Reduced Density Matrix Functional Theory at Finite Temperature

Dissertation

zu Erlangung des akademischen Grades
Doctor rerum naturalium

vorgelegt von

Tim Baldsiefen

Institut für Theoretische Physik
Freie Universität Berlin

Oktober 2012

Erstgutacher: Prof. Dr. E. K. U. Gross
Zweitgutachter: Prof. Dr. K. Schotte
Datum der Disputation: 31.10.2012

Eigenständigkeitserklärung

Hiermit versichere ich, dass ich die vorliegende Dissertationsschrift mit dem Titel *"Reduced Density Matrix Functional Theory at Finite Temperature"* selbständig und ohne die Benutzung anderer als der angegeben Hilfsmittel angefertigt habe. Die Stellen der Arbeit, die dem Wortlaut oder dem Sinn nach anderen Werken entnommen sind, wurden unter Angabe der Quelle kenntlich gemacht.

Berlin, den 10.10.2012

Abstract

Density functional theory (DFT) is highly successful in many fields of research. There are, however, areas in which its performance is rather limited. An important example is the description of thermodynamical variables of a quantum system in thermodynamical equilibrium. Although the finite-temperature version of DFT (FT-DFT) rests on a firm theoretical basis and is only one year younger than its brother, groundstate DFT, it has been successfully applied to only a few problems. Because FT-DFT, like DFT, is in principle exact, these shortcomings can be attributed to the difficulties of deriving valuable functionals for FT-DFT.

In this thesis, we are going to present an alternative theoretical description of quantum systems in thermal equilibrium. It is based on the 1-reduced density matrix (1RDM) of the system, rather than on its density and will rather cumbersomly be called finite-temperature reduced density matrix functional theory (FT-RDMFT). Its zero-temperature counterpart (RDMFT) proved to be successful in several fields, formerly difficult to address via DFT. These fields include, for example, the calculation of dissociation energies or the calculation of the fundamental gap, also for Mott insulators.

This success is mainly due to the fact that the 1RDM carries more directly accessible "many-body" information than the density alone, leading for example to an exact description of the kinetic energy functional. This sparks the hope that a description of thermodynamical systems employing the 1RDM via FT-RDMFT can yield an improvement over FT-DFT.

Giving a short review of RDMFT and pointing out difficulties when describing spin-polarized systems initiates our work. We will then lay the theoretical framework for FT-RDMFT by proving the required Hohenberg-Kohn-like theorems, investigating and determining the domain of FT-RDMFT functionals and by deriving several properties of the exact functional. Subsequently, we will present a perturbative method to iteratively construct approximate functionals for FT-RDMFT. The minimization of the corresponding first-order functional is shown to be equivalent to a solution of the finite-temperature Hartree-Fock (FT-HF) equations. We will then present a self-consistent minimization scheme, much like the Kohn-Sham minimization scheme in DFT, and show that it can also be employed to effectively and efficiently minimize functionals from RDMFT.

Finally, we will investigate the temperature-dependent homogeneous electron gas (HEG), employing various techniques which include finite-temperature many-body perturbation theory (FT-MBPT) and FT-RDMFT. We will focus on the description of the magnetic phase diagram and the temperature-dependent quasi-particle spectrum for collinear as well as chiral spin configurations.

Table of Contents

List of Figures

List of Tables

List of Abbreviations

1RDM	1-reduced density matrix.
2RDM	2-reduced density matrix.
BB	Buijse-Baerends/Müller functional.
BBCN	Corrections to the Buijse-Baerends/Müller functional.
BOW	Baldsiefen and Gross 2012 functional.
BOW-TIE	Trans-channel interaction energy version of the BOW functional.
CDFT	Current density functional theory.
CGA	xc functional by Csányi, Goedecker and Arias.
COHSEX	Coulomb hole plus screened exchange approximation.
DFT	Density functional theory.
EPX	Effective potential expansion method.
EQ	Equilibrium.
FM	Ferromagnetic.
FP-LAPW	Full potential linearily augmented plane waves.
FT-DFT	Finite-temperature density functional theory.
FT-HF	Finite-temperature Hartree-Fock.
FT-MBPT	Finite-temperature many-body perturbation theory.
FT-RDMFT	Finite-temperature reduced matrix functional theory.
GGA	Generalized gradient approximation.
GS	Ground state.
GZ	Gori-Giorgi and Ziesche.
HEG	Homogeneous electron gas.
HF	Hartree-Fock.
HS	Hilbert-Schmidt.
KAPPA	Baldsiefen 2010 FT-RDMFT correlation functional.
KAPPA-TIE	Trans-channel interaction energy version of the KAPPA functional.
LDA	Local density approximation.
LRDMA	Local 1RDM approximation.
LSDA	Local spin density approximation.
MBPT	Many-body perturbation theory.

MC	Monte-Carlo.
ML/ML-SIC	Marques-Lathiotakis empirical functional.
NO	Natural orbitals.
ON	Occupation numbers.
PBE	Perdew-Burke-Ernzerhof functional.
PM	Paramagnetic.
PNOF/0	Piris natural orbital functionals.
PP	Partially polarized.
PSS	Planar spin spirals.
PWCA	Perdew and Wang parametrization of Monte-Carlo results for the HEG by Ceperley and Alder.
RDMFT	Reduced density matrix functional theory.
RPA	Random phase approximation.
SC	Self-consistent.
SC-DFT	Superconductiong density functional theory.
SDO	Statistical density operator.
SDW	Spin density waves.
SW	Spin waves.
TD-DFT	Time-dependent density functional theory.
XC	Exchange-correlation.

1 Introduction

Already 86 years have past since Schrödinger formulated the fundamental equation of quantum mechanics [1]. Although this equation is in principle capable of describing all nonrelativistic quantum systems completely, its solution is practically impossible for most many-particle systems. The wavefunction keeps track of all coordinates of all particles, making it such a tremendeously complicated object that an actual numerical determination is out of reach of classical computation techniques at present and presumably will be so in the forseeable future.

From a practical point of view it certainly appears inefficient to retain all information contained in the wavefunction, if in the end one is interested in averaged quantities, like the energy for example. It therefore suggests the search for objects other than the wavefunction and methods other than solving the Schrödinger equation to determine the groundstate (gs) properties of a quantum mechanical system. The most important relation, utilized for this purpose, is the variational principle, singling out the groundstate as the state which minimizes the energy of the system. If one could describe the energy of a state by an object of lower dimensionality than the wavefunction, one could utilize the variational principle to find the groundstate energy. There is, however, one important nicety in this procedure. In the minimization process, one has to know which objects are physical, i.e. stem from a wavefunction of the correct symmetry. This problem prevents one from using the variational principle in combination with the Green's function or the 2-reduced density matrix [2], which otherwise would be able to yield the exact gs energy.

On the other hand, the conditions for the density to be physical are known and rather simple, namely the requirements of semipositivity and normalizability. It is by virtue of the work of Hohenberg and Kohn [3] that we know that the density also contains all the information needed to determine the groundstate energy. The formulation of a density functional theory (DFT) is therefore well founded.

The cost one has to pay for the lower dimensionality of the density is that the functional dependence on the density of the observables is generally not known and has to be approximated. A major improvement in the context of DFT was the introduction of a Kohn-Sham system [4], i.e. a noninteracting system, having the same groundstate density as the interacting one. The functional for the energy of the interacting system then consists of four parts. These are the functional for the noninteracting kinetic energy of the Kohn-Sham system, the Hartree energy functional, describing the classical part of the interaction energy, the exchange energy functional, paying tribute to Pauli's exclusion principle, and finally the remaining part, the correlation energy functional. Finding approximations for the correlation part is the main obstacle in DFT. Two of the most prominent approximations, the local density approximation (LDA) [3] and the generalized gradient approximation (GGA) [5], show remarkable success in many different applications, e.g. in determining gs energies and structure constants. Both approximations are based on Monte-Carlo (MC) results for the homogeneous electron gas (HEG) which underlines the importance of this simple model system.

Because of the success of the original formulation of DFT, a wide range of extensions has emerged in the past decades, expanding the realm of possible applications. They can be cast roughly into two groups. The first one represents different varieties of Hamiltonians, leading to e.g. spin-DFT [6, 7], which is capable of describing spin-polarized systems, current density functional theory (CDFT) [8], describing systems in external magnetic fields, or superconducting DFT (SC-DFT) [9], treating superconducting states. The second group deals with problems which go beyond groundstate calculations, like time-dependent DFT (TD-DFT) [10], describing the time evolution of a system, or finite-temperature DFT (FT-DFT) [11], trying to determine thermodynamic properties of quantum systems in thermodynamic equilibrium.

All these extensions of DFT are theoretically well founded but are not necessarily equally successful in their respective fields of application. Two prominent examples for physical problems where DFT struggles are the calculation of dissociation energies [12, 13] and the determination of the fundamental gap of Mott insulators. Futhermore, FT-DFT in general fails to achieve accuracies comparable to those of gs-DFT. This is unfortunate, in view of the wide variety of possible

applications. These include e.g. the description of phase transitions, either magnetic [14, 15] or superconducting [16, 17], the description of warm matter [18] and hot plasmas [19, 20, 21], femtochemistry at surfaces of solids [22], the description of shock waves in hot dense gases [23, 24], or the composition of different phases of water in the interior of giant planets [25].

With regard to the zero-temperature case, there are several approaches to remedy existing problems. One promising approach is reduced density matrix functional theory (RDMFT) which employs the 1-reduced density matrix (1RDM) rather than the density as central variable. In contrast to DFT, this theory, based on a theorem by Gilbert [26], is capable of describing systems subject to a nonlocal external potential. Such potentials are sometimes used as mathematical tools [27, 28] and are therefore an important consideration. The theory of RDMFT is successful in calculating dissociation energy curves [29, 30, 31, 32] and predicting fundamental gaps for atoms and molecules [31, 33] as well as for Mott insulators [34].

The main concern of this work, motivated by the success of RDMFT at zero temperature, is to lay the theoretical framework of a finite-temperature version of RDMFT (FT-RDMFT) and investigate its properties and performance.

We have divided the thesis in the following way:

After presenting a selection of mathematical prerequisites in **Section 2**, we shall give a short review of RDMFT in **Section 3**. From an investigation of several existing approximations we will be able to define a new exchange-correlation functional which is capable of describing the correlation energy of a homogeneous electron gas to unprecedented accuracy. It furthermore recovers important qualitative features of the momentum distribution, a capability most existing functionals are missing. Then, by using only Monte-Carlo results for the groundstate energy of a HEG, we will be able to demonstrate that a certain class of correlation functionals in RDMFT is bound to fail when applied to the spin-polarized HEG. The investigation of this problem will give some valuable insight into the relation of correlation contributions which stem from interactions of electrons of the same spin compared to electrons with different spin.

In **Section 4** we will lay the mathematical framework of FT-RDMFT. This will include proving a Hohenberg-Kohn-like theorem as well as investigating the domain of functionals. Special attention is given to the question of equilibrium-V-representability. This is how 1RDMs which come from an equilibrium state, corresponding to a Hamiltonian with fixed two-particle interaction and some external potential, can be characterized. As we will point out repeatedly in this work, this question is of more than just mathematical interest, which also explains why its zero-temperature counterpart in DFT received considerable attention during the course of the theoretical development of DFT [35, 36, 37, 38].

Also in FT-RDMFT, some part of the free energy functional has to be approximated. Accordingly, the success of FT-RDMFT depends strongly on the quality of these approximations. To guide the development of correlation functionals, in **Section 5** we will derive various properties of the exact free energy functional. One major tool utilized for this is the concept of uniform coordinate scaling, which proved to be very useful also in the context of DFT [39, 40, 41, 42] and FT-DFT [43].

Utilizing the fact that in FT-RDMFT there is a Kohn-Sham system, in **Section 6** we will establish a methodology to construct FT-RDMFT correlation functionals using the powerful methods of finite-temperature many-body perturbation theory (FT-MBPT). By construction, these functionals satisfy most exact properties derived in the previous section.

Having laid a solid theoretical foundation, in **Section 7** we will then turn to the problem of numerical minimization of FT-RDMFT functionals. We will develop a self-consistent minimization scheme which will be able to effectively and efficiently minimize functionals from FT-RDMFT as well as RDMFT.

In the final **Section 8** we will investigate the effect of several FT-RDMFT functionals on the magnetic phase diagram of the HEG . The results will be compared to results from Monte-Carlo calculations as well as FT-MBPT approximations. We will furthermore be able to employ FT-RDMFT to calculate the finite-temperature Hartree-Fock dispersion relations for both a collinear as well as a

chiral spin configuration.

We have chosen to make each chapter of this thesis relatively self contained. We hope that this will increase its usefulness as a reference work and we are gladly willing to pay the price of a higher degree of redundancy.

Throughout this thesis, unless mentioned otherwise, we will use atomic units ($e = m_e = \hbar = 1$).

2 Mathematical prerequisites

The theory of RDMFT, both at zero as well as finite temperature, to a large extent relies on the same theoretical concepts. Accordingly, before proceeding with the investigation of RDMFT, we are going to introduce some important mathematical requisites in the following:

Section	Description
2.1	We will define the Hamiltonian, mostly used in this thesis, especially focussing on spin notation.
2.2	We will then define the statistical density operator (SDO) and 1RDM of a quantum
2.3	system and investigate some of their properties.
2.4	Finally, we will briefly introduce the concept of the HEG. It will become an important testing system for RDMFT at both zero as well as finite temperature.

Related publications: [44]

2.1 Hamiltonian and spin notation

In the course of this work, we will focus mainly on systems subject to a two-particle interaction $\hat{W}$ and a generally nonlocal external potential $\hat{V}_{ext}$. In combination with the kinetic energy part, described by $\hat{T}$, this yields the following Hamiltonian:

$$\hat{H} = \hat{T} + \hat{W} + \hat{V}_{ext}. \tag{2.1}$$

A subject of major interest will be temperature-driven magnetic phase transitions. We will therefore have to keep track of the spin quantum number. Not to overload notation, we will combine the spin index σ with the spacial index $\boldsymbol{r}$ into the joint variable $x = (\sigma, \boldsymbol{r})$. Integrals over x then refer to a spin summation and a spacial integration: $\int dx = \sum_\sigma \int d^3 r$. The second-quantized forms of the operators, introduced before, then become

$$\hat{T} = \int dx \lim_{x' \to x} \left(-\frac{\nabla^2}{2} \right) \hat{\Psi}^+(x') \hat{\Psi}(x) \tag{2.2}$$

$$\hat{V}_{ext} = \int dx dx' v_{ext}(x, x') \hat{\Psi}^+(x') \hat{\Psi}(x) \tag{2.3}$$

$$\hat{W} = \int dx dx' w(x, x') \hat{\Psi}^+(x') \hat{\Psi}^+(x) \hat{\Psi}(x) \hat{\Psi}(x'), \tag{2.4}$$

where $\{\hat{\Psi}\}$ are the common fermionic field operators. The most important type of interaction in this work is the Coulomb interaction, whose kernel $w(x, x')$ is given by

$$w(x, x') = \frac{1}{|\boldsymbol{r} - \boldsymbol{r}'|}. \tag{2.5}$$

2.2 Statistical density operator (SDO)

A quantum mechanical system is generally described by a SDO, i.e. a weighted sum of projection operators on the underlying Hilbert space $\mathcal{H}$.

$$\hat{D} = \sum w_i |\psi_i\rangle\langle\psi_i|, \quad 0 \le w_i \le 1, \quad \sum_i w_i = 1, \tag{2.6}$$

where $\{\psi_i\}$ constitutes a basis of $\mathcal{H}$. The set of all possible SDOs, yielding a particle number N, will be denoted by $\mathfrak{D}^N$.

$$\mathfrak{D}^N = \left\{ \hat{D} \mid \hat{D} \text{ as defined in Eq. (2.6) with } \text{Tr}\{\hat{D}\hat{N}\} = N \right\}, \tag{2.7}$$
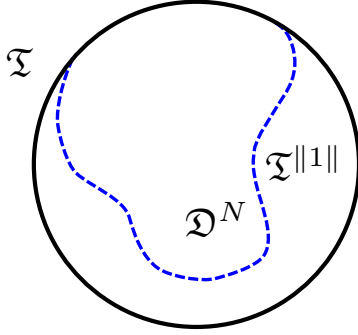
2.1.a: Hierarchy of spaces as defined in Eqs. (2.9),(2.11), and (2.7)
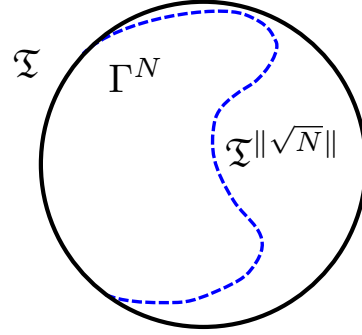
2.1.b: Hierarchy of spaces as defined in Eqs. (2.9),(2.23), and (2.22)

Figure 2.1: Sketch of the spaces of ensemble-N-representable SDOs and 1RDMs and their embedment in a Banach space.

where the particle number operatore $\hat{N}$ is defined as

$$\hat{N} = \int dx \hat{\Psi}(x)^+ \hat{\Psi}(x). \tag{2.8}$$

By definition, $\mathfrak{D}^N \subset \mathfrak{T}$, where $\mathfrak{T}$ is the set of all trace-class operators, i.e. compact operators with finite trace.

$$\mathfrak{T} = \left\{ \hat{A} \mid \hat{A} \text{ trace-class} \right\} \tag{2.9}$$

To define a distance between SDOs, we introduce the Hilbert-Schmidt (HS) norm $\| \cdot \|_{HS}$.

$$\|\hat{A}\|_{HS} = \sqrt{\text{Tr}\{\hat{A}^+ \hat{A}\}} \tag{2.10}$$

$\mathfrak{T}$ together with $\| \cdot \|_{HS}$ therefore constitutes a Banach space, i.e. a complete normed vector space which we will simply denote by $\mathfrak{T}$ in the following. From Eq. (2.6), we see that every $\hat{D} \in \mathfrak{D}^N$ has a HS-norm smaller or equal to 1. $\mathfrak{D}^N$ is therefore a subset of the norm closed ball $\mathfrak{T}^{\|1\|}$ of radius 1.

$$\mathfrak{T}^{\|1\|} = \left\{ \hat{A} \mid \|\hat{A}\|_{HS} \leq 1 \right\} \tag{2.11}$$

It follows that $\mathfrak{D}^N \subset \mathfrak{T}^{\|1\|} \subset \mathfrak{T}$ as depicted in Figure 2.1.a. This property, i.e. the embedment of $\mathfrak{D}^N$ in a norm closed subset ($\mathfrak{T}^{\|1\|}$) of a Banach space ($\mathfrak{T}$) will become crucial for the investigation of properties of the universal functional in FT-RDMFT in Section 4.3.

2.3 1-reduced density matrix (1RDM)

The 1RDM $\gamma(x, x')$ of a system, whose state is described by $\hat{D}$, is formally defined with the help of the field operators $\{\hat{\Psi}(x)\}$.

$$\gamma(x, x') = \text{Tr}\{\hat{D}\hat{\Psi}^+(x')\hat{\Psi}(x)\} \tag{2.12}$$

By definition, $\gamma(x, x')$ is hermitean and can therefore be written in spectral representation as

$$\gamma(x, x') = \sum_i n_i \phi_i^*(x')\phi_i(x). \tag{2.13}$$

The eigenstates $\{\phi_i(x)\}$ of the 1RDM are called natural orbitals (NO) and the eigenvalues $\{n_i\}$ occupation numbers (ON) [45]. It is sometimes desirable to treat spin and spacial variables separately. To this end we introduce a two-component (Pauli) spinor notation,

$$\Phi_i(\boldsymbol{r}) = \left(\begin{array}{c} \phi_{i1}(\boldsymbol{r}) \\ \phi_{i2}(\boldsymbol{r}) \end{array} \right), \tag{2.14}$$

where $\phi_{i\sigma}(\boldsymbol{r}) = \phi_i(x) = \phi_i(\sigma, \boldsymbol{r})$ ($\sigma = 1, 2$) are the orbitals of Eq. (2.13). The 1RDM can then be written as a matrix in spin space as

$$\gamma(\boldsymbol{r}, \boldsymbol{r}') = \sum_i n_i \Phi_i^\dagger(\boldsymbol{r}') \otimes \Phi_i(\boldsymbol{r}) \tag{2.15}$$

$$= \left(\begin{array}{cc} \gamma_{11}(\boldsymbol{r}, \boldsymbol{r}') & \gamma_{12}(\boldsymbol{r}, \boldsymbol{r}') \\ \gamma_{21}(\boldsymbol{r}, \boldsymbol{r}') & \gamma_{22}(\boldsymbol{r}, \boldsymbol{r}') \end{array} \right) = \sum_i n_i \left(\begin{array}{cc} \phi_{i1}^*(\boldsymbol{r}')\phi_{i1}(\boldsymbol{r}) & \phi_{i2}^*(\boldsymbol{r}')\phi_{i1}(\boldsymbol{r}) \\ \phi_{i1}^*(\boldsymbol{r}')\phi_{i2}(\boldsymbol{r}) & \phi_{i2}^*(\boldsymbol{r}')\phi_{i2}(\boldsymbol{r}) \end{array} \right) \tag{2.16}$$

There are some cases in which one can treat different spin channels separately. One of these special cases is the particulary important situation of collinear spin configuration. For these systems, the natural orbitals are so-called spin orbitals, i.e. spinors containing only one spin component. We characterize these spin orbitals by an additional index.

$$\Phi_{i1}(\boldsymbol{r}) = \left(\begin{array}{c} \phi_{i1}(\boldsymbol{r}) \\ 0 \end{array} \right), \Phi_{i2}(\boldsymbol{r}) = \left(\begin{array}{c} 0 \\ \phi_{i2}(\boldsymbol{r}) \end{array} \right) \tag{2.17}$$

This then leads to a 1RDM where every 2x2 matrix in Eq. (2.16) contains only one nonvanishing entry, either the 11 or the 22 one. Hence the complete 1RDM is diagonal w.r.t. the spin coordinate,

$$\gamma_{\sigma\sigma'}(\boldsymbol{r}, \boldsymbol{r}') = \delta_{\sigma\sigma'} \sum_i n_{i\sigma} \phi_{i\sigma}^*(\boldsymbol{r}')\phi_{i\sigma}(\boldsymbol{r}), \tag{2.18}$$

where $n_{i\sigma}$ are the occupation numbers of the special spinors $\Phi_{i\sigma}(\boldsymbol{r})$ of Eq. (2.17). Another special case where this seperation is possible is the case of spin spiral states which will be dealt with in Section 8.4.2.

Because we want to establish a functional theory, based on a variational scheme over 1RDMs, it is important to know which 1RDMs stem from a physical state $\hat{D}$, as defined in Eq.(2.6). Fortunately, as Coleman showed [46], this set of 1RDMs is simply characterized by the following constraints on the ONs and NOs of the 1RDMs.

Theorem 2.1. [ensemble-N-representability]
Let $\gamma(x, x') = \sum_i n_i \phi_i^*(x')\phi_i(x)$. There exists a SDO $\hat{D} \in \mathfrak{D}^N$ so that $\mathrm{Tr}\{\hat{D}\hat{\Psi}^+(x')\hat{\Psi}(x)\} = \gamma(x, x')$ if and only if

$$0 \le n_i \le 1, \tag{2.19}$$

$$\sum_i n_i = N, \tag{2.20}$$

$\{\phi_i\}$ forms a complete orthonormal set. $\tag{2.21}$

A 1RDM, which fulfills these requirements is said to be ensemble-N-representable.

The set of all ensemble-N-representable 1RDMs is denoted by Γ^N.

$$\Gamma^N = \left\{ \gamma \mid \gamma \text{ fulfills Eqs. } (2.19),(2.20), \text{ and } (2.21) \right\} \tag{2.22}$$

In analogy to our investigation of SDOs, we see that every ensemble-N-representable 1RDM $\gamma \in \Gamma^N$ has a Hilbert-Schmidt norm smaller or equal to $\sqrt{N}$. Γ^N is therefore embedded in the norm closed ball $\mathfrak{T}^{\|\sqrt{N}\|}$ of radius $\sqrt{N}$.

$$\mathfrak{T}^{\|\sqrt{N}\|} = \left\{ \hat{A} \mid \|\hat{A}\|_{HS} \leq \sqrt{N} \right\} \tag{2.23}$$

The hierarchy of sets is then $\Gamma^N \subset \mathfrak{T}^{\|\sqrt{N}\|} \subset \mathfrak{T}$ as depicted in Figure 2.1.b.

We show in Appendix A.1 that an ON n_i bears the following important information. It reflects the contribution of its corresponding NO ϕ_i to the state of the system. If one expands $\{\psi_i\}$ in Eq. (2.6) in Slater determinants constructed from the NOs, then n_i/N is the relative frequency of occurrence of the orbital ϕ_i. E.g. a state, consisting only of a single projection operator on a Slater determinant of orbitals ϕ_i (a noninteracting, nondegenerate groundstate) will yield ONs which are either 0 or 1. On the other hand, a thermodynamical equilibrium (eq) state will have contributions from all possible eigenstates of the Hamiltonian. Therefore, every NO will contribute and all ONs will be bigger 0. Furthermore, they will be also smaller than 1, because otherwise that would imply that states, not containing the orbital, would not contribute to the equilibrium state. A more detailed proof of this argument is presented in Appendix A.2

Another important property of the 1RDM was shown by Löwdin in 1954 [45]. If one uses the NOs as basis functions for the Slater determinants in a configuration interaction (CI) expansion, then one achieves the most rapid convergence. This fact, however, cannot simply be exploited because the gs-1RDM is not known a priori.

Finally, following from Eq. (2.12), we point out that the density $n(x)$ is simply given as the diagonal of the 1RDM.

$$n(x) = \gamma(x, x) \tag{2.24}$$

If one is interested in the spin-resolved density n_σ, which has to be done when considering systems subject to magnetic fields, then one can take only the spacial diagonal to get

$$n_\sigma(\boldsymbol{r}) = \gamma_{\sigma\sigma}(\boldsymbol{r}, \boldsymbol{r}). \tag{2.25}$$

2.4 Homogeneous electron gas (HEG)

In the course of this work, we will be concerned mostly with systems subject to Coulomb interactions, as defined in Eq. (2.5). This interaction, as well as the kinetic energy operator, is spacially invariant, i.e. $w(\boldsymbol{r}, \boldsymbol{r}') = w(\boldsymbol{r} - \boldsymbol{r}')$. If the external potential also fulfills this property, then the full Hamiltonian commutes with the displacement operator $\hat{J} = e^{i\hat{\boldsymbol{P}} \cdot \hat{\boldsymbol{r}}}$ with $\hat{\boldsymbol{P}}$ being the momentum operator. Consequently, all eigenstates of $\hat{H}$ can be chosen to be momentum eigenstates as well. Accordingly, the Green's function, as well as the 1RDM, is also spacially invariant, yielding a constant density. Because of this constant density the system is usually termed homogeneous electron gas (HEG). The HEG constitutes a central model system for the theoretical description of many particle quantum systems and an extensive investigation of it can be found in Ref. [47].

If one considers local potentials, the requirement of spacial invariance can only be fulfilled by a constant potential. Following from the Hohenberg-Kohn theorem [3], one can characterize the HEG completely by the density. Rather than using the density itself it is common practice to use the Wigner-Seitz radius r_s instead. It is given as the radius of a sphere of constant density which contains one electron.

$$r_s = \left(\frac{3}{4\pi n} \right)^{1/3} \tag{2.26}$$

The Fermi wavevector k_F, the Fermi energy ε_F, and the Fermi temperature T_F are then defined as

$$k_F = \left(3\pi^2 n\right)^{\frac{1}{3}} = \left(\frac{9}{4}\pi\right)^{\frac{1}{3}} r_s^{-1} \tag{2.27}$$

$$\varepsilon_F = \frac{k_F^2}{2} \tag{2.28}$$

$$T_F = \frac{\varepsilon_F}{k_B}, \tag{2.29}$$

where k_B is Boltzmann's constant with $k_B = 3.17 \cdot 10^{-6}(Ha/K)$. When considering spin-dependent systems, one has to use the full spin-resolved density. For collinear spin configurations one can either use the diagonal elements of the the spin-resolved densities $n^\uparrow$ and $n^\downarrow$ or one can use the averaged density or Wigner-Seitz radius in combination with the polarization ξ.

$$\xi = \frac{n^\uparrow - n^\downarrow}{n^\uparrow + n^\downarrow} \tag{2.30}$$

The Fermi variables from Eqs. (2.27)-(2.29) can then also be defined for the different spin channels.

$$n_\sigma = n(1 \pm \xi) \tag{2.31}$$

$$k_{F\sigma} = k_F(1 \pm \xi)^{\frac{1}{d}} \tag{2.32}$$

$$\varepsilon_{F\sigma} = \varepsilon_F(1 \pm \xi)^{\frac{2}{d}} \tag{2.33}$$

$$T_{F\sigma} = T_F(1 \pm \xi)^{\frac{2}{d}}, \tag{2.34}$$

where d denotes the number dimensions of the HEG.

The gs-energy of the HEG has been calculated for the spin-polarized case in three dimensions [48, 49] and for the paramagnetic case in two dimensions [50, 51]. These results have also been readily parametrized [52, 49]. Because these results are very accurate, the HEG is often used as a testing system in theoretical solid state physics. Furthermore, the 3D-results are employed in the very successful local density approximation (LDA) of DFT, where the correlation energy of a nonuniform system $E_c^{nu}[n(\boldsymbol{r})]$ is calculated as the average of the correlation energy per particle of the HEG $e_c(n)$:

$$E_c^{nu}[n(\boldsymbol{r})] = \int d\boldsymbol{r} n(\boldsymbol{r}) e_c(n(\boldsymbol{r})). \tag{2.35}$$

The treatment of the HEG is greatly simplified by the fact that the external potential is only a constant. In the course of this work, however, we will also have to deal with nonlocal external potentials. The requirement of spacial invariance then leads to the following form for $\hat{V}_{ext}$.

$$\hat{V}_{ext\ \sigma\sigma'} = \int d\boldsymbol{k} v_{ext\ \sigma\sigma'}(\boldsymbol{k}) \hat{n}_{\sigma\sigma'}(\boldsymbol{k}), \tag{2.36}$$

where $v_{ext\ \sigma\sigma'}(k)$ is the Fourier transform of $v_{ext\ \sigma\sigma'}(\boldsymbol{r} - \boldsymbol{r}')$ and $\hat{n}_{\sigma\sigma'}(\boldsymbol{k})$ is the momentum density operator. Gilbert showed [26] that for these potentials the density alone is not sufficient anymore and one has to resort to the 1RDM. The ONs of a HEG describe what is usually called the momentum distribution. The determination of the gs-momentum distribution is complicated, because the gs-energy is relatively insensitive to small changes in the ONs. This then usually leads to big statistical variances in the determination of the gs-momentum distribution via Monte-Carlo calculations. It was Takada and Kita [53] who, for the case of the three-dimensional HEG, derived a self-consistency relation between the momentum distribution and the correlation energy which allows to test the accuracy of momentum distributions. It also allows the development of an effective potential expansion (EPX) method [54] to calculate the momentum distributions to high accuracy. Gori-Giorgi and Ziesche [55] then derived a parametrization for the gs-momentum distribution of the HEG for $r_s < 12$, both checking against Monte-Carlo as well as EPX results.

3 Zero-temperature RDMFT

DFT proved to be highly successful in the description of several properties of many-particle quantum systems. However, although in principle exact, it has to rely on approximations for the correlation energy which will inevitably fail to describe all possible systems accurately. An investigation of the failures of DFT can then lead to a better understanding of the basic processes governing the quantum world and stimulate the derivation of improved functionals and techniques.

One example for a theory, which rests on the same theoretical concepts as DFT, is RDMFT, employing the 1RDM as central variable rather than the density. The aim of this part of our work is to introduce the main concepts of RDMFT and discuss their accomplishments and shortcomings and to propose possible improvements. We will structure this section as the following:

Section	Description
3.1	We start this section by giving a short introduction to the theoretical foundations of RDMFT, reviewing several approximate functionals.
3.2	The construction of an LDA for RDMFT is complicated by several difficulties. We will review some of these obstacles and propose improvements.
3.3	One improvement will be the development of a novel correlation functional for RDMFT. It is shown to be able to reproduce the gs-energy of the HEG for a wide range of densities more accurately than most common RDMFT functionals. It will furthermore be able to reproduce the effects of depletion of low momentum states in the momentum distribution as well as occupation of all high momentum states, leading to a qualitatively better description of the gs-momentum distribution.
3.4	Finally, we will consider the description of magnetic systems. Using only results from Monte-Carlo calculations, we will be able to show that a certain class of RDMFT functionals is intrinsically incapable of describing polarized systems accurately.

Related publications: [44, 56]

3.1 Theoretical foundations

At zero temperature, the system is from now on assumed to be in a nondegenerate groundstate, so that its SDO $\hat{D}$ is given by a single projection operator:

$$\hat{D} = |\Psi_{gs}\rangle\langle\Psi_{gs}|. \tag{3.1}$$

The energy of the system is then given by

$$E = E_k[\gamma] + V_{ext}[\gamma] + W[\Gamma^{(2)}] \tag{3.2}$$

$$E_k[\gamma] = \int dx \lim_{x' \to x} \left(-\frac{\nabla^2}{2}\right) \gamma(x', x) \tag{3.3}$$

$$V_{ext}[\gamma] = \int dx dx' v_{ext}(x, x') \gamma(x', x) \tag{3.4}$$

$$W[\Gamma^{(2)}] = \int dx dx' w(x, x') \Gamma^{(2)}(x, x'; x, x'), \tag{3.5}$$

where $\Gamma^{(2)}$ is the 2-reduced density matrix (2RDM) of the system, defined as

$$\Gamma^{(2)}(x_1, x_2; x_3, x_4) = \frac{N(N-1)}{2} \text{Tr}\{\hat{D}\hat{\Psi}^+(x_4)\hat{\Psi}^+(x_3)\hat{\Psi}^+(x_1)\hat{\Psi}^+(x_2)\}. \tag{3.6}$$

The corresponding 1RDM $\gamma(x, x')$ can be calculated from $\Gamma^{(2)}$ via

$$\gamma(x, x') = \frac{2}{N-1} \int dx_2 \Gamma^{(2)}(x, x_2; x', x_2). \tag{3.7}$$

We conclude that knowledge of $\Gamma^{(2)}$ is sufficient to calculate the corresponding energy exactly. One might try to exploit this fact in combination with the variational principle to find the gs-energy of the system by a minimization of the energy functional as defined in Eq.(3.2) w.r.t. the 2RDM. One difficulty arising in this procedure is the problem of ensemble-N-representability (see Section 2.3) of the 2RDM. This is the question of how a 2RDM, coming from a state of the correct symmetry via Eq. (3.6), can be characterized. Although the conditions are known in principle [57, 58], they are too complicated to be used in a numerical procedure. The apparent possiblity of an exact description of a quantum gs led to an tremendous effort to approx-mate the exact conditions to be treated in practical terms [59, 60, 61, 62, 63, 64, 2]. So far, however, one was only successful in deriving several simple separate necessary or sufficient conditions, but not an inclusive combination of both.

On the other hand, as we have seen in Section 2.3, the conditions for the 1RDM to be ensemble-N-representable are known exactly and rather simple (see Thm. 2.1). Because the density is simply related to the 1RDM via Eq. 2.24, the Hohenberg-Kohn theorem justifies the incorporation of the 1RDM as central variable.

$$W[\Gamma^{(2)}] = W[\gamma] \tag{3.8}$$

As Gilbert showed in 1975 [26], the nonlocal nature of the 1RDM allows the treatment of nonlocal potentials, which sometimes appear in model Hamiltonians [27, 28]. This is a problem formerly inaccessible via DFT.

An important difference between DFT and RDMFT concerns the uniqueness of the mapping between external potentials and 1RDMs. Assume e.g. the following two potentials.

$$v(x, x') = v_{HF}(x, x') \tag{3.9}$$
$$v'(x, x') = v_{HF}(x, x') + \alpha \gamma_{gs}(x, x'), \tag{3.10}$$

where $v_{HF}(x, x')$ denotes the Hartree-Fock potential and $\gamma_{gs}(x, x')$ is the corresponding gs-1RDM. Both potentials yield the same gs-determinant for systems with a discrete spectrum and sufficiently small α. Therefore, the mapping of external potentials to the corresponding gs-1RDMs is not unique. However, we were able to show in Appendix A.3 that in general, the one-to-one correspondence between potential and wavefunction persists if and only if there are no pinned ONs, i.e. no ONs equal to 0 or 1. The case described above exhibits only pinned states and can therefore be be seen as an extreme case of our general result from Appendix A.3. Following these considerations, it is now interesting to investigate the properties of the gs-1RDMs of an interacting system with regard to the distribution of their ONs.

When dealing with Coulomb systems, i.e. systems with a two-particle interaction with $w(x, x') = 1/|\boldsymbol{r} - \boldsymbol{r}'|$, the following important statement was shown [65].

Theorem 3.1. [Cusp condition]
The gs-1RDM of a Coulomb system has an infinite number of occupied orbitals, i.e. orbitals with ON $n_i > 0$.

Proof [of Theorem 3.1]
The original proof is rather involved and we therefore give an alternative simpler version in the following.
As Kato showed in 1957 [66], the divergence of the Coulomb interaction for vanishing interparticle distances leads to a nucleus-electron as well as an electron-electron cusp in the gs-wavefunction. This gs-wavefunction is an element of the general N-particle Hilbert space of the system and can therefore

be expanded in any basis of this Hilbert space. Furthermore, we know that one can create an N-particle basis by constructing all possible N-particle Slater determinants of a fixed one-particle basis. Because in a Slater determinant a particular one-particle wavefunction "does not know" about the coordinates of another, the electron-electron cusp condition cannot be fulfilled by a superposition of a finite number of Slater determinants. One therefore needs an infinite number of Slater determinants to reproduce the cusp and therefore the gs-wavefunction of a Coulomb-system. This argument is valid for all one-particle bases, including the set of NOs of the gs-1RDM. If an infinite number of N-particle wavefunctions contributes, then the number of contributing one-particle NOs also has to be infinite, concluding the proof. ∎

We know from Sec. 2.3 that a 1RDM with partially occupied ONs cannot be the 1RDM of a nondegenerate gs. Therefore, in combination with Thm. 3.1, we conclude that in RDMFT, there exists no Kohn-Sham system for Coulomb systems. We whould like to point out, however, that a degenerate noninteracting system is capable of reproducing a 1RDM with partially occupied NOs [67], but the degree of degeneracy is equal to the number of partially occupied states, which for a Coulomb system is infinite.

The main task of RDMFT is now to find accurate approximations for the interaction energy in terms of the 1RDM. It is common practice to separate the classical Hartree energy E_H and the exchange energy E_x, which is induced by Pauli's inclusion principle. The remainder will then be called the correlation energy:

$$W[\gamma] = E_H[\gamma] + E_x[\gamma] + E_c[\gamma] \tag{3.11}$$

$$E_H[\gamma] = \frac{1}{2} \int dx dx' w(x, x') \gamma(x, x) \gamma(x', x') \tag{3.12}$$

$$E_x[\gamma] = -\frac{1}{2} \int dx dx' w(x, x') \gamma(x, x') \gamma(x', x) \tag{3.13}$$

$$E_c[\gamma] = W[\gamma] - E_H[\gamma] - E_x[\gamma]. \tag{3.14}$$

We see from Eq. 3.3 that, in contrast to DFT, the kinetic energy functional is known exactly in terms of the 1RDM . Therefore, the correlation energy in RDMFT does not contain any kinetic contribution. This has some conceptual advantages, for example the simpler behaviour of $E_c[\gamma]$ under coordinate scaling (see Section 5.3).

Before we review several existing functionals in RDMFT, we should like to mention the respective areas of success. RDMFT is capable of describing several properties of small systems quite accurately. These include dissociation curves of several small open-shell molecules, references of which will be given in the next section. Furthermore, RDMFT was also shown to be able to predict correctly the fundamental gap of small systems [68, 69, 33] as well as of strongly correlated Mott insulators [34, 33], the latter being an extremely difficult task within DFT. However, the accurate description of magnetic systems and their properties is not very satisfactory. We will try to shed some light on the intrinsic problems of an RDMFT description of these systems in Section 3.4 and propose some conceptual improvements.

Starting with the derivation of the famous Müller functional [70] in 1984, there emerged several functionals trying to incorporate the correlation energy in the framework of RDMFT. The most common class of functionals, namely the exchange-correlation (xc) functionals $E_{xc}[\gamma]$ will be discussed in the following section.

3.1.1 Exchange-correlation functionals

Most energy functionals in RDMFT try to incorporate correlation via a modification of the exchange functional Eq. (3.13). The resulting functionals are accordingly called exchange-correlation

functionals and can generally be written as

$$E_{xc}[\gamma] = E_x[\gamma] + E_c[\gamma] \tag{3.15}$$

$$E_{xc}[\gamma] = -\frac{1}{2} \sum_{ij} f(n_i, n_j) \int dx dx' w(x, x') \phi_i^*(x') \phi_i(x) \phi_j^*(x) \phi_j(x'). \tag{3.16}$$

Choosing $f^x(n_i, n_j) = n_i n_j$ reproduces the exchange-only functional, neglecting correlation completely.

The first approximation to $f(n_i, n_j)$ was done by Müller in 1984 [70] leading to $f^{Mueller}(n_i, n_j) = \sqrt{n_i n_j}$. The same approximation was rederived almost 20 years later from a different ansatz by Buijse and Baerends [71] and is therefore sometimes also called BB functional. This Müller functional was able to describe correctly the dissociation limit of several small dimers of open-shell atoms but it overestimates the correlation energy quite considerably. Goedecker and Umrigar [72] attributed this fact to the inclusion of self-interaction terms in the Müller functional, proposing a remedy by omitting the diagonal terms of $f^{Mueller}(n_i, n_j)$. They succeeded in improving correlation energies but failed to retain the good results for the dissociation limit [73]. Inveigled by the simplicity of the form of the xc approximation and the primary success of the Müller functional, Gritsenko, Pernal and Baerends developed what is now known as the BBC1, BBC2 and BBC3 functionals [29]. The key difference in their approach is the different treatment of orbitals which were occupied or unoccupied in a Hartree-Fock (HF) solution (termed strongly and weakly occupied in the following). In addition, BBC2 and BBC3 effectively mix parts of the exchange and Müller functionals. A similar approach was taken by Piris et al. [74]. Their approach differs slightly in the distinction of strongly and weakly occupied orbitals, removes parts of the self interaction (PNOF0) and tries to incorporate particle-hole symmetry (PNOF). These more elaborate functionals BBC1/2/3 and PNOF/0 are capable of reproducing good dissociation energies as well as correlation energies.

Whereas the previous functionals are mainly derived from physical arguments, Marques and Lathiotakis [75] pursued a different way by proposing a two-parameter Padé form for $f(n_i, n_j)$. These parameters are then optimized to minimize the deviation of correlation energies when applied to the molecules of the G2 and G2-1 sets. The resulting functionals are called ML and ML-SIC, either including or excluding self interaction. The ML and ML-SIC functionals achieve an unprecedented precision, reaching the accuracy of second-order Møller-Plesset perturbation theory for the calculation of the correlation energies. An overview of several of these functionals as well as the corresponding energies for many molecules can be found in Ref. [76].

Another rather empirical functional, which will become important in this work, was derived by Sharma et al. [34]. They realized that both the exchange-only functionals as well as the Müller functional can be seen as instances of a more general functional, namely the α or Power functional, described by $f^\alpha(n_i, n_j) = (n_i n_j)^\alpha$. Because the Müller functional underestimates the correlation energy, one expects to improve the results for values of α between 0.5 and 1. This assumption proved to be valid [31], leading to an accurate description of the dissociation energy curve of H2 (a discussion of the performance of several DFT functionals for this problem can be found in [77]).

So far, we have only considered small finite systems. Because the xc functional should in principle be general, it is now instructive to investigate how the different functionals perform for extended systems. We therefore turn to the description of a HEG via RDMFT in the following section.

3.2   The problem of the construction of an RDMFT-LDA

One reason for the wide acceptance of DFT as the method of choice for modern day quantum computations is the tremendous success of the LDA. Because of this success, one should like to derive a similar approximation in the framework of RDMFT. But there arise some conceptual problems.

In DFT, one only has to calculate the correlation-energy of the HEG as a function of the constant density n. In RDMFT, on the other hand, one has to calculate it for all possible density matrices $\gamma(\boldsymbol{r}-$

$\boldsymbol{r}'$) that are compatible with translational invariance, i.e. for all possible momentum distributions $n(\boldsymbol{k})$. The correlation-energy per volume of the HEG in RDMFT therefore becomes a *functional*, $\varepsilon_c^{HEG}[n(\boldsymbol{k})]$, of $n(\boldsymbol{k})$ rather than just a function of n. Under the assumption that such a functional was accessible, the local 1RDM approximation (LRDMA) of RDMFT is defined in the following way.

$$E_c^{LRDMA}[\gamma(\boldsymbol{r}, \boldsymbol{r}')] := \int d^3R \, \varepsilon_c^{HEG}[\gamma(\boldsymbol{k}, \boldsymbol{R})], \tag{3.17}$$

where E_c^{LRDMA} is the approximate correlation-energy of a nonuniform system and $\gamma(\boldsymbol{k}, \boldsymbol{R})$ describes the Wigner transform of the 1RDM of the nonuniform system under study:

$$\gamma(\boldsymbol{k}, \boldsymbol{R}) = \int d^3s \, \gamma(\boldsymbol{R} + \boldsymbol{s}/2, \boldsymbol{R} - \boldsymbol{s}/2) e^{i\boldsymbol{k}\cdot\boldsymbol{s}}. \tag{3.18}$$

This procedure is similar to the definition of the LDA in SC-DFT [78, 9]. While there are many LDA constructions conceivable that correctly reduce to the homogeneous limit, Eq. (3.17) is the only definition that correctly reproduces the correlation energy of a *weakly inhomogeneous* electron gas [78].

A parametrization of $\varepsilon_c^{HEG}[n(\boldsymbol{k})]$ has not been carried out so far and remains an important task for the future. An extension of the LRDMA fomalism to spin-dependent systems and systems at finite temperature is conceptually straightforward. However, the explicit calculation of the temperature-dependent $\varepsilon_c^{HEG}[n(\boldsymbol{k}), T]$, although in principle possible by means of path integral Monte-Carlo techniques [79], is rather involved, due to the fermionic sign problem [80].

An alternative approach for further theoretical development in RDMFT and FT-RDMFT therefore consists in the derivation of approximate correlation functionals for the HEG and their implementation in a (FT-)LRDMA. We point out that a functional in FT-RDMFT should not only reproduce an accurate eq-free energy but also has to yield a good momentum distribution.

As a first step, we investigated the performance of several of the previously mentioned RDMFT functionals for the calculation of the correlation energy of the HEG. The results are shown in Figure 3.1. The CGA functional [81], which relies on an approximate tensor product expansion of the 2RDM, was derived explicitly to describe the HEG and succeeds to do so for high densities but fails for low ones, including the important range of metallic densities $1 < r_s < 6$. From the functionals mentioned so far, only the α functional is capable of describing the correlation energy over the whole range of densities considerably accurately. Worth mentioning is the fact that the energy of the HEG for the Müller functional can be solved analytically, so long as there are no fully occupied states. It can be shown [82] that this is the case if and only if $r_s > 5.77$.

To make any statements about whether or not a given functional reproduces an accurate momentum distribution, we will have to rely on the results by Gori-Giorgi and Ziesche [55] which we introduced briefly in Section 2.4. Three important properties of the momentum distribution derived from these results are listed in the following list.

(1) Nonzero occupation of all high momentum states [83] which can be understood by the help of the electronic cusp condition [65, 44].

(2) A discontinuity and rather symmetrical behaviour of the momentum distribution at the Fermi level (as also suggested by Landau-Liquid theory).

(3) Depletion of low momentum states.

All functionals mentioned so far succeed in recovering property (1). This is due to the large value of the derivative $\frac{\partial E_{xc}[\gamma]}{\partial n_i}$ for $n_i \to 0$. All but the ML/ML-SIC functionals show a divergence for this derivative which will then lead to a partial occupation of all states. The ML/ML-SIC functionals exhibit only a very big, but finite, derivative. Therefore, states of very high momentum are not to be expected to show partial occupation. When it comes to the description of property (2), only

Figure 3.1: Correlation energy of the three-dimensional electron gas. The black dashed line denotes Monte-Carlo results in the PWCA [52] parametrization. The other labels are explained in Sections 3.1.1 and 3.3. For $r_s > 1$, which includes the metallic density range, the BOW functional shows an unprecedented accuracy.

the BBC and the PNOF functionals recover a discontinuity at the Fermi surface. This is due to the discontinuous change in $f(n_i, n_j)$ when changing from a strongly occupied state to a weakly occupied one. We should like to point out that this discontinuous behaviour is not intrinsically necessary to produce a discontinuous momentum distribution. We have managed to achieve the same feature for model functionals which were partially like the exchange-only functional, but shifted by a constant, i.e. $f^{test}(n_i, n_j) = (n_i n_j + c)$ on an area around the Fermi level. The discontinuity, created by the BBC functionals, shows wrong behaviour when changing r_s. Although expected to decrease with decreasing density, it increases [84]. Furthermore, the behaviour around the Fermi level is not symmetric. Neither does it qualitatively resemble the Monte-Carlo results. Property (3), a qualitatively correct depletion of low momentum states, is not fulfilled by the investigated functionals. Only the BBC1, BBC2 and PNOF functionals show a small decrease of occupation, but not nearly as much as prevalent in the exact momentum distributions.

We believe that the depletion of low momentum states is an important physical effect which must be recovered by an RDMFT functional. Motivated by this credo, we are going to design an appropriate functional in the following section.

3.3 BOW functional

We wish to construct an xc functional which is capable of reproducing both the occupation of high momentum states as well as the depletion of low momentum ones. We will not focus on the discontinuity at the Fermi level and propose it as a task for future studies.

Considering the occupation of high momentum states, we will be guided by the success of the α functional and include a term of $(n_i n_j)^\alpha$ in our functional. To achieve a depletion of low momentum states we then require our functional to have a vanishing derivative for $n_i = n_j = 1$. In this way it is possible to reduce the occupation number of fully occupied orbitals without changing the energy. As the exchange contribution is negative, this excess charge can be used to lower the energy. The variational principle will therefore lead to a groundstate where the orbitals are never fully occupied. A possible choice of functional with vanishing derivative for full occupation could then
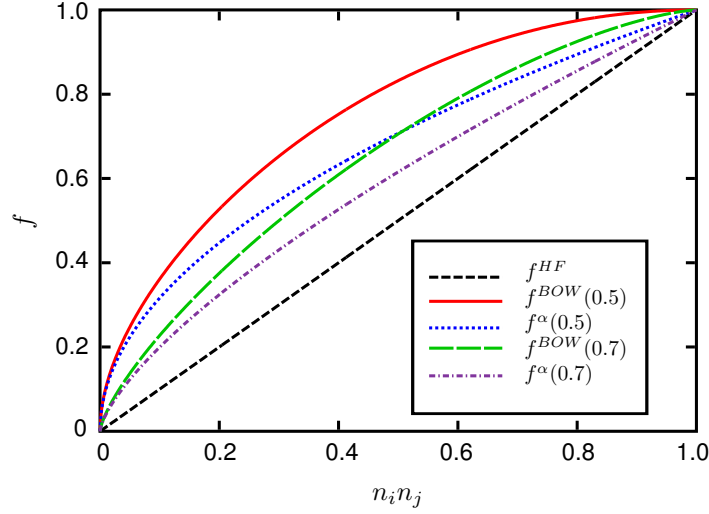
Figure 3.2: Occupation number dependence function f for the BOW and α functionals for different values of the parameter α. The Hartree-Fock function is reproduced by both functionals with $\alpha = 1$.

be $f(n_i, n_j) = ((n_i n_j)^\alpha - \alpha n_i n_j)/(1 - \alpha)$. We found, however, that this choice underestimates the correlation-energy considerably. The partially occupied states are given too much influence on the energy. We therefore introduce a simple counter-term to decrease this effect. It incorporates the inverse of the α functional, leading to our final choice for the xc functional, which we will call BOW functional in the following.

$$E_{xc}^{BOW}[\gamma; \alpha] = -\frac{1}{2} \sum_{ij} f^{BOW}(n_i, n_j; \alpha) \int dx dx' w(x, x') \phi_i^*(x') \phi_i(x) \phi_j^*(x) \phi_j(x') \tag{3.19}$$

$$f^{BOW}(n_i, n_j; \alpha) = (n_i n_j)^\alpha - \alpha n_i n_j + \alpha - \alpha(1 - n_i n_j)^{1/\alpha} \tag{3.20}$$

As a necessary property, the BOW-functional leads to the reproduction of the exchange-only functional for uncorrelated momentum distributions

$$f^{BOW}(n_i, n_j; \alpha)|_{n_i n_j = 0} = 0 \tag{3.21}$$

$$f^{BOW}(n_i, n_j; \alpha)|_{n_i = n_j = 1} = 1. \tag{3.22}$$

Furthermore, we recover the exchange-only functional by choosing $\alpha = 1$, i.e. $f^{BOW}(n_i, n_j; 1) = f^x(n_i, n_j)$. We can now use the parameter α to tune the influence of correlation. We show $f^{BOW}(n_i, n_j; \alpha)$ and the function from the α-functional $f^\alpha(n_i, n_j; \alpha) = (n_i n_j)^\alpha$ for several values of α in Figure 3.2. A decrease in α leads to a bow-like shape which lead to our choice of name. As we show in Figure 3.1, with the right choice of α the BOW functional is capable of describing the correlation energy for $r_s > 1$ very accurately, exceeding the precision of all other functionals. Its performance for higher densities becomes less superb but is still considerably accurate compared to its contestants.

We can now turn to the actual problem we were concerned with in the beginning, namely the description of the gs-momentum distribution. As we can see in Figure 3.3, the BOW functional is successful in describing both occupation of high momentum states as well as depletion of low momentum ones. Because of the success in describing both energy quantitatively as well as momentum distribution qualitatively for the three-dimensional (3D) HEG, we also investigated the performance
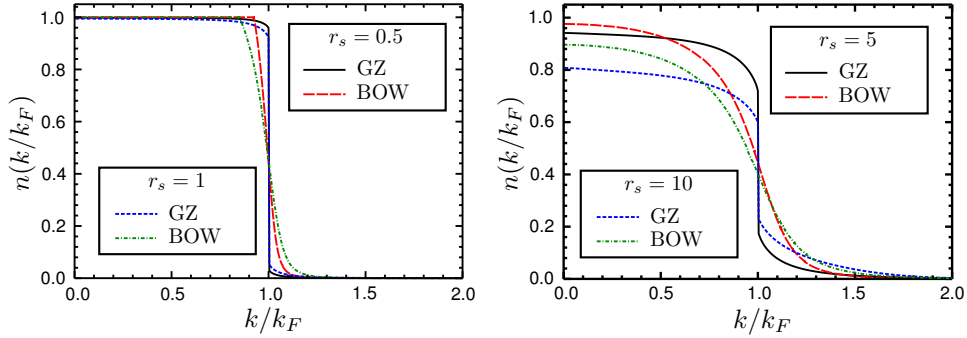
Figure 3.3: Momentum distributions of the HEG for $r_s \in \{0.5, 1, 5, 10\} a.u.$ from the parametrization by Gori-Giorgi and Ziesche (GZ) [55] and from the BOW functional for $\alpha = 0.56$. Low momentum state depletion, high momentum state occupation, and symmetrical behaviour around the Fermi level are reproduced.
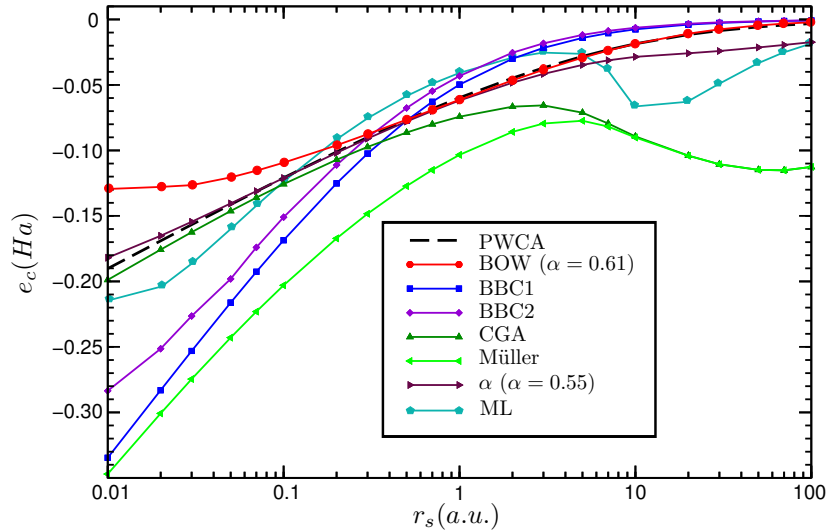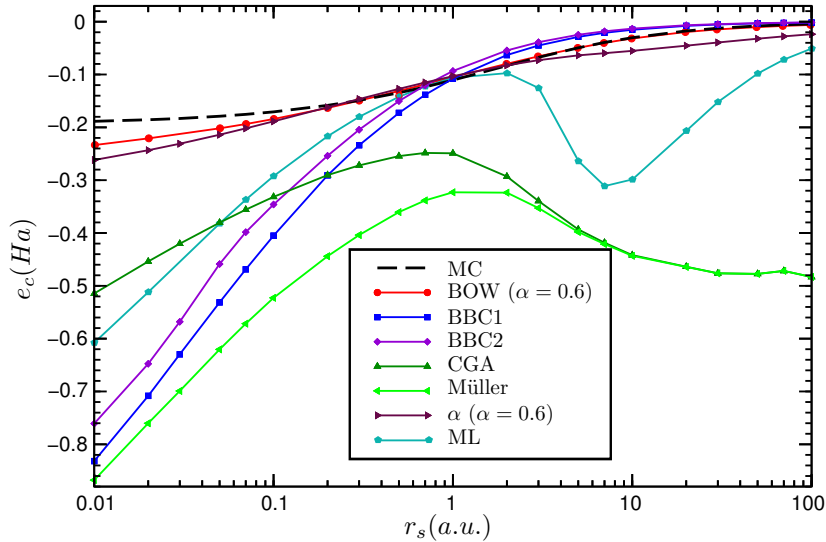

Figure 3.4: Correlation energy of the two-dimensional electron gas. The black dashed line denotes Monte-Carlo results in the Attaccalite [50] parametrization. The other labels are explained in Sections 3.1.1 and 3.3.

of the different functionals for the two-dimensional (2D) HEG. The correlation energies of a 2D-HEG are known from Monte-Carlo calculations and are readily parametrized [50, 51]. We show the results in Figure 3.4. As one can see, also for the 2D-HEG, the BOW functional succeeds in describing the correlation energy over the whole range of densities.

In summary, the BOW functional shows remarkable success in describing the correlation energy of the HEG, both in 3 and 2 dimensions, over a wide range of densities ($0.01 < r_s < 100$), including the range of metallic densities ($1 < r_s < 6$). It, for the first time, manages to qualitatively correctly describe the depletion of low momentum states, an exact property known from Monte-Carlo results. The reproduction of a discontinuity at the Fermi level is a task for the future. To achieve this property, one could follow the idea of the BBC and PNOF functionals to describe states above and below the Fermi energy differently which will then lead to a discontinuity.

3.4   The problem of the description of magnetic systems

As mentioned in the previous section, a formulation of an RDMFT-LDA and an RDMFT-LSDA is theoretically possible but has not been carried out so far. The energy differences between different magnetic phases of the HEG become very close for low densities. Therefore, even in Monte-Carlo calculations, the estimates for the critical Wigner-Seitz radius r_c, where a phase transition between an unpolarized and totally polarized configuration occurs, vary. Ceperley and Alder [48] find $r_c = 75a.u.$ whereas Zhong et al. [85] find $r_s = 50a.u.$. An approximate functional in RDMFT would need to exhibit a very high accuracy to be able to reproduce the phase transition in the HEG, which seems to be a hard problem to solve. However, because physical systems usually show phase transitions for much lower densities, one suspects/hopes that a medium accuracy would suffice. In the following, we should like to elucidate why the use of a functional of the kind of Eq. (3.16) will have severe difficulties to achieve even a mediocre accuracy in describing spin-polarized systems.

When trying to describe spin-polarized systems in collinear configuration, the kinetic, the external potential, and the exchange part can be separated into a sum of contributions from only spin-up and only spin-down NOs and ONs. To describe the xc functional for a spin-polarized system, a common approach in RDMFT is to make the same ansatz of spin-channel seperability,

$$E_{xc}[\gamma] = E_{xc}[\gamma_{\uparrow\uparrow}, \gamma_{\downarrow\downarrow}] = E_{xc}^S[\gamma_{\uparrow\uparrow}] + E_{xc}^S[\gamma_{\downarrow\downarrow}], \tag{3.23}$$

where $\gamma_{\uparrow\uparrow}$ and $\gamma_{\downarrow\downarrow}$ are the diagonal elements of the 1RDM γ from Eq. (2.16) and $E^S[\gamma]$ denotes the separated functional.

We claim that such an approximation is intrinsically incapable of describing both spin-polarized and spin-unpolarized configurations together. The underlying reason for this problem is that a separable functional might describe accurately the correlation contributions, which arise from interactions of the electrons of the same spin (i.e. inner-spin-channel correlation), but will not be able to describe the contribution coming from the correlation of electrons of different spin (i.e. inter-spin-channel correlation). In the following, we will elaborate on this problem by considering a spin-polarized HEG (see Section 2.4). We will again rely on the PWCA[52] parametrization of the polarization-dependent correlation energies.

For a collinear spin configuration, the fundamental quantities are the spin-up density $n_\uparrow$ and the spin-down density $n_\downarrow$ and the energy can be written as $E(n_\uparrow, n_\downarrow)$. If the assumption of spin-cannel seperability is valid, the following two relations would hold:

$$E(n_\uparrow, n_\downarrow) = E(n_\uparrow, 0) + E(0, n_\downarrow) =: E^F \tag{3.24}$$

$$E(n_\uparrow, n_\downarrow) = \frac{1}{2}\left(E(n_\uparrow, n_\uparrow) + E(n_\downarrow, n_\downarrow)\right) =: E^P. \tag{3.25}$$

In Eq. (3.24) the partially polarized system is given as a sum of two fully polarized, i.e. ferromagnetic systems, whereas in Eq. (3.25) one constructs the partially polarized one out of two unpolarized, i.e. paramagnetic systems, hence the notations E^F and E^P.

We can now investigate, if Eqs. (3.24) and (3.25) are valid for the case of a partially polarized HEG by calculating the differences between the exact, i.e. Monte-Carlo, results and the expected results E^F and E^P:

$$\Delta^F = E - E^F \tag{3.26}$$

$$\Delta^P = E - E^P. \tag{3.27}$$

The results are shown in Figure 3.5. As we can see in Figure 3.5.a, Δ^F vanishes by construction for a totally polarized system ($\xi = 1$). Decreasing the polarization then leads to a decrease of Δ^F, i.e. $E < E^F$. Because in E^F the inter-spin-channel correlation is neglected, we deduce that it has to be negative. Considering the paramagnetic case in Figure 3.5.b, we see that again by construction Δ^P vanishes, now for the paramagnetic configuration ($\xi = 0$) and then increases with

3.5.a: Energy differences Δ^F from Eq. (3.26)

3.5.b: Energy differences Δ^P from Eq. (3.27)

3.5.c: Relative energy deviations δ^F from Eq. (3.28)

3.5.d: Relative energy deviations δ^P from Eq. (3.29)
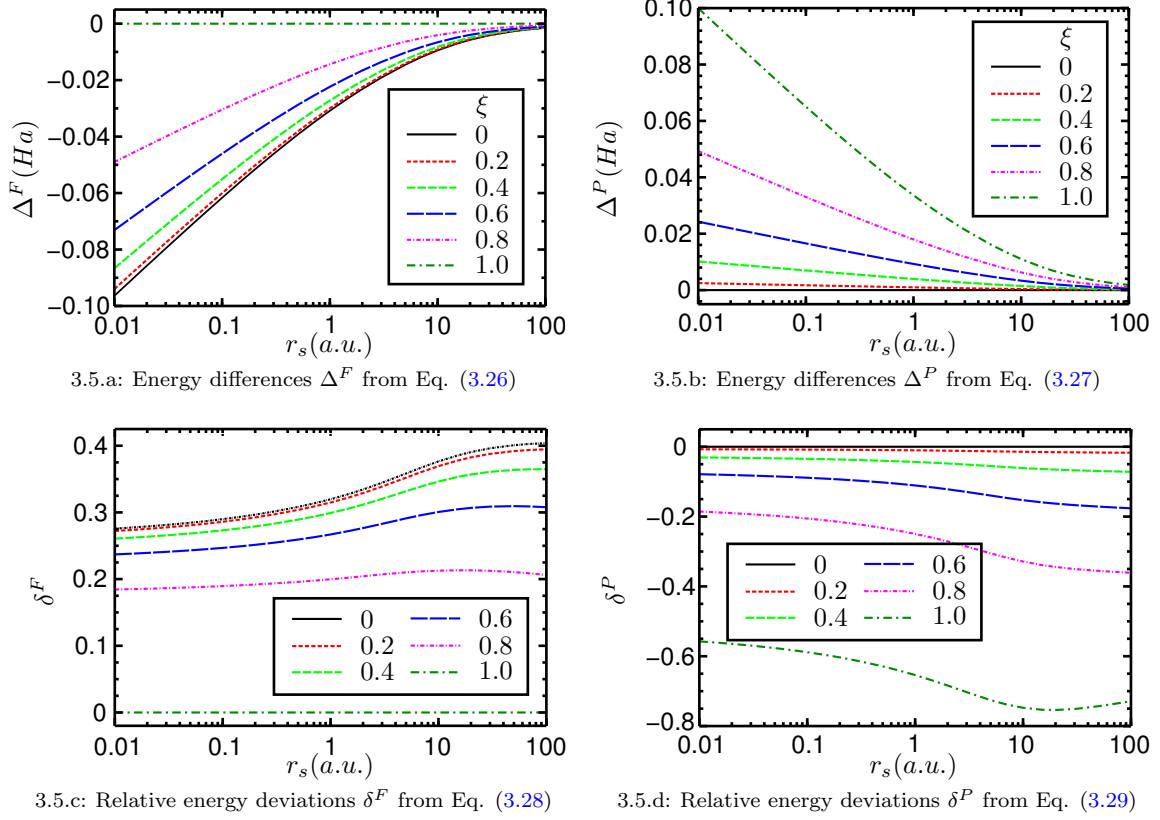
Figure 3.5: Energy difference Δ^F and Δ^P and relative energy fractions δ^F and δ^P as defined in Eqs. (3.26) - (3.29) with respect to r_s for different values of the polarization ξ.

increasing polarization. This can be understood by realizing that E^P basically double counts the inter-spin-channel correlation contribution, leading to $E > E^P$.

In RDMFT, the only correlation contribution comes from the interaction alone. We therefore should like to know how the inter-spin-channel correlation contribution relates to this correlation contribution W_c. We can use the PWCA parametrization of the correlation contributions to the energy to calculate $W_c = E_c - T_c$ and investigate the following two fractions:

$$\delta^F = \frac{\Delta^F}{W_c} \tag{3.28}$$

$$\delta^P = \frac{\Delta^P}{W_c}. \tag{3.29}$$

The results are shown in Figure 3.5. We see that by assuming spin-channel seperability, one will yield errors for the correlation energy of up to 40%. However, a remarkable feature of Figures 3.5.c and 3.5.d is that the relative deviations over the whole range of considered densities vary only slightly. Apparently, both inner- as well as inter-spin-channel correlation are affected in the same way by a change in the density, leading to only a small change in their fraction. This result becomes important at the end of this section, where we model the inner-spin-channel correlation by a term similar to the inter-spin-channel contribution.

The importance of the previous results lies in the following. Let us assume that we found a spin-channel separable functional, which described the polarized (unpolarized) HEG perfectly.

3D											
ξ	0.0	0.1	0.2	0.3	0.4	0.5	0.6	0.7	0.8	0.9	1.0
α	0.56	0.56	0.56	0.57	0.57	0.57	0.58	0.59	0.61	0.63	0.66
BOW	0.61	0.61	0.61	0.62	0.62	0.63	0.63	0.64	0.65	0.67	0.69

2D											
ξ	0.0	0.1	0.2	0.3	0.4	0.5	0.6	0.7	0.8	0.9	1.0
α	0.63	0.63	0.63	0.63	0.64	0.64	0.65	0.66	0.67	0.7	0.74
BOW	0.66	0.66	0.66	0.67	0.67	0.68	0.69	0.71	0.73	0.76	0.80

Table 3.1: Best parameters to describe the correlation energy of a HEG in three and two dimensions in the range $1 < r_s < 100$ for the α and BOW functionals.

Applying this functional now to an unpolarized (polarized) HEG will inevitably yield an error of about 30%-40% in the correlation energy. Most of the previously introduced functionals (Müller, BBC1/2/3,PNOF/0,ML,ML-SIC,CGA) are spin-channel separable and there seems to be no easy way to remedy this problem. The α and BOW functionals, on the other hand, offer a simple way out of the seperability dilemma because they exhibit one parameter. Making this parameter polarization-dependent makes the functional inseparable and offers an easy solution to the problem, given that the functionals also describe the partially polarized systems accurately. We investigated the α and BOW functionals for partially polarized systems and found a good agreement of the correlation energies for the respective best parameters. We show the resulting parameters in Table 3.1. However, although both the α as well as the BOW functional with polarization-dependent parameter describe the correlation energy qualitatively correctly, they fail to predict a phase transition between paramagnetic and ferromagnetic phases. This is due to the fact that a smaller coefficient in the low density limit in both functionals leads to a bigger contribution to the correlation energy and therefore, by reproducing the energy for intermediate densities well, they favour the paramagnetic phase for low density, where the phase transition should occur.

This is a serious backlash because the phase transition is a physical property of considerable interest. Because in Section 8 we want to study the phase diagram of the HEG at finite temperatures, we will now propose a rather phenomenological way to recover the phase transition at zero temperature. From the good agreement of the α as well as of the BOW functional results with the Monte-Carlo results for fully polarized configurations, we deduce that one can, at least to some extent, describe the inner-spin-channel correlation effects by employing the exchange integral. We therefore propose to use a similar approach to include the opposite-spin-channel contributions additionally. Our expression for this "trans-channel interaction energy" (BOW-TIE) modification reads with an explicit mentioning of the spin index

$$E_{xc}^{BOW-TIE}[\gamma] = -\frac{1}{2} \sum_{ij\sigma} f^{BOW}(n_{i\sigma}, n_{j\sigma}; \alpha^P) K(i,j)-$$

$$c \sum_{ij} \left((n_{i\uparrow}n_{j\downarrow})^{\alpha^U} (1 - n_{i\uparrow}n_{j\downarrow})^{\alpha^U} \right) K(i,j). \quad (3.30)$$

$K(i,j)$ represents the exchange integral, corresponding to the NOs ϕ_i and ϕ_j and α^P stand for the best parameter for the description of the fully polarized HEG. The second term in Eq. 3.30 vanishes for a spin-polarized system and contributes increasingly with decreasing polarization. The coefficients α^U and c are fitted to reproduce a critical density closer to the Monte-Carlo result while maintaining the good overall accuracy of the correlation-energy for different spin polarizations. The

	α^P	α^U	c
BOW-TIE	0.70	2.0	0.19

Table 3.2: Optimal parameters for the TIE-version of the BOW xc functional as defined in Eq. (3.30).

resulting parameters are shown in Table 3.2 and lead to an instantaneous phase transition at a critical density of $r_c \approx 28a.u.$.

We should like to emphasize again that we did not deduce this opposite-spin-channel contribution from higher principles but rather postulated it to create a model functional which reproduces the critical density of the HEG more accurately. With a different choice for the inter-spin channel correlation energy, i.e. one which favours partially polarized configurations more strongly, one might be able to get rid of the instantaneous transition between unpolarized and polarized phases and reproduce a qualitatively correct continuous quantum phase transition.

This functional can then later on be used as a model function to study the effect of temperature on the magnetic phase diagram of the HEG.

3.5   Summary and outlook

In this section we gave a short review of the theoretical foundations of RDMFT at zero temperature. We then investigated the performance of several popular xc functionals for the HEG in three and two dimensions. Apart from the accurate description of the gs-energy we laid our focus on the reproduction of the gs-momentum distribution. We found out that most functionals used in actual calculations fail to yield a depletion of low momentum states. We therefore designed a functional, the BOW functional, which is capable of reproducing exactly this feature in a qualitatively correct manner. It also reproduces the gs-energies for $1a.u. < r_s < 100a.u.$ to unprecedented accuracy.

We then turned to the problem of the description of partially polarized systems. We showed that most of the functionals used in actual calculations are intrinsically incapable of describing both the unpolarized as well as the polarized HEG together. We attributed this problem to the property of spin-channel seperability. Motivated by these considerations we proposed two ways to construct explicitly non spin-channel separable functionals. The first one constitutes of making the functional parameter polarization-dependent. This procedure applied to the α and BOW functional succeeded in qualitatively reproducing the gs-energies of the 3D- and 2D-HEG but because of wrong low density behaviour failed to reproduce the magnetic phase transition between unpolarized and polarized configurations. The second procedure introduces an explicit coupling between the diagonal elements of the spin-dependent 1RDM. By choosing appropriate parameters for this interaction, we were able to reproduce the gs-energies accurately including a magnetic phase transition at $r_s \approx 40a.u.$. This functional will later on be used as a testing functional for investigation of the effect of temperature on the free energy phase diagram of the 3D-HEG (see Section 8).

There are several open questions to be dealt with in the future. For example, one should try to modify the BOW functional to reproduce the discontinuity of the momentum distribution at the Fermi surface. Another topic, which is of considerable interest, is the theoretical justification of the postulated coupling between the diagonal elements of the spin-dependent 1RDM. As this effect seems to be able to reproduce the main features of the gs-energy of a partially polarized HEG, it would be desirable to get a more physical than phenomenological understanding of it. Finally, one would have to apply the "not spin-channel separable" functionals to real systems and investigate the magnetic properties of the respective gs-configurations.

4 Finite-temperature RDMFT (FT-RDMFT)

After giving a short review of RDMFT at zero temperature in Section 3, we will now allow the system to exchange particles and energy with its surrounding. We will pursue the goal of laying a solid foundation for the description of quantum systems in grand canonical thermodynamic equilibrium, using the 1RDM as central variable. The resulting theory will be called FT-RDMFT.

It was shortly after the original work by Hohenberg and Kohn [3] that Mermin extended their proofs to grand canonical ensembles. He proved that no two local potentials can yield the same eq-density and therefore paved the way for a finite-temperature version of DFT (FT-DFT). This original formulation of FT-DFT, just like its zero-temperature counterpart, is only valid for densities which are equilibrium-V-representable, i.e. eq-densities corresponding to some external potential $\hat{V}$. In general, it is not known how this set of densities can be characterized, which leads to some mathematical difficulties, for example the problem of defining a functional derivative. It was Lieb [37] who reformulated DFT using the concept of Legendre-transforms, solving several of these conceptual mathematical problems. The same path was followed by Eschrig [86], putting FT-DFT on a solid mathematical footing. Knowing about these stumbling blocks, but without the claim of absolute mathematical rigor, we are going to investigate the theoretical foundations of FT-RDMFT as thoroughly as possible in this section. The outline will be as follows:

Section	Description
4.1	At first, we are going to define the problem we are interested in, namely the description of quantum mechanical system in grand canonical equilibrium. We will then repeat how standard quantum mechanics approaches this problem and investigate properties of functionals of the SDO. We will later be able to translate most of these properties to the functionals in FT-RDMFT.
4.2	We will then state a proof of a Hohenberg-Kohn theorem for quantum systems in grand canonical equilibrium with possibly nonlocal external potential. This allows the formulation of a functional theory employing the 1RDM. We will furthermore extend the domain of the functionals to the whole set of ensemble-N-representable 1RDMs Γ^N.
4.3	To aid further investigations, we will then investigate some mathematical properties of the FT-RDMFT functionals, focussing on convexity and lower semicontinuity.
4.4	Subsequently we will consider the question of equilibrium-V-representability, i.e. the question, how 1RDMs, which come from an equilibrium state, can be characterized. We will find that the set of equilibrium-V-representable 1RDMs Γ^V lies dense in the set of ensemble-N-representable 1RDMs Γ^N, a result which will become considerably important for the remainder of this work.
4.5	Finally, we will investigate how the results from our considerations of grand canonical ensembles translate to the case of microcanonical and canonical ones.

Related publications: [44]

4.1 Physical situation and standard quantum mechanical treatment
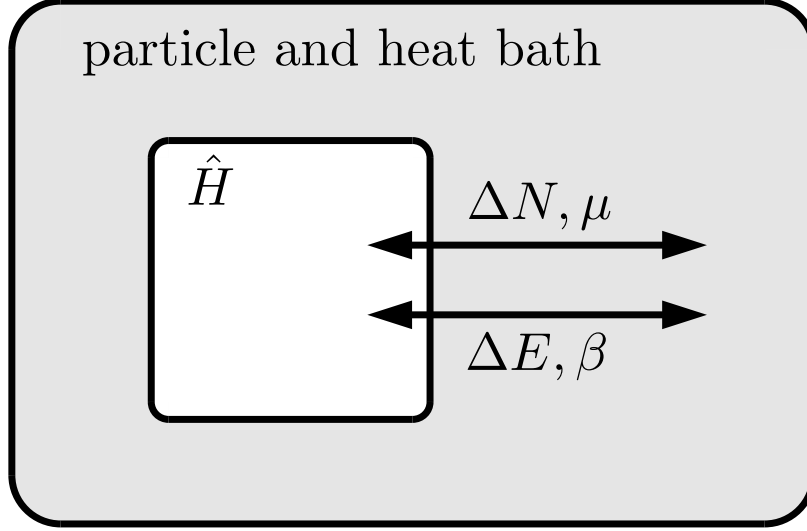
Figure 4.1: Sketch of a grand canonical ensemble. The subsystem, governed by Hamiltonian $\hat{H}$, exchanges energy E and particles N with the surrounding infinite bath. The strength of the couplings to the bath is governed by the two Lagrangian multipliers μ and β.

In contrast to the zero-temperature problem, we will now allow the system to exchange energy and particles with an infinite bath. The exchange of particles then requires an extension of the N-particle Hilbert space to the Fock space $\mathcal{H}$, which is given as the direct sum of symmetrized tensor products of the one-particle Hilbert space h.

$$\mathcal{H} = \bigoplus_{n=0}^{\infty} \hat{S} h^{\otimes n} \tag{4.1}$$

Instead of the energy, the main thermodynamic variable of this system is the grand potential Ω. For a given state $\hat{D}$, the grand potential is given by

$$\Omega[\hat{D}] = \mathrm{Tr}\{\hat{D}(\hat{H} - \mu\hat{N} + 1/\beta \ln \hat{D})\}. \tag{4.2}$$

The Lagrangian parameters μ (the chemical potential) and $1/\beta = k_B T$ (the temperature) describe the couplings to the particle and heat bath. The entropy of the system is then defined as

$$S[\hat{D}] = -\mathrm{Tr}\{\hat{D} \ln \hat{D}\}, \tag{4.3}$$

which, from the definition of $\hat{D}$ in Eq. (2.6), is positive definite. The equilibrium state is now defined as the state which minimizes Eq. (4.2), leading to the finite-temperature variational principle (the Gibbs principle).

$$\Omega[\hat{D}] > \Omega[\hat{D}_{eq}], \quad \text{for all } \hat{D} \neq \hat{D}_{eq} \tag{4.4}$$

It was shown in Ref. [11] that the equilibrium state $\hat{D}_{eq}$ is uniquely given by

$$\hat{D}_{eq} = e^{-\beta(\hat{H} - \mu\hat{N})}/Z_{eq} \tag{4.5}$$

$$Z_{eq} = \mathrm{Tr}\{e^{-\beta(\hat{H} - \mu\hat{N})}\}. \tag{4.6}$$

4.2.a: Convexity   4.2.b: Lower semicontinuity
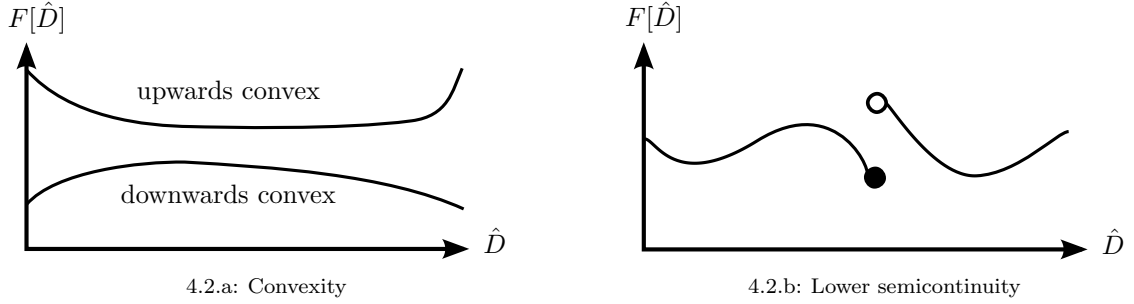
Figure 4.2: Illustration of the concepts of convexity and lower semicontinuity

Z_{eq} is called the partition function and allows a simple representation of the equilibrium grand potential $\Omega_{eq} = \Omega[\hat{D}_{eq}]$.

$$\Omega_{eq} = -1/\beta \ln Z_{eq} \tag{4.7}$$

We will now introduce the set of 1RDMs which come from an eq-state. They will be called equilibrium-V-representable and are defined as the following.

Definition 4.1. [equilibrium-V-representability]
If , for a given 1RDM γ, there exists a potential $\hat{V}$, so that

$$\gamma(x,x') = \mathrm{Tr}\left\{ \frac{e^{-\beta(\hat{T}+\hat{V}+\hat{W})}}{Z} \hat{\Psi}^+(x')\hat{\Psi}(x) \right\}, \tag{4.8}$$

then γ is called equilibrium-V-representable (eq-V-representable). The set of all eq-V-representable 1RDMs is denoted by Γ^V.

$$\Gamma^V = \left\{ \gamma \mid \gamma \ \text{eq-V-representable} \right\} \tag{4.9}$$

The conditions for an arbitrary 1RDM to be eq-V-representable are not known and the only knowledge we have about this set so far is that it is a subset of Γ^N and therefore also of $\mathfrak{T}^{\|\sqrt{N}\|}$ and $\mathfrak{T}$ (see Section 2.3).

$$\Gamma^V \subseteq \Gamma^N \subset \mathfrak{T}^{\|\sqrt{N}\|} \subset \mathfrak{T} \tag{4.10}$$

However, in Section 4.4 we will be able to show that the set Γ^V is dense in the set Γ^N. This means that given any $\gamma \in \Gamma^N$, there is a $\gamma \in \Gamma^V$ arbitrarily close to it (employing the Banach-space norm). This will become crucial for the investigation of properties of the exact functionals in FT-RDMFT (see Section 5) and for the development of a methodology to derive approximate functionals (see Section 6). But before digging into the theoretical treatment of FT-RDMFT, we are going to have a closer look at the properties of $\Omega[\hat{D}]$ and $S[\hat{D}]$ in the following. The reason for this is that, by the virtue of Theorem 4.8, we will be able to translate most of these exact properties to the functionals in FT-RDMFT.

4.1.1 Properties of thermodynamic variables

The two main properties are convexity and lower semicontinuity as defined in the following and illustrated in Figures 4.2.a and 4.2.b.

Definition 4.2. [Convexity]
A functional $\hat{F}[\hat{D}]$ is called upwards (downwards) convex if for all $\hat{D}_1, \hat{D}_2$ and for all $\lambda \in \mathbb{R}$ with $0 \leq \lambda \leq 1$:

$$F[\lambda \hat{D}_1 + (1-\lambda)\hat{D}_2] \leq (\geq)\lambda F[\hat{D}_1] + (1-\lambda)F[\hat{D}_2] \tag{4.11}$$

Definition 4.3. [Lower semicontinuity]
Let $\hat{D}_k$ converge (weakly) to $\hat{D}$. A functional $F[\hat{D}]$ is called (weakly) lower semicontinuous, if

$$F[\hat{D}] \leq \liminf_{k \to \infty} F[\hat{D}_k] \tag{4.12}$$

Because in [FT-RDMFT](#) the equilibrium state will be found by a minimization of a grand potential functional $\Omega[\gamma]$, the convexity property will prove to be very useful. Furthermore, the property of lower semicontinuity (l.s.c.) will become important when dealing with the problem of [eq](#)-V-representability in Section [4.4](#). For an investigation of the convexity and continuity properties of the thermodynamic variables, we are now going to introduce the concept of relative entropy [87, 88]. For two density matrices $\hat{A}$ and $\hat{B}$, the relative entropy is defined as

$$\mathfrak{S}[\hat{A}, \hat{B}] = \text{Tr}\{\hat{A}(\ln \hat{A} - \ln \hat{B})\}. \tag{4.13}$$

$\mathfrak{S}[\hat{A}, \hat{B}]$ can be related to the grand potential of the system, by setting $\hat{A} = \hat{D}$ and $\hat{B} = \hat{D}_{eq}$

$$\mathfrak{S}[\hat{D}, \hat{D}_{eq}] = \beta(\Omega[\hat{D}] - \Omega_{eq}) \tag{4.14}$$

and to the entropy by setting $\hat{A} = \hat{D}$ and $\hat{B} = 1$.

$$\mathfrak{S}[\hat{D}, 1] = -\beta S[\hat{D}] \tag{4.15}$$

The relative entropy $\mathfrak{S}[\hat{A}, \hat{B}]$ was shown to be upwards convex in both arguments [89], i.e. if $\hat{A} = \lambda \hat{A}_1 + (1-\lambda)\hat{A}_2$, $\hat{B} = \lambda \hat{B}_1 + (1-\lambda)\hat{B}_2$, and $0 \leq \lambda \leq 1$, then

$$\mathfrak{S}[\hat{A}, \hat{B}] \leq \lambda \mathfrak{S}[\hat{A}_1, \hat{B}_1] + (1-\lambda)\mathfrak{S}[\hat{A}_2, \hat{B}_2]. \tag{4.16}$$

By using Eqs. (4.14) and (4.15), this property translates directly to $\Omega[\hat{D}]$ and $S[\hat{D}]$.

$$\Omega[\lambda \hat{D}_1 + (1-\lambda)\hat{D}_2] \leq \lambda \Omega[\hat{D}_1] + (1-\lambda)\Omega[\hat{D}_2] \tag{4.17}$$
$$S[\lambda \hat{D}_1 + (1-\lambda)\hat{D}_2] \geq \lambda S[\hat{D}_1] + (1-\lambda)S[\hat{D}_2] \tag{4.18}$$

Because $\hat{A}$ and $\hat{B}$ do not necessarily commute, the following representation of $\mathfrak{S}[\hat{A}, \hat{B}]$ [90] will be useful.

$$\mathfrak{S}[\hat{A}, \hat{B}] = \sup_{\lambda} \left((1/\lambda)\left(S[\lambda\hat{A} + (1-\lambda)\hat{B}] - \lambda S[\hat{A}] - (1-\lambda)S[\hat{B}] \right) \right) \tag{4.19}$$

$\mathfrak{S}[\hat{A}, \hat{B}]$ was shown in [90] to be lower semicontinuous with respect to the trace norm. The requirement of norm convergence can be softened and the modified proof is stated in the following.

Theorem 4.4. [Lower semicontinuity]
Let $\{\hat{A}_k\}$ and $\{\hat{B}_k\}$ be infinite series of density operators. If there are $\hat{A}$ and $\hat{B}$, so that $\text{Tr}\{\hat{P}(\hat{A}_k - \hat{A})\} \to 0$ and $\text{Tr}\{\hat{P}(\hat{B}_k - \hat{B})\} \to 0$, for every finite-dimensional projection operator $\hat{P}$, then

$$\mathfrak{S}[\hat{A}, \hat{B}] \leq \liminf_{k \to \infty} \mathfrak{S}[\hat{A}_k, \hat{B}_k] \tag{4.20}$$

Proof [of Theorem 4.4]
We will use the following two relations.

$$\text{Tr}\{\hat{A}\} = \sup_{\hat{P}} \text{Tr}\{\hat{P}\hat{A}\} \tag{4.21}$$

$$\text{Tr}\{\hat{P}\hat{A}\} \leq \|\hat{P}\|\text{Tr}\{\hat{A}\}, \tag{4.22}$$

where the norm $\|\cdot\|$ is the operator norm. From the conditions $\text{Tr}\{\hat{P}(\hat{A}_k - \hat{A})\} \to 0$ and $\text{Tr}\{\hat{P}(\hat{B}_k - \hat{B})\} \to 0$ it follows that for all $0 \leq \lambda \leq 1$

$$\text{Tr}\{\hat{P}(\lambda\hat{A}_k + (1-\lambda)\hat{B}_k - \lambda\hat{A} - (1-\lambda)\hat{B})\} \to 0. \tag{4.23}$$

Because $\hat{A}_k, \hat{B}_k, \hat{A}$, and $\hat{B}$ have only semipositive eigenvalues and because $x \ln x$ is a continuous, finite function on $[0 : \infty)$, this leads to

$$\text{Tr}\{\hat{P}(\hat{S}[\lambda\hat{A}_k + (1-\lambda)\hat{B}_k)]\} \to \text{Tr}\{\hat{P}(\hat{S}[\lambda\hat{A} + (1-\lambda)\hat{B}])\}. \tag{4.24}$$

Realizing that $\|\hat{P}\| = 1$ and using Eqs. (4.19) and (4.24), one can conclude the proof:

$$\mathfrak{S}[\hat{A}, \hat{B}] = \sup_{\hat{P}, \lambda} \left((1/\lambda)\text{tr}\left\{ \hat{P}\left(\hat{S}[\lambda\hat{A} + (1-\lambda)\hat{B}] - \lambda\hat{S}[\hat{A}] - (1-\lambda)\hat{S}[\hat{B}] \right) \right\} \right) \tag{4.25}$$

$$\leq \liminf_{k \to \infty} \mathfrak{S}[\hat{A}_k, \hat{B}_k]. \tag{4.26}$$

∎

This result can again be related to the grand potential and entropy by setting $\hat{A}_k = \hat{D}_k$ and $\hat{B}_k = \hat{D}_{eq}$ and $\hat{A}_k = \hat{D}_k$ and $\hat{B}_k = 1$ respectively.

Corollary 4.5. *Let $\{D_k\}$ be an infinite series of density operators, so that $\text{Tr}\{\hat{P}(\hat{D}_k - \hat{D})\} \to 0$ for all finite-dimensional projection operators $\hat{P}$. Then*

$$\Omega[\hat{D}] \leq \liminf_{k \to \infty} \Omega[\hat{D}_k] \tag{4.27}$$

$$S[\hat{D}] \geq \liminf_{k \to \infty} S[\hat{D}_k]. \tag{4.28}$$

After reviewing several important concepts from standard quantum mechanics we can now turn to the formulation of a finite-temperature version of RDMFT.

4.2 Mathematical foundation of FT-RDMFT

As mentioned in the introduction, Mermin [11] showed that there is a one-to-one correspondence between the eq-density n_{eq} and the SDO $\hat{D}_{eq}$ for a system with local external potential. Since the diagonal of the 1RDM gives the density ($n(x) = \gamma(x, x)$) it follows that for such systems there is also a one-to-one correspondence between the $\hat{D}_{eq}$ and the equilibrium 1RDM γ_{eq} (see Figure 4.3).

In 1974 Gilbert [26] extended the zero-temperature Hohenberg-Kohn theorems to systems with nonlocal external potential. In these systems, the groundstate is not uniquely determined by the density anymore but by the 1RDM. In the following, we will show that for such a system at finite temperature the 1RDM is still sufficient to describe the equilibrium properties. This will be achieved by showing that the map between $\hat{D}_{eq}$ and $\gamma_{eq}(x, x')$ is invertible which in turn implies the existence of a grand potential functional $\Omega[\gamma]$
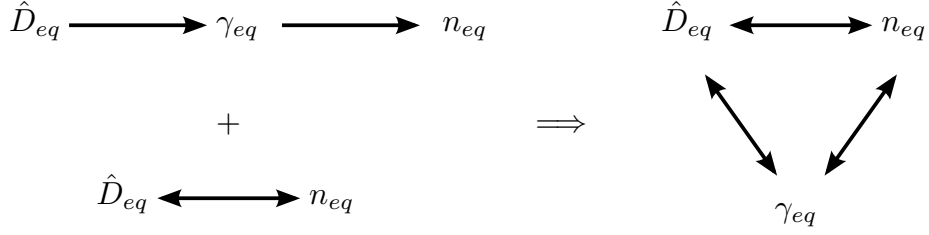
Figure 4.3: The one-to-one map between $\hat{D}$ and n implies the existence of a one-to-one map between $\hat{D}$ and γ.

4.2.1 Existence of grand potential functional $\Omega[\gamma]$

We want to point out that in the subsequent discussion, we explicitly consider only eq-V-representable 1RDMs $\gamma(x, x')$ (see Def. 4.1) which we do not know how to characterize. This lack of knowledge of the constraints on the domain of $\Omega[\gamma]$ might pose a serious problem in the course of numerical minimization. Fortunately, in Section 4.3 we will be able to extend the domain to the full set of Γ^N, which is easy to deal with. The proof of the existence of a one-to-one mapping between the eq-SDO $\hat{D}_{eq}$ (see Eq.(4.5)) and the eq-1RDM (see Eq.(2.12)) can be divided in two parts. First, the one-to-one mapping between $\hat{D}_{eq}$ and the external potential minus the chemical potential $(v_{ext}(x, x') - \mu)$ will be shown, then the one-to-one correspondence between $(v_{ext}(x, x') - \mu)$ and $\gamma_{eq}(x, x')$ is proven.

- $\hat{D}_{eq} \overset{1-1}{\longleftrightarrow} (v_{ext}(x, x') - \mu)$:

Let $\hat{H}$ and $\hat{H}'$ be two different Hamiltonians and assume they lead to the same SDO $\hat{D}$. $\hat{H}'$ shall differ from $\hat{H}$ only by a one-particle potential contribution $\hat{U}$. With Eq. (4.5) this reads

$$e^{-\beta(\hat{H} - \mu\hat{N})}/Z = e^{-\beta(\hat{H} + \hat{U} - \mu\hat{N})}/Z'. \tag{4.29}$$

where Z and Z' are the partition functions (e.g. $Z = \text{Tr}\{e^{-\beta(\hat{H} - \mu\hat{N})}\}$). Solving Eq. (4.29) for $\hat{U}$ yields

$$\hat{U} = \int dx dx' u(x', x)\hat{\psi}^+(x')\hat{\psi}(x) = -\frac{1}{\beta}\ln\frac{Z}{Z'}, \tag{4.30}$$

We now need to show that there is no one-particle potential $u(x, x') \neq 0$ which fulfills this equality, thereby contradicting our initial assumption. To proceed, we assume three different Slater determinants $|X_1\rangle = |1, 0, 0, ...\rangle, |X_2\rangle = |0, 1, 0, ...\rangle$, and $|X_3\rangle = |1, 1, 0, ...\rangle$ in the basis $\{\chi_i\}$. The potential in this basis is denoted by $u_{ij} = \int dx dx' u(x', x)\chi_i^*(x')\chi_j(x)$. Calculating the expectation value of both sides of Eq. (4.30) w.r.t. these three Slater determinants we get the following system of equations

$$-\frac{1}{\beta}\ln\frac{Z}{Z'} = u_{11} = u_{22} = u_{11} + u_{22}, \tag{4.31}$$

which can only be fulfilled by $u_{11} = u_{22} = 0$ and $Z = Z'$. A repetition of this argument for all possible bases then shows that only $\hat{U} = 0$ fulfills Eq. (4.30) which in turn proves the one-to-one correspondence between $\hat{D}_{eq}$ and $(v_{ext}(x, x') - \mu)$. It has to be noted that this proof intrinsically relies on the fact that in the case of grand canonical ensembles we work in a Fock space, i.e. a Hilbert space with varying particle number. If we had restricted ourselves to a canonical situation, i.e. a Hilbert space with fixed particle number, we would have found that the external potential is uniquely determined only up to within an additional constant.

• $(v_{ext}(x, x') - \mu) \overset{1-1}{\longleftrightarrow} \gamma(x, x')$:

In order to prove the one-to-one correspondence between $(v_{ext}(x, x') - \mu)$ and $\gamma_{eq}(x, x')$, we assume that $\hat{H}$ and $\hat{H}'$ differ only in their external potentials. The corresponding grand potentials are given by

$$\Omega[\hat{D}_{eq}] = \text{Tr}\{\hat{D}_{eq}(\hat{H} - \mu\hat{N} + 1/\beta \ln \hat{D}_{eq})\} \tag{4.32}$$

$$\Omega'[\hat{D}'_{eq}] = \text{Tr}\{\hat{D}'_{eq}(\hat{H}' - \mu'\hat{N} + 1/\beta \ln \hat{D}'_{eq})\}, \tag{4.33}$$

where $\hat{D}_{eq}$ and $\hat{D}'_{eq}$ are defined according to Eq. (4.5). The variational principle (Eq. (4.4)) then leads to

$$\Omega[\hat{D}_{eq}] < \Omega[\hat{D}'_{eq}] \tag{4.34}$$

$$= \text{Tr}\{\hat{D}'_{eq}(\hat{H} - \mu\hat{N} + 1/\beta \ln \hat{D}'_{eq})\} \tag{4.35}$$

$$= \Omega'[\hat{D}'_{eq}] + \text{Tr}\{\hat{D}'_{eq}((\hat{H} - \mu\hat{N}) - (\hat{H}' - \mu'\hat{N}))\}. \tag{4.36}$$

Now, by exchanging primed and unprimed objects, one obtains

$$\Omega[\hat{D}_{eq}] < \Omega'[\hat{D}'_{eq}] + \int dx dx' ((v_{ext}(x, x') - \mu) - (v'_{ext}(x, x') - \mu'))\gamma'(x', x) \tag{4.37}$$

$$\Omega'[\hat{D}'_{eq}] < \Omega[\hat{D}_{eq}] + \int dx dx' ((v'_{ext}(x, x') - \mu') - (v_{ext}(x, x') - \mu))\gamma(x', x) \tag{4.38}$$

Adding these two equations leads to the following relation.

$$\int dx dx' ((v'_{ext}(x, x') - \mu') - (v_{ext}(x, x') - \mu))(\gamma(x', x) - \gamma'(x', x)) > 0 \tag{4.39}$$

The existence of two different sets of external and chemical potentials yielding the same eq-1RDM lets the integral in Eq.(4.39) vanish which leads to a contradiction. Hence, the initial assumption is falsified.∎

This proof of the existence of a one-to-one mapping between $\hat{D}_{eq}$ and γ_{eq}, allows us to define the grand potential as a functional of the 1RDM.

$$\Omega[\gamma_{eq}] = \text{Tr}\{\hat{D}[\gamma_{eq}](\hat{H} - \mu\hat{N} + 1/\beta \ln(\hat{D}[\gamma_{eq}]))\} \tag{4.40}$$

In Eq. (4.40) the contributions from the external and the chemical potential can be separated yielding the definition of a universal functional $\mathcal{F}[\gamma_{eq}]$ for FT-RDMFT which then reads

$$\Omega[\gamma_{eq}] = \int dx dx' (v_{ext}(x, x') - \mu)\gamma_{eq}(x, x') + \mathcal{F}[\gamma_{eq}] \tag{4.41}$$

$$\mathcal{F}[\gamma_{eq}] = \text{Tr}\{\hat{D}[\gamma_{eq}](\hat{T} + \hat{W} + 1/\beta \ln \hat{D}[\gamma_{eq}])\}. \tag{4.42}$$

As mentioned before, this functional $\mathcal{F}[\gamma]$ is defined only on the set Γ^V of 1RDMs coming from SDOs of the form of Eq. (4.5), which we do nt know how to characterize. Fortunately, as we will show in the following section, we can extend the domain by using a different formulation for the universal functional.

4.2.2 Lieb formulation of the universal functional

Analoguous to the Lieb-formulation [91, 37] of DFT, we start by restating the variational principle.

$$\Omega_{eq} = \min_{\hat{D} \in \mathfrak{D}^N} \Omega[\hat{D}] \tag{4.43}$$

Because every $\hat{D} \in \mathfrak{D}^N$ yields a 1RDM $\gamma \in \Gamma^N$, we can divide the minimization as follows:

$$\Omega_{eq} = \min_{\gamma \in \Gamma^N} \inf_{\hat{D} \in \mathfrak{D}^N \to \gamma} \Omega[\hat{D}[\gamma]]. \tag{4.44}$$

The infimum in Eq. (4.44) appears because for a 1RDM $\gamma \in \{\Gamma^N \backslash \Gamma^V\}$, i.e. a 1RDM which is not eq-V-representable, it is not clear so far if there exists a minimizing SDO $\hat{D} \to \gamma$. We will come back to this question in Section 4.3.1 and show that there is in fact a minimizing $\hat{D}$ in Eq. (4.44) for all $\gamma \in \Gamma^N$. Therefore, in the following we replace the infimum by a minimum.

We can now separate the external potential part from Eq. (4.44) to get

$$\Omega_{eq} = \min_{\gamma \in \Gamma^N} \left(\mathfrak{F}[\gamma] + \int dx dx' (v_{ext}(x,x') - \mu)\gamma(x',x) \right), \tag{4.45}$$

where the universal functional $\mathfrak{F}[\gamma]$ is defined as

$$\mathfrak{F}[\gamma] = \min_{\hat{D} \in \mathfrak{D}^N \to \gamma} \mathrm{Tr}\{\hat{D}(\hat{T} + \hat{W} + 1/\beta \ln \hat{D})\}. \tag{4.46}$$

The grand potential functional $\Omega[\gamma]$ is then given by

$$\Omega[\gamma] = \mathfrak{F}[\gamma] + \int dx dx' (v_{ext}(x,x') - \mu)\gamma(x',x). \tag{4.47}$$

The equilibrium grand potential is now found by a minimization of the functional $\Omega[\gamma]$:

$$\Omega_{eq} = \min_{\gamma \in \gamma^N} \Omega[\gamma]. \tag{4.48}$$

(The corresonding zero-temperature formulation is also sometimes referred to as the *grand canonical ensemble formulation* [92]).

We would also like to establish an Euler-Lagrange equation for the eq-1RDM γ_{eq} of the following kind.

$$\left. \frac{\delta F[\gamma]}{\delta \gamma(x',x)} \right|_{\gamma_{eq}} + v_{ext}(x,x') = \mu \tag{4.49}$$

However, the question of the existence of a functional derivative of the exact $F[\gamma]$ at the equilibrium 1RDM is not answered so far and is subject to continued studies (also in DFT this question is still under discussion [93]). In an approximate treatment, however, one will most likely define a functional $F^{approx}[\gamma]$ for which the functional derivative exists, justifying the use of the Euler-Lagrange equation in a minimization scheme. Two differences to the case of zero-temperature RDMFT have to be pointed out here. Because at zero temperature, the minimizing 1RDM can be on the boundary of the domain Γ^N (i.e. one can have ONs equal to 0 or 1), the Euler-Lagrange equation does not take the form of Eq. (4.49) but has to incorporate the constraints on the eigenvalues of the 1RDM by further Kuhn-Tucker multipliers [94]. In the case of FT-RDMFT, where the eq-1RDM refers to a grand canonical ensemble, we pointed out in Section 2.3 that there cannot be ONs on the boundary of Γ^N, rendering these additional multipliers unnecessary.

The second, and maybe more important difference, concerns the existence of a Kohn-Sham system. We have seen in Section 3 that because of the cusp condition, there exists no Kohn-Sham system in RDMFT at zero temperature (see Thm. 3.1). In the following section we will show that in FT-RDMFT this drawback disappears and that there exists a noninteracting system which in grand canonical equilibrium reproduces the eq-1RDM of an interacting system. We will also show, how the corresponding Kohn-Sham Hamiltonian can be constructed directly from the ONs and NOs of the interacting 1RDM. This direct construction is a conceptual advantage over DFT, where the Kohn-Sham Hamiltonian had to be found by an inversion of the Kohn-Sham equation which is in general a nontrivial task and has to be done by iterative methods [95].

4.2.3 Kohn-Sham system for FT-RDMFT

To show the existence of a Kohn-Sham system in the context of FT-RDMFT, it is instructive to consider an arbitrary noninteracting system, defined by the one-particle Hamiltonian $\hat{H}_s^{(1)}$ with eigenvalues ε_i and eigenfunctions $\phi_i(x)$.

$$\hat{H}_s^{(1)} = \sum_i \varepsilon_i |\phi_i\rangle\langle\phi_i| \tag{4.50}$$

For a grand canonical ensemble at chemical potential μ, the eq-1RDM is then [96] given by

$$\gamma_{eq}(x, x') = \sum_i n_i \phi_i^*(x')\phi_i(x), \tag{4.51}$$

where the ONs n_i are determined completely by the eigenvalues $\{\varepsilon_i\}$ and the chemical potential μ (we show the explicit derivation in Appendix A.4):

$$n_i = \frac{1}{1 + e^{\beta(\varepsilon_i - \mu)}}. \tag{4.52}$$

This relation can be inverted to give the Kohn-Sham energies in terms of the corresponding ONs and the chemical potential:

$$\varepsilon_i - \mu = \frac{1}{\beta} \ln\left(\frac{1 - n_i}{n_i}\right). \tag{4.53}$$

From Eq.(4.53), it is now possible to construct the Kohn-Sham Hamiltonian from a given 1RDM. Its eigenfunctions are given by the NOs of the 1RDM while the eigenvalues are defined up to a common constant by Eq.(4.53). This is of course just possible, if the 1RDM has no ONs equal to 0 or 1, but as we have pointed out in Section 2.3 and Appendix A.2, this cannot be for an eq-1RDM of a grand canonical ensemble.
Defining the kinetic operator in the basis of NOs ($t_{ij} = \langle\phi_i|\hat{T}|\phi_j\rangle$), the effective one-particle potential $v_{eff}(x, x')$ can be expressed as

$$v_{eff}(x, x') = \sum_{i,j}(\delta_{ij}\varepsilon_i - t_{ij})\phi_i^*(x')\phi_j(x) \tag{4.54}$$

which is generally nonlocal in spatial coordinates. The existence of a Kohn-Sham system now suggests the definition of correlation functionals following the ideas of DFT.

4.2.4 Functionals in FT-RDMFT

In contrast to DFT, in the framework of RDMFT the functionals for the kinetic energy $E_k[\gamma]$, the Hartree energy $E_H[\gamma]$, and the exchange energy $E_x[\gamma]$ of the interacting system are known exactly. For now, we postulate that the functional forms of these contributions stay the same for finite-temperature ensembles. A detailed investigation of the correlation functional in Section 6 will prove this assumption to be valid. Furthermore, the entropy of a noninteracting system with eq-1RDM γ, i.e. the Kohn-Sham entropy $S_0[\gamma]$, is a trivial functional of the ONs of the 1RDM (see Appendix A.4). The grand potential functional is then given by

$$\Omega[\gamma] = \Omega_k[\gamma] + \Omega_{ext}[\gamma] - \mu N[\gamma] - 1/\beta S_0[\gamma] + \Omega_H[\gamma] + \Omega_x[\gamma] + \Omega_c[\gamma], \tag{4.55}$$

where the individual contributions are defined as follows:

$$\Omega_k[\gamma] = \int dx' \lim_{x \to x'} \left(-\frac{\nabla^2}{2} \right) \gamma(x,x') \tag{4.56}$$

$$N[\gamma] = \int dx \gamma(x,x) \tag{4.57}$$

$$\Omega_{ext}[\gamma] = \int dx dx' v_{ext}(x,x') \gamma(x',x) \tag{4.58}$$

$$\Omega_H[\gamma] = \frac{1}{2} \int dx dx' w(x,x') \gamma(x,x) \gamma(x',x') \tag{4.59}$$

$$\Omega_x[\gamma] = -\frac{1}{2} \int dx dx' w(x,x') \gamma(x,x') \gamma(x',x) \tag{4.60}$$

$$S_0[\gamma] = -\sum_i \left(n_i \ln n_i + (1-n_i) \ln(1-n_i) \right). \tag{4.61}$$

The universal functional $F[\gamma]$ can then be written as

$$F[\gamma] = \Omega_k[\gamma] - 1/\beta S_0[\gamma] + \Omega_H[\gamma] + \Omega_x[\gamma] + \Omega_c[\gamma]. \tag{4.62}$$

We can now show that neglecting correlation completely will lead to a grand potential functional whose minimization is equivalent to a solution of the finite-temperature Hartree-Fock (FT-HF) equations.

4.2.5 Finite-temperature Hartree-Fock (FT-HF)

Neglecting $\Omega_c[\gamma]$ in Eq. (4.55) yields the following functional

$$\begin{aligned} \Omega[\gamma] = &\int dx' \lim_{x \to x'} \left(-\frac{\nabla^2}{2} \right) \gamma(x,x') + \int dx v_{ext}(x,x') \gamma(x',x) - \mu \int dx \gamma(x,x) + \\ &\frac{1}{2} \int dx dx' w(x,x') \gamma(x,x) \gamma(x',x') - \frac{1}{2} \int dx dx' w(x,x') \gamma(x,x') \gamma(x',x) + \\ &1/\beta \sum_i (n_i \ln n_i + (1-n_i) \ln(1-n_i)). \end{aligned} \tag{4.63}$$

In equilibrium at finite temperature there will be no pinned states, i.e. no states with ONs equal to 0 or 1. Furthermore, Eq. (4.63) is an explicit functional of the 1RDM. Therefore, the functional derivative w.r.t. the 1RDM exists and at the minimum, the functional fulfills the following Euler-Lagrange equation:

$$\frac{\delta \Omega[\gamma]}{\delta \gamma(x',x)} = 0. \tag{4.64}$$

We will now apply this condition to the correlation-free functional from Eq.(4.63) and project the result on the i-th NO. This will then lead to the FT-HF equations.

$$\begin{aligned} 0 = &\int dx' \phi_i(x') \frac{\delta \Omega[\gamma]}{\delta \gamma(x',x)} \tag{4.65} \\ = &\left(-\frac{\nabla^2}{2} \right) \phi_i(x) + \int dx' v_{ext}(x,x') \phi_i(x') - \int dx' w(x,x') \gamma(x,x') \phi_i(x') + \\ &\left(\int dx' w(x,x') \gamma(x',x') \right) \phi_i(x) - \varepsilon_i \phi_i, \tag{4.66} \end{aligned}$$

where in the last term we used Eq.(4.53). As a first valuable result from our investigation of FT-RDMFT we therefore derived an alternative way to solve the FT-HF equations by a minimization rather than by iterative diagonalization. We will use this fact in Section 8.4 to investigate the temperature dependence of the quasi-particle dispersion relation as well as the magnetic phase diagram for collinear and chiral spin configurations in FT-HF. We will now turn to a more thorough investigation of the mathematical foundations of FT-RDMFT.

4.3 Properties of the universal functional

We showed in Section 4.2.1 that a quantum mechanical system with fixed interaction and with local or nonlocal external potential, which is in grand canonical equilibrium, can be described solely by its 1RDM. Furthermore, we established a one-to-one correspondence between the external potential minus the chemical potential and the 1RDM $((v_{ext}(x,x') - \mu) \longleftrightarrow \gamma(x,x'))$. Therefore, the grand potential can be written as a functional of the 1RDM.

$$\Omega[\gamma] = F[\gamma] + \int dx dx' \gamma(x',x)(v_{ext}(x,x') - \mu) \tag{4.67}$$

4.3.1 Existence of minimum

We are now going to show that we were allowed to replace the infimum from Eq. (4.44) by a minimum in Eq. (4.46). This is important, because it leads to a one-to-one mapping between the ensemble-N-representable 1RDMs and a subset $\mathfrak{D}_L^N$ of $\mathfrak{D}^N$ which allows one to translate several exact properties of the SDO grand potential functional $\Omega[\hat{D}]$ to the corresponding 1RDM-functional $\Omega[\gamma]$.

The corresponding problem in DFT was dealt with for zero-temperature DFT in Refs. [37, 38] with an equivalent outcome. We will follow a very similar path now in the context of FT-RDMFT. We will have to deal with questions of convergence on Banach-spaces. In particular, we need the concept of weak-* convergence and the Banach-Alaoglu theorem, which we restate in the following.

Definition 4.6. [Weak-* convergence]
Let B be a Banach space and B^* its dual space. A series $f_k \in B^*$ is said to be weak- convergent, if for all $x \in B$*

$$\lim_k (f_k(x) - f(x)) \to 0. \tag{4.68}$$

Theorem 4.7. [Banach-Alaoglu theorem]
Let B be a Banach space and B^* its dual space. Let $B^*_{\|1\|}$ be a norm-closed subset of radius 1, i.e.

$$B^*_{\|1\|} = \{f \in B^* | \|f\|_{B^*} \le 1\}. \tag{4.69}$$

Then $B^*_{\|1\|}$ is compact with respect to the weak- topology (see Def. 4.6).*

With these two tools at hand, we will be able to prove the existence of a minimal SDO $\hat{D}$ in Eq. 4.44.

Theorem 4.8. $[(\gamma \in \Gamma^N) \xleftrightarrow{1-1} (\hat{D} \in \mathfrak{D}_L^N \subset \mathfrak{D}^N)]$
For every $\gamma \in \Gamma$, there exists a density operator $\hat{D} \in \mathfrak{D}^N$ with $\hat{D} \to \gamma$, so that

$$F[\gamma] = \mathrm{Tr}\{\hat{D}(\hat{H}_0 + 1/\beta \ln \hat{D})\}, \tag{4.70}$$

i.e. the infimum in Eq. (4.44) is a minimum

Proof of theorem 4.8 Let $\{\hat{D}_k\}$ be a sequence of density operators with $\hat{D}_k \in \mathfrak{D}^N \subset \mathfrak{T}$, so that each $\hat{D}_k \to \gamma$ and

$$\lim_{k \to \infty} \mathrm{Tr}\{\hat{D}_k(\hat{H}_0 + 1/\beta \ln \hat{D}_k)\} = F[\gamma]. \tag{4.71}$$

We will divide the proof in three parts and show

(1) There exists a $\hat{D}$ with $\hat{D}_k \to \hat{D}$ in some sense/topology

(2) This $\hat{D}$ yields γ

(3) $\hat{D}$ fulfills $\mathrm{Tr}\{\hat{D}(\hat{H}_0 + 1/\beta \ln \hat{D})\} = F[\gamma]$.

(1) There exists a $\hat{D}$ with $\hat{D}_k \to \hat{D}$ in some sense/topology:
From Section 2.2 we know that for each density operator the Hilbert-Schmidt norm yields $\|\hat{D}_k\| \leq 1$, i.e. $\hat{D}_k \in \mathfrak{T}^{\|1\|}$. By the virtue of the Banach-Alaoglu theorem 4.7 we know that there is a $\hat{D}$ with $\|\hat{D}\| \leq 1$, so that $\hat{D}_k \overset{*}{\to} \hat{D}$ in the weak-$*$ topology (see Definition 4.6). By definition, $\hat{D}_k$ are trace class operators. The set of trace class operators is the dual of the set of compact operators. The weak-$*$ convergence therefore implies that for all compact operators $\hat{A}$

$$\mathrm{Tr}\{(\hat{D}_k - \hat{D})\hat{A}\} \to 0. \tag{4.72}$$

This implies that each matrix element of $\hat{D}_k$ converges weakly against the corresponding one of $\hat{D}$ which then implies that the eigenvalues of $\hat{D}$ are between 0 and 1.
(2) $\hat{D}$ yields γ:
Although each $\hat{D}_k$ yields the same 1RDM we will now for didactical reasons denote them by γ_k. We now want to use the weak-$*$ convergence of $\hat{D}_k$ to prove the weak convergence of γ_k. Because we chose all $\gamma_k = \gamma$, this would then also imply strong convergence and therefore $\hat{D} \to \gamma$. We denote the 1RDM resulting from $\hat{D}$ by $\overline{\gamma}$. $\overline{\gamma}$ is trace class. The dual of the set of trace class operators are bounded operators. Therefore, $\gamma_k \to \overline{\gamma}$ weakly if and only if for all bounded f

$$\int dx dx' (\gamma_k(x, x') - \overline{\gamma}(x, x')) f(x', x) \to 0. \tag{4.73}$$

To relate the 1RDMs with their corresponding SDOs, we now introduce the following operator.

$$\hat{M}_f = \int dx dx' f(x', x) \hat{\psi}^+(x') \hat{\psi}(x) \tag{4.74}$$

With this help, we can reformulate the requirement from Eq. (4.73) as

$$\mathrm{Tr}\{(\hat{D}_k - \hat{D})\hat{M}_f\} \to 0. \tag{4.75}$$

$\hat{M}_f$, although it originates from a bounded function $f(x, x')$ is not bounded, which is why we cannot just use Eq. (4.72) to proceed. However, we know that each eigenvalue of $\hat{M}_f$ is finite. We now introduce an arbitrary finite-dimensional projection operator $\hat{P}$. Then the product $\hat{M}_f \hat{P}$ is compact again. The left hand side of Eq. (4.75) can therefore be written as

$$\mathrm{Tr}\{(\hat{D}_k - \hat{D})\hat{M}_f \hat{P}\} + \mathrm{Tr}\{(\hat{D}_k - \hat{D})\hat{M}_f(1 - \hat{P})\}. \tag{4.76}$$

Because of Eq.(4.72), we know that for any choice of compact $\hat{P}$, the first part of Eq.(4.76) goes to zero. We now just have to show that we can always choose a $\hat{P}$, so that for every ϵ the second term in Eq. (4.76) will fall below ϵ. This would show weak convergence of γ_k. It is here that our proof differs from the DFT version [37]. This is because γ and f are not diagonal in the same basis, i.e. the spatial one. We will proof that the second term in Eq. (4.76) falls below ϵ by showing that both

terms individually do. We remember that the expectation values of $\text{Tr}\{\hat{D}_k \hat{M}_f\}$ and $\text{Tr}\{\hat{D}\hat{M}_f\}$ are finite by construction. Furthermore, the eigenvalues of $\hat{D}_k$ and $\hat{D}$ are positive. Considering the $\hat{D}_k$ operators, this implies that one can always find an M_0 so that for all $M > M_0$

$$\sum_{i=M+1}^{\infty} w_{k\ i} \langle \psi_{k\ i} | \hat{M}_f | \psi_{k\ i} \rangle < \varepsilon. \tag{4.77}$$

The same argument applies to $\hat{D}$ which then proofs that, given any $\varepsilon > 0$, we can find a M s.t. the right hand side of Eq. (4.76) surpasses ε. To elucidate this statement, we go back to the definition of weak convergence. We want to show that for all ε, there is one K, s.t. for all $k > K$, $|\text{Tr}\{(\hat{D}_k - \hat{D})\hat{M}_f\}| < \varepsilon$. We now choose an ε and K_1. Because of Eq. (4.77) we know that there is an M, s.t. for all $k > K_1$ $\text{Tr}\{(\hat{D}_k - \hat{D})\hat{M}_f(1 - \hat{P}_M)\} < \varepsilon$. We furthermore know from the weak-* convergence of $\hat{D}_k$ that there is also a K_2, s.t. $\text{Tr}\{(\hat{D}_k - \hat{D})\hat{M}_f P_M\} < \varepsilon$ for all $k > K_2$. Then choosing the bigger one of K_1 and K_2 as K yields the proof of weak convergence of $\gamma_k \to \gamma$. And because we chose $\gamma_k = \gamma$ this then finally leads to $\hat{D} \to \gamma$. We have therefore shown that the weak-* convergence implies weak convergence. This is due to the fact that the p-1 norm, or absolute value norm of all $\hat{D} \in \mathfrak{D}^N$ is bounded (it is in fact by construction equal to 1). This is not true for all elements of $\mathfrak{T}^{\|1\|}$ because of which generally weak-* and weak convergence differ.

(3) $\hat{D}$ fulfills $\text{Tr}\{\hat{D}(\hat{H}_0 + 1/\beta \ln \hat{D})\} = F[\gamma]$:

As before, we use that a finite-dimensional projection $\hat{P}$ is compact. Replacing $\hat{A}$ in (4.72) with $\hat{P}$, one gets

$$\text{Tr}\{\hat{P}(\hat{D}_k - \hat{D})\} \to 0. \tag{4.78}$$

Using Corollary 4.5 and Eq. (4.46), one gets

$$\text{Tr}\{\hat{D}(\hat{H}_0 + 1/\beta \ln \hat{D})\} = F[\gamma], \tag{4.79}$$

where the equality sign follows from the definition of $\hat{D}_k$ as the minimizing sequence.

The existence of a minimizing $\hat{D}$ in Eq. (4.44) for all $\gamma \in \Gamma^N$ now simplifies the proof that the functionals $F[\gamma]$ and therefore also $\Omega[\gamma]$ are convex and lower semicontinuous.

4.3.2 Lower semicontinuity

Theorem 4.9. [Semicontinuity of $F[\gamma]$]
Let $\gamma_k, \gamma \in \Gamma^N$ with $\gamma_k \to \gamma$ weakly. Then the following relation holds:

$$F[\gamma] \leq \liminf_{k \to \infty} F[\gamma_k]. \tag{4.80}$$

Proof of theorem 4.9 Because of Theorem 4.8, for each γ_k there exists a $\hat{D}_k$, so that $F[\gamma_k] = \text{Tr}\{\hat{D}_k(\hat{H}_0 + 1/\beta \ln \hat{D}_k)\}$. This defines a sequence $\hat{D}_k$ which by the Banach-Alaoglu theorem converges against a $\hat{D}$ in the weak-* topology. Following the same steps as in the proof of Theorem 4.8 one can show $\hat{D} \to \gamma$ weakly. Again using Eq. (4.27) yields

$$F[\gamma] \leq \text{Tr}\{\hat{D}(\hat{H}_0 + 1/\beta \ln \hat{D})\} \tag{4.81}$$
$$\leq \liminf_{k \to \infty} F[\gamma_k]. \tag{4.82}$$

4.3.3 Convexity

Theorem 4.10. [Convexity of $F[\gamma]$]
Let $\gamma_1, \gamma_2 \in \Gamma^N$ and $0 \leq \lambda \leq 1$, then

$$F[\lambda\gamma_1 + (1-\lambda)\gamma_2] \leq \lambda F[\gamma_1] + (1-\lambda)F[\gamma_2]. \tag{4.83}$$

Proof of theorem 4.10 Because of Theorem 4.8 there exist $\hat{D}_1 \rightarrow \gamma_1$ and $\hat{D}_2 \rightarrow \gamma_2$. Therefore, using Eq. 4.17 and removing the external contribution proves the theorem.

We have thus managed to derive the general properties of convexity and lower semicontinuity of the exact grand potential functional in FT-RDMFT. Convexity is important when one considers a numerical minimization of a functional, lower semicontinuity, on the other hand, will help us in the following section to address the question of eq-V-representability in FT-RDMFT.

4.4 Eq-V-representability

For every potential $\hat{V}$, the eq-SDO $\hat{D}_{eq}$ can be constructed via Eq. (4.5). This density operator then yields an eq-1RDM $\gamma(x, x')$ via Eq. (2.12). Following from Definition 4.1, such an eq-1RDM is called eq-V-representable. This section is now concerned with the question of how the set of all eq-V-representable 1RDMs can be classified. The zero-temperature counterpart in DFT, the question of V-representability, has been dealt with already at early stages of the theoretical development of DFT. It has been proven that the set of V-representable densities coincides with the set of N-representable densities for finite-dimensional state spaces [35], for general quantum lattice systems [97] and for systems with coarse-grained densities [38]. On the other hand, it was shown that the same statement is invalid for general infinite-dimensional spaces [98, 37]. As an illustrative example, Ref. [62] demonstrates how the spaces of N- and V-representable densities differ for a simple model interaction.

It has to be noted that the treatment of this problem is of more than just purely mathematical interest. The assumption of eq-V-representability allows a detailed investigation of properties of the exact correlation functionals in FT-RDMFT (see Section 5) as well as allows the development of a methodology to derive correlation functionals by employing methods from many-body perturbation theory (see Section 6).

Following ideas of Lieb's prolific work [37], we will be able to show that the set of all eq-V-representable 1RDMs Γ^V lies dense in the set of all ensemble-N-representable 1RDMs Γ^N. Therefore, for any given 1RDM γ, there is a eq-V-representable $\bar{\gamma}$ arbitrarily close to it. But to show this, we will have to rephrase the definition of eq-V-representability by the help of the universal functional $F[\gamma]$, as defined in Eq. (4.46). To disencumber notation, we are going to omit the notion of the two spatial coordinates in integrals and arguments of potentials and 1RDMs in the following.

Definition 4.11. [Eq-V-representability II]
If, for a given $\gamma_0 \in \Gamma^N$, there exists a potential v_0, s.t.

$$\inf_{\gamma \in \Gamma^N} \left(F[\gamma] + \int v_0 \gamma \right) = F[\gamma_0] + \int v_0 \gamma_0, \tag{4.84}$$

then γ_0 is called eq-V-representable.

At first glance, it might seem that the existence of a minimum in Eq. (4.84) could be fulfilled easily for all $\gamma_0 \in \Gamma^N$ by setting $v_0 = -\frac{\delta F[\gamma]}{\delta \gamma_0}$. But there is one important problem. The existence of a functional derivative of $F[\gamma]$ on the whole set of Γ^N is not known so far. In fact, the same problem occurs in zero-temperature DFT. Initially, it was claimed [99] that the DFT-universal Lieb-functional $F^{DFT}[\rho]$ is differentiable for all ensemble-V-representable densities and nowhere else. But quite recently, new light was shed on this particular field of subject [93] and it seems that this

statement cannot be uphold without further constraints on the domain of $F^{DFT}[\rho]$. Fortunately, as it will turn out, the question of eq-V-representability in FT-RDMFT can be dealt with also without the use of functional derivatives. To further investigate this question we have to introduce the concept of continuous tangent functionals.

Definition 4.12. *Let F be a real functional on a subset A of a Banach space B and let $\gamma_0 \in A$. A linear functional L on B is said to be a tangent functional (tf) at γ_0 if and only if for all $\gamma \in A$*

$$F[\gamma] \geq F[\gamma_0] - L[\gamma - \gamma_0]. \tag{4.85}$$

If L is furthermore continuous, then it is called a continuous tangent functional (ctf). We can now prove the following important theorem.

Theorem 4.13. *The universal functional $F[\gamma]$ has a unique continuous tangent functional at every eq-V-representable 1RDM and nowhere else.*

Proof [of Theorem 4.13]
• ctf $\Rightarrow$ eq-V:
The proof is done by reductio ad absurdo. Suppose $F[\gamma]$ exhibits a ctf at γ_0, but γ_0 is not eq-V-representable. Denoting the ctf as $\tilde{v}$ it follows:

$$F[\gamma] \geq F[\gamma_0] - \int \tilde{v}(\gamma - \gamma_0) \tag{4.86}$$

$$F[\gamma] + \int \tilde{v}\gamma \geq F[\gamma_0] + \int \tilde{v}\gamma_0 \tag{4.87}$$

$$\inf_{\gamma \in \Gamma^N} \left(F[\gamma] + \int \tilde{v}\gamma \right) \geq F[\gamma_0] + \int \tilde{v}\gamma_0, \tag{4.88}$$

where the equality sign is fulfilled for γ_0. But we assumed in the beginning that γ_0 is not eq-V-representable and therefore the infimum on the left of Eq. (4.88) should never be assumed for any γ. This leads to a contradiction and proves that the existence of a continuous tangent functional at γ_0 implies the eq-V-representability of γ_0.

• eq-V $\Rightarrow$ ctf:
By definition of eq-V-representability (see Eq.(4.84)) we deduce the following relation

$$F[\gamma_0] + \int v_0\gamma_0 = \inf_{\tilde{\gamma} \in \Gamma^N} \left(F[\tilde{\gamma}] + \int v_0\tilde{\gamma} \right) \tag{4.89}$$

$$\leq F[\gamma] + \int v_0\gamma \quad \text{for all } \gamma \tag{4.90}$$

which immediately proves the existence of a continuous tangent functional.

$$F[\gamma] \geq F[\gamma_0] - \int v_0(\gamma - \gamma_0) \tag{4.91}$$

Uniqueness is then proven by assuming the existence of a different ctf $\tilde{v} \neq v_0$. One is then again lead to Eqs. (4.86)-(4.88). But because $\tilde{v} \neq v_0$, Eq. (4.88) will again be violated, proving the uniqueness of the ctf. ∎

Theorem 4.13 transforms the question of eq-V-representability to the question of the existence of a unique ctf. We have shown already in Theorems 4.10 and 4.9 that $F[\gamma]$ is convex and lower semicontinuous and we can therefore use the following theorem.

Theorem 4.14. [Bishop-Phelps theorem]
Let F be a lower semicontinuous convex functional on a real Banach space B. F can take the value $+\infty$, but not everywhere. Suppose $\gamma_0 \in B$ and $v_0 \in B^*$ with $F[\gamma_0] < \infty$. For every $\varepsilon > 0$, there exists $\gamma_\varepsilon \in B$ and $v_\varepsilon \in B^*$ so that

1. $\|v_\varepsilon - v_0\| \leq \varepsilon$

2. v_ε *is ctf to F at γ_ε*

3. $\varepsilon \|\gamma_\varepsilon - \gamma_0\| \leq F[\gamma_0] + \int v_0 \gamma_0 - \inf_{\gamma \in B}\{F[\gamma] + \int v_0 \gamma\}$.

Part 3 of theorem 4.14 makes an assertion about distances between elements in B. We can use this to prove the final theorem of this section

Theorem 4.15. *For any given 1RDM $\gamma \in \Gamma^N$ there exists a sequence $\gamma_k \in \Gamma^N$, so that*

1. $\gamma_k \rightarrow \gamma$

2. *F has a ctf at each γ_k, i.e. each γ_k is eq-V-representable.*

This theorem is equivalent to the statement that Γ^V is dense in Γ^N.

Proof [of Theorem 4.15]
The right hand side of part 3 of Theorem 4.14 is finite and independent of ε. We will denote it by Δ_0.

$$\Delta_0 = F[\gamma_0] + \int v_0 \gamma_0 - \inf_{\gamma \in \Gamma^N}\left\{F[\gamma] + \int v_0 \gamma\right\} \tag{4.92}$$

We now choose a set $\{\varepsilon_k\}$ with $\varepsilon_k = k/\Delta_0$. From Theorem 4.14 we also know that for each of these ε_k we can find a 1RDM γ_k, so that

$$\|\gamma_k - \gamma_0\| \leq \Delta_0/\varepsilon = 1/k. \tag{4.93}$$

Finally part 2 of Theorem 4.14 then ensures eq-V-representability of γ_k. ∎

With this final proof, we have succeeded in laying a firm theoretical basis for FT-RDMFT. As the derivation of our results rested mainly on a few general properties of quantum systems in (grand canonical) equilibrium we will now investigate how these results translate if one considers different ensembles, i.e. microcanonical or canonicl ones.

4.5   Relation to microcanonical and canonical formulations

The main results of this section rely only on the properties of the sets of SDOs and 1RDMs considered, the variational principle, and on the convexity and lower semicontinuity of the SDO-functionals. The fact that one works with a grand canonical ensemble is only required in the investigation of the existence of a Kohn-Sham system. All other results can be translated to the cases of microcanonical and canonical ensembles with an appropriate replacement of the main thermodynamical variables to energy or free energy respectively. One might wonder how the claim that also for microcanonical ensembles Γ^V should be dense in Γ^N is compatible with the statement that there is no Kohn-Sham system in zero-temperature RDMFT. The solution to this apparent contradiction is that our results do not claim that the corresponding potential will not lead to degeneracies in the noninteracting Hamiltonian. If one allows the noninteracting system to be degenerate, then there is a Kohn-Sham system in RDMFT [67].

Because the description of systems in canonical equilibrium will ultimately become important in our investigation of phase transitions of the HEG in Section 8, we will briefly state the required

concepts in the following. The appropriate Hilbert space for the description of canonical ensembles of particle number N is given by the N-particle subspace $\mathcal{H}^N$ of the Fock space $\mathcal{H}$ of Eq. (4.1)

$$\mathcal{H}^N = \hat{S} h^{\otimes N}, \tag{4.94}$$

and the SDOs are weighted sums of projection operators on $\mathcal{H}^N$:

$$\hat{D}^c = \sum_\alpha w_{\alpha N} |\Psi_{\alpha N}\rangle \langle \Psi_{\alpha N}|, \quad w_{\alpha N} \geq 0, \sum_{\alpha,} w_{\alpha N} = 1. \tag{4.95}$$

The variational principle which governs this situation involves the free energy F rather than the grand potential:

$$F[\hat{D}] = \text{Tr}\{\hat{D}(\hat{H} + 1/\beta \ln \hat{D})\}. \tag{4.96}$$

The corresponding eq-SDO is given by

$$\hat{D}^c_{eq} = \frac{e^{-\beta\hat{H}}}{\text{Tr}\{e^{-\beta\hat{H}}\}}, \tag{4.97}$$

where $\hat{H}$ is now the N-particle Hamiltonian of the system. We already see from Eq. (4.97) that the external potential is only defined up to a constant, i.e. there are infinitely many potentials, all yielding the same canonical eq-1RDM. The Lieb-construction now allows to define a canonical universal functional $\mathfrak{F}^c[\gamma]$ on the whole domain of ensemble-N-representable 1RDMs as

$$\mathfrak{F}^c[\gamma] = \inf_{\hat{D} \in \mathcal{H}^N \to \gamma} \text{Tr}\{\hat{D}(\hat{T} + \hat{W} + 1/\beta \ln \hat{D})\}. \tag{4.98}$$

The equilibrium of the system is then found by a minimization of the free energy functional

$$F[\gamma] = \mathfrak{F}^c[\gamma] + V_{ext}[\gamma]. \tag{4.99}$$

So far, the formulation of FT-RDMFT for canonical ensembles follows in the same steps as for grand canonical ones and is equally well founded. As pointed out before, the main difference to the grand canonical ensemble occurs when we investigate the canonical Kohn-Sham system. As in the grand canonical case the NOs of an eq-1RDM of a noninteracting system will be given by the eigenstates of the one-particle Hamiltonian and the ONs will lie in the interior of the set of ensemble N-representable 1RDMs. However, because there is no simple analytic relation between the eigenvalues of the one-particle Hamiltonian and the ONs as in Eq. (4.52), we do not know if every 1RDM with $0 < n_i < 1$ is a canonical eq-1RDM and we can only state that the set of noninteracting canonical eq-1RDMs lies dense in the set of ensemble-N-representable ones. If we know that a given 1RDM corresponds to a noninteracting canonical equilibrium the corresponding potential has to be found by iterative methods similar to [95]. The reason why the construction of the noninteracting Hamiltonian from the canonical eq-1RDM is more complicated than in the grand canonical case lies in the fact that the exponent of the eq-SDO in a canonical ensemble contains only N-particle contributions which will become important in our derivation of a perturbative method to approximate FT-RDMFT-functionals in Section 6.

In general, FT-RDMFT functionals describing either a canonical or a grand canonical equilibrium are different. However, considering the special case of the system being in the thermodynamic limit, the thermodynamic variables, and therefore also the corresponding functionals, of grand canonical and canonical ensembles coincide. We can therefore use a functional for the grand potential $\Omega[\gamma]$ to calculate the free energy

$$F[\gamma] = \Omega[\gamma] + \mu N[\gamma]. \tag{4.100}$$
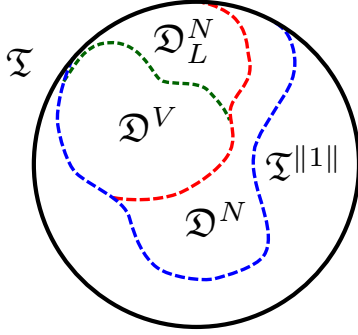
4.4.a: Hierarchy of spaces as defined in Eqs. (2.9),(2.11), and (2.7)
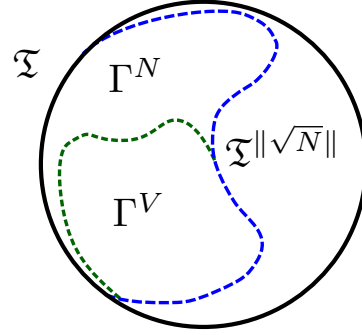
4.4.b: Hierarchy of spaces as defined in Eqs. (2.9),(2.23), and (2.22)

Figure 4.4: Sketch of all relevant spaces of SDOs and 1RDMs and their embedment in a Banach space.

4.6 Summary and outlook

We started this section by giving a definition of the physical system we are interested in, i.e. quantum mechanical systems in grand canonical equilibrium. We then reviewed how standard quantum mechanics approaches this problem, focussing on the description via functionals of SDOs. Subsequently, we derived several properties of these functionals, e.g. convexity and lower semicontinuity. Because employing a SDO in a variational principle is far from being applicable in calculations, we then laid the mathematical foundation for the description of grand canonical ensembles via a functional theory w.r.t. 1RDMs. The corresponding existence-theorem (see Section 4.2.1) justifies this formulation for all eq-V-representable 1RDMs, implying a one-to-one correspondence between Γ^V and $\mathfrak{D}^V$, the set of all eq-V-representable SDOs. However, because it is not known how to characterize Γ^V we then used a formulation of the FT-RDMFT functionals similar to the Lieb construction in DFT. We were then able to show that the Lieb construction leads to an extension of the one-to-one correspondence to Γ^N. I.e. for every $\gamma \in \Gamma^N$, there is a $\hat{D} \in \mathfrak{D}^N$, so that Eq. (4.46) attains its minimum for $\hat{D}$. The set of all $\hat{D}$, corresponding to a γ via Eq. (4.46) is denoted by $\mathfrak{D}_L^N$. In summary, the mappings are as follows

$$\mathfrak{D}^N \xleftrightarrow{\text{many-1}} \Gamma^N \tag{4.101}$$

$$\mathfrak{D}^V \xleftrightarrow{\text{1-1}} \Gamma^V \tag{4.102}$$

$$\mathfrak{D}_L^N \xleftrightarrow{\text{1-1}} \Gamma^N. \tag{4.103}$$

We show a sketch of the several sets defined in this section in Figure 4.4. Subsequently, using the previous results, we were then able to show that the set Γ^V is dense in Γ^N, i.e. given a $\gamma^N \in \Gamma^N$, there is a $\gamma^V \in \Gamma^V$ arbitrarily close to it. This will prove to be important in the investigation of exact properties of the FT-RDMFT functionals in Section 5 as well as for the development of a methodology to derive approximate functionals via methods from FT-MBPT in Section 6. In Figure 4.5 we depict the logical outline of this section, backing up the importance of these mathematical considerations.

Finally, we investigated, how our results, which were orginally derived for grand canonical ensembles, translate to microcanonical and canonical ones. We found that the only difference concerns the existence, i.e. construction of the appropriate Kohn-Sham systems and that the general formulation of a canonical version of FT-RDMFT is theoretically well founded.
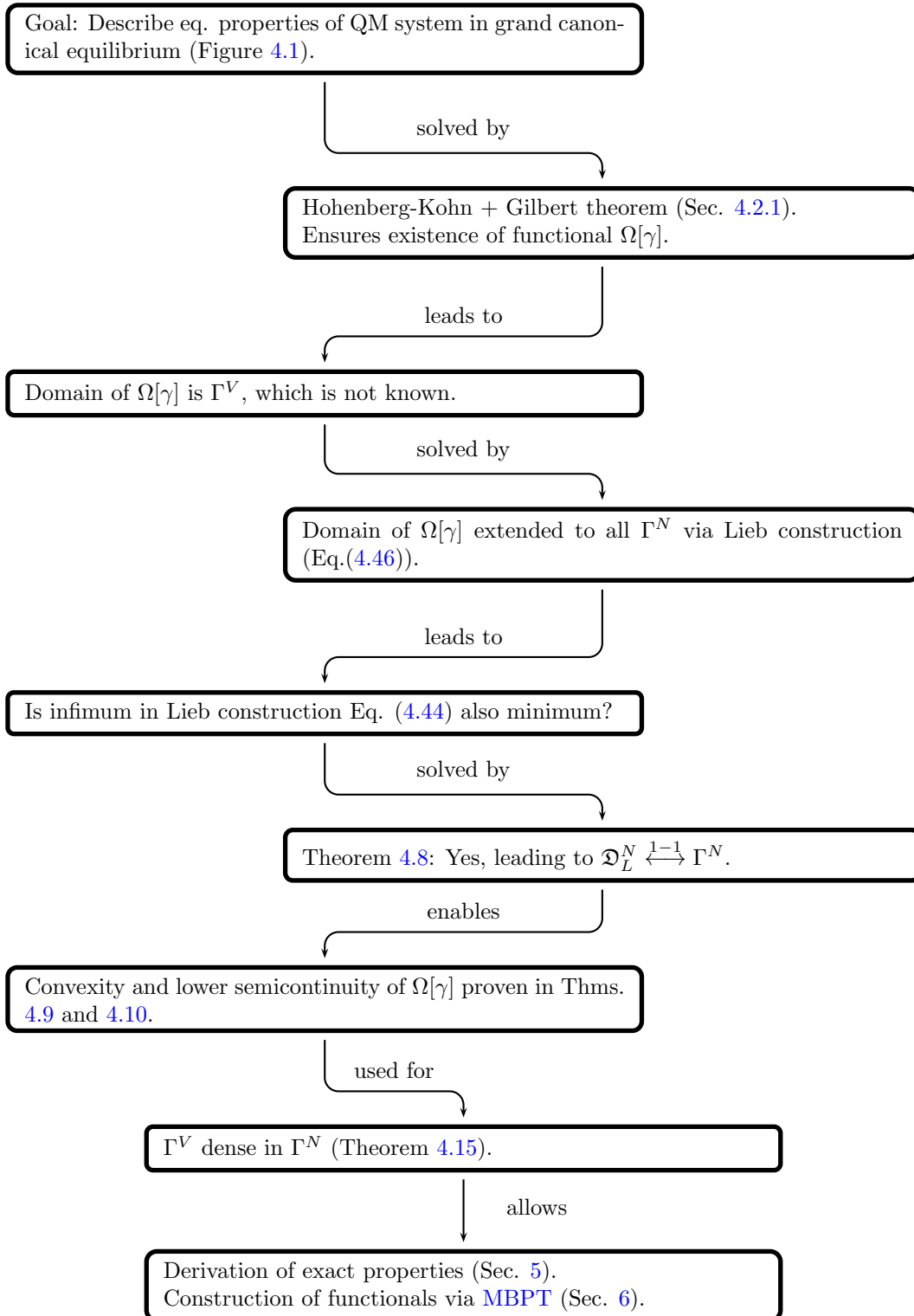
Figure 4.5: Logical outline of Section 4

5 Properties of the exact FT-RDMFT functionals

In the previous section, we laid the foundations for the description of grand canonical ensembles via FT-RDMFT. What remains to be done is the development of correlation functionals. Rather than stumbling through the dark, it will be helpful to know properties of the exact correlation functional which may guide the development of approximations. As a motivating example from DFT, we should like to mention the PBE functional [5] which incorporates exact coordinate scaling relations, leading to an increase in accuracy over a wide range of applications. We are going to structure this section as folows:

Section	Description
5.1	Using the variational principle, we will show that the correlation functionals of the grand potential $\Omega_c[\gamma]$ as well as separately the interaction $W_c[\gamma]$ and entropy $S_c[\gamma]$ are always negative.
5.2	We will then express the correlation grand potential functional $\Omega_c[\gamma]$ through the correlation interaction functional $W_c[\gamma]$ via the method of adiabatic connection.
5.3	Introducing the concept of uniform coordinate scaling, we can then derive several exact relations between the different correlation contributions.
5.4	Finally, we will be able to derive properties of the correlation functionals, linking the behaviour at different temperatures and interaction strengths.

Related publications: [100]

It is worth pointing out that in the derivation of all these exact properties, the concept of eq-V-representability (see Section 4.4) plays a central role. We always assume that a given 1RDM can be seen as an eq-1RDM of a noninteracting as well as of an interacting system. To help the reader distinguish between results and derivations, we chose to put the exact relations in frames in this section. Furthermore, we will use a temperature variable τ, measured in units of k_B: $\tau = 1/\beta$.

5.1 Negativity of the correlation functionals Ω_c, W_c, S_c

As mentioned before, we assume eq-V-representability. Therefore, a given 1RDM can be seen as the eq-1RDM of either an interacting or a noninteracting system with eq-SDOs $\hat{D}_w$ and $\hat{D}_0$. The variational principle Eq. (4.4) then yields

$$\Omega_w[\hat{D}_w] < \Omega_w[\hat{D}_0] \tag{5.1}$$

$$\Omega_0[\hat{D}_0] < \Omega_0[\hat{D}_w], \tag{5.2}$$

where Ω_w, Ω_0 denote the grand potentials of the interacting and noninteracting system respectively. It is now in order to define the correlation contributions to interaction energy $W_c[\gamma]$, entropy $S_c[\gamma]$, and grand potential $\Omega_c[\gamma]$ as

$$W_c[\gamma] = \mathrm{Tr}\{(\hat{D}_w[\gamma] - \hat{D}_0[\gamma])\hat{W}\} \tag{5.3}$$

$$S_c[\gamma] = -\mathrm{Tr}\{\hat{D}_w[\gamma]\ln\hat{D}_w[\gamma]\} + \mathrm{Tr}\{\hat{D}_0[\gamma]\ln\hat{D}_0[\gamma]\} \tag{5.4}$$

$$\Omega_c[\gamma] = W_c[\gamma] - \tau S_c[\gamma]. \tag{5.5}$$

Because $\hat{D}_w[\gamma]$ and $\hat{D}_0[\gamma]$, by construction, both yield the same 1RDM, the respective expectation values of one-particle operators will yield the same result. Therefore, Eqs. (5.1) and (5.2) reduce to

$$\mathrm{Tr}\{\hat{D}_w[\gamma](\hat{W} + \tau\ln\hat{D}_w[\gamma])\} < \mathrm{Tr}\{\hat{D}_0[\gamma](\hat{W} + \tau\ln\hat{D}_0[\gamma])\} \tag{5.6}$$

$$\mathrm{Tr}\{\hat{D}_0[\gamma]\ln\hat{D}_0[\gamma]\} < \mathrm{Tr}\{\hat{D}_w[\gamma]\ln\hat{D}_w[\gamma]\}. \tag{5.7}$$

This can be used to get our first exact relations for the correlation energy, entropy, and grand potential.

$$S_c[\gamma] < 0 \tag{5.8}$$
$$W_c[\gamma] < \tau S_c[\gamma] < 0 \tag{5.9}$$
$$\Omega_c[\gamma] < 0 \tag{5.10}$$

We will now proceed by deriving an adiabatic connection formula between $\Omega_c[\gamma]$ and $W_c[\gamma]$.

5.2 Adiabatic connection formula

We consider a parameter-dependent Hamiltonian of the form

$$\hat{H}^\lambda = \hat{T} + \hat{V}_0 + \lambda \hat{W}. \tag{5.11}$$

For this Hamiltonian, the grand potential functional, as defined in Eq. 4.46, becomes

$$\Omega^\lambda[\gamma] = \min_{\hat{D} \to \gamma} \mathrm{Tr} \left\{ \hat{D} \left(\hat{H}^\lambda - \mu \hat{N} + \tau \ln \hat{D} \right) \right\} \tag{5.12}$$

$$= \min_{\hat{D} \to \gamma} \left(\mathrm{Tr} \left\{ \hat{D} \left(\hat{H}^\lambda + \hat{V}^\lambda[\gamma] - \mu \hat{N} + \tau \ln \hat{D} \right) \right\} - \mathrm{Tr} \left\{ \hat{D} \hat{V}^\lambda[\gamma] \right\} \right). \tag{5.13}$$

$\hat{V}^\lambda[\gamma]$ is chosen so that the eq-1RDM of $\hat{H}^\lambda + \hat{V}^\lambda[\gamma]$ is γ for each λ. Because $\hat{V}^\lambda[\gamma]$ is a one-particle operator, the last term in Eq. 5.14 can be taken out of the minimization. The minimizing SDO is then given by the equilibrium operator $\hat{D}^\lambda[\gamma] = e^{-\beta(\hat{H}^\lambda + \hat{V}^\lambda[\gamma] - \mu \hat{N})}/Z^\lambda$ and the grand potential functional becomes

$$\Omega^\lambda[\gamma] = \mathrm{Tr} \left\{ \hat{D}^\lambda[\gamma] \left(\hat{H}^\lambda + \hat{V}^\lambda[\gamma] - \mu \hat{N} + \tau \ln \hat{D}^\lambda[\gamma] \right) \right\} - \mathrm{Tr} \left\{ \hat{D}[\gamma] \hat{V}^\lambda[\gamma] \right\}. \tag{5.14}$$

$\hat{D}[\gamma]$ can be chosen to be any SDO yielding γ, i.e. also a λ-independent one. For each λ, the first term on the right hand side of Eq. (5.14) describes a system in equilibrium with 1RDM γ. Taking the derivative with respect to λ therefore does not yield a contribution from the derivatives of the SDO $\hat{D}^\lambda[\gamma]$ and the total derivative of the grand potential functional $\Omega^\lambda[\gamma]$ w.r.t. λ becomes

$$\frac{d\Omega^\lambda[\gamma]}{d\lambda} = \mathrm{Tr} \left\{ \hat{D}^\lambda[\gamma] \left(\hat{W} + \frac{d}{d\lambda} \hat{V}^\lambda[\gamma] \right) \right\} - \frac{d}{d\lambda} \mathrm{Tr} \left\{ \hat{D}[\gamma] \hat{V}^\lambda[\gamma] \right\}. \tag{5.15}$$

Again using the one-particle character of $\hat{V}^\lambda[\gamma]$ and integrating Eq. (5.15) yields

$$\Omega[\gamma] = \Omega^0[\gamma] + \int_0^1 d\lambda \, \mathrm{Tr} \left\{ \hat{D}^\lambda[\gamma] \hat{W} \right\} \tag{5.16}$$

The Hartree and exchange functionals (Eqs. (4.59) and (4.60)) separately fulfill this equation and are substracted. This then leads to

$$\Omega_c[\gamma] = \int_0^1 \frac{d\lambda}{\lambda} W_c^\lambda[\gamma], \tag{5.17}$$

where $W_c^\lambda[\gamma] = \mathrm{Tr}\{(\hat{D}^\lambda[\gamma] - \hat{D}^0[\gamma])\lambda \hat{W}\}$. The correlation grand potential therefore can be interpreted as a coupling constant average over the correlation interaction energy, i.e. over the interaction energy difference between a noninteracting and an interacting ensemble. It is interesting to note a similarity between DFT and FT-RDMFT at this point. In DFT, the method of adiabatic connection expresses
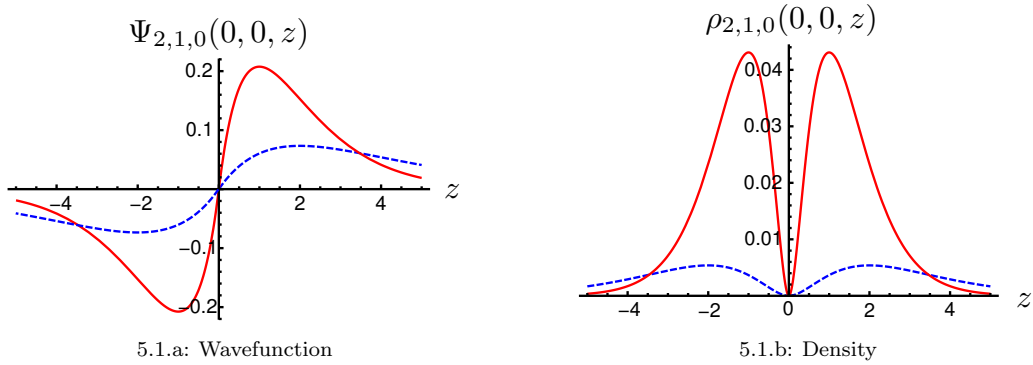
5.1.a: Wavefunction

5.1.b: Density

Figure 5.1: Hydrogen wavefunctions $\Psi_{n,l,m}(x,y,z)$ and densities $\rho_{n,l,m}(x,y,z)$ for $n=2, l=1, m=0$ on the z-axis. The blue dashed graphs denote the unscaled functions whereas the red graphs follow from a a uniform coordinate scaling by a factor of 2 according to Eq. (5.19).

the correlation energy $E_c[n]$ through $W_c[n]$. The kinetic correlation contribution $T_c[n] = T^1[n] - T^0[n]$ is therefore completely taken care of by the coupling constant integration. In FT-RDMFT, where there is no kinetic correlation contribution, the coupling constant integration manages to take care of the entropic correlation contribution $S_c[\gamma] = S^1[\gamma] - S^0[\gamma]$. It seems surprising that both kinetic as well as entropic contributions, which are naïvely expected to be very different in nature, are dealt with equivalently in the different frameworks of DFT and FT-RDMFT.

Employing the method of uniform coordinate scaling, we can now proceed to derive several further exact properties of the different contributions to the exact functional in FT-RDMFT.

5.3   Uniform coordiante scaling

The method of uniform coordinate scaling proved to be a valuable tool in the derivation of exact properties of the functionals in zero-temperature DFT as well as FT-DFT. In DFT, it was successfully used to derive several scaling inequalities of the correlation functionals [40] as well as for determining bounds for the xc functional [41]. Some of the exact uniform scaling relations were later incorporated into the famous PBE functional [5]. Furthermore, as we will demonstrate in Section 5.4, one can make a connection between coordinate scaling and a combined coupling constant and temperature scaling. The TD-DFT equivalent was exploited in Ref. [42] to determine the correlation energy of the HEG from the frequency-dependent exchange-correlation kernel to assess the quality of several approximations for the kernel. The method of uniform coordinate scaling is not restriced to a specific form of the SDO, describing the quantum mechanical state, and can therefore also be used to derive exact properties of the exact functionals in FT-DFT [43]. This situation however, compared to FT-RDMFT, is complicated by the fact that the correlation functional in FT-DFT consists of three different contributions, kinetic, interaction, and entropic, whereas in FT-RDMFT the kinetic part is treated exactly. We might therefore claim that in this particular aspect FT-RDMFT is advantageous compared to FT-DFT, because it allows a more detailed investigation of exact properties via uniform coordinate scaling.

To introduce the concept of coordinate scaling, we consider an arbitrary element $|\psi\rangle$ of the Hilbert space under consideration. Its spatial representation is given by $\psi(r_1, ..., r_N) = \langle r_1, ..., r_N | \psi \rangle$. One now introduces a transformation $\hat{U}(\lambda)$, so that

$$\psi_\lambda(r_1, ..., r_N) := \langle r_1, ..., r_N | \hat{U}(\lambda) | \psi \rangle \tag{5.18}$$

$$= \lambda^{3N/2} \psi(\lambda r_1, ..., \lambda r_N). \tag{5.19}$$

We illustrate the effect of scaling in Figure 5.1. It then seems natural to define a "scaled" operator

$\hat{O}_\lambda = \hat{U}(\lambda)\hat{O}\hat{U}(1/\lambda)$. For this operator it follows that

$$\langle\psi_\lambda|\hat{O}_\lambda|\psi_\lambda\rangle = \langle\psi|\hat{O}|\psi\rangle. \tag{5.20}$$

The scaled operators for kinetic energy, particle interaction, and particle number can be simply related to their unscaled counterparts:

$$\hat{T}_\lambda = \frac{1}{\lambda^2}\hat{T} \tag{5.21}$$

$$\hat{W}_\lambda = \frac{1}{\lambda}\hat{W} \tag{5.22}$$

$$\hat{N}_\lambda = \hat{N}. \tag{5.23}$$

We would now like to know, how the exact 1RDM functionals in FT-RDMFT behave under scaling of the 1RDM. From the explicit forms of $\Omega_k[\gamma], \Omega_H[\gamma], \Omega_x[\gamma]$, and $S_0[\gamma]$ (Eqs. (4.56) - (4.61)) one can immediately deduce

$$T[\gamma_\lambda] = \lambda^2\Omega_k[\gamma] \tag{5.24}$$

$$\Omega_H[\gamma_\lambda] = \lambda\Omega_H[\gamma] \tag{5.25}$$

$$\Omega_x[\gamma_\lambda] = \lambda\Omega_x[\gamma] \tag{5.26}$$

$$S_0[\gamma_\lambda] = S_0[\gamma]. \tag{5.27}$$

$W_c[\gamma], S_c[\gamma]$ and $\Omega_c[\gamma]$ are not known explicitly, but we can derive exact relations for their behaviour under coordinate scaling. We will use the fact that a scaled SDO $\hat{D}_\lambda[\gamma]$ leads to a scaled 1RDM γ_λ. This can be recast in the more convenient form

$$\hat{D}_{\frac{1}{\lambda}}[\gamma_\lambda] \to \gamma. \tag{5.28}$$

$\hat{D}_{\frac{1}{\lambda}}[\gamma_\lambda]$ now decribes a system with interaction $\hat{W}_{\frac{1}{\lambda}}$. We can again use the variational principle to get

$$\mathrm{Tr}\{\hat{D}[\gamma](\hat{W} + \tau \ln \hat{D}[\gamma])\} \leq \mathrm{Tr}\{\hat{D}_{\frac{1}{\lambda}}[\gamma_\lambda](\hat{W} + \tau \ln \hat{D}_{\frac{1}{\lambda}}[\gamma_\lambda])\} \tag{5.29}$$

$$\mathrm{Tr}\{\hat{D}_{\frac{1}{\lambda}}[\gamma_\lambda](\hat{W}_{\frac{1}{\lambda}} + \tau \ln \hat{D}_{\frac{1}{\lambda}}[\gamma_\lambda])\} \leq \mathrm{Tr}\{\hat{D}[\gamma](\hat{W}_{\frac{1}{\lambda}} + \tau \ln \hat{D}[\gamma])\}. \tag{5.30}$$

With the help of Eqs. (5.22) and using the scaling behaviour of Ω_H, Ω_x, and S_0, this can be written as

$$W_c[\gamma] - \tau S_c[\gamma] \leq \frac{1}{\lambda}W_c[\gamma_\lambda] - \tau S_c[\gamma_\lambda] \tag{5.31}$$

$$W_c[\gamma_\lambda] - \tau S_c[\gamma_\lambda] \leq \lambda W_c[\gamma] - \tau S_c[\gamma], \tag{5.32}$$

which directly yields the following relation.

$$\lambda(\tau S_c[\gamma_\lambda] - \tau S_c[\gamma]) < W_c[\gamma_\lambda] - \lambda W_c[\gamma] < \tau S_c[\gamma_\lambda] - \tau S_c[\gamma] \tag{5.33}$$

Eqs.(5.31),(5.32), and (5.33) now allow us to find exact relations for the correlation functionals.

$$\boxed{(\lambda - 1)\tau S_c[\gamma_\lambda] \leq \Omega_c[\gamma_\lambda] - \lambda\Omega_c[\gamma] \leq (\lambda - 1)\tau S_c[\gamma]} \tag{5.34}$$

$$\boxed{\begin{aligned}(1 - \lambda)(W_c[\gamma_\lambda] - \lambda W_c[\gamma]) &\geq 0 \\ (1 - \lambda)(S_c[\gamma_\lambda] - S_c[\gamma]) &\geq 0\end{aligned}} \tag{5.35}$$
$$\tag{5.36}$$

From Eq. (5.35) it follows that $W_c[\gamma_\lambda] > \lambda W_c[\gamma]$ for $\lambda < 1$. Because $W_c < \tau S_c$ (Eq. (5.9)) this implies

$$W_c[\gamma_\lambda] \xrightarrow{\lambda \to 0} 0 \tag{5.37}$$

$$S_c[\gamma_\lambda] \xrightarrow{\lambda \to 0} 0 \tag{5.38}$$

$$\Omega_c[\gamma_\lambda] \xrightarrow{\lambda \to 0} 0. \tag{5.39}$$

The correlation contributions vanish in the limit $\lambda \to 0$. We can now derive differential equations, relating the different correlation functionals. It will be instructive to use the variational principle in a different form.

$$0 = \frac{d}{d\lambda} \left(\Omega[\hat{D}_{\frac{1}{\lambda}}[\gamma_\lambda]] \right)\Big|_{\lambda=1} \tag{5.40}$$

As usual, getting rid of the one-particle operators, we obtain

$$0 = \frac{d}{d\lambda} \operatorname{Tr} \left\{ \hat{D}_{\frac{1}{\lambda}}[\gamma_\lambda] \left(\frac{1}{\lambda}\hat{W}_{\frac{1}{\lambda}} + \tau \ln(\hat{D}_{\frac{1}{\lambda}}[\gamma_\lambda]) \right) \right\}\Big|_{\lambda=1} \tag{5.41}$$

which gives the following differential equation:

$$W[\gamma] = \frac{d}{d\lambda} \left(W[\gamma_\lambda] - \tau S[\gamma_\lambda] \right)|_{\lambda=1}. \tag{5.42}$$

Ω_H, Ω_x, and S_0 fulfill this equation separately and can be substracted. Applying the remaining correlation functionals to γ_ν and consecutively renaming $\nu \to \lambda$ yields

$$W_c[\gamma_\lambda] = \lambda \frac{d}{d\lambda} \Omega_c[\gamma_\lambda]. \tag{5.43}$$

Because $\Omega_c[\gamma_\lambda]$ vanishes in the limit $\lambda \to 0$ (Eq.(5.39)) the solution of Eq.(5.43) is given by

$$\Omega_c[\gamma_\lambda] = \int_0^\lambda \frac{d\mu}{\mu} W_c[\gamma_\mu]. \tag{5.44}$$

From Eq. (5.5) we can furthermore derive

$$S_c[\gamma_\lambda] = \lambda^2 \left(\frac{\partial}{\partial\lambda} \frac{1}{\lambda} \Omega_c[\gamma_\lambda] \right) \tag{5.45}$$

which can be used to finally relate $W_c[\gamma_\lambda]$ and $S_c[\gamma_\lambda]$.

$$\frac{d}{d\lambda} \tau S_c[\gamma_\lambda] = \lambda \frac{d}{d\lambda} \left(\frac{1}{\lambda} W_c[\gamma_\lambda] \right). \tag{5.46}$$

From Eq. (5.43) we see that $\Omega_c[\gamma]$ is monotonically decreasing with λ. We can show that this is also true for $W_c[\gamma]$ and $S_c[\gamma]$. For this purpose we expand the functionals in Eqs. (5.35) and (5.36) around $\lambda = 1$. We then replace $\gamma \to \gamma_\mu$ and subsequently substitute $\lambda\mu \to \lambda$.

$$\frac{d}{d\lambda} \Omega_c[\gamma_\lambda] = \frac{1}{\lambda} W_c[\gamma_\lambda] < 0 \tag{5.47}$$

$$\frac{d}{d\lambda} W_c[\gamma_\lambda] < \frac{d}{d\lambda} \Omega_c[\gamma_\lambda] < 0 \tag{5.48}$$

$$\frac{d}{d\lambda} S_c[\gamma_\lambda] < 0 \tag{5.49}$$
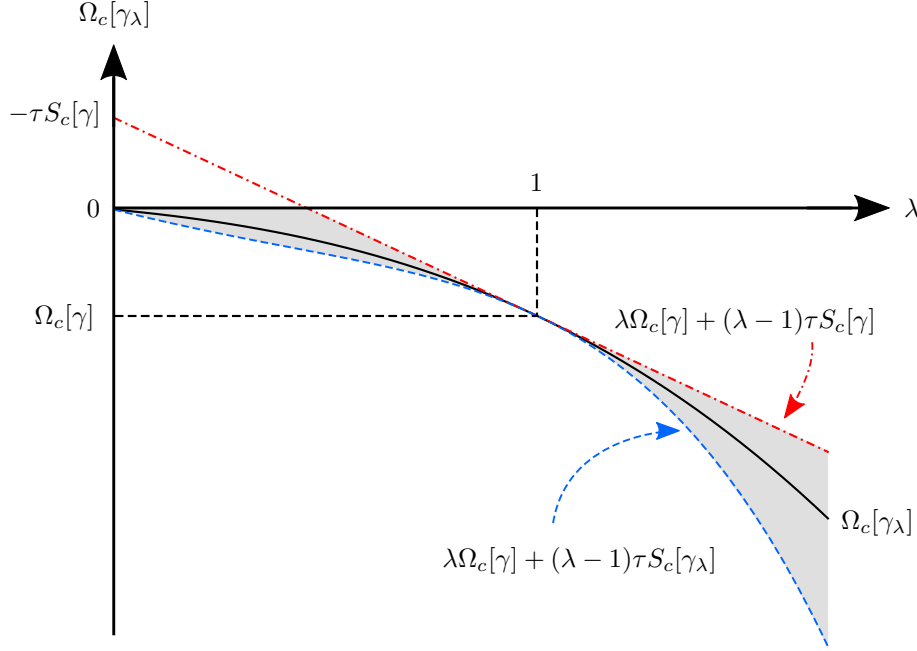
Figure 5.2: Given an approximation for $\Omega_c[\gamma]$, one can test if $\Omega_c[\gamma_\lambda]$ fulfills the exact conditions derived so far. Both its first and second derivatives w.r.t λ have to be negative (Eqs. (5.47) and (5.51)). Furthermore, it has to lie in the allowed (grey shaded) area, defined by the relations in Eq. (5.34) and the negativity constraint (5.10). $S_c[\gamma_\lambda]$ is to be derived from Eq. (5.45).

Finally, we can also prove negativity of the second derivative of $\Omega_c[\gamma_\lambda]$ with respect to λ by differentiating Eq. (5.47) and using Eq. (5.48).

$$\frac{d^2}{d\lambda^2}\Omega_c[\gamma_\lambda] = -\frac{1}{\lambda^2}W_c[\gamma_\lambda] + \frac{1}{\lambda}\frac{d}{d\lambda}W_c[\gamma_\lambda] < -\frac{1}{\lambda^2}W_c[\gamma_\lambda] + \frac{1}{\lambda}\frac{d}{d\lambda}\Omega_c[\gamma_\lambda] \tag{5.50}$$

$$\boxed{\frac{d^2}{d\lambda^2}\Omega_c[\gamma_\lambda] < 0} \tag{5.51}$$

To give a more descriptive representation of the relations, derived so far, we sketch the behaviour of a model-functional in Figure 5.2.

We will now have a closer look at Eq. (5.44). It looks very similar to our adiabatic connection formula in Eq. (5.17). To further investigate this similarity, we will show in the following section that a coordinate scaling is equivalent to an appropriate scaling of the temperature as well as of the interaction strength of the system.

5.4   Temperature and interaction scaling

Because we will now work with systems at different temperatures and interaction strengths, we will include these parameters as arguments. The scaled equilibrium SDO for a system at temperature $\tau = 1/\beta$ and interaction strength w is then given by

$$\hat{D}_\lambda(\tau, w)[\gamma] = e^{-\beta(\hat{T}/\lambda^2 + \hat{V}_\lambda[\gamma] + \hat{W}/\lambda - \mu\hat{N})}/Z_\lambda. \tag{5.52}$$

One knows that $\hat{D}_\lambda[\gamma]$ yields γ_λ and can therefore deduce

$$\hat{D}_\lambda(\tau, w)[\gamma] = \hat{D}(\lambda^2\tau, \lambda w)[\gamma_\lambda]. \tag{5.53}$$

With this relation and the scaling relations from Eqs. (5.21),(5.22), and (5.23) we can show that all contributions to the grand potential functional show the same behaviour under scaling. They acquire a prefactor of λ^2 while the temperature is scaled by $1/\lambda^2$ and the interaction strength by $1/\lambda$. This reads for the correlation functionals as

$$W_c(\tau, w)[\gamma_\lambda] = \lambda^2 W_c(\tau/\lambda^2, w/\lambda)[\gamma] \tag{5.54}$$

$$\tau S_c(\tau, w)[\gamma_\lambda] = \lambda^2 \frac{\tau}{\lambda^2} S_c(\tau/\lambda^2, w/\lambda)[\gamma] \tag{5.55}$$

$$\Omega_c(\tau, w)[\gamma_\lambda] = \lambda^2 \Omega_c(\tau/\lambda^2, w/\lambda)[\gamma]. \tag{5.56}$$

We can now rewrite Eq.(5.44) for $\lambda = 1$ and compare it with Eq.(5.17).

$$\Omega_c(\tau, w)[\gamma] = \int_0^1 \frac{d\lambda}{\lambda} W_c(\tau, \lambda w)[\gamma] \tag{5.57}$$

$$\Omega_c(\tau, w)[\gamma] = \int_0^1 d\lambda \lambda W_c(\tau/\lambda^2, w/\lambda)[\gamma] \tag{5.58}$$

Eqs. (5.57) and (5.58) accomplish to relate the temperature and interaction strength dependence of the correlation functionals. They can be used to test, if an approximate $\Omega_c^{approx}(\tau, w)[\gamma]$ shows a physical temperature and interaction strength dependence, i.e. if it respects Eqs. (5.57) and (5.58).

5.5 Summary and outlook

In this section, we focussed on the task of deriving properties of the exact FT-RDMFT functionals. Under the assumption of eq-V-representability, we could employ the variational principle to prove the negativity of the separate correlation contributions W_c, S_c, and Ω_c. The variational principle furthermore allowed us to express the correlation contribution to the grand potantial Ω_c via a coupling constant integration over the correlation contribution to the interaction W_c which is very similar to the method of adiabatic connection in DFT. We then employed the method of uniform coordinate scaling. This allowed us, on one hand, to derive differential equations, relating the different correlation functionals and, on the other hand, led to the derivation of bounds for the scaled correlation contributions. Finally, we were able to relate uniform coordinate scaling to a scaling of temperature and interaction.

The properties, derived in this section, can be used to test existing approximate functionals in FT-RDMFT or guide the development of new ones. Further progress in the determination of exact properties could be achieved by considering exact properties known from zero-temperature RDMFT like particle-hole symmetry or size consistency. Another useful investigation could be concerned with the derivation of exact bounds on the correlation grand potential e.g. in the spirit of the Lieb-Oxford bound in DFT [101].

We present in the next section a rigorous method to develop approximate grand potential functionals by employing methods of FT-MBPT. As a first application of the results derived in the present section, we will show that these functionals fulfill all exact relations derived so far under a few conditions.

6 Constructing approximate functionals

After deriving the mathematical foundations of FT-RDMFT in Section 4, we now turn to the problem of deriving approximate functionals for the grand potential functional $\Omega[\gamma]$. One key difference to RDMFT is the fact that at finite temperature there exists a Kohn-Sham system (see Section 4.2.3). We shall employ this fact in the development of a methodology to construct functionals using the powerful methods of FT-MBPT. The unperturbed system will then be the Kohn-Sham system, rather than just the original system stripped from its interaction part. This section will be structured as follows:

Section	Description
6.1	We will start by pointing out the conceptual problems of employing FT-MBPT to derive correlation functionals in FT-RDMFT.
6.2	We will then show how these problems can be solved by introducing a modified perturbation, consisting of the original two-particle interaction together with an appropriate one-particle correction.
6.3	The method introduced will have one major conceptual uncertainty, namely the assumption of eq-V-representability of the 1RDMs under consideration. We will point out why the results from Section 4.4 prevent this uncertainty from having notworthy impact on our method, therefore both substantiating our perturbative scheme as well as justifying our efforts from Section 4.4.
6.4	Finally, we will investigate how arbitrary diagrams in our method will behave under uniform coordinate scaling. We will find that they naturally fulfill most of the exact conditions derived in Section 5.

Related publications: [44, 56]

6.1 Why not use standard FT-MBPT?

To better understand the conceptual differences between a standard FT-MBPT treatment and our approach of FT-RDMFT, we will give a short review of FT-MBPT in the following.

Let the system under consideration be governed by a Hamiltonian $\hat{H} = \hat{H}_0 + \hat{W}$, where $\hat{H}_0$ is a one-particle operator and $\hat{W}$ represents a two-particle interaction (see Eqs. (2.4)). The question FT-MBPT tries to answer can be phrased as follows:

"Given a Hamiltonian $\hat{H}$, a temperature τ, and a chemical potential μ. What are the thermodynamic equilibrium properties of the system?"

The central assumption of FT-MBPT is then that the two-particle interaction $\hat{W}$ can be treated as a perturbation. In grand canonical equilibrium, the noninteracting system, governed by $h_0(x, x') = \sum_i \varepsilon_i \phi_i^*(x')\phi_i(x)$, exhibits the following finite-temperature, or Matsubara, Green's function $\mathcal{G}^0(x, \nu, x', \nu')$ [102].

$$\mathcal{G}^0(x, \nu, x', \nu') = \sum_i \phi_i(x)\phi_i^*(x')e^{-(\varepsilon_i-\mu)(\nu-\nu')} \begin{cases} n_i & , \nu > \nu' \\ n_i - 1 & , \nu > \nu' \end{cases} \tag{6.1}$$

The eq-1RDM is then given as the temperature diagonal of $\mathcal{G}^0(x, \nu, x', \nu')$

$$\gamma^0(x, x') = \mathcal{G}^0(x, \nu, x', \nu^+) = \sum_i n_i \phi_i^*(x')\phi_i(x), \tag{6.2}$$
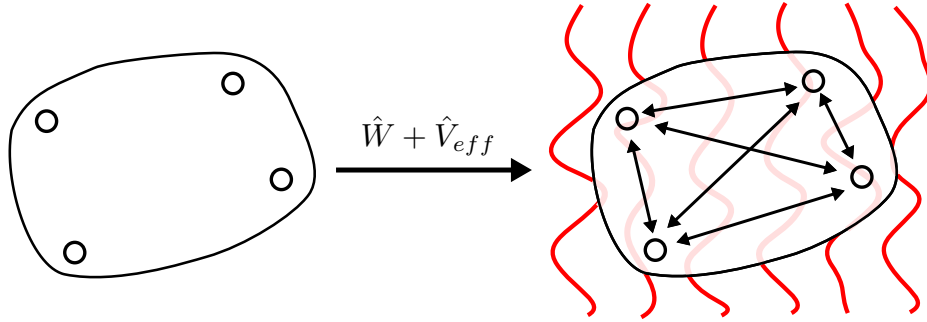
$$\mathcal{G}^0(x, 0, x', 0^+) = \gamma(x, x') = \mathcal{G}(x, 0, x', 0^+)$$

Figure 6.1: Perturbation in FT-RDMFT. It consists of a two-particle interaction (arrows) and an additional nonlocal one-particle potential (wavy lines), designed to leave the 1RDM invariant.

where the eigenvalues ε_i and occupation numbers n_i are related via the Fermi distribution (see Eqs. (4.52) and (4.53)).

$$n_i = \frac{1}{1 + e^{\beta(\varepsilon_i - \mu)}} \tag{6.3}$$

$$\varepsilon_i = \frac{1}{\beta} \ln\left(\frac{1 - n_i}{n_i}\right) + \mu \tag{6.4}$$

We see that knowledge of the noninteracting 1RDM determines the noninteracting Green's function completely. By the virtue of the finite-temperature version of Wick's theorem [102], one can now relate the interacting and noninteracting systems by using the method of Feynman diagrams. In this procedure, the chemical potential (and the temperature) is held constant. But this means that in general the interacting system has a different particle number from the noninteracting one. If the particle numbers are not the same, then surely also the 1RDMs are different. In FT-RDMFT however, the question one is asking differs from the one in FT-MBPT. It reads

"Given a Hamiltonian $\hat{H}$ and a temperature τ, what are the thermodynamic properties of the interacting system with eq-1RDM γ?"

Therefore, one explicitly has the interacting 1RDM at hand. If one should now resort to just using a perturbative expansion from FT-MBPT one would encounter the problem that the noninteracting 1RDMs and therefore also the noninteracting Green's function would not be known. Therefore, the Feynman diagrams appearing in a perturbative expansion of the interacting Green's function cannot be evaluated. Our approach to solve this conceptual problem is the introduction of an additional, in general nonlocal, one-particle potential which lets the 1RDM stay invariant under this new perturbation. We depict this idea in Figure 6.1. Accordingly, the interacting and noninteracting 1RDMs would be the same and one could easily calculate the noninteracting Green's function. We should like to acknowledge that a similar approach was pursued in the course of DFT [103]. There, in accordance with the nature of DFT, the additional one-particle potential was local and designed to keep the density constant.

6.2   Methodology of modified perturbation theory

After these preliminary considerations, we can proceed to derive Feynman rules to construct approximate functionals for $\Omega[\gamma]$. We start from the adiabatic connection formula Eq. (5.16) which we will restate in the following:

$$\Omega[\gamma] = \Omega^0[\gamma] + \int_0^1 d\lambda \operatorname{Tr}\left\{ \hat{D}^\lambda[\gamma]\hat{W} \right\}. \tag{6.5}$$

The λ-dependent SDO is given by

$$\hat{D}^\lambda[\gamma] = e^{-\beta(\hat{T} + \hat{V}^\lambda[\gamma] + \lambda\hat{W} - \mu\hat{N})}/Z, \tag{6.6}$$

where $V^\lambda[\gamma]$ is chosen so that $\gamma(x, x') = \operatorname{Tr}\{\hat{D}^\lambda[\gamma]\Psi^+(x')\hat{\Psi}(x)\}$ stays invariant with respect to λ. It is now known (e.g.[104], p.230) that $\langle\lambda\hat{W}\rangle_\lambda = \operatorname{Tr}\{\hat{D}^\lambda[\gamma]\lambda W\}$ can be calculated from the Green's function of the system under consideration

$$\langle\lambda\hat{W}\rangle_\lambda = \frac{1}{2}\int dxdx' \lim_{\nu'\to\nu^+} \left(-\delta(x - x')\frac{\partial}{\partial\nu} - k_0(\lambda)(x, x') \right)\mathcal{G}^\lambda(x, \nu, x', \nu'), \tag{6.7}$$

where $\beta = 1/\tau$ and $k_0(\lambda)$ is defined by $\hat{K}_0(\lambda) = \hat{T} + \hat{V}_0 - \mu\hat{N} + \hat{V}^\lambda[\gamma]$. As explained before, we can now relate the interacting system with its Kohn-Sham system which allows to express the resulting Feynman diagrams in terms of the ONs and NOs of the 1RDM. The Hamiltonian of this noninteracting system is given by $\hat{K}_0(0)$. Eq. (6.7) therefore is rewritten as

$$\langle\lambda\hat{W}\rangle_\lambda = \frac{1}{2}\int dxdx' \lim_{\nu'\to\nu^+} \left(-\delta(x - x')\frac{\partial}{\partial\nu} - k_0(0)(x, x') \right)\mathcal{G}^\lambda(x, \nu, x', \nu') +$$
$$\frac{1}{2}\int d^3x d^3x' \left(v^0[\gamma](x', x) - v^\lambda[\gamma](x', x) \right)\gamma(x, x'). \tag{6.8}$$

Now, methods of FT-MBPT can be applied. The unperturbed Hamiltonian is $\hat{K}_0(0)$ whereas the interacting one reads $\hat{K}(\lambda) = \hat{K}_0(\lambda) + \lambda\hat{W}$. This defines the perturbation as $(\lambda\hat{W} + \hat{V}^\lambda - \hat{V}^0)$. The one-particle part will be denoted by v_{eff}^λ:

$$v_{eff}^\lambda = v^\lambda - v^0. \tag{6.9}$$

The perturbation now consists of a two-particle interaction $\lambda w(\boldsymbol{r}, \boldsymbol{r}')$ and a possibly nonlocal one-particle interaction $v_{eff}^\lambda(\boldsymbol{r}, \boldsymbol{r}')$. The proof of Wick's theorem is still applicable for this kind of perturbation and the same Feynman graphs appear (see Table 6.1).

In the special situation of a temperature-independent Hamiltonian and a spatially uniform system, Eq. (6.8) can be written in a compact form.

$$\langle\lambda\hat{W}\rangle_\lambda^{unif} = \frac{1}{2}\left(\text{⬤}\Sigma^* - \text{⬳} \right), \tag{6.10}$$

where Σ^* denotes the irreducible self energy. In practice, one has to select a particular set of Feynman diagrams. We will demonstrate in the following section that the requirement that both interacting and noninteracting systems exhibit the same eq-1RDM is sufficient for an elimination of the Kohn-Sham potential contributions. We will be left with diagrams containing only two-particle interactions and noninteracting Green's functions which can be calculated using the Feynman rules of Appendix A.5.
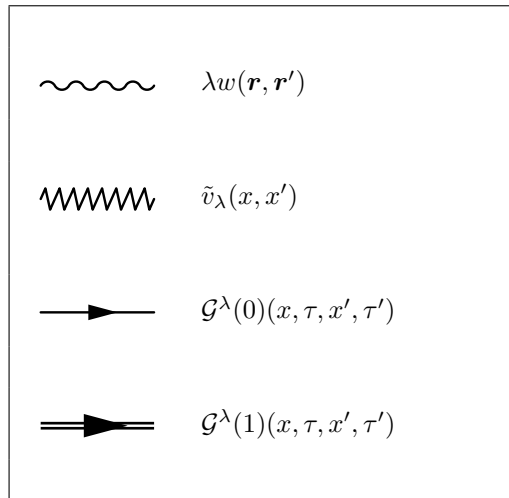
Table 6.1: Feynman graph contributions for the construction of correlation functionals in FT-RDMFT

6.2.1 Elimination of V_{eff}

In Figure 6.2 we show all contributions to the interacting Green's function $\mathcal{G}(x, \nu, x', \nu')$ up to second-order in w and v_{eff}. We now expand v_{eff} in orders of w as

$$v_{eff} = v_{eff}^{(1)} + v_{eff}^{(2)} + \dots .$$ (6.11)

It is now possible to iteratively solve for the different contributions for $v_{eff}^{(n)}$ from the requirement $\mathcal{G}(x, 0, x', 0^+) = \mathcal{G}^0(x, 0, x', 0^+)$. It can be recast in terms of Feynman diagrams as

  (6.12)

The interacting and noninteracting 1RDMs are required to be equal. Therefore, we are led to the conditional equation for v_{eff}.

  (6.13)
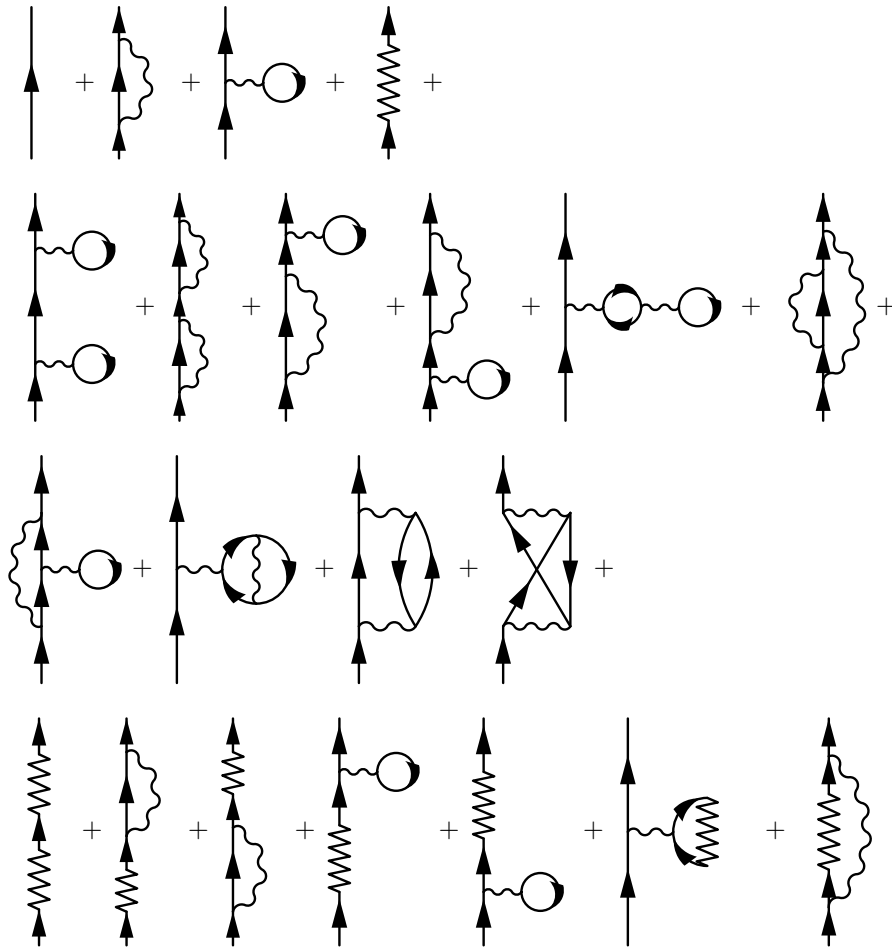
Figure 6.2: Contributions to the interacting Green's function $\mathcal{G}(x, \nu, x', \nu')$ up to second-order in $\hat{W}$ and $\hat{V}_{eff}$

We can now utilize Eq. (6.13) to solve for $v_{eff}^{(1)}$ by only considering first-order contributions. We get

$$(6.14)$$

$$\int dy dy' \int_0^\beta d\nu d\nu' v_{eff}^{(1)}(y, y') \delta(\nu - \nu') \mathcal{G}^0(x, 0, y, \nu) \mathcal{G}^0(y', \nu', x', 0^+)$$

$$= - \int dy dy' \int_0^\beta d\nu d\nu' w(y, y') \delta(\nu - \nu') \mathcal{G}^0(x, 0, y, \nu) \mathcal{G}^0(y, \nu, y', \nu') \mathcal{G}^0(y', \nu', x', 0^+) -$$

$$\int dy dy' \int_0^\beta d\nu d\nu' w(y, y') \delta(\nu - \nu') \mathcal{G}^0(x, 0, y, \nu) \mathcal{G}^0(y, \nu, x', 0^+) \mathcal{G}^0(y, \nu, y', \nu') \quad (6.15)$$

We can now replace the noninteracting Green's function with expression Eq. (6.1). It is exactly here that the nonlocality of the 1RDM pays off, because we can use the orthonormality and completeness of $\{\phi\}$ and the fact that $0 < \tau < \beta$ to get

$$v_{eff}^{(1)}(x, x') = -\delta(x - x') \int dy w(x, y) \gamma(x', x') - w(x, x') \gamma(x, x'), \quad (6.16)$$

or, in terms of Feynman diagrams,

 (6.17)

This result bears the following important information. Up to first order in the interaction, the Kohn-Sham potential $\hat{V}_{eff}$ cancels completely the interaction contributions coming from $\hat{W}$, implying that the Green's functions of the noninteracting and interacting system are equal. This represents the result we obtained in Section 4.2.5, namely that the first-order functional in FT-RDMFT is equivalent to finite-temperature Hartree-Fock theory which is effectively a noninteracting theory.

The next step is now to replace all first-order contributions to v_{eff} by Eq. (6.17). There will be many cancellations of diagrams and we get for the second-order contribution to the Kohn-Sham potential $v_{eff}^{(2)}$

 (6.18)

The solution of this equation is rather more complicated than the corresponding one from first-order diagrams. The reason for this is that the in and outgoing Green's functions will have different temperature arguments. As a simplification we write

 (6.19)

Written in spatial representation, this becomes

$$\int dy dy' \int_0^\beta d\tau d\tau' v_{eff}^{(1)}(y, y') \delta(\tau - \tau') \mathcal{G}^0(x, 0, y, \tau) \mathcal{G}^0(y', \tau', x', 0^+)$$

$$= - \int dy dy' \int_0^\beta d\tau d\tau' M(y, \tau, y', \tau') \mathcal{G}^0(x, 0, y, \tau) \mathcal{G}^0(y', \tau', x', 0^+) \quad (6.20)$$

which will be solved by

$$v_{eff}^{(2)} = \frac{\sum_{ij} \phi_i(x)\phi_j^*(x') \int_0^\beta d\nu d\nu' M_{ij}(\nu,\nu') e^{\nu(\varepsilon_i - \mu)} e^{-\nu'(\varepsilon_j - \mu)}}{\int_0^\beta e^{\nu'(\varepsilon_i - \varepsilon_j)}}, \tag{6.21}$$

where
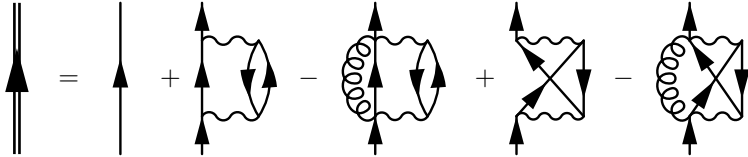
$$M_{ij}(\nu,\nu') = \int dy dy' M(x,\nu,x',\nu') \phi_i(x')\phi_j^*(x). \tag{6.22}$$

An evaluation of Eq. (6.21) with the appropriate $M(x,\nu,x',\nu')$ then yields the second-order contribution to v_{eff}. Exactly in the same fashion as before we could now replace all appearing $v_{eff}^{(2)}$ and solve for the third-order term $v_{eff}^{(3)}$. We would be led to an equation just like Eq. (6.19) with different $M(x,\nu,x',\nu')$ and therefore to an Eq. (6.19) which would then yield the third-order contribution. Applying this method iteratively therefore determines v_{eff}. We would now like to point out a small sublety. It seems that by the arguments above, one could solve for v_{eff} for any given 1RDM $\gamma \in \Gamma^N$. This would lead to the conclusion that all $\Gamma^N = \Gamma^V$. The flaw in this argument is the assumption that the perturbation expansion of $\mathcal{G}$ converges. This question of convergence of perturbation expansions is a very complicated and so far generally unsolved problem in FT-MBPT. Therefore, we cannot conclude $\Gamma^N = \Gamma^V$. However, given any FT-MBPT approximation for $\mathcal{G}$ we can still calculate the corresponding v_{eff}.

It is now possible, to express v_{eff} in terms of Feynman diagrams by the introduction of an additional graphical contribution.

 $$= \frac{\sum_{ij} \phi_i(x)\phi_j^*(x') \int_0^\beta d\nu d\nu' M_{ij}(\nu,\nu') e^{\nu(\varepsilon_i - \mu)} e^{-\nu'(\varepsilon_j - \mu)}}{\int_0^\beta e^{\nu'(\varepsilon_i - \varepsilon_j)}}. \tag{6.23}$$

Combining our first-order and second-order results, we get the following expression for the interacting Green's function.

 $$\tag{6.24}$$

Any choice of diagrams leads to an approximation for $\mathcal{G}(x,\nu,x',\nu')$ from which we can derive $\Omega[\gamma]$ via Eqs. (5.16) and (6.7).

Considering now only the first-order contribution to the grand potential functional, we can justify our claim from Section 4.2.4 that the form of the Hartree and exchange functionals from zero-temperature RDMFT carry over to the finite-temperature case. The first-order functional $\Omega_{xc}^{(1)}$ is given in terms of Feynman diagrams as

$$\Omega_{xc}^{(1)}[\gamma] = \text{} \tag{6.25}$$

which translates to Eqs. (4.59) and (4.60).

$$\Omega_{xc}[\gamma] = \frac{1}{2} \int dx dx' w(x,x') \gamma(x,x) \gamma(x',x') - \frac{1}{2} \int dx dx' w(x,x') \gamma(x,x') \gamma(x',x) \tag{6.26}$$

In the case of a translationally invariant Hamiltonian, Eq. (6.10) allows a simple representation of the grand potential functional up to second order:

$$\Omega_{xc}^{(2)}[\gamma] = \quad\text{(diagrams)}\quad + \quad\text{(diagrams)}\quad + \quad\text{(diagrams)}\quad + \quad\text{(diagrams)}\quad . \tag{6.27}$$

We want to point out that an inclusion of higher-order diagrams will lead to contributions to Ω_c including the new Feynman graphs introduced in Eq. (6.23). Up to second order they are cancelled by the effective potential contribution in Eq. 6.10.

Applied to the HEG, the first and third diagrams in Eq. 6.27 are diverging. The first one is then cancelled by the positive background charge and the third one is usually subjected to an RPA screening, rendering it finite. We will investigate the behaviour of the different contributions to the xc functional as described in Eq. 6.27 in Section 8.4.

Having derived a methodology to iteratively construct functionals for FT-RDMFT, we will now come back to the problem already mentioned in the introduction to Section 6, namely the question of eq-V-representability of the 1RDMs under consideration.

6.3 Importance of eq-V-representability

Starting from a noninteracting 1RDM $\gamma \in \Gamma^N$ we explicitly assumed that it was also eq-V-representable for interaction $\hat{W}$. But this might contain the following conceptual problem. Generally speaking, the perturbative procedure is only valid on Γ^V. Let us now assume that all the assumptions of FT-MBPT are well fulfilled and that we derived a good functional $\Omega[\gamma]$. Good means that a minimization of $\Omega[\gamma]$ on Γ^V yields a minimum close to the exact one. Applying this functional on $\Gamma^N \backslash \Gamma^V$, it is not at all justified to assume that the functional retains its good behaviour, i.e. that one is not led to a completely different minimum on $\Gamma^N \backslash \Gamma^V$. We illustrate this problem in Figure 6.3. In summary, the problem is that one minimizes a functional, which is well behaved on one set, on a bigger set, where there is nothing known about its behaviour. It is now that Theorem 4.15 unveils its importance. It states that Γ^V is dense in Γ^N, which ensures that given any 1RDM $\gamma^N \in \Gamma^N$ there is another 1RDM $\gamma^V \in \Gamma^V$ arbitrarily close to it. Because the functionals derived from FT-MBPT will be considerably smooth, this means that $\Omega[\gamma^N]$ will be arbitrarily close to $\Omega[\gamma^V]$. Therefore, a minimization of $\Omega[\gamma]$ over the full set Γ^N will lead to a minimum arbitrarily close to the minimum over Γ^V (see Figure 6.3).
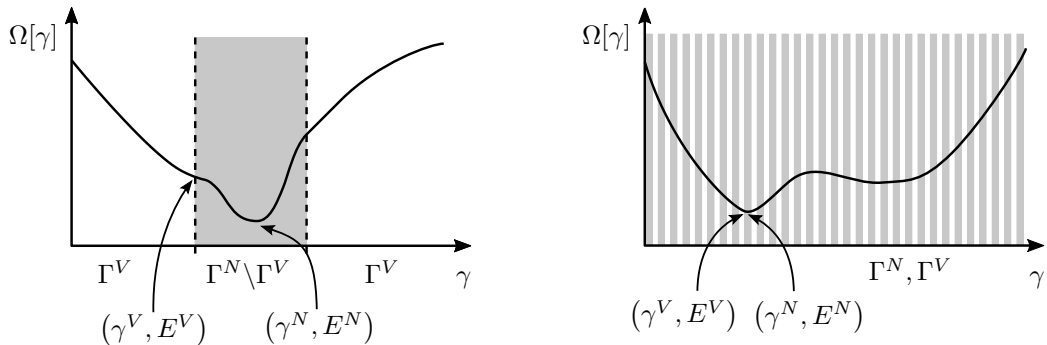
6.3.a: Γ^V not being dense in Γ^N: Minima on different sets can be very different.

6.3.b: Γ^V dense in Γ^N: Minima on different sets are infinitesimal close.

Figure 6.3: Illustration of the importance of eq-V-representability in the context of functional construction via FT-MBPT. The grey regions in both figures denote the set $\Gamma^N \backslash \Gamma^V$. In Figure 6.3.b this region is enlarged for graphical purposes.

6.4 Scaling behaviour

We can now investigate how the single diagrams appearing in a certain approximation to $\Omega_c[\gamma]$ behave under scaling of the 1RDM, temperature and interaction strength. We will consider a scaling of the 1RDM first. From Eqs. (6.1) and (6.4) we see that, with $k_0(x, x') = h_0(x, x') - \mu$, we get

$$k_0[\gamma_\lambda](x, x') = \lambda^3 k_0[\gamma](\lambda x, \lambda x') \tag{6.28}$$

$$\mathcal{G}^0[\gamma_\lambda](x, \nu, x', \nu') = \lambda^3 \mathcal{G}^0[\gamma](\lambda x, \nu, \lambda x', \nu'). \tag{6.29}$$

A general n-th order contribution to the interacting Green's function contains

- n interaction lines
- 2n+1 $\mathcal{G}^0$ lines
- 2n interior points.

A variable substitution in the integrals $x \to x/\lambda$ then yields a factor of λ^{-3} for each inner node. In addition, this variable substitutions will give a factor of λ for each Coulomb interaction line. Combining these observations, we see that an arbitrary n-th order contribution scales as follows.

$$\mathcal{G}^{\xi(n)}[\gamma_\lambda](x, \nu, x', \nu') = \lambda^{n+3} \mathcal{G}^{\xi(n)}[\gamma](\lambda x, \nu, \lambda x', \nu') \tag{6.30}$$

A final variable substitution in Eq.(6.7) then yields

$$\Omega_c^{(n)}[\gamma_\lambda] = \lambda^n \Omega_c^{(n)}[\gamma]. \tag{6.31}$$

Using Eqs. (5.44) and (5.45) to define $W_c[\gamma]$ and $S_c[\gamma]$, we get

$$W_c^{(n)}[\gamma_\lambda] = \lambda^n W_c^{(n)}[\gamma] = n\Omega_c^{(n)}[\gamma_\lambda] \tag{6.32}$$

$$\tau S_c^{(n)}[\gamma_\lambda] = \lambda^n \tau S_c^{(n)}[\gamma] = (n-1)\Omega_c^{(n)}[\gamma_\lambda]. \tag{6.33}$$

We immediately see that if a diagram fulfills $\Omega_c^{(n)}[\gamma] < 0$, then the exact relations (5.8), (5.9), (5.10),(5.47), (5.48), and (5.49) are fulfilled.

To show that Eqs. (5.34), (5.35), and (5.36) are also fulfilled, we prove the validity of Eqs. (5.31) and (5.32), as restated in the following.

$$W_c[\gamma] - \tau S_c[\gamma] \leq \frac{1}{\lambda} W_c[\gamma_\lambda] - \tau S_c[\gamma_\lambda] \tag{6.34}$$

$$W_c[\gamma_\lambda] - \tau S_c[\gamma_\lambda] \leq \lambda W_c[\gamma] - \tau S_c[\gamma] \tag{6.35}$$

Taking the difference of the left (L) and right (R) sides of Eq. (6.34) and using Eqs. (6.32) and (6.33) we get

$$L - R = (1 - n\lambda^{n-1} + (n-1)\lambda^n)\Omega_c[\gamma] \tag{6.36}$$

$$\frac{\partial}{\partial \lambda}(L - R) = n(n-1)(\lambda^{n-1} - \lambda^{n-2}). \tag{6.37}$$

We see that for $\lambda = 1 : L - R = 0$. Furthermore, the derivative with respect to λ is bigger 0 for $\lambda < 1$ and smaller 0 for $\lambda > 1$. It follows that $L - R \leq 0$. For Eq. (6.35) we get

$$L - R = (\lambda^n - n\lambda + (n-1))\Omega_c[\gamma] \tag{6.38}$$

$$\frac{\partial}{\partial \lambda}(L - R) = n(\lambda^{n-1} - 1). \tag{6.39}$$

The same argument as before again proves $L - R \leq 0$. These two results prove the validity of Eqs. (5.31) and (5.32) and therefore of Eqs. (5.34), (5.35), and (5.36).

It is now also possible to show the equivalence of Eqs. (5.57) and (5.58) for these approximations. We therefore investigate an arbitrary nth-order contribution to $\mathcal{G}^\lambda$ under scaling of temperature and interaction. Again using Eqs. (6.1) and (6.4), we acquire

$$k_0(\eta\tau)[\gamma](x, x') = \eta k_0(\tau)[\gamma](x, x') \tag{6.40}$$

$$\mathcal{G}^0(\eta\tau)[\gamma](x, \nu, x', \nu') = \mathcal{G}^0(\tau)[\gamma](x, \eta\nu, x', \eta\nu'). \tag{6.41}$$

Because the Coulomb interaction is instantaneous, $\mathcal{G}^{\xi(n)}$ contains only n temperature integrations. Therefore,

$$\mathcal{G}^{\xi(n)}(\eta\tau, \kappa w)[\gamma](x, \nu, x', \nu') = \eta^{-n}\kappa^n \mathcal{G}^{\xi(n)}(\tau, w)[\gamma](x, \eta\nu, x', \eta\nu'). \tag{6.42}$$

From Eq. (6.7), we finally arrive at

$$W_c^{(n)}(\eta\tau, \kappa w)[\gamma] = \eta^{1-n}\kappa^n W_c^{(n)}(\tau, w)[\gamma] \tag{6.43}$$

which fulfills Eq. (5.54) and therefore proves the equivalence of Eqs. (5.57) and (5.58). The previous results can be combined to get a complete description of the scaling behaviour of an arbitrary nth-order contribution to the grand potential functional.

$$\boxed{\Omega_c^{(n)}(\eta\tau, \kappa w)[\gamma_\lambda] = \eta^{1-n}\kappa^n \lambda^n \Omega_c^{(n)}(\tau, w)[\gamma]} \tag{6.44}$$

6.5 Summary and outlook

Employing the fact that in FT-RDMFT there is a Kohn-Sham system, we derived a methodology to construct approximate functionals by using diagramatic techniques from FT-MBPT. Because in the standard FT-MBPT treatment the chemical potential is held fixed, the interacting and noninteracting systems will not have the same eq-1RDM. In FT-RDMFT, however, we need to determine the various contributions to the grand potential for a given 1RDM, i.e. the goal is to construct a functional of the 1RDM using FT-RDMFT. We solved this problem by introducing an additional one-particle potential which renders the 1RDM invariant under the perturbation. We investigated the resulting perturbative expansion and showed that for every choice of contributing interaction diagrams the one-particle contribution can be uniquely determined. We also showed that the first-order functional has the same form as the zero-temperature one with an inclusion of the noninteracting entropy functional, which justifies the assumption of Section 4.2.4. Additionally, we pointed out the importance of our investigation of eq-V-representability for the considerations in this section. Finally, we investigated, how the resulting approximate functionals behave under scaling of coordinates, temperature and interaction strength and showed that, under a few conditions, they fulfill all exact properties derived in Section 5.

After these theoretical considerations, one has to investigate how different choices of diagrams, or classes of diagrams, perform when applied to model and real systems. We do so in Section 8.6, considering both second-order Born as well as RPA diagrams.

Continuing our considerations regarding systems in canonical equilibrium from Section 4.5, we restate that the exponent of the eq-SDO in a canonical ensemble contains only N-particle contributions. This is rather unfortunate because the finite temperature version of Wick's theorem explicitly relies on the interplay of states of different particle numbers and is therefore invalid for canonical ensembles. Accordingly our perturbative methods will not be valid for the construction of functionals for the description of systems in canonical equilibrium.

7 Numerical treatment

We have shown in Section 4.2.1 that it is possible to describe a quantum mechanical system in grand canonical equilibrium with the help of the 1RDM. One can find the eq-1RDM by a minimization of a grand potential functional $\Omega[\gamma]$ over a certain set of 1RDMs. This set was shown in Section 4.2.2 to be easily determined by simple constraints on the ONs and NOs of the 1RDMs (see Eqs.(2.19)-(2.21)). To approximate the exact functional, one could now either use the method we introduced in Section 6 or simply guess a functional, guided by physical insight and tested against exact properties, e.g. the ones derived in Section 5. Regardless of the origin of a functional, one will eventually have to minimize it. Because at zero temperature there exists no Kohn-Sham system in RDMFT (see Thm. 3.1 Section 3.1), one usually resorts to direct minimization schemes [105, 106]. However, because at finite temperature there exists a Kohn-Sham system (see Section 4.2.3), this handicap disappears and we will be able to construct a self-consistent (sc) minimization scheme for FT-RDMFT. Furthermore, we will show that this procedure can also be used to minimize functionals from zero-temperature RDMFT to arbitrary accuracy. Therein, one will construct a noninteracting system at finite temperature which reproduces the eq-1RDM of an interacting system at zero temperature. The remainder of this section is structured as follows:

Section	Description
7.1	We are going to review the main concept of minimization via a self-consistent scheme employing a noninteracting effective system. This will help in understanding the capabilities and limitations of our procedure. It also paves the way for improvements in our scheme, like the introduction of a temperature tensor in Section 7.3.
7.2	We will then define the Hamiltonian describing the effective noninteracting system in grand canonical equilibrium. It will be given completely in terms of the derivatives of the functional $\Omega[\gamma]$ w.r.t. the ONs and NOs.
7.3	Inspired by considerations in Section 7.1 we are able to greatly improve the adaptability of the effective system. This will be done by introducing a state-dependent temperature tensor for the effective noninteracting system. We then present a computational scheme for a self-consistent minimization procedure employing this noninteracting system.
7.4	To analytically investigate our minimization scheme, we can do a perturbative small-step expansion. We derive requirements on the effective temperature tensor to ensure a decrease of the functional $\Omega[\gamma]$ at each iteration step.
7.5	Paying tribute to the possible inaccuracy of numerical derivatives, we then derive two derivative-based convergence measures which allow to judge the convergence of the minimization with respect to ONs and NOs.
7.6	Finally, we are going to investigate the performance of the Kohn-Sham minimization scheme. We therefore implemented it in the FP-LAPW-Code Elk [107]. As an example we minimize a common RDMFT functional applied to LiH and discuss achievements and shortcomings.

Related publications: [108]

7.1 Key idea of self-consistent minimization

We are now going to have a closer look at the idea of a minimization by employing an arbitrary noninteracting system. The functional, which we want to minimize, shall be denoted by $\Omega[\gamma]$ and its domain shall be given by Γ^N. If one considers the functional as a functional of ONs and NOs, then it describes a grand potential surface on the set of allowed $\{n_i\}$ and $\{\phi_i\}$. For a given 1RDM γ_k, the question arising is where one would assume the next 1RDM γ_{k+1} so that one will move downwards
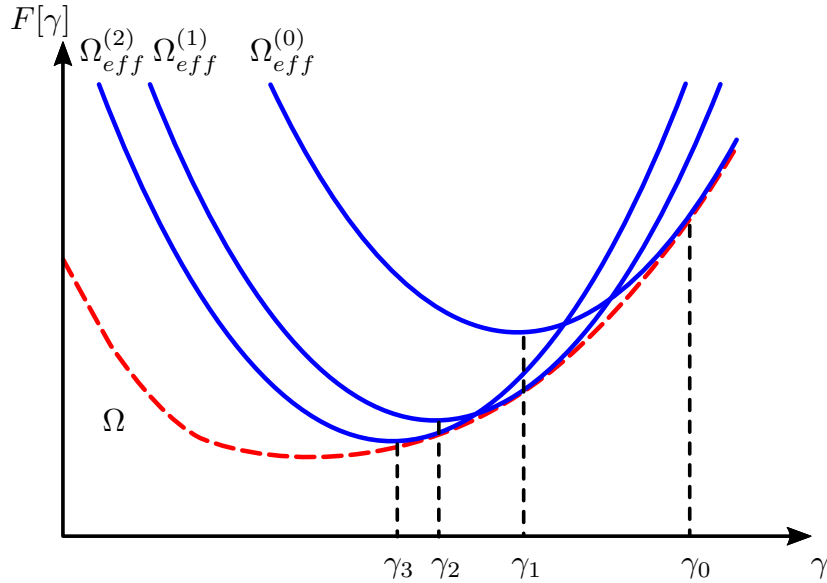
Figure 7.1: Iterative minimization of $\Omega[\gamma]$ (red dashed line) by employing effective noninteracting functionals $\Omega_{eff}^{(n)}[\gamma]$ (blue solid lines).

on the grand potential surface. A standard approach to this problem is the use of steepest-descent methods. Therein, one will use the first derivatives with respect to the ONs and NOs and take a step along the smallest slope. The main problem of this approach is the incorporation of the auxiliary conditions on the ONs and NOs. These are the boundedness of the ONs $0 \leq n_i \leq 1$, the particle number conservation $\sum_i n_i = N$, and most importantly, because most difficulty, the orthonormality of the NOs. Usually, the orthonormality of the NOs will be enforced by applying an orthonomalization algorithm to the NOs after they have been modified, using the information provided by the functional derivatives $\delta\Omega[\gamma]/\delta\phi_i$. These orthonormalization procedures can change several orbitals quite significantly which can lead to a slow convergence of the minimization routines.

The main idea of a self-consistent minimization scheme is now to approximate the grand potential surface by a simpler one whose minimum, incorporating all auxiliary constraints, can be found easily. In our situation, we take the information about the derivatives of $\Omega[\gamma]$ at γ_k and construct an effective noninteracting system in grand canonical equilibrium whose grand potential functional Ω_{eff} has the same functional derivative in γ_k. The minimum of this grand potential surface is found by a diagonalisation of the effective Hamiltonian and an occupation of the new ONs according to the Fermi-Dirac distribution. The resulting eq-1RDM will then serve as the starting point γ_{k+1} for the subsequent iteration. This idea is schematically sketched in Figure 7.1. We should like to point out that this method intrinsically incorporates the constraints on the ONs and NOs and we will not have to apply subsequent orthonormalizations or the like. The success of this scheme, of course, relies on the similarity of the grand potential surfaces of $\Omega[\gamma]$ and $\Omega_{eff}[\gamma]$. However, we know from Theorem 4.10 that both $\Omega[\gamma]$ and $\Omega_{eff}[\gamma]$ are upwards convex. This ensures that one will eventually arrive at the minimum of Ω, given appropriately small step lengths. These considerations also show the necessity of an upwards convexity of approximate functionals. If this feature was not satisfied a minimization might end up in a local minimum. This problem, however, is prevalent in most minimization schemes which use only the information of the first derivatives.

We will now proceed to derive the variational equations, guiding the determination of γ_{k+1}.

7.2 Effective Hamiltonian

We will restate the interacting as well as the noninteracting grand potential functionals in the following (see Eqs. (4.56)-(4.61)):

$$\Omega[\gamma] = \Omega_k[\gamma] + V_{ext}[\gamma] + \Omega_{Hxc}[\gamma] - \mu N[\gamma] - 1/\beta S_0[\gamma] \tag{7.1}$$

$$\Omega_{eff}[\gamma] = \Omega_k[\gamma] + V_{eff}[\gamma] - \mu_0 N[\gamma] - 1/\beta_0 S_0[\gamma]. \tag{7.2}$$

We combined the Hartree, exchange, and correlation contributions to the grand potential into $\Omega_{Hxc}[\gamma]$. We explicitly allow the Kohn-Sham system to have a different temperature β_0 from the interacting one. The effective noninteracting system is now constructed so that the derivatives of the interacting as well as of the noninteracting functional (Eqs. (7.1) and (7.2)) coincide:

$$\frac{\delta\Omega_{eff}[\gamma]}{\delta\gamma(x,x')} = \frac{\delta\Omega[\gamma]}{\delta\gamma(x,x')}. \tag{7.3}$$

The effective Hamiltonian in spatial representation then becomes

$$h_{eff}[\gamma](x,x') = t[\gamma](x,x') + v_{ext}[\gamma](x,x') + v_{Hxc}[\gamma](x,x') +$$
$$\left(\frac{1}{\beta_0} - \frac{1}{\beta}\right)\sigma[\gamma](x,x') + (\mu_0 - \mu)\delta(x - x'), \tag{7.4}$$

where

$$v_{Hxc}[\gamma](x,x') = \frac{\delta\Omega_{Hxc}[\gamma]}{\delta\gamma(x,x')} \tag{7.5}$$

$$\sigma[\gamma](x,x') = \frac{\delta S_0[\gamma]}{\delta\gamma(x,x')}. \tag{7.6}$$

We want to use the chain rule for the functional derivative. We therefore need the derivatives of the ONs and NOs with respect to γ. They can be obtained using first-order perturbation theory, leading to

$$\frac{\delta n_k}{\delta\gamma(x',x)} = \phi_k^*(x')\phi_k(x) \tag{7.7}$$

$$\frac{\delta\phi_k(y)}{\delta\gamma(x',x)} = \sum_{l\neq k}\frac{\phi_l^*(x')\phi_k(x)}{n_k - n_l}\phi_l(y) \tag{7.8}$$

$$\frac{\delta\phi_k^*(y)}{\delta\gamma(x',x)} = \sum_{l\neq k}\frac{\phi_k^*(x')\phi_l(x)}{n_k - n_l}\phi_l^*(y). \tag{7.9}$$

In the following, it will be useful to work in the basis of NOs. An arbitrary function $g(x,x')$ is then represented by g_{ij}, where

$$g_{ij} = \int dx dx' \phi_i^*(x)g(x,x')\phi_j(x'). \tag{7.10}$$

The effective Hamiltonian is then represented by its matrix elements $h_{eff\ ij}$ in the basis of the NOs

$$h_{eff\ ij} = \delta_{ij}\left(\frac{\partial\Omega[\gamma]}{\partial n_i} + \mu_0 + \frac{\sigma_i}{\beta_0}\right) + \frac{1 - \delta_{ij}}{n_i - n_j}\int dy\left(\frac{\delta\Omega[\gamma]}{\delta\phi_i(y)}\phi_j(y) - \frac{\delta\Omega[\gamma]}{\delta\phi_j^*(y)}\phi_i^*(y)\right), \tag{7.11}$$

where the entropic contribution σ_i is given by

$$\sigma_i = \frac{\partial S_0[\gamma]}{\partial n_i} = \ln\left(\frac{1 - n_i}{n_i}\right). \tag{7.12}$$

The offdiagonal elements are exactly those Pernal [109] derived in her approach for the derivation of an effective potential for RDMFT. They are also simply related to the ones Piris and Ugalde [106] introduced in their method for an orbital minimization. It has to be noted, however, that in our approach the diagonal elements are not free to choose but are determined by the thermodynamic ensemble. We also see that one can control the change in the 1RDM by tuning β_0. If β_0 was small, i.e. if the corresponding effective temperature was high, the diagonal part of $\hat{H}_{eff}$ will be bigger compared to the offdiagonal parts. Therefore, after a diagonalisation of $\hat{H}_{eff}$, the orbitals will change less. Accordingly, in the limit of $\beta \to 0$, the offdiagonal elements of $\hat{H}^{eff}$ can be neglected and the diagonal elements will be given by the entropic contribution σ_i/β, i.e. $h_{ij}^{eff} = \delta_{ij}\varepsilon_i = \delta_{ij}\sigma_i/\beta$. If one would now, starting from a set of ONs $\{n_i\}$, construct a new set of ONs $\{n_i'\}$ from this effective Hamiltonian via Eqs. (4.52) and (4.53) then one finds that the ONs are left invariant, i.e. $n_i' = n_i$. We will further investigate the behaviour of our self-consistent minimization scheme for small β_0 in Section 7.4.

Before we construct a self-consistent scheme for the minimization of $\Omega[\gamma]$, in the following we will show how the concept of a temperature tensor greatly enhances the adaptability of the Kohn-Sham system which will improve the performance of the minimization procedure.

7.3 Temperature tensor

So far, we treated temperature as a single parameter in the definition of our effective Hamiltonian. We will show now how the concept of a temperature tensor crucially increases our variational freedom. The following considerations will be instructive. In a self-consistent minimization scheme, for a given 1RDM, we construct a known (noninteracting) functional whose first derivative coincides with the one from the interacting functional. For a fixed β_0, the parameter, responsible for this fitting, is μ_0. β_0 can now be varied to modify how narrow the noninteracting grand potential surface will be. However, second derivatives with respect to the ONs may differ quite substantially and a value of β_0 which describes the grand potential surface w.r.t. one ON well might describe others quite badly. A simple example would be a quadratic two-state model functional $\Omega[n_1, n_2]$ without orbital dependence.

$$\Omega[n_1, n_2] = \frac{\alpha_1}{2}(n_1 - 0.5)^2 + \frac{\alpha_2}{2}(n_2 - 0.5)^2 \tag{7.13}$$

$$= \Omega_1[n_1] + \Omega_2[n_2] \tag{7.14}$$

A choice of $\alpha_1 = 50$ and $\alpha_2 = 1$ leads to $h_{eff\ 11} = \varepsilon_1 = -0.225 + \mu$ and $h_{eff\ 22} = \varepsilon_2 = 0.00450 + \mu$ in Eq. (7.11). The corresponding projected grand potential surfaces are plotted in Figure 7.3 for $\beta_0 = 0.11$. As one can see, the choice of $\beta_0 = 0.11$ models the first grand potential surface quite well, but the second one fails to be reproduced. One would like to have some sort of adaptive β_0 which can be related to the second derivatives. However, before one can use such a construct, one has to confirm that it corresponds to a grand potential surface whose minimum can easily be found.

We are now going to show that this is possible by a slight variation of the definition of grand canonical ensembles. We consider the following generalized SDO-grand potential functional

$$\mathfrak{G}[\hat{D}] = \text{Tr}\{\hat{D}(\hat{\mathcal{B}}(\hat{H} - \mu\hat{N}) + \ln\hat{D})\}, \tag{7.15}$$

where $\hat{\mathcal{B}}$ is an arbitrary hermitean operator on the Fock-space. The same proof as in [11] now leads to the following variational principle

$$\mathfrak{G}[\hat{D}] \geq \mathfrak{G}[\hat{D}_{eq}], \tag{7.16}$$

where the equality is only fulfilled if $\hat{D} = \hat{D}_{eq}$.

$$\hat{D}_{eq} = e^{-\hat{\mathcal{B}}(\hat{H} - \mu\hat{N})}/Z_{eq} \tag{7.17}$$

$$Z_{eq} = \text{Tr}\{e^{-\hat{\mathcal{B}}(\hat{H} - \mu\hat{N})}\} \tag{7.18}$$

7.2.a: First ON, $\alpha_1 = 50$

7.2.b: Second ON, $\alpha_2 = 1$

Figure 7.2: Projected grand potential surfaces for the model of Eq. (7.13) with $\alpha_1 = 50, \alpha_2 = 1, \beta_0 = 0.11$.

For a noninteracting Hamiltonian and a $\hat{\mathcal{B}}$ for which $[\hat{\mathcal{B}}, \hat{H}] = 0$ the Fermi Dirac relation reads

$$n_i = \frac{1}{e^{\beta_i(\varepsilon_i - \mu)} + 1} \tag{7.19}$$

$$\varepsilon_i - \mu = \frac{1}{\beta_i} \ln\left(\frac{1 - n_i}{n_i}\right), \tag{7.20}$$

where β_i denotes the i-th eigenvalue of $\hat{\mathcal{B}}$. This leads to the following expression for the grand potential

$$\Omega[\gamma] = \sum_i \left(n_i(\varepsilon_i - \mu) + \frac{1}{\beta_i}(n_i \ln n_i + (1 - n_i)\ln(1 - n_i)) \right) \tag{7.21}$$

$$= \sum_i \Omega_i[n_i, \beta_i]. \tag{7.22}$$

Where in the case of a scalar temperature we just had one parameter to construct our effective noninteracting system, we now have one for each ON. A straightformard utilization of this freedom would be to let the second derivatives of the energy functional with respect to the ONs of the interacting functional and the noninteracting one be proportional to each other, i.e.

$$\beta_i = \eta \frac{\partial^2 S_0[\gamma]}{\partial n_i^2} \bigg/ \frac{\partial^2 \Omega[\gamma]}{\partial n_i^2} \tag{7.23}$$

$$= \eta \frac{1}{n_i(1 - n_i)} \left(\frac{\partial^2 \Omega[\gamma]}{\partial n_i^2}\right)^{-1}, \tag{7.24}$$

where η, the proportionality factor, is the only global parameter. In our model (Eq. (7.13)), this yields

$$\beta_i = \frac{\eta}{\alpha_i} \frac{1}{n_i(1 - n_i)}. \tag{7.25}$$

$\eta = 1$ lets the second derivatives of interacting and noninteracting functional be equal whereas an increase (decrease) of η leads to a spreading (compression) of the noninteracting grand potential surface. As can be seen from Figure 7.3, with a good choice of η (in our model $\eta = 0.5$) one can reproduce the different grand potential surfaces simultaneously.
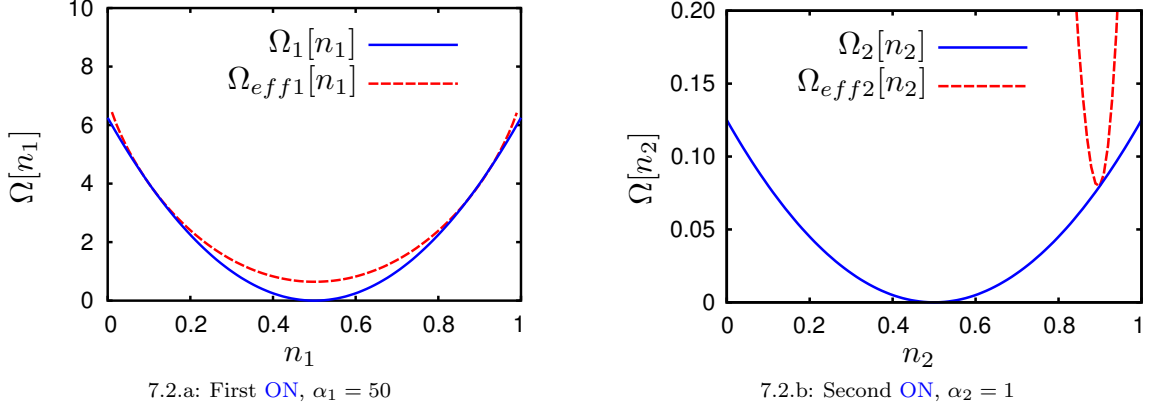
7.3.a: First ON, $\beta_0 = .5$

7.3.b: Second ON, $\beta_2 = 5.55$
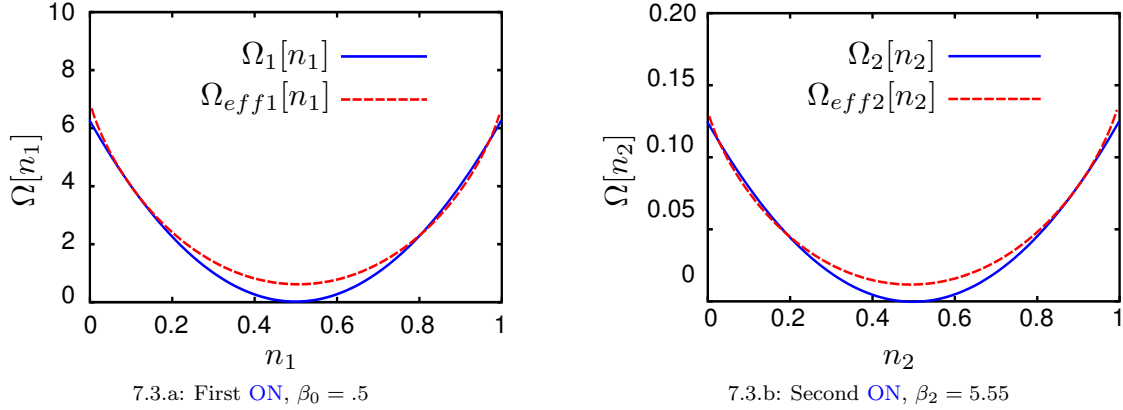
Figure 7.3: Projected grand potential surfaces for the model of Eq. (7.13) with $\alpha_1 = 50, \alpha_2 = 1$. The choice of $\eta = 0.5$ leads to $\beta_1 = 0.11$ and $\beta_2 = 5.55$.

We can now construct a self-consistent scheme for the minimization of $\Omega[\gamma]$ which we sketch in Figure 7.4. Every iteration of this scheme requires a change in NOs and therefore an update of the derivatives w.r.t. the NOs. This might prove to be expensive and one might be interested in a procedure which only minimizes the ONs and leaves the NOs invariant. Fortunately, the minimization scheme can easily be modified to accomplish this task. The effective Hamiltonian H^{eff} is simply assumed to be diagonal, i.e. one only populates the diagonal elements following Eq. (7.11). The eigenvalues, i.e. the diagonal elements, of H^{eff}, will then yield a new set of ONs via Eq. (7.19). Assigning the new ONs to the frozen orbitals is straightforward because a given ON n_i leads to a specific $\varepsilon_i' = h_{ii}^{eff}$ which in turn leads to an unambiguously defined n_i'. The last step in the minimization scheme, the mixing of 1RDMs, is straightforward, because Γ^N is a convex set.

7.4 Small step investigation

We showed in the previous considerations that one can employ the Kohn-Sham system in FT-RDMFT to construct a self-consistent minimization scheme. However, this does not ensure that an application of this scheme will actually lead to a minimum of the functional. This is a common problem of minimization schemes, but in the following we are going to show that for small step lengths our method will definitely lead to a decrease of the value of the functional under consideration. As we argued at the end of Section 7.2, choosing a smaller β_0 will lead to smaller changes in ONs and NOs. Starting from a given 1RDM γ, we therefore apply first-order perturbation theory to get the modified 1RDM γ'. By the virtue of Eq. (7.11), γ leads to the effective Hamiltonian $\hat{H}_{eff}$. A diagonalization under the assumptions of first-order perturbation theory then yields the following new eigenvalues ε_i' and eigenstates ϕ_i'.

$$\varepsilon_i' = h_{eff\ ii} \tag{7.26}$$

$$\phi_i'(x) = \phi_i(x) + \sum_{j \neq i} \frac{h_{eff\ ji}}{\varepsilon_i - \varepsilon_j} \phi_j(x) \tag{7.27}$$

The new ONs, resulting from our modified eigenenergies, become

$$n_i' = \frac{1}{1 + e^{\beta_i(\varepsilon_i' - \mu - \Delta_\mu)}}, \tag{7.28}$$

1.) diagonalize $\gamma^{(k)}(x,x') = \sum_i n_i^{(k)} \phi_i^{(k)*}(x') \phi_i^{(k)}(x)$

2.) from $\left\{ n_i^{(k)} \right\}$ and $\left\{ \phi_i^{(k)} \right\}$ calculate $\hat{H}_{eff}^{(k)}$ by Eq. (7.11)

3.) diagonalize $\hat{H}_{eff}^{(k)}$ to get a new set of $\left\{ \varepsilon_i^{(k+1)} \right\}$ and $\left\{ \phi_i^{(k+1)}(x) \right\}$

4.) construct $\left\{ n_i^{(k+1)} \right\}$ using Eq. (7.20) and find $\mu_0^{(k+1)}$ so that $\sum_i n_i^{(k+1)} = N$

5.) from $\left\{ \phi_i^{(k+1)}(x) \right\}$ and $\left\{ n_i^{(k+1)} \right\}$ build new 1RDM $\tilde{\gamma}(x,x')$

6.) mixing of $\tilde{\gamma}(x,x')$ with $\gamma^{(k)}(x,x')$ yields $\gamma^{(k+1)}(x,x')$
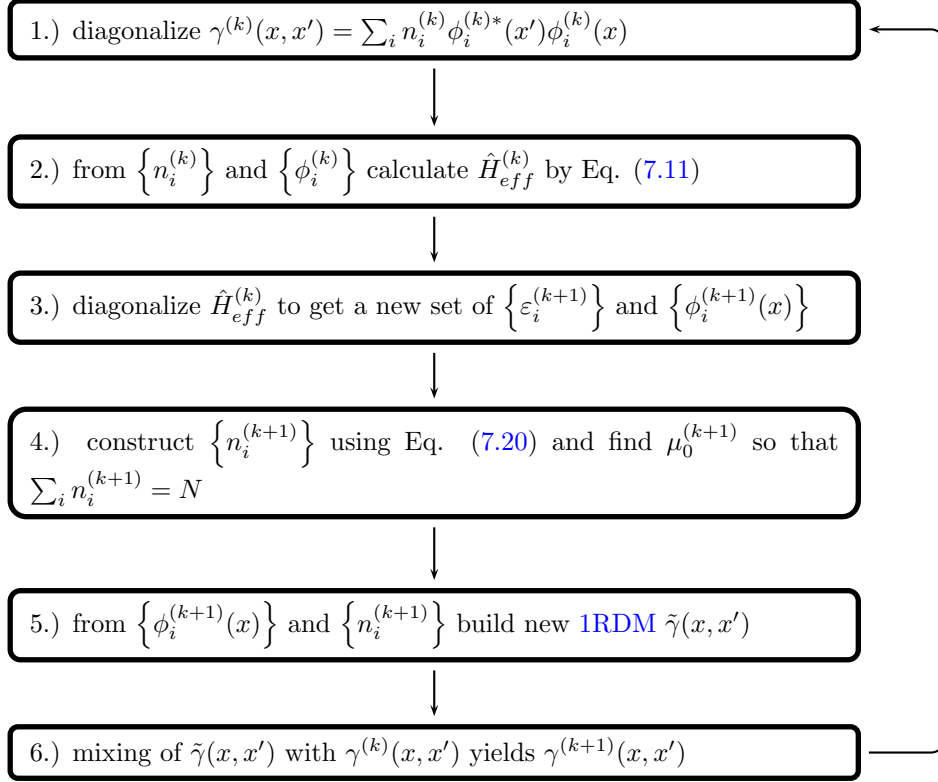
Figure 7.4: Self-consistent minimization scheme in FT-RDMFT

where one had to introduce the chemical potential correction Δ_μ to ensure particle number conservation. With Eq. (7.12) one gets

$$n_i' = \frac{n_i}{n_i + (1-n_i)e^{\beta_i\left(\frac{\partial\Omega}{\partial n_i} - \Delta_\mu\right)}}. \tag{7.29}$$

Expanding Δ_μ in orders of β_i and subsequently Eq. (7.29) for small β_i, we get

$$\delta n_i = n_i' - n_i \tag{7.30}$$

$$= \beta_i n_i(n_i - 1)\left(\frac{\partial\Omega[\gamma]}{\partial n_i} - \Delta_\mu^{(0)}\right). \tag{7.31}$$

This result is very similar to the steepest-descent method with an additional factor of $n_i(n_i - 1)$. This additional term tries to keep the ONs in the allowed set $0 < n_i < 1$. $\Delta_\mu^{(0)}$ can now be found by the requirement of particle number conservation:

$$\Delta_\mu^{(0)} = \frac{\sum_i \beta_i n_i(n_i - 1)\frac{\partial\Omega[\gamma]}{\partial n_i}}{\sum_i \beta_i n_i(n_i - 1)}. \tag{7.32}$$

The overall change in the 1RDM up to first order in β_i is then given by

$$\Delta\gamma_{ij} = \gamma'_{ij} - \delta_{ij}n_i \tag{7.33}$$

$$= \delta_{ij}\delta n_i + (1 - \delta_{ij})\frac{n_i - n_j}{\varepsilon_i - \varepsilon_j}h_{eff\ ij}. \tag{7.34}$$

The grand potential changes accordingly as

$$\Delta\Omega = \int dxdx' \frac{\delta\Omega[\gamma]}{\delta\gamma(x,x')}\Delta\gamma(x',x) \tag{7.35}$$

$$= \sum_{ij} \frac{\delta\Omega[\gamma]}{\delta\gamma_{ij}}\Delta\gamma_{ji} \tag{7.36}$$

$$= \underbrace{\sum_i \delta n_i \frac{\partial\Omega[\gamma]}{\partial n_i}}_{\Delta\Omega_1} + \underbrace{\sum_{i \neq j} \frac{n_i - n_j}{\varepsilon_i - \varepsilon_j}|h_{eff\ ij}|^2}_{\Delta\Omega_2}. \tag{7.37}$$

We see that the grand potential change $\Delta\Omega$ separates into two parts. $\Delta\Omega_1$ determined by the change in ONs, and $\Delta\Omega_2$ coming from the change in NOs. In the following we are going to investigate these two different contributions separately.

7.4.1   Occupation number (ON) contribution

We will now show that the first term in Eq. (7.37), which is due to the change in ONs, is always negative for appropriately small step lengths.

$$\Delta\Omega_1 := \sum_i \delta n_i \frac{\partial\Omega[\gamma]}{\partial n_i} \tag{7.38}$$

$$= \sum_i \beta_i n_i(n_i - 1)\left(\frac{\partial\Omega[\gamma]}{\partial n_i} - \Delta_\mu^{(0)}\right)\frac{\partial\Omega[\gamma]}{\partial n_i} \tag{7.39}$$

$$= \sum_i \beta_i n_i(n_i - 1)\left(\frac{\partial\Omega[\gamma]}{\partial n_i}\right)^2 - \frac{\left(\sum_i \beta_i n_i(n_i - 1)\frac{\partial\Omega[\gamma]}{\partial n_i}\right)^2}{\sum_i \beta_i n_i(n_i - 1)} \tag{7.40}$$

For brevity, we introduce $c_i = \frac{\beta_i n_i(n_i-1)}{\sum_i \beta_i n_i(n_i-1)}$, which leads to

$$\Delta\Omega_1 = \left(\sum_j \beta_j n_j(n_j - 1)\right)\sum_i c_i\left(\left(\frac{\partial\Omega[\gamma]}{\partial n_i}\right)^2 - \left(\sum_k c_k \frac{\partial\Omega[\gamma]}{\partial n_k}\right)^2\right) \tag{7.41}$$

$$= \left(\sum_j \beta_j n_j(n_j - 1)\right)\sum_i c_i\left(\frac{\partial\Omega[\gamma]}{\partial n_i} - \sum_k c_k \frac{\partial\Omega[\gamma]}{\partial n_k}\right)^2. \tag{7.42}$$

Because every ON n_i fulfills $0 < n_i < 1$ and every β_i is greater 0, this leads to the conclusion

$$\Delta\Omega_1 \leq 0. \tag{7.43}$$

7.4.2   Natural orbital (NO) contribution

We can now turn to the second term in Eq. (7.37) which represents the functional change due to the change in NOs.

$$\Delta\Omega_2 = \sum_{i \neq j} \frac{n_i - n_j}{\varepsilon_i - \varepsilon_j}|h_{eff\ ij}|^2 \tag{7.44}$$

By using Eq. (7.20) this transforms to

$$\Delta\Omega_2 = \sum_{i \neq j} \frac{n_i - n_j}{\frac{1}{\beta_i} \ln\left(\frac{1-n_i}{n_i}\right) - \frac{1}{\beta_j} \ln\left(\frac{1-n_j}{n_j}\right)} |h_{eff\ ij}|^2. \tag{7.45}$$

We see that for an arbitrary choice of β_i, we cannot ensure the negativity of $\Delta\Omega_2$. But if we use a constant β_0, we get

$$\Delta\Omega_2 = \beta_0 \sum_{i \neq j} \frac{n_i - n_j}{\ln\left(\frac{n_j(1-n_i)}{n_i(1-n_j)}\right)} |h_{eff\ ij}|^2, \tag{7.46}$$

which is nonpositive.

$$\Delta\Omega_2 \leq 0 \tag{7.47}$$

We have shown that for small enough β_i, the ON change will always decrease the grand potential, regardless of whether one chooses a constant temperature or a temperature tensor. When considering changes in the NOs, one has to fall back to constant temperature to ensure a decrease of the functional value.

7.5 Convergence measures

We have now all the necessary tools at hand to iteratively minimize a functional $\Omega[\gamma]$. We need, however, some measures to judge if a calculation is converged. There are two main reasons why using the grand potential itself as convergence measure is disadvantageous.

Firstly, often the calculation of derivatives is not accurate and consequently a derivative-based minimization may lead to a fixpoint where $\Omega[\gamma]$ is not minimal. This leads to a sign change of the convergence measure and implementing the strict decrease of grand potential as a requirement of the minimization procedure will then lead to a result depending on the starting point. To illustrate this problem we consider a simple parabola $\Omega(x) = ax^2$ whose minimum is at $x = 0$. Let us now assume that the calculation of the derivative is only approximate and leads to a constant error δ. The derivatives then do not describe the surface given by $\Omega(x)$ but rather one defined by $\bar{\Omega}(x) = ax^2 + \delta x$ whose minimum will be at $\bar{x} = -d/(2a)$. If one would now approach this minimum coming from the left with a series of positions $\{x_i\}$, then $\Omega(x_i)$ will be monotonously decreasing. At the point of convergence its value will be $\Omega(\bar{x}) = d^2/(4a)$. If, on the other hand, we would have approached the minimum coming from the right, i.e. starting at $x = \infty$, then we would have passed through the minimum of $\Omega(x)$ and the series $\Omega(x_i)$ would exhibit a valley. Incorporating the grand potential $\Omega(x)$, or rather the change in grand potential, as convergence measure would therefore prevent the minimization to approach the true minimum of $\bar{\Omega}(x)$ and lead to two different points of convergence, depending on the starting position.

Secondly, because the true minimal grand potential is not known, one would have to judge convergence from the change in $\Omega[\gamma]$ after iterating the minimization routine, i.e. a small change in $\Omega[\gamma]$ indicates a relative closeness to the real minimum. This might pose a problem if the minimum of the grand potential surface, as defined by the derivatives of $\Omega[\gamma]$, is very shallow or, worse, if the minimization procedure leads to a slow approach to the minimum. An example for such a situation is discussed in Section 7.6.3.

Because of these problems, we would rather use a strictly positive convergence measure which goes to 0 if the 1RDM approaches the minimum of the grand potential surface, as defined by the derivatives of $\Omega[\gamma]$. We will establish our choice of convergence measures on the following two observations.

- In the minimum, the derivatives with respect to the ONs will be equal for unpinned states.

- In the minimum, the effective Hamiltonian $\hat{H}_{eff}$ will be diagonal.

The first observation allows us to define a convergence measure χ_n^2 for a minimization with respect to the ONs.

$$\chi_n^2 = \frac{1}{N_{unpinned}} \sum_i^{N_{unpinned}} \left(\frac{\partial \Omega}{\partial n_i} - \mu \right)^2 \tag{7.48}$$

$$\mu = \frac{1}{N_{unpinned}} \sum_i^{N_{unpinned}} \frac{\partial \Omega}{\partial n_i} \tag{7.49}$$

The second statement leads to the following definition of χ_ϕ^2 as a convergence measure for a minimization with respect to the NOs.

$$\chi_\phi^2 = \frac{1}{N-1} \frac{\sum_{i \neq j}^N |h_{eff\ ij}|^2}{\sum_i \varepsilon_i^2} \tag{7.50}$$

If a minimization is converging, both measures should approach 0.

7.6 Sample calculations

We test the self-consistent procedure for the case of solid LiH at zero temperature by using the FP-LAPW code Elk [107]. The exchange-correlation energy will be modelled by the α functional $E_{xc}^\alpha[\gamma]$, as defined in Section 3.1.1.

$$E_{xc}^\alpha[\gamma] = -\frac{1}{2} \sum_{ij} n_i^\alpha n_j^\alpha \int dx dx' w(x,x') \phi_i^*(x') \phi_i(x) \phi_j^*(x) \phi_j(x') \tag{7.51}$$

We choose this functional because it exhibits several properties making it difficult to be minimized. As in the case of the HEG in Section 3.2, it will lead to several fully occupied, i.e. pinned states. These lie on the boundary of the domain of the effective grand potential functional $\Omega_{eff}[\gamma]$. The minimization of the α functional is therefore a good test for the minimization scheme leading to boundary minima. Furthermore, the α functional exhibits divergencies in the derivatives w.r.t. the ONs for $n_i \to 0$. If, in the minimum, there will be ONs close to 0 (and there will be if one considers enough NOs) this might lead to convergence problems of the minimization. We will now investigate the performance of the self-consistent minimization scheme w.r.t. ON- and NO-convergence.

7.6.1 Occupation number (ON) minimization

We have minimized the α functional for $\alpha = 0.565$ with three methods. First we used the steepest-descent method, as implemented in Elk, then we used the self-consistent FT-RDMFT minimization with constant β_0, and finally we used a temperature tensor β_i of the form of Eq. (7.24) with parameter η. In all three methods, we chose all parameters to achieve fastest convergence. The results, which are shown in Figures 7.5.a-7.5.f, show that both self-consistent minimizations lead to a faster convergence than steepest-descent. A dramatic increase in the speed of convergence is then achieved by employing a temperature tensor. The slow decrease of χ_n^2 in Figures 7.5.d and 7.5.f for the steepest-descent- and constant β_0-methods can be attributed to the following fact. For these two methods, the ONs, which will be pinned at the equilibrium, approach their final values quite slowly. Therefore, their derivatives contribute to χ_n^2 via Eq. (7.48) even after several iterations.

7.5.a: Energy: 1 k-point

7.5.b: ON-Variance: 1 k-point

7.5.c: Energy: 2x2x2 k-points

7.5.d: ON-Variance: 2x2x2 k-points

7.5.e: Energy: 3x3x3 k-points

7.5.f: ON-Variance: 3x3x3 k-points
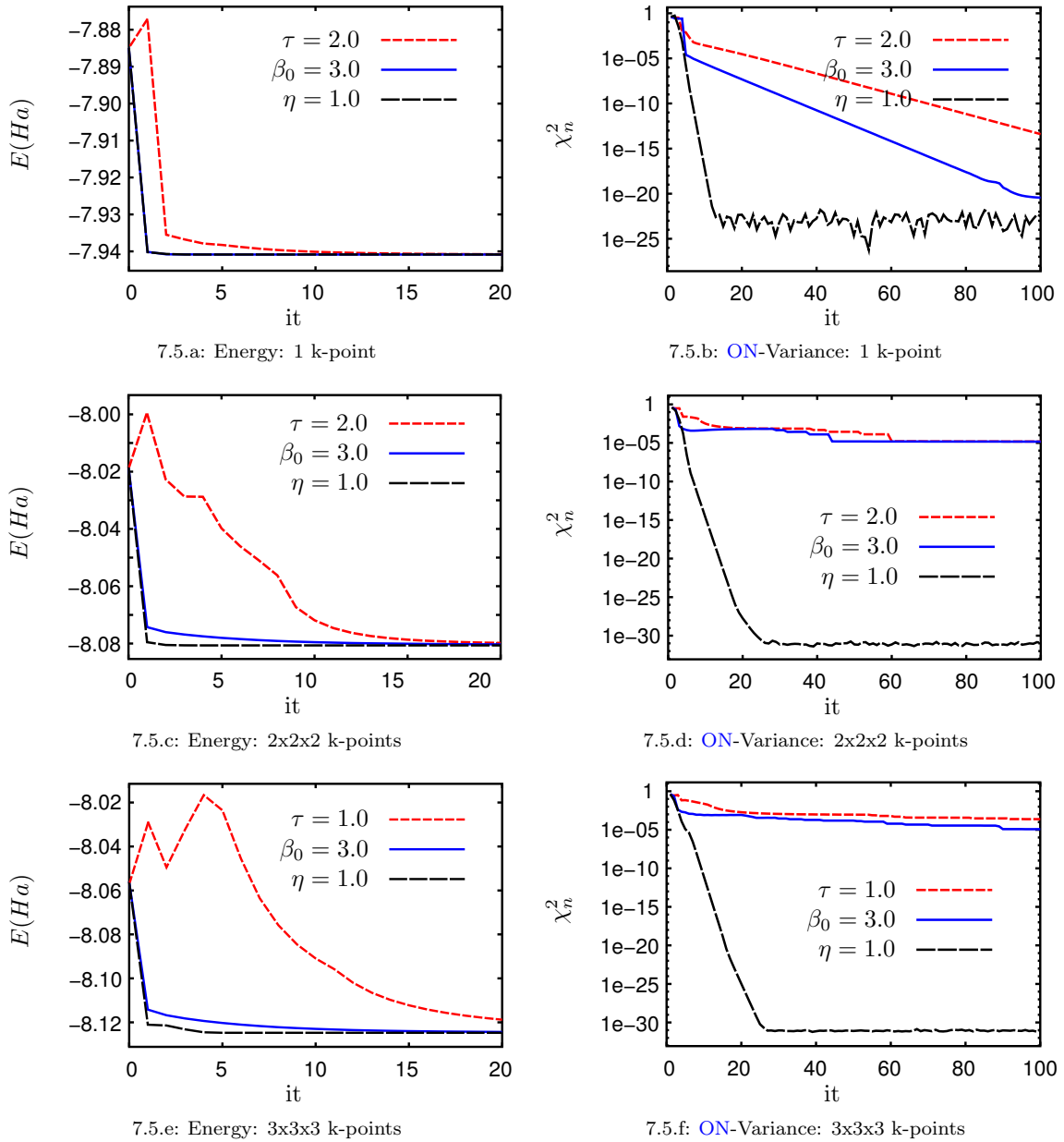
Figure 7.5: Energy E and ON-convergence measure χ_n for ON minimizations of the α functional, with $\alpha = 0.565$, applied to LiH. The red, short dashed lines stand for a steepest-descent minimization, the blue, solid ones for a sc-Kohn-Sham minimization with constant β_0, and the black, long dashed ones for a sc-Kohn-Sham minimization with adaptive β_i. τ denotes the value for he parameter "*taurdmn*" in Elk, whereas β_0 and η are defined via Eqs. (7.2) and (7.23).

7.6.2 Full minimization

We can now turn to the problem of minimizing $E[\gamma]$ with respect to both ONs and NOs. We find that the overall performance of this full minimization is greatly improved by introducing a ON-minimization after every NO-minimization step (see Figure 7.4). Because we have seen in the previous section that this can be done very efficiently and effectively, this increases the runtime of a full minimization run only negligibly. The deeper reason for the improvement of the convergence by inclusion of an ON-minimization is the following. It might happen that two states ϕ_i and ϕ_j have similar eigenvalues in $\hat{H}_{eff}$ but considerably different ONs. A diagonalisation of $\hat{H}_{eff}$ might then yield a strong mixing between these states. If the ONs were not updated, one might be led away from the minimum of the energy functional. A subsequent ON-minimization remedies this problem and assigns the optimal ON for each NO. We show a sketch of the full minimization scheme in Figure 7.6. An application of this scheme to LiH then leads to the results depicted in Figure 7.7. Again, we see a tremendous increase in speed and accuracy for the self-consistent minimization scheme compared to the steepest-descent method. The steepest-descent method shows a very slow convergence, which can be attributed to the orthonormalization of NOs. Furthermore, the increase of the energy curves in Figures 7.7.c and 7.7.e is due to the approximative nature of the derivatives. As we have pointed out before, the minimization procedure is only guided by the values of the derivatives (see Eq. (7.11)) and it will not minimize the energy surface defined by $E[\gamma]$ but rather one defined by the approximate derivatives. Coincidentally, the starting point for the minimization of $E[\gamma]$, as shown in Figure 7.6, leads to a path to the minimum of the approximate energy surface which leads through a part of the exact surface which has a lower value. Coming from another starting point this would not necessarily have been the case. This starting point dependence always exists if the derivatives are approximate which solidifies the argument that the energy should not be used as convergence measure.
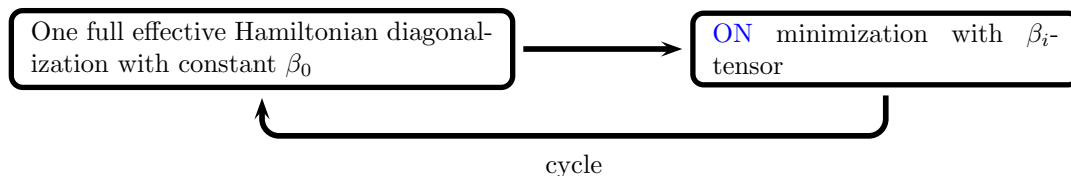
Figure 7.6: Full minimization scheme

7.7.a: Energy: 1 k-point

7.7.b: NO-Variance: 1 k-point

7.7.c: Energy: 2x2x2 k-points

7.7.d: NO-Variance: 2x2x2 k-points

7.7.e: Energy: 3x3x3 k-points

7.7.f: NO-Variance: 3x3x3 k-points
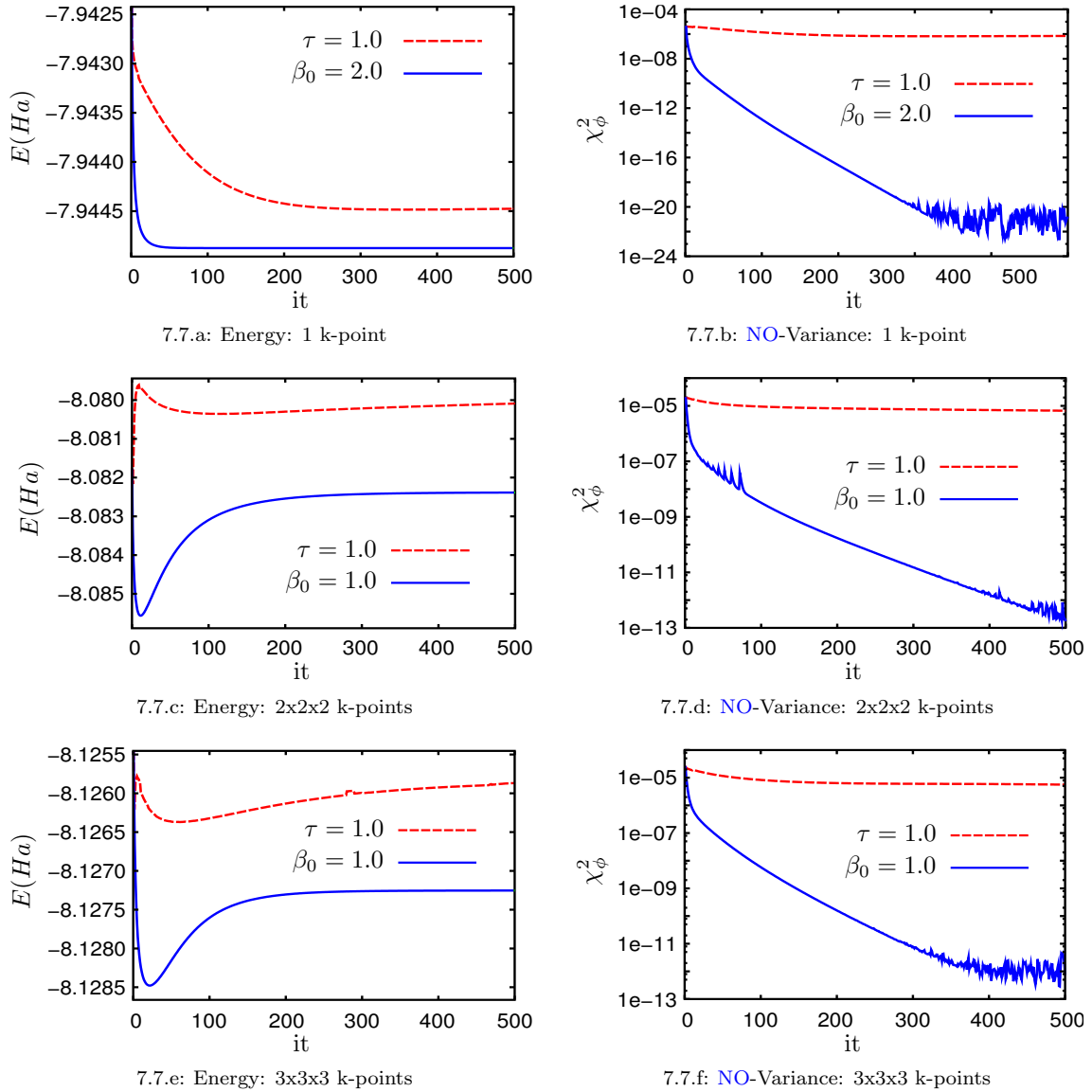
Figure 7.7: Energy E and NO-convergence measure χ_ϕ for NO minimizations of the α functional, with $\alpha = 0.565$ applied to LiH. Both variables are plotted against the number of NO changes. After each change in NO there follows a complete ON minimization. The red, dashed lines stand for a steepest-descent minimization whereas the blue, solid ones depict a sc-Kohn-Sham minimization with constant β_0. τ denotes the parameter value for *taurdmc* in Elk, whereas β_0 is defined via Eq. (7.2).

7.8.a: Energy: 3x3x3 k-points   7.8.b: NO-Variance: 3x3x3 k-points
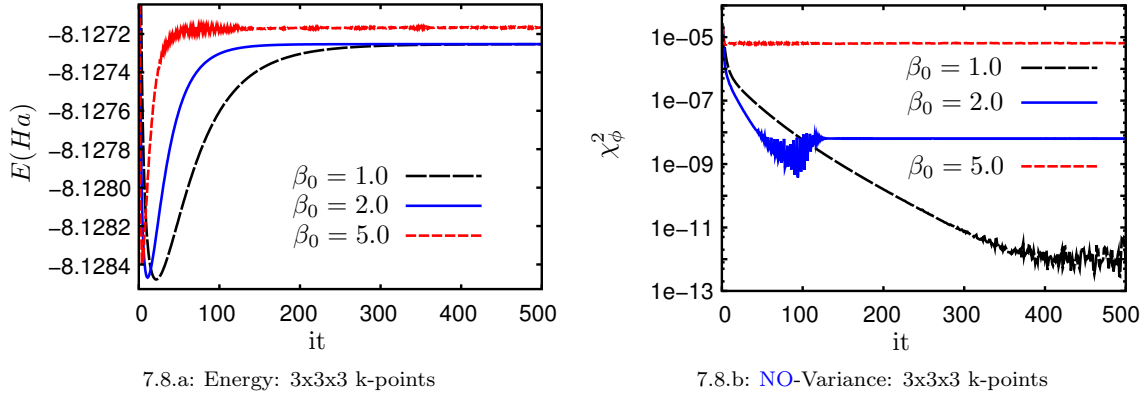
Figure 7.8: NO-convergence for different effective temperatures.

7.6.3 Summary and outlook

In this section, we introduced a self-consistent minimization scheme in the theoretical framework of FT-RDMFT. We then defined measures which allow us to judge the convergence of a calculation without having to resort to the energy. This was necessary because the numerical derivatives are usually not accurate enough. We could show that this self-consistent procedure is superior in many aspects compared to the steepest-descent method, especially considering a minimization w.r.t. the NOs. The important parameter in the minimization scheme is the effective temperature β_0 and the speed of convergence crucially depends on it. In Figure 7.8 we show the behaviour of the minimization scheme for three different choices of β_0. $\beta_0 = 1$ represents the optimal value, i.e. the value for which the convergence measure χ^2_ϕ decreases the fastest. We see that the energy reaches its fixpoint after approximately 300 iterations. An increase of β_0 to $\beta_0 = 2$ seemingly speeds up the energy convergence, but from χ^2_ϕ one can see that after about 100 iterations the minimization fails to diagonalize h_{eff} any further. The changes in the 1RDM, whose amplitudes are determined by β_0, become too big and the 1RDM jumps around the fixpoint of the energy. Without considering χ^2_ϕ, this would have been difficult to detect, which illustrates the importance of a convergence measure which is independent of the energy value. One might argue that this choice of β_0 still leads to a fixpoint very close to the optimal one, but this cannot be ensured for all problems and all choices of β_0 and therefore has to be seen in the actual example as rather accidental, i.e. fortunate. A further increase of β_0 to $\beta_0 = 5$ then exposes this problem more clearly. The energy apparently reaches a fixpoint. But this fixpoint is considerably above the optimal one. Just having the energy at hand, this might have been difficult to detect. But χ^2_ϕ directly shows that the minimization is far from being converged.

One important feature, which can be extracted from Figure 7.8, is that all three parameters lead to a similar energy vs. iteration curve. Apparently, a minimization-run with β_0 being too big is able to lead to the vicinity of the fixpoint. A utilization of this fact would now be to use an adaptive β_0 rather than a constant one. One could start with a big β_0 till the energy does not change anymore and than decrease β_0 until χ^2_ϕ surpasses the convergence threshold.

8 Applications

The initial success of DFT can be attributed mainly to the remarkable performance of the LDA. As pointed out in Section 3.2, a similar formulation in the framework of RDMFT is complicated by the fact that one would have to consider a HEG subject to nonlocal external potentials. This is in principle possible via Monte-Carlo techniques, but it has not been carried out so far. The testing of RDMFT functionals could therefore only be done for HEGs with local external potentials. In grand canonical ensembles the situation becomes even worse. The calculation of the exact equilibrium grand potential of a HEG at finite temperature is in principle possible via the method of Path integral Monte-Carlo. However, the fermion sign problem renders these calculations extremely difficult and expensive at low temperatures [80]. Therefore, to the best of our knowledge, there exists no parametrization of the equilibrium grand potential or free energy of a HEG at finite temperature. Accordingly, one has to resort to the description of grand canonical systems by approximate means. There exists wide variety of different approaches to accomplish this task. These include the introduction of approximate model interactions [85, 110], the utilization of the dielectric formulation (employing various approximations, including the hypernetted chain approximation [19, 111], the modified convolution approximation [112, 113] and the equation-of-motion approach of Singwi, Tosi, Land and Sjölander [114, 115, 116]), the mapping of quantum systems to classical systems at finite temperature [20, 117], and the utilization of FT-MBPT, including non-diagrammatic local field corrections to the RPA [118, 119, 120, 121, 122, 123, 124]. Because there are no exact results, a quantitative testing of approximate FT-RDMFT functionals is not possible. However, one can still investigate their qualitative behaviour. Because we will be interested in magnetic phase transitions, we will focus on the qualitatively correct description of the phase diagram of the HEG. We will structure the remainder of this section as follows:

Section	Description
8.1	We will start with a short clarification of the nomenclature used concerning phase transitions and phase diagrams.
8.2	We will then investigate the HEG, replacing the Coulomb interaction by a contact interaction. We will calculate the phase diagram and discuss shortcomings of this approximation.
8.3	As a second approach, we will review how standard FT-MBPT approaches the problem, correcting preliminary results by [119] and calculating the magnetic phase diagram of the HEG in collinear spin configuration.
8.4	Subsequently, we will incorporate our novel approach of FT-RDMFT. Using the first-order/exchange-only functional we will calculate the magnetic phase diagram for both collinear spin configuration as well as planar spin spiral states.
8.5	Using the equivalence of the first-order FT-RDMFT functional with FT-HF theory, we will investigate the temperature dependence of the quasi-particle spectrum for both collinear and spin spiral configurations.
8.6	Closing, we will focus on the problem of the description of correlation effects. Starting with the inclusion of correlation functionals from DFT we will proceed to employ phenomenological correlation functionals from RDMFT at zero temperature. Subsequently, we will incoporate the perturbative methodology as derived in Section 6.2 and show that a straightforward utilization might lead to the problem of variational collapse. Finally, we will present a procedure to avoid this collapse, utilizing exact properties of the finite temperature polarization propagator.

Related publications: [125, 56]

8.1 Magnetic phase transitions in the HEG

In this section, eventually we want to test FT-RDMFT applied to the HEG. In particular, we want to calculate the free energy magnetic phase diagram. This, however, needs some clarification. In the development of FT-RDMFT in Section 4, we explicitly considered grand canonical ensembles. There were two main reasons for this restriction. The first one concerns the Kohn-Sham system for canonical ensembles. From Section 4.5 we know that the set of eq-V-representable 1RDMs also in the case of canonical ensembles lies dense in the set of ensemble-N-representable 1RDMs. However, it is not clear, how one could recover the Kohn-Sham potential from a given 1RDM. The inversion in Eq. (4.53) is valid only for grand canonical ensembles. The second reason was that the FT-MBPT is also defined only for grand canonical ensembles. A formulation of a FT-MBPT for canonical ensembles breaks down in the proof of the corresponding Wick's theorem. This proof explicitly requires that the traces involved are defined on the full Fock space and not just on an N-particle Hilbert space. This does not disprove the possibility of a perturbation theory for canonical ensembles. It just shows that the methods derived for grand canonical ensembles cannot be translated easily. Accordingly, the variational principle refers to the grand potential rather than the free energy of the system. We therefore have to assume that the system is in the thermodynamic limit, which will allow us to calculate the canonical free energy $F^{c.}$ from the grand canonical $\Omega^{g.c.}$ grand potential as

$$F^{c.} = \Omega^{g.c.} + \mu N. \tag{8.1}$$

However, in the case of small finite systems embedded in a temperature bath, this assumption need not be valid and might be a source of possible deviations between calculations and measurements, requiring further investigation [126].

The phase diagram is now constructed by calculation and comparison of free energies of different phases. When considering phase transitions we will use a terminology in the spirit of Ehrenfests characterization, i.e. if the derivative of the free energy changes discontinuously w.r.t. a certain order parameter, then we call it a first-order phase transition. If on the other hand it changes continuously, then we call it a second-order phase transition. In Figure 8.1 we show an example coming from the first-order functional of FT-RDMFT as discussed later in Section 8.4. Therein we assumed a collinear spin configuration where the polarization ξ_{eq} of the eq-state is the order parameter. We then calculated the free energy for various values of the Wigner-Seitz radius r_s and the polarization ξ. We denote the minimal free energy for fixed density by the thick black line. We see that with an increase of r_s we first encounter a first-order phase transition between the unpolarized and the polarized state. Increasing r_s even further will ulimately lead to a second-order phase transition back to the unpolarized state.

Although the exact magnetic phase diagram of the HEG in collinear spin configuration is not known, we can still derive general properties of it from the following considerations. Let us first consider the zero-temperature case. In collinear configuration, we expect that the kinetic energy favours an unpolarized gs. This is due to the fact that the kinetic energy operator in Eq. (2.2) is a spin-independent one-particle operator. An eigenstate to the kinetic energy operator of spin character $\uparrow$ will therefore yield the same energy expectation value as the corresponding $\downarrow$-state. We now assume that the states $\psi_{i\sigma}$ are ordered w.r.t. their kinetic energy expectation values. If now $\psi_{0\uparrow}$ is occupied we see from the previous considerations that it is favourable to occupy $\psi_{0\downarrow}$ next, rather than $\psi_{1\uparrow}$. The same argument extends to all spin-independent one-particle Hamiltonians. The interaction on the other hand corresponds to a two-particle operator (see Eq.(2.4)). We are concerned with the Coulomb interaction whose spatial representation reads $w(x, x') = 1/|\boldsymbol{r} - \boldsymbol{r}'|$. Because of the divergence of the interaction for $\boldsymbol{r} \to \boldsymbol{r}'$ one can now argue that the interaction yields a big energy contribution if the different wavefunctions have a big spatial overlap. The two states $\psi_{i\uparrow}$ and $\psi_{i\downarrow}$ have maximal spatial overlap and it is therefore resonable to state that the Coulomb interaction generally favours a polarized configuration. The explicit form of the kinetic energy leads to an approximate r_s^{-2} dependence. To estimate the density dependence of the Coulomb interaction, we can, as a first step, consider a classical system. With the inclusion of an appropriate background
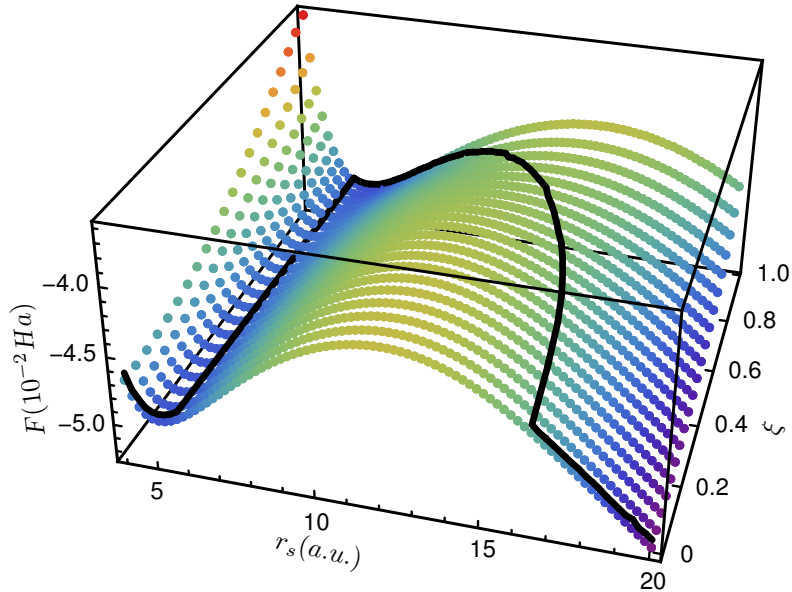
Figure 8.1: Free energy w.r.t. the polarization ξ and r_s at $T = 5000K$ from the first-order FT-RDMFT functional. The black line denotes the equilibrium free energy for a fixed r_s. At $r_s \approx 5.8 a.u.$ a first-order phase transition between paramagnetic and ferromagnetic phases takes place. An increase in r_s then leads to a second-order phase transition back to the paramagnetic state.

charge, we can then deduce from the form of $w(x, x')$ that it shows an r_s^{-1} behaviour, which is also the leading term in the quantum case. For an increase of r_s, we therefore expect a magnetic phase transition at a critical density r_c between an unpolarized configuration and a polarized one. The nature of this phase transition cannot be determined by the previous simple arguments and has to be investigated in detail. Monte-Carlo calculations confirm the previous considerations, suggesting a continuous phase transition at a critical Wigner-Seitz radius of around $r_c \approx 60 a.u.$ ([48]:$r_c \approx 75 a.u.$, [85]:$r_c \approx 50 a.u.$).

We can now investigate how the situation will change when the entropy, as defined in Eq. (4.3), is included. The entropy value is determined solely by the statistical weights w_i from Eq. (2.6).

$$S[\hat{D}] = \sum_i w_i \ln w_i \tag{8.2}$$

We have shown in Eq. (4.18) in Section 4.1.1 that $S[\hat{D}]$ is a convex functional of the SDO $\hat{D}$. This implies that generally the entropy favours a configuration where more states are occupied. In the unpolarized configuration, there are twice as many states to be occupied, compared to the polarized configuration, which leads to the conclusion that the entropy generally favours a paramagnetic configuration. As mentioned before, the entropy depends only on the statistical weights w_i and shows no explicit density dependence. Because of the r_s^{-2} and r_s^{-1} dependencies of the kinetic energy and the Coulomb interaction we expect the relative effect of entropy to be increased with increasing r_s. Furthermore, we expect the phase transitions to take place when the entropy contributions becomes comparable to the energy. The characteristic energy of a system is given by the Fermi energy ε_F and the corresponding Fermi temperature is $T_F = \varepsilon_F/k_B$ (see Eqs. (2.28) and (2.29)). Because the kinetic energy has less relative influence for bigger r_s we also expect that the phase transition from polarized to unpolarized configurations happens at larger relative temperatures $t = T/T_F$ for increasing r_s. We summarize our expectations in Table 8.1 and show a sketch of a generic phase

1. At zero temperature, with increasing r_s there will be a phase transition between unpolarized and polarized configurations.

2. The phase transition at zero temperature is continuous, i.e. of second order.

3. An increase in temperature will eventually favour an unpolarized state.

4. The effect of temperature is increased for increasing r_s, leading to a faster decrease of a polarized phase.

5. The phase transitions occur for temperatures comparable to the Fermi temperature T_F.

6. For increasing r_s the phase transition from polarized to unpolarized configurations occurs for higher values of the temperatures compared to the Fermi temperature T_F.

Table 8.1: General assumptions about behaviour of the phase diagram of the HEG in collinear configuration.

diagram fulfilling our conclusions in Figure 8.2. We should like to emphasize again that the previous considerations are rather general and the resulting assumptions are of qualitative nature. We do not claim that e.g. for small temperatures a slight increase in temperature might not lead to a favourisation of a phase which is more structured, as we will actually find out in Section 8.4.2, considering a spin spiral configuration.

In the remainder of this section, we will call an unpolarized state paramagnetic (PM) and a fully polarized collinear state ferromagnetic (FM). A partially polarized state will be denoted by the abbreviation PP. Furthermore, from now on we will consider energy densities, rather than total
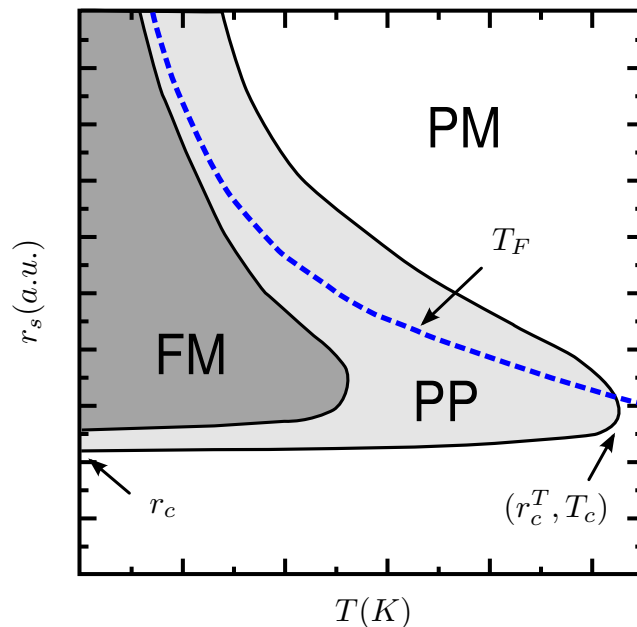

Figure 8.2: Expected qualitative behaviour of the phase diagram of the HEG in collinear configuration. FM: ferromagnetic phase, PM: paramagnetic phase, PP: partially polarized phase. The dotted blue line denotes the Fermi temperature T_F.

energies. Not to overload the notation we will denote these densities just as the total energies. I.e. Ω now refers to the grand potential density.

After these clarifications, we will now review previous approximations for the spin-dependent free energy of a HEG. The resulting phase diagrams will then be interpreted and qualitatively compared to the general expected properties as listed in Table 8.1 and shown in Figure 8.2.

8.2 Homogeneous electron gas with contact interaction

We assume a HEG in collinear spin configuration. The momentum distributions of the spin channels shall be denoted by $n_\sigma(\boldsymbol{k})$. The density n is then given by

$$n = \int \frac{d^3k}{(2\pi)^3}(n_\uparrow(\boldsymbol{k}) + n_\downarrow(\boldsymbol{k})). \tag{8.3}$$

The different contributions to the free energy density of a noninteracting system are given entirely in terms of the momentum distribution.

$$\Omega_{k\sigma} = \frac{1}{n}\int\frac{d^3k}{(2\pi)^3}\frac{k^2}{2}n_\sigma(\boldsymbol{k}) \tag{8.4}$$

$$\Omega_{ext\sigma} = \frac{1}{n}\int\frac{d^3k}{(2\pi)^3}n_\sigma(\boldsymbol{k})v_{ext\sigma}(\boldsymbol{k}) \tag{8.5}$$

$$n_\sigma = \frac{1}{n}\int\frac{d^3k}{(2\pi)^3}n_\sigma(\boldsymbol{k}) \tag{8.6}$$

$$S_{0\sigma} = -\frac{1}{n}\int\frac{d^3k}{(2\pi)^3}\left(n_\sigma(\boldsymbol{k})\ln n_\sigma(\boldsymbol{k}) + (1 - n_\sigma(\boldsymbol{k})\ln(1 - n_\sigma(\boldsymbol{k})))\right) \tag{8.7}$$

$$F = \sum_\sigma\left(\Omega_{k\sigma} + \Omega_{ext\sigma} - 1/\beta S_{0\sigma}\right) \tag{8.8}$$

As mentioned in Section 8.1, without interaction or external potential, the HEG will always be paramagnetic because kinetic energy as well as entropy favour this configuration.

One way to include interaction was proposed by Zong, Lin and Ceperley [85]. They argue that the interaction is sufficiently screened to be effectively modelled by a Stoner-type contact interaction. Taking account of the Pauli principle, this interaction explicitly couples only particles of opposite spin. Its spatial representation therefore behaves like

$$w^S(x, x') \propto (1 - \delta_{\sigma_1\sigma_2})\delta(\boldsymbol{r} - \boldsymbol{r}'). \tag{8.9}$$

At this point, we should like to point out some inconsistencies in the literature. In Eq. (8) of Ref. [85], the r_s-dependence of the interaction is denoted to be 2 orders higher than the one of the kinetic energy. This however would lead to the result that the interaction energy per particle would be density independent, just like the entropy. Furthermore, Ω_W^S is intrinsically favouring a spin-polarized state. Therefore, for big r_s, where the kinetic energy will be negligible, there will ultimately form a balance between the interaction and the entropy which will eventually lead to the unphysical result of a nonvanishing ferromagnetic phase. This is not shown in Figure 8 of Ref. [85] and we believe that Eq. (8) of that reference contains a typo. To get the correct density dependence of the contact interaction we use that the Coulomb interaction is $\propto r_s^{-1}$ whereas the δ-function is $\propto r_s^{-3}$. We therefore set

$$w^S(x, x') \propto r_s^2(1 - \delta_{\sigma_1\sigma_2})\delta(\boldsymbol{r} - \boldsymbol{r}'). \tag{8.10}$$

This interaction is now included as a first-order perturbation on top of the noninteracting HEG. Introducing the interaction strength parameter g, the interaction grand potential is then simply written with the help of the polarization ξ as

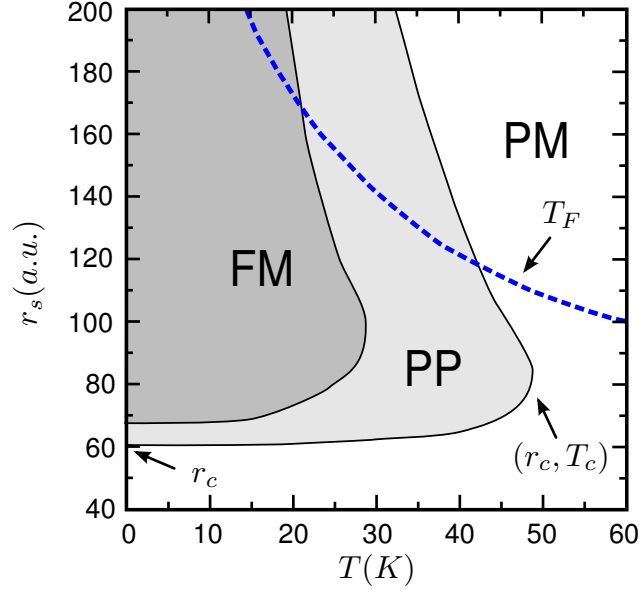$$\Omega_W^S = gr_s^{-1}(1 - \xi^2). \tag{8.11}$$

Figure 8.3: Collinear phase diagram of the HEG for a contact interaction. FM: ferromagnetic phase, PM: paramagnetic phase, PP: partially polarized phase. The dotted blue line denotes the Fermi temperature T_F.

If g is chosen big enough, there will be a ferromagnetic region in the phase diagram. The strength of the interaction is now determined by the requirement of the reproduction of the zero-temperature critical Wigner-Seitz radius $r_c \approx 60 a.u.$, which yields $g \approx 0.0102$. The resulting phase diagram is shown in Figure 8.3. We see that the simple Stoner model is capable of reproducing most of the exact properties from Table 8.1. However, the critical temperature T_c at r_c is too low compared to the Fermi temperature. In the following sections we are going to investigate if we can get a qualitatively better phase diagram by more eleborate theoretical means.

8.3 FT-MBPT

A different approach to the calculation of the phase diagram of the HEG employs FT-MBPT, a compact review of which can be found e.g. in [104] or [127]. We will restate the expression for the noninteracting free energy F_0:

$$F_0 = \Omega_k - 1/\beta S_0. \tag{8.12}$$

The kinetic energy and entropy contributions are given in Eqs. (8.4) and (8.7). The momentum distribution in FT-MBPT is given by the Fermi distribution of the noninteracting system.

$$n(\boldsymbol{k}) = \frac{1}{1 + e^{\beta(\varepsilon(\boldsymbol{k}) - \mu)}} \tag{8.13}$$

$$\varepsilon(\boldsymbol{k}) = \frac{k^2}{2} \tag{8.14}$$

It is justified to assume that most of the interesting physical properties of a metallic system are mainly determined by the behaviour at the Fermi surface. It will therefore prove to be helpful to work with reduced variables for temperature and momentum.

$$t = \frac{T}{T_F} \quad , \quad \underline{\boldsymbol{k}} = \frac{\boldsymbol{k}}{k_F} \tag{8.15}$$

The polarization-dependent quantities are given by

$$t_\sigma = t(1 \pm \xi)^{-\frac{2}{3}} \quad , \quad \underline{\boldsymbol{k}}_\sigma = \underline{\boldsymbol{k}}(1 \pm \xi)^{-\frac{1}{3}}. \tag{8.16}$$

Under these transformations, the momentum distribution becomes

$$n_\sigma(\underline{\boldsymbol{k}}) = \frac{1}{1 + e^{\underline{k}^2/t - \alpha(t_\sigma)}}, \tag{8.17}$$

where the fugacity $\alpha = \beta\mu$ only depends on the reduced temperature t rather than on both T and k_F separately [128] and is determined by the following equation.

$$\frac{2}{3}t^{-\frac{3}{2}} = \int_0^\infty dx \frac{\sqrt{x}}{1 + e^{x - \alpha}} \tag{8.18}$$

A further simplification can be achieved by the introduction of the Fermi-Dirac integrals $F_j(x)$ [129].

$$F_j(x) = \frac{1}{\Gamma(j+1)} \int_0^\infty dz \frac{z^j}{1 + e^{z - x}} \tag{8.19}$$

Together with the reduced variables, they allow the noninteracting contributions to the free energy to be written in a more compact form.

$$n_\sigma = \frac{3}{8}\pi^{\frac{1}{2}} t^{\frac{3}{2}} F_{\frac{1}{2}}(\alpha_\sigma) \tag{8.20}$$

$$E_{k\sigma} = \frac{9}{32}\pi^{\frac{1}{2}} k_F^2 t^{\frac{5}{2}} F_{\frac{3}{2}}(\alpha_\sigma) \tag{8.21}$$

$$\mu_\sigma = \frac{1}{2}k_F^2 t \alpha_\sigma \tag{8.22}$$

$$S_{0\sigma} = \left(\frac{15}{16}\pi^{\frac{1}{2}} t^{\frac{3}{2}} F_{\frac{3}{2}}(\alpha_\sigma) - \alpha_\sigma n_\sigma \right) \tag{8.23}$$

Relation (8.18) then becomes

$$\frac{4}{3}\pi^{-\frac{1}{2}} t_\sigma^{-\frac{3}{2}} = F_{\frac{1}{2}}(\alpha_\sigma). \tag{8.24}$$

The Fermi-Dirac integrals, or the closely related Polylogarithms, are included in most modern numerical libraries (e.g. GSL [130]). This makes the calculation of the noninteracting contributions to the free energy very efficient. We can now investigate the effect of the inclusion of different diagrams from FT-MBPT.

8.3.1 Exchange-only

Including the first-order diagram leads to the following expression for the free energy:

$$F = F_0 + \int_0^1 \frac{d\lambda}{\lambda} \underbrace{}_{\to \Omega_x} \tag{8.25}$$

$$= \Omega_k - 1/\beta S_0 + \Omega_x. \tag{8.26}$$

The exchange diagram is linear in the coupling constant λ and we can therefore drop the integration. The exchange contribution of spin channel σ to the free energy is then given as

$$\Omega_{x\sigma} = -\frac{1}{n} \int \frac{d^3 k}{(2\pi)^3} \frac{d^3 q}{(2\pi)^3} W(\boldsymbol{k} - \boldsymbol{q}) n_\sigma(\boldsymbol{k}) n_\sigma(\boldsymbol{q}), \tag{8.27}$$
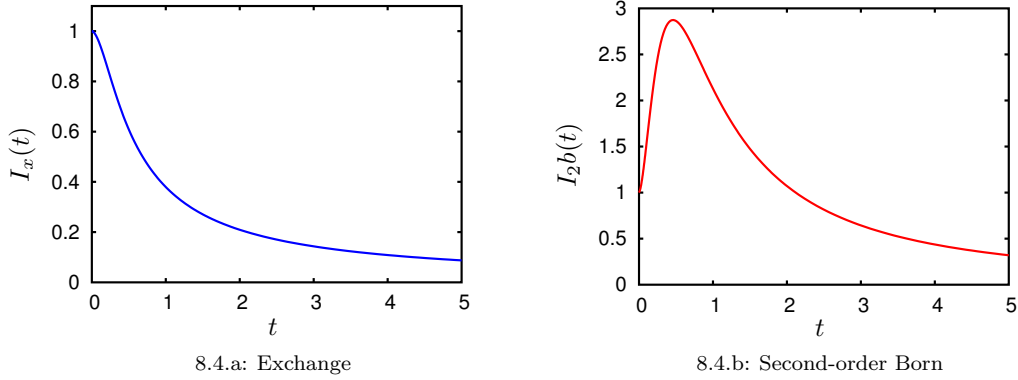
8.4.a: Exchange

8.4.b: Second-order Born

Figure 8.4: Universal functions $I_x(t)$ and $I_{2b}(t)$ as defined in Eqs. (8.30) and (8.42).

with the Fourier transform of the Coulomb interaction

$$W(\boldsymbol{k}) = \frac{4\pi}{k^2}. \tag{8.28}$$

When considering reduced variables, we see that the k_F-dependence can be separated from the integral in Eq. (8.27). We can therefore introduce a universal function $I_x(t)$, leading to the following expressions [128]:

$$\Omega_{x\sigma}(t) = -(1 \pm \xi)^{\frac{4}{3}} k_F \frac{3}{8} \pi^{-1} I_x(t_\sigma) \tag{8.29}$$

$$I_x(t) = \int dx \int dy \frac{x}{1 + e^{\frac{x^2}{t} - \alpha(t)}} \frac{y}{1 + e^{\frac{y^2}{t} - \alpha(t)}} \ln \frac{(x+y)^2}{(x-y)^2}. \tag{8.30}$$

We show $I_x(t)$ in Figure 8.4.a. $I(x)$ is a smooth, monotonically decreasing function with known high temperature limit $4/9t^{-1}$. It can therefore efficiently be parametrized or tabulated. A density change can then be incorporated into $\Omega_{x\sigma}$ by an appropriate change of t and a change of the prefactor in Eq. (8.29). This makes the calculation of the exchange contribution very fast.

We investigated the magnetic phase transitions for collinear spin configuration and show a sketch of the phase diagram in Figure 8.5.

We see that we recover the zero-temperature Hartree-Fock critical density of $r_c \approx 5.54 a.u.$. This was to be expected, because at zero temperature the first-order zero-temperature many-body perturbation theory (MBPT) approximation is known to be equivalent to the Hartree-Fock approximation. An increase in temperature now leads to an increase of the effect of entropy which itself favours a paramagnetic configuration. Therefore, above the critical temperature $T_c \approx 9800K$ we will only encounter the paramagnetic equilibrium configuration. Due to the $1/r_s$-dependence of Ω_x the phase diagram in Figure 8.5 reproduces several features expected from our general considerations, listed in Table 8.1 and sketched in Figure 8.2. However, the zero temperature phase transition is first-order and the resulting critical Wigner-Seitz radius is one order of magnitude below the ones expected from quantum Monte-Carlo calculations ($r_c \approx 60.a.u.$). We conclude that higher-order contributions in the perturbative expansion of the free energy are required for a more accurate description of the phase diagram. As a first choice, we will consider the famous RPA diagrams in the following.

Figure 8.5: Collinear phase diagram of the HEG from FT-MBPT including only the exchange contribution. FM: ferromagnetic phase, PM: paramagnetic phase, PP: partially polarized phase. The thick dashed red line denotes first-order phase transitions. The dotted blue line denotes the Fermi temperature T_F.

8.3.2 Exchange + RPA

The RPA ring-diagrams were shown to reproduce the high-temperature low-density classical limit as well as the zero-temperature high-density quantum limit of the correlation energy, i.e. the $\ln r_s$ dependence for small r_s [131, 132]. An inclusion of these diagrams then leads to the following free energy expression.

$$F = F_0 + \int_0^1 \frac{d\lambda}{\lambda} \left(\underbrace{\text{⬡}}_{\to \Omega_x} + \underbrace{\text{⬡}}_{\to \Omega_r} \right) \tag{8.31}$$

$$= \Omega_k - 1/\beta S_0 + \Omega_x + \Omega_r \tag{8.32}$$

Carrying out the coupling constant integration, the RPA contribution becomes

$$\Omega_r = \frac{1}{n}\frac{1}{2\beta} \int \frac{d^3q}{(2\pi)^3} \sum_{a=-\infty}^{\infty} \Big(\ln(1 - W(\boldsymbol{q})\chi(\boldsymbol{q},\nu_a)) + W(\boldsymbol{q})\chi(\boldsymbol{q},\nu_a) \Big), \tag{8.33}$$

where the discrete frequencies ν_a are given by

$$\nu_a = \frac{2\pi a}{\beta}. \tag{8.34}$$
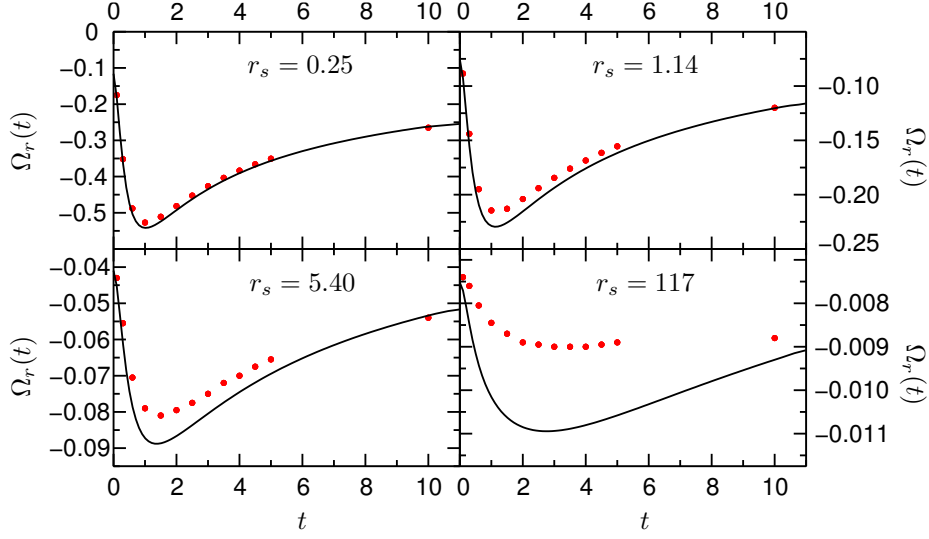
Figure 8.6: RPA contributions to the free energy density of a HEG at finite temperature. The lines denote our fully numerical results. The dots show the results from Ref. [119].

The polarization insertion $\chi(q, \nu_a)$ is given as a sum over its different spin contributions $\chi(\boldsymbol{q}, \nu_a) = \sum_\sigma \chi_\sigma(\boldsymbol{q}, \nu_a)$.

$$\chi_\sigma(\boldsymbol{q}, \nu_a) = -\int \frac{d^3k}{(2\pi)^3} \frac{n_\sigma(\boldsymbol{k} + \boldsymbol{q}) - n_\sigma(\boldsymbol{k})}{\mathrm{i}\nu_a - (\varepsilon_\sigma(\boldsymbol{k} + \boldsymbol{q}) - \varepsilon_\sigma(\boldsymbol{k}))} \tag{8.35}$$

We will now again change to reduced variables. Using the spatial invariance of the system, we are able to integrate over angles in Eqs. (8.33) and (8.35) [123]:

$$\Omega_r = \frac{k_F^2 t}{8\pi^2} \int d\underline{q}\,\underline{q}^2 \sum_{a=-\infty}^{\infty} \Big(\ln(1 - W(\underline{q})\chi(\underline{q}, \nu_a)) + W(\underline{q})\chi(\underline{q}, \nu_a) \Big) \tag{8.36}$$

$$\chi_\sigma(\underline{q}, \nu_a) = -\frac{1}{(2\pi)^2} \frac{k_{F\sigma}}{\underline{q}} \int d\underline{k} \frac{\underline{k}}{1 + e^{\underline{k}^2/t_\sigma - \alpha(t_\sigma)}} \ln\left(\frac{(2\pi a t_\sigma)^2 + (\underline{q}^2 + 2\underline{k}\underline{q})^2}{(2\pi a t_\sigma)^2 + (\underline{q}^2 - 2\underline{k}\underline{q})^2} \right). \tag{8.37}$$

Gupta and Rajagopal calculated the RPA contributions for the unpolarized HEG in 1982 ([119, 121]). Due to the tremendous increase in computational power since these preliminary calculations, we were able to fully calculate the integrals in Eqs. (8.36) and (8.37) for arbitrary choices of parameters. Our results are limited only by the accuracy of the numerical integration routines. We show our findings as well as the results from Refs. [119] and [121] in Figure 8.6. For $t \to 0$ we reproduce the values reported from Gupta and Rajagopal. For $t > 0$, however, our results start to differ and increasingly so for bigger r_s. Nonetheless, because we did not use any approximations in our calculation of the integrals in Eqs. (8.36) and (8.37), we expect our results to be accurate. Whereas the exchange contribution to the free energy decreases with temperature, from Figure 8.6 we see that the RPA-correlation contribution for low temperatures gains influence and reaches its maximum absolute value at around the Fermi temperature. This illustrates the need for an inclusion of correlation effects in the description of warm matter.

As a test of our finite-temperature calculations we investigated the low-temperature behaviour of Ω_r. We therefore calculated Ω_r for three small temperatures $t = \{0.001, 0.005, 0.01\}$ and extrapolated to $t = 0$ using a quadratical fit. We compare these extrapolated results with explicit zero-temperature
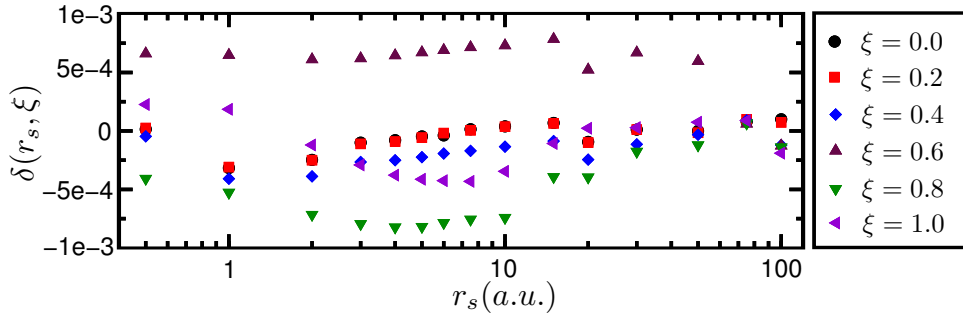
Figure 8.7: Relative deviation of RPA energies from a zero-temperature calculation [133] and our extrapolated finite-temperature results.
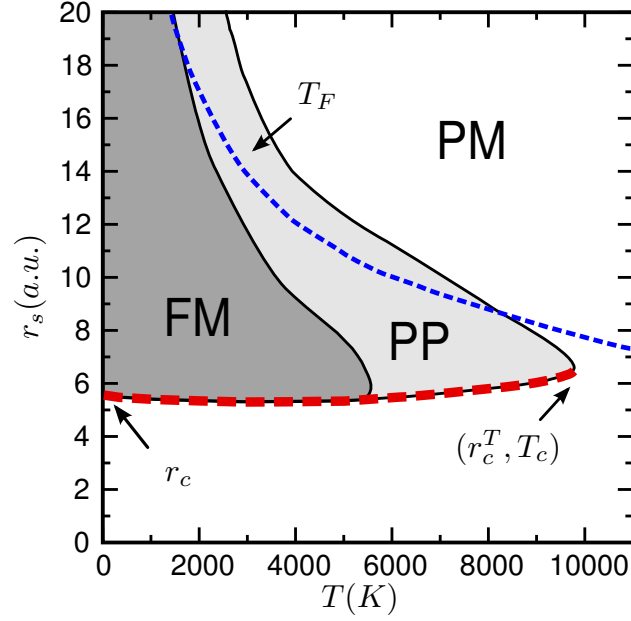

Figure 8.8: Collinear phase diagram of the HEG from FT-MBPT including the exchange and RPA contributions. FM: ferromagnetic phase, PM: paramagnetic phase, PP: partially polarized phase. The thick dashed red line denotes first-order phase transitions. The dotted blue line denotes the Fermi temperature T_F.

calculations from Vosko and Perdew [133]. We show the relative deviation in Figure 8.7 and point out that over the whole range of densities and polarizations the relative deviation lies below 0.001. This backs up our confidence in the accuracy of our numerical results.

In Figure 8.8 we show the phase diagram of the HEG resulting from the exchange plus RPA free energy in Eq. (8.32). The zero temperature phase transition stays first-order and its critical density r_c increases to $\approx 18 a.u.$. However, the critical temperature T_c is $\approx 270K$ which is far below the corresponding Fermi temperature $T_F \approx 1600K$. Apparently, the inclusion of RPA diagrams overestimates the ambition of the HEG to assume a paramagnetic configuration. To remedy this problem, we will in the following include the second-order Born diagrams in our free energy expression.

8.3.3 Exchange + RPA + second-order Born

As was pointed out in Ref. [134], the second-order Born diagram is the only diagram of second-order contributing to the free energy if one requires the noninteracting and interacting systems to have the same particle number. The other second-order diagrams cancel. This is very similar to the derivation of the methodology in Section 6. There we found that the other second-order diagrams disappear if one requires the two systems to exhibit the same 1RDM, which of course also leads to the same particle number. The resulting expression for the free energy is now

$$
F = F_0 + \int_0^1 \frac{d\lambda}{\lambda} \left(\underbrace{\vcenter{\hbox{}}}_{\to \Omega_x} + \underbrace{\vcenter{\hbox{}}}_{\to \Omega_{2b}} + \underbrace{\vcenter{\hbox{}}}_{\to \Omega_r} \right) \tag{8.38}
$$

$$
= \Omega_k - 1/\beta S_0 + \Omega_x + \Omega_{2b} + \Omega_r \tag{8.39}
$$

Carrying out the coupling constant integration in Eq. (8.38) (or rather replacing it by a factor of $1/2$ for Ω_{2b}) we arrive at the following expression for the second-order Born contribution from spin channel σ.

$$
\Omega_{2b\sigma} = \frac{1}{n} 2^{-10} \pi^{-9} \int d^3k \int d^3p \int d^3q
$$
$$
\frac{W(\boldsymbol{q}) W(\boldsymbol{k}+\boldsymbol{p}+\boldsymbol{q}) n_\sigma(\boldsymbol{k}) n_\sigma(\boldsymbol{p})(1-n_\sigma(\boldsymbol{k}+\boldsymbol{q}))(1-n_\sigma(\boldsymbol{p}+\boldsymbol{q}))}{\varepsilon(\boldsymbol{k}+\boldsymbol{q}) + \varepsilon(\boldsymbol{p}+\boldsymbol{q}) - \varepsilon(\boldsymbol{k}) - \varepsilon(\boldsymbol{p})}. \tag{8.40}
$$

As for the exchange contribution, the calculation of the second-order Born (Ω_{2b}) contribution is hugely simplified by the fact that, by changing to reduced variables, the explicit k_F-dependence can be separated from the momentum integrals.

$$
\Omega_{2b\sigma}(t) = \frac{(1\pm\xi)}{2} \Omega_{2b\sigma}(0) I_{2b}(t_\sigma) \tag{8.41}
$$

$$
I_{2b}(t) = -\frac{3}{\Omega_{2b\sigma}(0)} 2^{-6} \pi^{-5} \int d^3\underline{k} \int d^3\underline{p} \int d^3\underline{q} \frac{n(\underline{q}) n(\underline{k}+\underline{p}+\underline{q})(1-n(\underline{k}+\underline{q}))(1-n(\underline{p}+\underline{q}))}{\underline{k}^2 \underline{p}^2 \underline{k}\cdot\underline{p}} \tag{8.42}
$$

$$
\Omega_{2b\sigma}(0) = \left(\frac{\ln 2}{6} - \frac{3}{4\pi^2} \zeta(3) \right), \tag{8.43}
$$

where ζ is Riemann's Zeta-function. The zero-temperature limit of Ω_{2b} was calculated analytically in Ref. [135] and the high-temperature limit of $I_{2b}(t)$ can be shown to be $\sim t^{-3/2}$. For a translationally invariant system, the dimensionality of the integral in Eq. (8.42) can be reduced to six. In Appendix A.6 we present a form of $\Omega_{2b\sigma}$ which is appropriate for numerical integration. We calculated the universal functional for various values of t and show it in Figure 8.4.b. We note that, as in the case of $I_x(t)$, we can parametrize or tabulate $I_{2b}(t)$ which leads to a tremendous decrease of the computational cost for the calculation of Ω_{2b}. One important observation, we should like to point out here, is that $\Omega_{2b\sigma}$ is independent of the density.

The phase diagram corresponding to the free energy approximation from Eq. (8.39) is shown in Figure 8.9. For $T = 0$ we recover the RPA critical Wigner-Seitz radius of $r_c \approx 18 a.u.$. An increase of the temperature then leads to a phase transition from a paramagnetic to a ferromagnetic configuration in the density range of $r_s \in \{4, 19\} a.u.$ which is in contrast to the third property from Table 8.1. Furthermore, the critical radius r_c^T is reduced to $r_c^T \approx 4 a.u.$ and the critical temperature is increased to $T_c \approx 16000 K$. To understand these unexpected effects, we show the
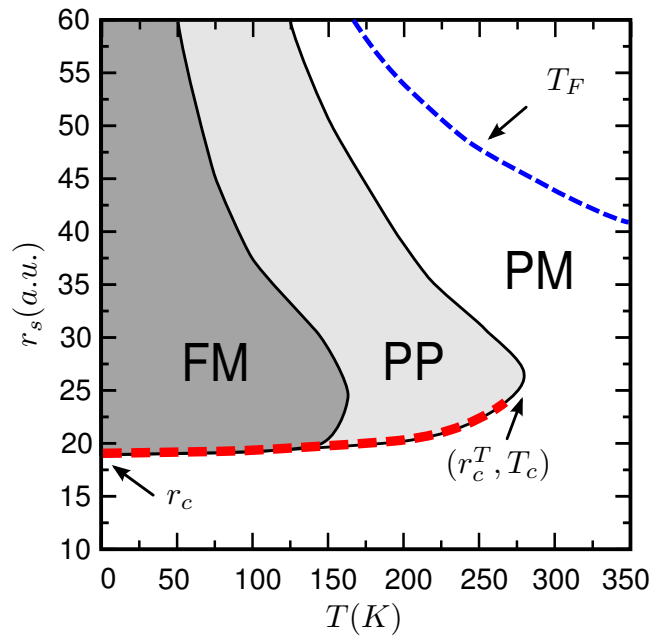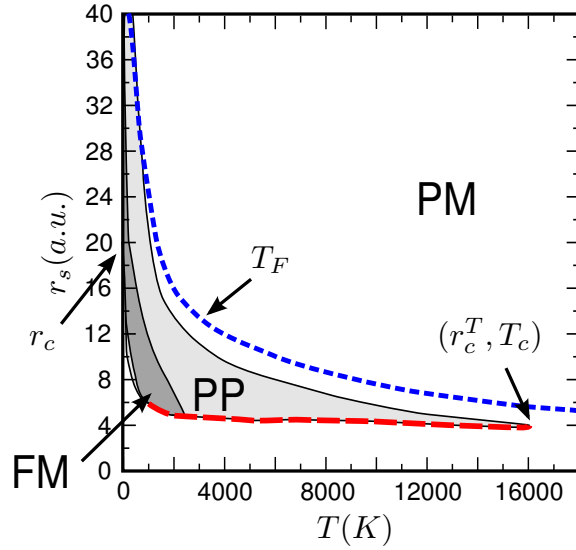
Figure 8.9: Collinear phase diagram of the HEG from FT-MBPT including exchange, RPA and second-order Born contributions. FM: ferromagnetic phase, PM: paramagnetic phase, PP: partially polarized phase. The thick dashed red line denotes first-order phase transitions. The dotted blue line denotes the Fermi temperature T_F.

contributions from the noninteracting free energy, the exchange energy, the RPA energy, and the second-order Born contribution in Figure 8.10 for $r_s = 7 a.u.$ and different polarizations. We see that the noninteracting as well as the RPA contributions always favour a paramagnetic configuration whereas the exchange contribution favours a ferromagnetic one. Furthermore, the energy differences between different polarizations stay almost constant for small temperatures. The second-order Born approximation, on the other hand, shows a qualitatively different behaviour. For $T = 0$, the reduced temperatures for the spin channels are the same ($t_\uparrow = t_\downarrow = 0$). From Eq. (8.41) we then conclude that $\Omega_{2b} = \Omega_{2b\uparrow} + \Omega_{2b\downarrow}$ is independent of the polarization. This explains why for $T = 0$ we recover the RPA critical density. Increasing the temperature then leads to a favourisation of the ferromagnetic configuration. As mentioned before, the energy differences of different polarizations coming from the other contributions stay almost invariant for small temperatures. This then explains the formation of a ferromagnetic configuration with increasing temperature for r_s slightly below r_c. We can also see from Figure 8.10 that the second-order Born contribution at about $t = 0.5$ starts to favour the paramagnetic configuration. Therefore, a further increase of the temperature will eventually yield a paramagnetic eq-state. We conclude this investigation by summarizing that the inclusion of the second-order Born approximation leads to a worse phase diagram compared to our assumptions from Figure 8.2. It both leads to a distinctive temperature-induced paramagnetic to ferromagnetic phase transition for $r_s \in \{4, 19\} a.u.$ and reduces the critical density r_c^T to a value even below the Hartree-Fock result.

After this investigation of several FT-MBPT approximations on the magnetic phase diagram of the HEG in collinear spin configuration, we will turn to the description via our new theory of FT-RDMFT.
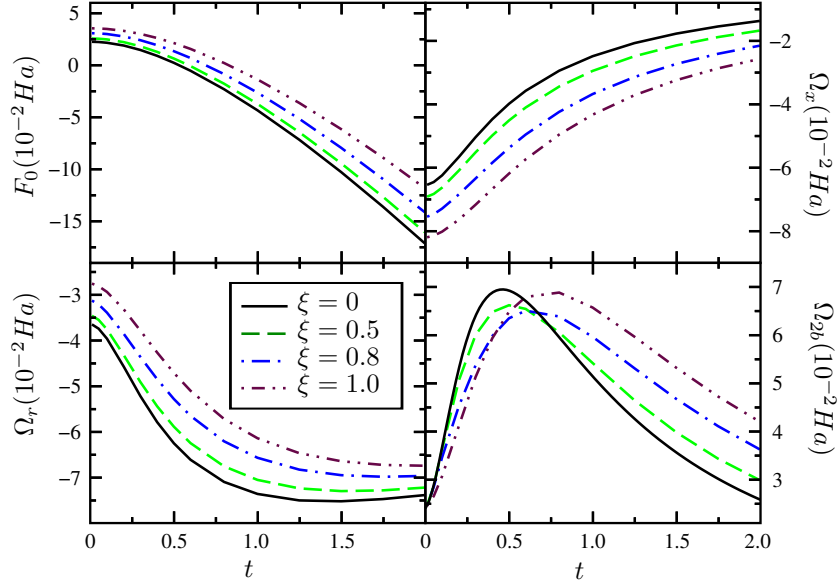
Figure 8.10: Clockwise from top left: noninteracting free energy, exchange, RPA and second-order Born contributions at $r_s = 7a.u.$ $(T_F \approx 11900K)$ versus the temperature T of the HEG for different polarizations ξ.

8.4 FT-RDMFT

We investigate the performance of our new theory of FT-RDMFT by choosing the first-order functional, i.e. the exchange-only functional from Sec. 6, as our free energy functional. One reason for this choice is that the results produce most of the features one might be interested in, in the investigation of the full system, e.g. first and second-order phase transitions between both collinear and spin spiral phases. Its simplicity also allows a more direct understanding and interpretation, serving as a guideline for more involved functionals. Another reason for the choice of this functional is that its minimization was shown in Section 4.2.5 to be equivalent to a solution of the FT-HF equations. The FT-HF solution can then serve as a starting point for various approximations in other theoretical frameworks. Because of its conceptual importance, the temperature dependence of the free energy of the HEG in FT-HF has been investigated [136, 137] but a thorough calculation of the corresponding phase diagram, including collinear and spin spiral phases, to the best of our knowledge has not been carried out so far, substantiating the importance of our calculations.

The expression for the free energy in the first-order FT-RDMFT approximation reads

$$F[\gamma] = F_0[\gamma] + \int_0^1 \frac{d\lambda}{\lambda} \underbrace{}_{\rightarrow \Omega_x} \tag{8.44}$$

$$= \Omega_k[\gamma] - 1/\beta S_0[\gamma] + \Omega_x[\gamma]. \tag{8.45}$$

The definitions for the different contributions are given in Eqs. (8.4)-(8.7),(8.27). But in contrast to the FT-MBPT treatment, in FT-RDMFT the momentum distribution $n(k)$ refers to the effective Kohn-Sham system and is subject to optimization. The choice of NOs then determines the symmetry of the system. In this work we will focus on NOs representing a collinear spin configuration in Section 8.4.1 and a planar spin wave configuration in Section 8.4.2.

8.4.1 Collinear spin configuration

The NOs describing a collinear spin state are plane waves. By discretizing, we assume the ONs to be constant in the small volumes V_i around the sample k-points $\boldsymbol{k}_i$ and hence the 1RDM is represented by the following expression.

$$\gamma(\boldsymbol{r} - \boldsymbol{r}') = \sum_{\sigma i} n_{\sigma i} \int_{V_i} \frac{d^3 k}{(2\pi)^3} e^{i\boldsymbol{k}\cdot(\boldsymbol{r}-\boldsymbol{r}')} \tag{8.46}$$

Therefore, the integrals in Eqs. (8.4)-(8.7),(8.27) become sums and we arrive at the final expression for the free energy functional.

$$F[\{n_{\sigma i}\}] = \Omega_k[\{n_{\sigma i}\}] - 1/\beta S_0[\{n_{\sigma i}\}] + \Omega_x[\{n_{\sigma i}\}] \tag{8.47}$$

The kinetic energy Ω_k, the entropy S_0, and the exchange energy Ω_x are given by

$$\Omega_k[\{n_{\sigma i}\}] = \sum_{\sigma,i} n_{\sigma i} t_i \tag{8.48}$$

$$S_0[\{n_{\sigma i}\}] = -\sum_{\sigma,i} \left(n_{\sigma i} \ln(n_{\sigma i}) + (1 - n_{\sigma i}) \ln(1 - n_{\sigma i}) \right) \omega_i \tag{8.49}$$

$$\Omega_x[\{n_{\sigma i}\}] = -\frac{1}{2} \sum_{\sigma,i,j} n_{\sigma i} n_{\sigma j} K_{i,j}, \tag{8.50}$$

where the integral weights are

$$t_i = \frac{1}{n} \int_{V_i} \frac{d^3 k}{(2\pi)^3} \frac{k^2}{2} \tag{8.51}$$

$$K_{i,j} = \frac{1}{n} \int_{V_i} \frac{dk_1^3}{(2\pi)^3} \int_{V_j} \frac{dk_2^3}{(2\pi)^3} \frac{4\pi}{(\boldsymbol{k} - \boldsymbol{k}')^2} \tag{8.52}$$

$$\omega_i = \frac{1}{n} \int_{V_i} \frac{d^3 k}{(2\pi)^3}. \tag{8.53}$$

The minimization of $F[\{n_{\sigma i}\}]$ w.r.t. the ONs has then to be performed under the constraints of particle number and polarization conservation $\sum_i n_{\sigma i} = n_\sigma$ and the fermionic requirement $0 \leq n_{\sigma i} \leq 1$. We employ the minimization methods derived in Section 7 which have proved to be very efficient and effective.

We now determine the eq-polarization as explained in Section 8.1 and depicted in Figure 8.1. The general behaviour of the phase transitions is the same, compared to the exchange-only treatment from FT-MBPT in Section 8.3.1. As we illustrate in Figure 8.11, an increase of r_s leads to a first-order phase transition between a paramagnetic and a ferromagnetic state and a subsequent second-order phase transition back to the paramagnetic state. An increase of the temperature then leads to an increase of the Wigner-Seitz radius, where the first-order phase transition occurs, and to a decrease of the Wigner-Seitz radius, where the paramagnetic configuration is assumed again. Interestingly, the nature of the phase transitions does not change, even at high temperatures.

In order to study the various contributions to the free energy separately, we plotted kinetic energy, exchange contribution, and entropy in Figure 8.12. We see that the entropy and exchange contributions always show a monotonically decreasing behaviour w.r.t. an increase in the polarization ξ. The kinetic energy, however, which is known at zero temperature to be monotonically increasing with ξ, actually becomes decreasing for high values of the reduced temperature $t = T/T_F$.

As we will see in the following, this somewhat counterintuitive effect is due to the fact that the exchange contribution hinders the temperature-induced smoothing of the momentum distributions and stronger so for the ferromagnetic configuration. To elucidate this argument we choose a density
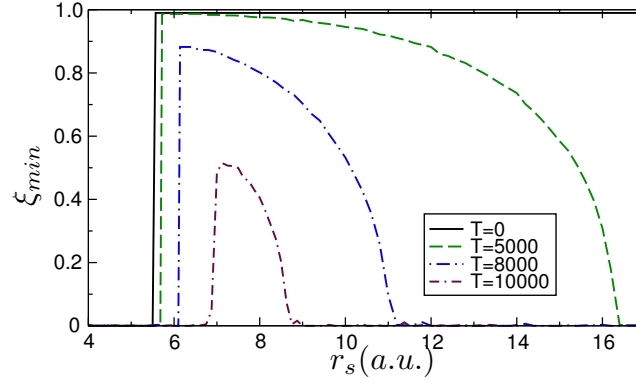
Figure 8.11: Equilibrium polarization ξ_{min} of the HEG for different r_s and T. Above $T = 6000K$ there is no fully polarized equilibrium state.
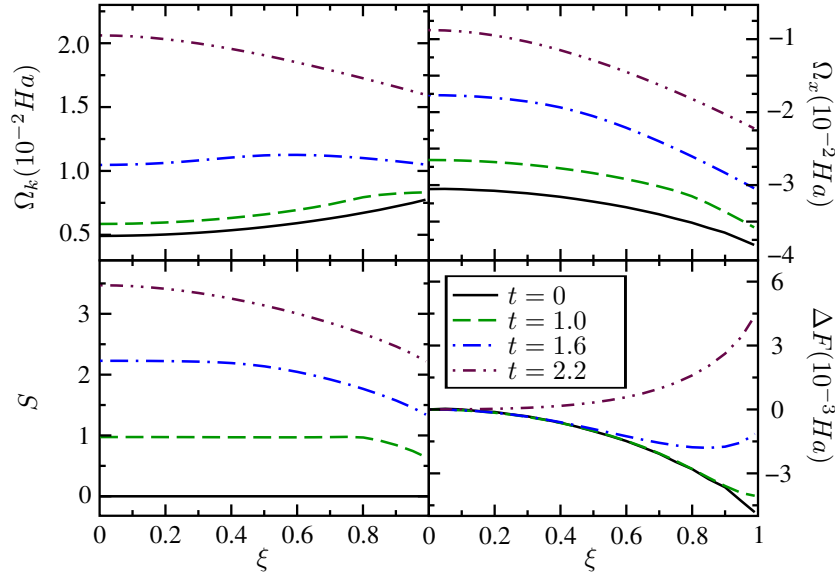
Figure 8.12: Clockwise from bottom left: entropy, kinetic energy, exchange energy and free energy at $r_s = 15a.u.$ ($T_F = 2590K$) versus the polarization ξ of the HEG for different reduced temperatures t. The free energy is origin-shifted for demonstration purposes.

which will yield a ferromagnetic solution at zero temperature ($r_s = 15a.u.$). Thermodynamic variables for both paramagnetic and ferromagnetic configurations as functions of the temperature are shown in Figure 8.13. The curves denoted by "FD" correspond to the FT-MBPT expressions, i.e. the FT-RDMFT functionals applied to Fermi-Dirac momentum distributions with the appropriate temperature. The FT-RDMFT functional is then minimized to give the curves denoted by "HF". The differences of the energies for ferromagnetic and paramagnetic configurations are then included as the "Δ_{1-0}" curves:

$$\Delta_{1-0} = \Omega(\xi = 1) - \Omega(\xi = 0). \tag{8.54}$$

We see that in the case of a noninteracting system, i.e. for the "FD" curves, the kinetic energies of paramagnetic and ferromagnetic configurations approach each other but do not cross. The fact that they converge for high temperatures can qualitatively be understood by the concept of different

Figure 8.13: Clockwise from bottom left: entropy, kinetic energy, exchange energy and free energy for the HF and the noninteracting functionals at $r_s = 15a.u.$ ($T_F = 2590K$) and $\xi = (0,1)$ versus the reduced temperature t of the HEG. The black dotted and the grey shaded lines denote the differences between the ferro- and paramagnetic configurations. The free energy 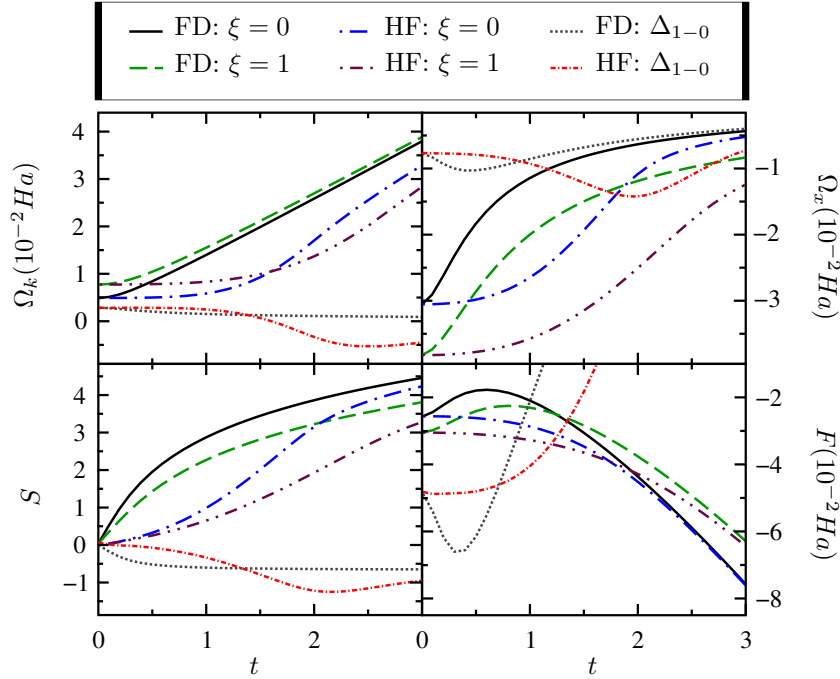differences are scaled by 10. The behaviour of the HF-curves can be explained by different "effective" Fermi temperatures.

"effective" Fermi temperatures T_F^* of the configurations. For the paramagnetic configuration at zero temperature the ONs occupy two Fermi spheres of radii $k_{F\uparrow}^u = k_{F\downarrow}^u = k_F$, one for each spin channel. Because in the ferromagnetic situation the ONs are restricted to only one spin channel there will also be only one Fermi sphere with increased radius $k_{F\uparrow}^p = 2^{\frac{1}{3}}k_F$ ($k_{F\downarrow}^p = 0$). Because the kinetic energies are proportional to $\sum_\sigma (k_{F\sigma})^2$ this explains the favourisation of the paramagnetic configuration at zero temperature. An increase in temperature will now lead to a smoothing of the Fermi sphere, i.e. the momentum distributions, and therefore to an overall increase of the kinetic energy. The quickness of the smoothing is determined mainly by the characteristic energy of the system, i.e. the Fermi energy, or, correspondingly, the Fermi temperature. Following from the arguments above, the paramagnetic configuration exhibits a smaller Fermi temperature when compared to the ferromagnetic configuration. This implies that the corresponding momentum distributions are smoothed more quickly which in turn leads to a relative increase of the kinetic energy of the paramagnetic configuration. This effect, hower, as we can see from Figure 8.13, is not big enough to let the kinetic energy curves cross and they converge for $T \to \infty$.

The situation changes if one includes the exchange contribution and minimizes w.r.t. the momentum distribution. The exchange contribution by itself is known to be minimal for a ferromagnetic configuration with a momentum distribution describing a sharp Fermi sphere. Because it does not couple different spin channels this also implies that, for general polarizations, the favourable configurations are the ones describing sharp Fermi spheres of appropriate radii. Ω_x therefore counteracts the effect of temperature which can be interpreted as an increase of the effective Fermi temperature T_F^*. As argued, this increase of T_F^* is stronger for the ferromagnetic configuration, which, in addition to our considerations of noninteracting systems above, then leads to a cross-over of the kinetic
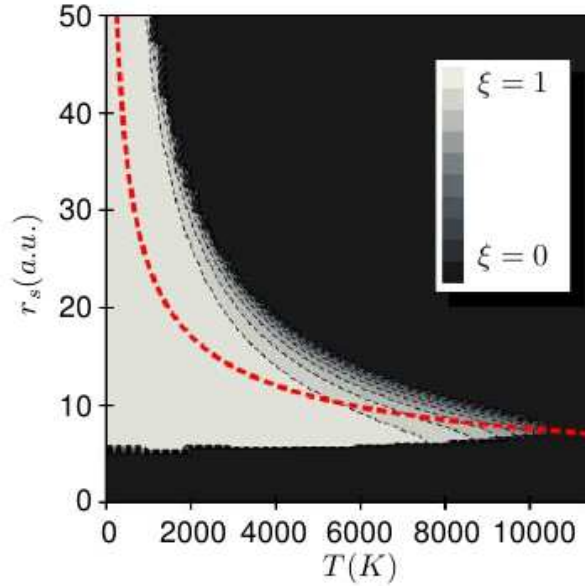
Figure 8.14: Phase diagram of the HEG for collinear spin configuration for the first-order FT-RDMFT functional. For $T < T_c$, when increasing r_s, the HEG shows both first and second-order phase transitions. The red dashed line denotes T_F.

energy curves in the FT-RDMFT treatment. These arguments can be applied to both entropic as well as exchange contributions, but there the ferromagnetic configuration exhibits a lower value for zero temperature, preventing a crossing of energy curves. The behaviour of the free energy is more complicated because the entropy enters negatively. It has to be pointed out, however, that in the case of "FD"-momentum distributions, i.e. in first order FT-MBPT, an increase of temperature first leads to an increase in the free energy before an eventually monotonic decrease. This is rather unphysical and can be appointed to the fact that the "FD"-momentum distribution is not acquired by any sort of variational principle. The "HF"-momentum distribution, one the other hand, is explicitly determined by a minimization procedure which leads to the qualitatively correct monotonical decrease of the free energy with temperature.

After these considerations, we now calculate the equilibrium polarization of the HEG for a wide range of densities and temperatures. The resulting magnetic phase diagram is shown in Figure 8.14. The critical Wigner-Seitz radius r_c, marking the zero-temperature magnetic transition between the paramagnetic and ferromagnetic phases, is the zero-temperature Hartree-Fock result of $r_c \approx 5.54a.u.$. On increasing the temperature, the ferromagnetic phase gets reduced until, after a critical point, it vanishes. The corresponding temperature T_c is calculated to be at about $10500K$ while the critical Wigner-Seitz radius r_c^T becomes $7.1a.u.$. A comparison of the phase diagrams for the exchange-only FT-MBPT treatment and the actual first-order FT-RDMFT functional shows that the ferromagnetic phase is slightly increased for the FT-RDMFT treament. This can be explained on the basis of the previous considerations. For temperatures similar or higher than the Fermi temperature, the FT-RDMFT treatment favours a ferromagnetic configuration, when compared to the FT-MBPT. This concludes our investigation of the phase diagram of the HEG in collinear spin configuration for the first-order functional. The effect of correlation is then discussed in Section 8.6.

We will in the following consider the explicitly noncollinear basis of planar spin spirals (PSS).

8.4.2 Planar spin spirals (PSS)

Although collinear plane waves as NOs respect the symmetry of the system, they do not necessarily yield the lowest free energy. Another possible choice are spin density waves (SDW) which are explicitly noncollinear but are still describable with a small set of parameters. The theoretical interest in SDW dates back to the beginning of modern many-body physics. It was in 1962 when Overhauser [138] proved that for the electron gas at zero temperature in Hartree-Fock approximation a state describing a SDW will yield energies below the energies provided by the collinear phases.

Using the framework of FT-RDMFT, we will now be able to investigate how the situation changes for a HEG in grand canonical equilibrium, restricting ourselves to the description of pure spin waves (SW). An investigation of SWs within zero-temperature RDMFT was done by Eich et al.[139] and we will repeat the most important concepts in the following. The NOs describing a SW are given by

$$\phi_{1\boldsymbol{k}}(\boldsymbol{r}) = \begin{pmatrix} \cos\left(\frac{\Theta_k}{2}\right) e^{-i\boldsymbol{q}\cdot\boldsymbol{r}/2} \\ \sin\left(\frac{\Theta_k}{2}\right) e^{i\boldsymbol{q}\cdot\boldsymbol{r}/2} \end{pmatrix} \frac{e^{i\boldsymbol{k}\cdot\boldsymbol{r}}}{\sqrt{V}} \tag{8.55}$$

$$\phi_{2\boldsymbol{k}}(\boldsymbol{r}) = \begin{pmatrix} -\sin\left(\frac{\Theta_k}{2}\right) e^{-i\boldsymbol{q}\cdot\boldsymbol{r}/2} \\ \cos\left(\frac{\Theta_k}{2}\right) e^{i\boldsymbol{q}\cdot\boldsymbol{r}/2} \end{pmatrix} \frac{e^{i\boldsymbol{k}\cdot\boldsymbol{r}}}{\sqrt{V}}, \tag{8.56}$$

where the wavevector $\boldsymbol{q}$ and the azimuthal angle Θ_k of the spin spirals are subject to variation. V denotes the Volume of the space under consideration. To distinguish the SW index from the spin index, we will denote it by b in the following. In the collinear basis, the 1RDM then becomes

$$\gamma_{\uparrow\uparrow}(\boldsymbol{r},\boldsymbol{r}';\boldsymbol{q},\Theta_k) = \int \frac{d^3k}{(2\pi)^3} \left(n_{1\boldsymbol{k}} \cos^2\left(\frac{\Theta_k}{2}\right) + n_{2\boldsymbol{k}} \sin^2\left(\frac{\Theta_k}{2}\right) \right) e^{i(\boldsymbol{k}-\boldsymbol{q}/2)\cdot(\boldsymbol{r}-\boldsymbol{r}')} \tag{8.57}$$

$$\gamma_{\uparrow\downarrow}(\boldsymbol{r},\boldsymbol{r}';\boldsymbol{q},\Theta_k) = \int \frac{d^3k}{(2\pi)^3} \frac{1}{2}(n_{1\boldsymbol{k}} - n_{2\boldsymbol{k}}) \sin(\Theta_k) e^{i\boldsymbol{k}\cdot(\boldsymbol{r}-\boldsymbol{r}')} e^{i\boldsymbol{q}/2\cdot(\boldsymbol{r}+\boldsymbol{r}')} \tag{8.58}$$

$$\gamma_{\downarrow\uparrow}(\boldsymbol{r},\boldsymbol{r}';\boldsymbol{q},\Theta_k) = \int \frac{d^3k}{(2\pi)^3} \frac{1}{2}(n_{1\boldsymbol{k}} - n_{2\boldsymbol{k}}) \sin(\Theta_k) e^{i\boldsymbol{k}\cdot(\boldsymbol{r}-\boldsymbol{r}')} e^{-i\boldsymbol{q}/2\cdot(\boldsymbol{r}+\boldsymbol{r}')} \tag{8.59}$$

$$\gamma_{\downarrow\downarrow}(\boldsymbol{r},\boldsymbol{r}';\boldsymbol{q},\Theta_k) = \int \frac{d^3k}{(2\pi)^3} \left(n_{1\boldsymbol{k}} \sin^2\left(\frac{\Theta_k}{2}\right) + n_{2\boldsymbol{k}} \cos^2\left(\frac{\Theta_k}{2}\right) \right) e^{i(\boldsymbol{k}+\boldsymbol{q}/2)\cdot(\boldsymbol{r}-\boldsymbol{r}')}. \tag{8.60}$$

The exchange contribution to the free energy is given by Eq. (4.66) as

$$\Omega_x[\gamma] = -\frac{1}{2} \sum_{\sigma_1\sigma_2} \int d^3r d^3r' w(\boldsymbol{r}-\boldsymbol{r}') \gamma_{\sigma_1\sigma_2}(\boldsymbol{r},\boldsymbol{r}') \gamma_{\sigma_2\sigma_1}(\boldsymbol{r}',\boldsymbol{r}). \tag{8.61}$$

For our choice of SWs as NOs this becomes for the Coulomb interaction

$$\Omega_x[\gamma] = -\frac{1}{2n} \int \frac{d^3k_1}{(2\pi)^3} \frac{d^3k_2}{(2\pi)^3} \frac{4\pi}{|\boldsymbol{k}_1-\boldsymbol{k}_2|^2}$$
$$\left[\sum_b (n_{b\boldsymbol{k}_1} n_{b\boldsymbol{k}_2}) \cos^2\left(\frac{\Theta_{\boldsymbol{k}_1}-\Theta_{\boldsymbol{k}_2}}{2}\right) + (n_{1\boldsymbol{k}_1} n_{2\boldsymbol{k}_2} + n_{2\boldsymbol{k}_1} n_{1\boldsymbol{k}_2}) \sin^2\left(\frac{\Theta_{\boldsymbol{k}_1}-\Theta_{\boldsymbol{k}_2}}{2}\right) \right]. \tag{8.62}$$

Interestingly, the exchange energy contribution shows no explicit dependence on the SW wavevector $\boldsymbol{q}$. We will from now on assume, that $\boldsymbol{q}$ is parallel to the z-axis which suggests the use of cylindrical coordinates. A vector $\boldsymbol{k}$ is then given by $\boldsymbol{k} = (k_z, k_\rho, \phi)$. We finally arrive at an expression for the

free energy functional, appropriate for numerical minimization

$$
\begin{aligned}
F[\boldsymbol{q}, \{n_{b,i}\}, \{\Theta_i\}] = \\
\sum_{bi} n_{bi} t_i + \frac{q^2}{8} - q \sum_i (n_{1i} - n_{2i}) \cos(\Theta_i) Q_i + \\
1/\beta \sum_{bi} \Big(n_{bi} \ln(n_{bi}) + (1 - n_{bi}) \ln(1 - n_{bi}) \Big) \omega_i - \\
\frac{1}{2} \sum_{bij} (n_{bi} n_{bj}) \cos^2 \left(\frac{\Theta_i - \Theta_j}{2} \right) K_{ij} - \sum_{ij} (n_{1i} n_{2j}) \sin^2 \left(\frac{\Theta_i - \Theta_j}{2} \right) K_{ij}.
\end{aligned}
\tag{8.63}
$$

The integral weights are defined in Eqs. (8.51)-(8.53) with the additional

$$
Q_i = \frac{1}{2n} \int_{V_i} \frac{d^3 k}{(2\pi)^3} k_z.
\tag{8.64}
$$

The magnetization of the HEG for SW-NOs is given by

$$
\boldsymbol{m}(\boldsymbol{r}) = - \begin{pmatrix} A \cos(\boldsymbol{q} \cdot \boldsymbol{r}) \\ A \sin(\boldsymbol{q} \cdot \boldsymbol{r}) \\ B \end{pmatrix}.
\tag{8.65}
$$

The two amplitudes A and B are determined via

$$
A = \frac{1}{2} \int \frac{d^3 k}{(2\pi)^3} (n_{1\boldsymbol{k}} - n_{2\boldsymbol{k}}) \sin(\Theta_{\boldsymbol{k}})
\tag{8.66}
$$

$$
B = \frac{1}{2} \int \frac{d^3 k}{(2\pi)^3} (n_{1\boldsymbol{k}} - n_{2\boldsymbol{k}}) \cos(\Theta_{\boldsymbol{k}}).
\tag{8.67}
$$

From now on, we will restrict ourselves to planar SWs, i.e. SWs for which the magnetization of the HEG in z-direction vanishes. As argued in [110] and [139], this planar configuration has a lower energy than a conical SW with nonvanishing z-component. These SWs will be called planar spin spirals (PSS) and the amplitude A of the PSS configuration becomes the order parameter.

The requirement of a vanishing z-component can be met by simple constraints on the ONs and NOs:

$$
n_{b k_\rho - k_z} = n_{b k_\rho k_z}
\tag{8.68}
$$

$$
\Theta_{k_\rho \pm |k_z|} = \frac{\pi}{2} (1 \mp a_{k_\rho |k_z|}).
\tag{8.69}
$$

As for the collinear case, we can define a PSS polarization ξ^{PSS}, using $N_1 = \sum_i n_{1i}$ and $N_2 = \sum_i n_{2i}$.

$$
\xi^{PSS} = \frac{N_1 - N_2}{N_1 + N_2}
\tag{8.70}
$$

If we now choose $\boldsymbol{q} = 0$ and $a_{k_\rho |k_z|} = 1$, then the PSS unpolarized state $\xi^{PSS} = 0$ corresponds to the paramagnetic state and the PSS polarized one $\xi^{PSS} = 1$ describes the ferromagnetic solution.

To understand the effect of an increase of $\boldsymbol{q}$ it is instructive to consider a fully polarized noninteracting system. We show a sketch of the $\boldsymbol{q}$-dependence of the Fermi surface in Figure 8.15. For $\boldsymbol{q} = 0$, the ONs describe a Fermi sphere of radius $2^{\frac{1}{3}} k_F$ around $\boldsymbol{k} = 0$. If one increases $\boldsymbol{q}$, one can derive from the first three terms in Eq. (8.63) and the symmetry relations (8.68), (8.69) that the Fermi sphere will divide symmetrically along the z-direction. If $\boldsymbol{q}$ supersedes $2k_F$, then there will be
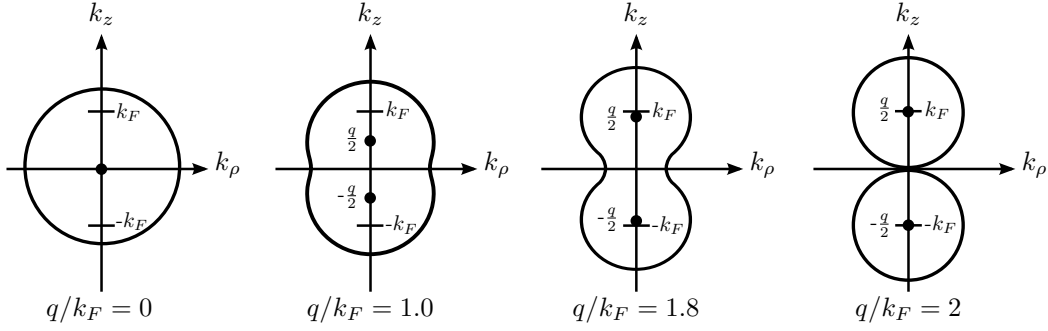
Figure 8.15: Sketch of $\boldsymbol{q}$-dependence of Fermi surface of a fully polarized PSS state.
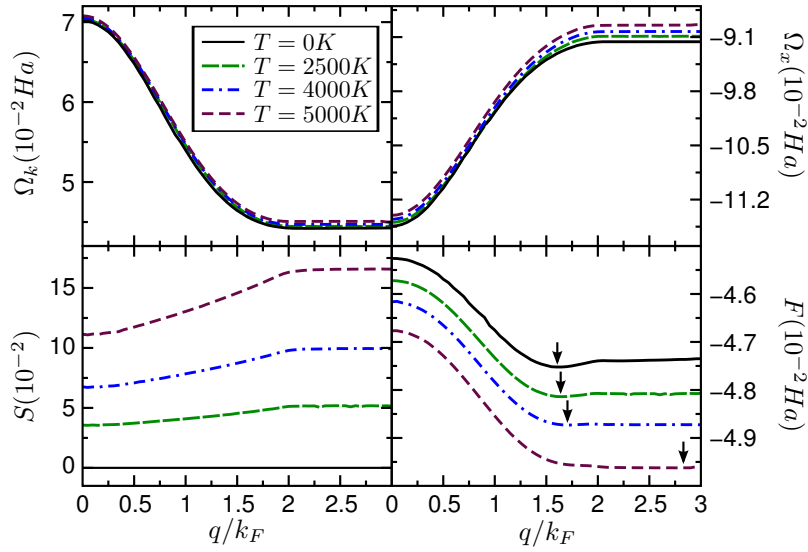
Figure 8.16: Clockwise from bottom left: entropy, kinetic energy, exchange energy and free energy at $r_s = 5.00$ ($T_F = 23300K$) versus the PSS $\boldsymbol{q}$-vector. The minimal free energies are denoted by the arrows.

two distinct Fermi spheres with radius k_F, centered at $k = -q/2$ and $k = q/2$ respectively and this configuration represents a paramagnetic collinear configuration. If one now includes temperature effects, then the momentum distribution around the Fermi surface will be smoothed. To reproduce the paramagnetic collinear configuration one therefore has to consider the limit $\boldsymbol{q} \to \infty$.

We can now minimize the free energy functional w.r.t. the ONs and orbital angles. For all of our calculations we found that the fully polarized PSS state yields the lowest free energy. In the following, we will therefore always consider fully polarized PSS configurations. The dependence of the entropy and the other thermodynamic variables on $\boldsymbol{q}$ at several temperatures is shown in Figure 8.16. The entropy displays a monotonically increasing, almost linear dependence which in turn leads to an increase of the optimal $\boldsymbol{q}$-vector (the $\boldsymbol{q}$ for which the free energy is minimal). This situation is depicted for $r_s = 5.50 a.u.$ in Figure 8.17 where we show the free energy and the amplitude of a PSS state w.r.t. $\boldsymbol{q}$ for several temperatures close to the critical temperature T_c^{PSS}. For temperatures below T_c^{PSS}, the free energy exhibits a minimum for finite $\boldsymbol{q}$. If the temperature is increased above T_c^{PSS}, q_{min} instantaneously jumps to a value bigger than $2k_F$, letting the amplitude of the PSS vanish. The jump in $\boldsymbol{q}$ at T_c^{PSS} therefore marks a first-order phase transition of the PSS phase where the amplitude of the optimal PSS is approaching zero instantaneously. In his work on SDWs
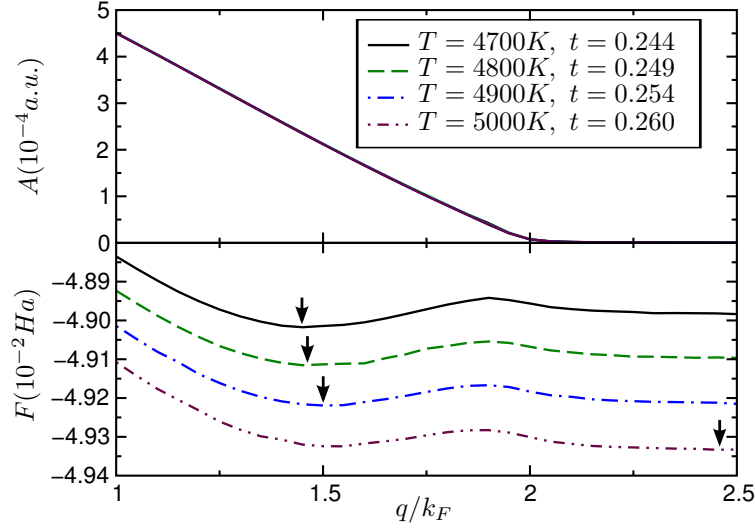
Figure 8.17: Amplitude A and free energy F for different $\boldsymbol{q}$ and T for $r_s = 5.5a.u.(T_F = 19200K)$. The amplitudes change only slightly when increasing the temperature, but the optimal $\boldsymbol{q}$ increases (arrows) discontinuously, letting the optimal amplitude A_{opt} vanish. This denotes a first-order phase transition in the PSS phase.

in an electron gas, Overhauser [138] made the conjecture that, on increasing the temperature, the optimal amplitude of the SDW state will approach zero continuously, giving rise to a second-order phase transition. Our results disprove the validity of this conjecture for PSS states for densities with Wigner-Seitz radii above $r_s \approx 4a.u.$.

We show the dependence of the amplitude of the optimal PSS w.r.t T for several r_s in Figure 8.18. For small $\boldsymbol{q}$ the amplitude increases slightly when increasing the temperature which seems to be surprising at first. Temperature is usually expected to favour states of higher disorder and one could therefore expect the amplitude to be reduced. However, in our calculations we encounter the following behaviour of the Fermi surface. For $q/k_F < 2$ the zero-temperature Fermi surface assumes an hourglass-like shape as depicted in Figure 8.15. We find that an increase of the temperature for small temperatures smoothes the Fermi surface but also leads to an increase of occupation at the "waist" of the hourglass. The angles are usually closer to $\pi/2$ for smaller values of k_z which then leads to an increase of the PSS amplitude A via Eq. 8.66. Furthermore, the free energy gain from this effect is bigger for smaller q which also leads to a decrease of the optimal $\boldsymbol{q}$-vector, increasing the amplitude even further. For higher temperatures these two effects become less important, leading to the eventual decrease of the optimal PSS-phase.

We have to point out, however, the numerical uncertainty of these findings. The energy differences for slightly changed momentum distributions are very small but the amplitude shows a much stronger dependence. This also explains the considerable variance of the calculated optimal amplitudes, as shown in Figure 8.18. However, we did a careful minimization of the functional with several k-point-mesh refinements and believe that our numerical findings are quantitatively correct. We have argued that for small temperatures the amplitude of a PSS state increases. The optimal $\boldsymbol{q}$-vector, on the other hand, changes only slightly. Therefore, for small temperatures the optimal amplitude increases. It was already mentioned in [139] that at zero temperature, the amplitude of the PSS decreases with decreasing r_s. Below a critical radius $r_c^{PSS} = 3.5$, we cannot resolve the amplitude of the PSS anymore. This reduction of the amplitude is mainly due to the fact that the energy difference between the paramagnetic and ferromagnetic phases increases and therefore the optimal $\boldsymbol{q}$ approaches $2k_F$ (see Figure 8.17). When considering finite temperatures, this leads to a decrease
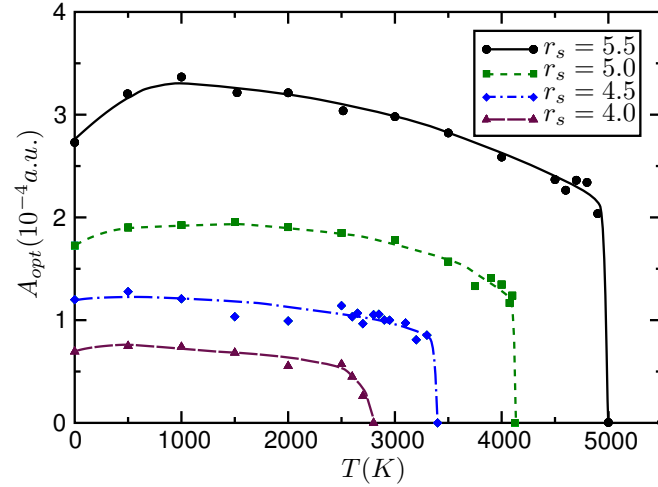
Figure 8.18: Amplitudes A_{opt} of the quilibrium PSS phases for different $r_s(\{4.0, 4.5, 5.0, 5.5\}a.u.)$ and T. The corresponding Fermi temperatures are $\{36400, 28800, 23300, 19200\}K$.

of the critical temperature T_c^{PSS}, as shown in Table 8.2.

For those r_s, for which a polarized configuration is favourable over an unpolarized one, a formation of a PSS was found to increase the free energy.

In Figure 8.19 we combine the results from the collinear NOs and the PSS NOs calculations to get a schematic diagram of the magnetic phase diagram of the HEG for the first-order FT-RDMFT functional.

The magnetic phase transition between paramagnetic and polarized phases for increasing r_s was shown to be first-order while the transition from polarized to paramagnetic phases for higher r_s is second-order. As can be seen from Figure 8.19, the second-order phase transitions occurs close to the Fermi temperature T_F. In summary, the collinear phase diagram, resulting from the first-order functional in FT-RDMFT, reproduces most features listed in Table 8.1 but it exhbits a first-order phase transition at zero temperature. Furthermore, it fails to reproduce a qualitatively correct r_c. The PSS phase shows a much stronger density dependence then the collinear phase and it is strongest for $4 \le r_s \le 6$. In this range we also see a temperature-driven first-order phase transition between a PSS state and the paramagnetic collinear state.

This concludes our investigation of the phase diagram of the HEG for the first-order FT-RDMFT functional. We have shown in Section 4.2.5 that the minimization of this first-order functional is equivalent to a solution of the FT-HF equations. In the following section we will therefore investigate the temperature dependence of the FT-HF single-particle dispersion relation for collinear as well as for PSS configurations.

$r_c(a.u.)$	4.0	4.5	5.0	5.5
$T_c(K)$	2700	3400	4100	5000

Table 8.2: Critical temperatures T_c^{PSS} above which no equilibrium PSS phase was found.
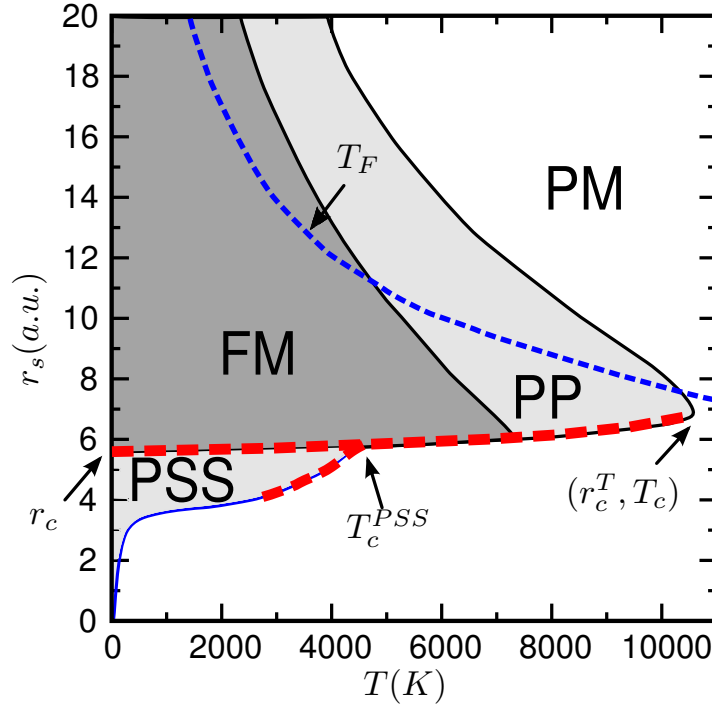
Figure 8.19: Phase diagram of the HEG in first-order FT-RDMFT (FT-HF) approximation. FM: ferromagnetic collinear phase, PM: paramagnetic collinear phase, PP: partially polarized collinear phase, PSS: planar spin spiral state. The thick dashed red line denotes first-order phase transitions. The dotted blue line denotes the Fermi temperature T_F.

8.5 FT-HF dispersion relations

At zero temperature, the HF dispersion relations for a collinear spin configuration can be calculated analytically to yield

$$\varepsilon_\sigma(k) = \frac{k^2}{2} - \frac{2}{\pi} f_d(k/k_{F\sigma}). \tag{8.71}$$

$f_d(x)$ denotes the dimension-dependent corrections. In three dimensions it reads

$$f_3(x) = \frac{1}{2} + \frac{1-x^2}{4x} \log \left| \frac{1+x}{1-x} \right|. \tag{8.72}$$

The two-dimensional correction is given by

$$f_2(x) = \begin{cases} E(x) & , x < 1 \\ x \left(E\left(\frac{1}{x}\right) - \left(1 - \frac{1}{x^2}\right) K\left(\frac{1}{x}\right) \right) & , x \geq 1 \end{cases},$$

where $E(x)$ and $K(x)$ are the complete elliptic integrals of the first and second kind.

At finite temperature, because of the entropy, the minimum of the free energy functional will always be assumed on the interior of Γ^N (see Eq. (2.22)), i.e. there will be no pinned states. Therefore, at the minimum of $F[\{n_i\}]$ from Eq. (8.47) the following relation holds

$$\frac{\partial F}{\partial n_i} = 0 = \frac{\partial \Omega_k}{\partial n_i} - \frac{1}{\beta} \frac{\partial S_0}{\partial n_i} + \frac{\partial \Omega_x}{\partial n_i}. \tag{8.73}$$

8.20.a: Three dimensions   8.20.b: Two dimensions

Figure 8.20: Hartree-Fock dispersion relation for the HEG in collinear spin configuration in three and two dimensions at $r_s = 5a.u.(T_F = 23300K)$ for different values of $t = T/T_F$. The black dotted line denotes the noninteracting relation $\varepsilon(k) = k^2/2$.

With the explict form of $S_0[\{n_i\}]$ of Eq. (8.49) this yields

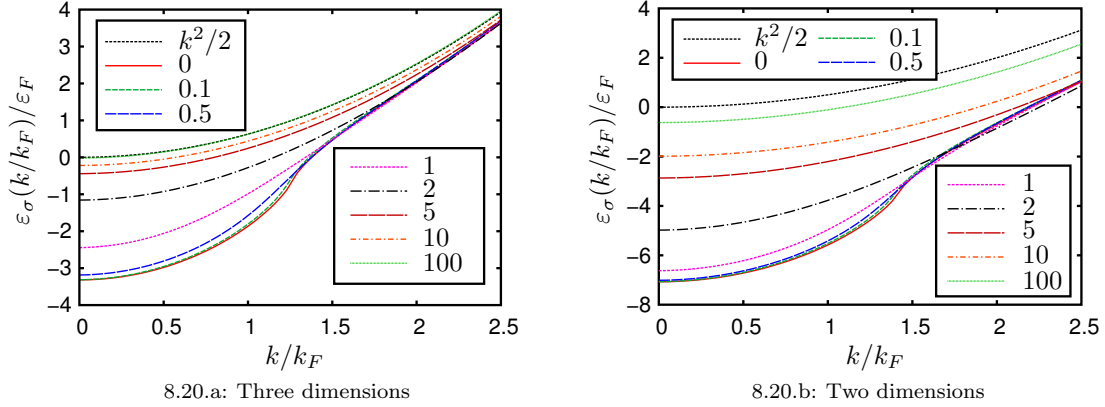$$\varepsilon_i - \mu = \frac{\partial \Omega_k}{\partial n_i} + \frac{\partial \Omega_x}{\partial n_i}, \tag{8.74}$$

which can be easily accessed numerically. We calculated the FT-HF dispersion relation for the fully polarized HEG in three and two dimensions for $r_s = 5a.u.$ and various values of t. The results are shown in Figure 8.20. Because of the full polarization, the Fermi surface is at $k/k_F = 2^{\frac{1}{d}}$, where d is the dimension of the HEG under consideration. Because the exchange contribution does not couple the different spin channels in collinear configuration, the unoccupied band shows the noninteracting dispersion relation $k^2/2$. For the occupied band at zero temperature we recover the exact relations to good agreement. An increase of the temperature then first lets the "valley" in the dispersion relation vanish and then secondly lets the eigenenergies approach the noninteracting relation, therefore closing the HF-gap. This can be understood from the thermal smoothing of the momentum distribution, induced by the entropy. Because NOs of very different quantum numbers generally have only small overlap, this leads to a decrease of the influence of the exchange contribution compared to the kinetic energy.

As a second choice for the NOs of the 1RDM we will now consider PSS states as defined in Section 8.4.2. The single-particle eigenenergies can be determined in the same way as for the collinear case (see Eq. (8.74)). We choose the same Wigner-Seitz radius $r_s = 5a.u.$ as in Figure 8.20 to allow for a comparison between the dispersion relations of collinear and PSS configurations. Considering a fully polarized PSS configuration with $q = 1.6$, we yield the dispersion relation shown in Figure 8.21. In Figure 8.21.a we show the zero-temperature PSS dispersion (T=0), the collinear ferromagnetic (FM) dispersion and the PSS dispersion corresponding to a noninteracting system (n.i.). The noninteracting PSS energies $e_b^0(k)$ are given simply by

$$e_b^0(k) = \frac{\left(k \pm \frac{q}{2}\right)^2}{2} - \frac{q^2}{8} = \frac{1}{2}(k^2 \pm kq). \tag{8.75}$$

As a first difference to the collinear case we see that the unoccupied band at zero temperature does not follow the noninteracting relation. This is due to the fact that the exchange contribution in Eq. (8.62) explicitly couples both PSS channels. In Figure 8.21.b we then demonstrate the effect of temperature on the PSS dispersion relation. As for the collinear configuration, the temperature first lets the "valley" in the dispersion relation of the occupied band disappear. With a further increase
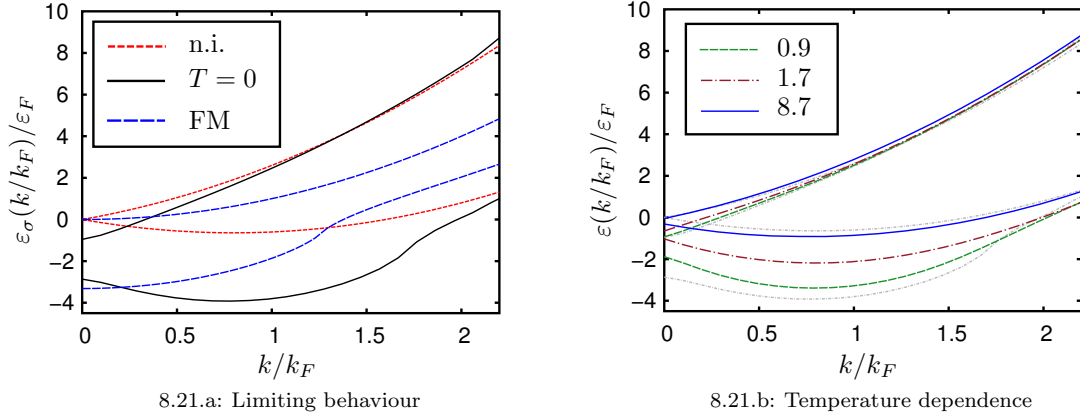
8.21.a: Limiting behaviour

8.21.b: Temperature dependence

Figure 8.21: Hartree-Fock dispersion relation for the PSS phase with $q = 1.6$ in the HEG at $r_s = 5a.u.(T_F = 23300K)$ for different values of $t = T/T_F$. Figure 8.21.a: The red short-dashed lines (n.i.) denote the noninteracting dispersions $\varepsilon(k/k_F)/\varepsilon_F = (k^2 \pm kq)/2$. The blue long-dashed lines (FM) represent the ferromagnetic collinear dispersions. The black solid line shows the PSS dispersion at $T = 0$. Figure 8.21.b: Dispersion relations for fully polarized PSS configurations at different reduced temperatures.

of the temperature, both unoccupied as well as occupied bands then approach the noninteracting dispersion relation.

The method of FT-RDMFT proved to be an efficient tool for the description of the eq-properties of the HEG at finite temperature in FT-HF approximation. An inclusion of correlation can now be achieved by an addition of an appropriate functional Ω_c to the first-order functional as defined in Eq. (8.50). In the following, we are going to investigate several choices of correlation functionals in the theoretical framework of FT-RDMFT and study their effect on the collinear magnetic phase diagram.

8.6 Correlation in FT-RDMFT

As a first class of candidates for correlation functionals in FT-RDMFT we will now investigate correlation functionals from DFT, both from zero, as well as from finite temperature frameworks.

8.6.1 DFT-LSDA correlation

The employment of correlation functionals from DFT in FT-RDMFT basically approximates the full 1RDM dependence of the correlation functional as a density-dependent one.

$$\Omega_c[\gamma] = \Omega_c^{DFT}[n] \tag{8.76}$$

We should like to point out that this approach exhibits an important intrinsic flaw. This becomes clear, if one reviews the minimization procedure for the case of local external potentials and separates the variation over 1RDMs in a combined variation over densities and a variation over the class of 1RDMs which yield a certain density:

$$F_{eq} = \min_{\gamma} F[\gamma] = \min_{n} \min_{\gamma \to n} F[\gamma] \tag{8.77}$$

$$= \min_{n} \left(\Omega_{ext}[n] + \Omega_H[n] + \Omega_c[n] + \min_{\gamma \to n} (\Omega_k[\gamma] - k_B T S_0[\gamma] + \Omega_x[\gamma]) \right). \tag{8.78}$$

As we assumed the correlation contribution to be independent of the particular form of the 1RDM as long as the diagonal, i.e. the density, stays the same we can take it out of the minimization

over 1RDMs. We find that the minimization over the 1RDMs now only contains kinetic, exchange, and entropy contributions. If the density n refers to a solution of the finite temperature Hartree-Fock equations to some external potential then we have shown in Section 4.2.5 that the constrained minimization of this combination of functionals gives the corresponding Hartree-Fock momentum distribution. The resulting 1RDM will in this sense be "uncorrelated". The severe problem with this result can be understood by considering the zero-temperature limit. Any choice of correlation functional in FT-RDMFT which just depends on the density will lead to a step function as the momentum distribution for low temperatures. As mentioned, this argument hinges on the assumption that the density n is a Hartree-Fock density of some external potential. In the case of the HEG this is obviously justified but for general systems with nonlocal external potential it is not clear if all densities share this property. Nonetheless the previous considerations show that for a wide class of external potentials, i.e. all which lead to a gs-density which is the Hartree-Fock density to some other external potential, the optimal 1RDM will be uncorrelated. This knowledge of the nature of the failure of DFT-functionals allows us to, at least partially, take account of these shortcomings in the following.

We are going to employ the correlation-energy of the electron gas as parametrized in the PWCA approximation. Remembering the conceptual difference between RDMFT and DFT, i.e. the knowledge of the exact kinetic energy functional, one might be tempted to remove the kinetic contribution from the PWCA-functional before employing it as a correlation-energy functional in RDMFT. This procedure, however, would be incorrect as will be explained below.

Based on our previous discussion of the intrinsic problems of the utilization of DFT functionals in RDMFT we know that the minimizing momentum distribution will be "uncorrelated", i.e. will reproduce the Hartree-Fock solution which becomes a step function $n^0(\boldsymbol{k})$ in the $T \to 0$ limit. If we removed the kinetic contribution the correlation-energy functional would be given by the interaction contribution W_c^{PWCA} alone and the free energy at density n would read

$$F \overset{T \to 0}{\equiv} \Omega_k[n^0(\boldsymbol{k})] + \Omega_x[n^0(\boldsymbol{k})] + W_c^{PWCA}(n). \tag{8.79}$$

Because the momentum distribution is a step function, this expression reproduces exactly the Monte-Carlo results without the kinetic contribution. This poses a problem because removing the kinetic contribution from a DFT-correlation functional yields an overall bad approximation. A straightforward remedy of this problem is the re-inclusion of the kinetic contribution to accomodate for the "uncorrelated" nature of the momentum distribution. Cashing in on our previous discussion we are therefore able to construct a FT-RDMFT functional which reproduces the exact Monte-Carlo results in the $T \to 0$ limit. The resulting phase diagram is shown in Figure 8.22.

By construction, we recover a critical Wigner-Seitz radius of $r_c \approx 70 a.u.$. However, we encounter several properties not expected from our considerations in Section 8.1. In the radius range of $20 a.u.$ to $70 a.u.$ with an increase of temperature we encounter a first-order phase transition to a partially polarized state. A further increase of temperature then leads to a second-order phase transition back to the paramagnetic configuration. Considering the density range defined by $70 a.u. < r_s < 90 a.u.$, the situation becomes worse. Starting from the ferromagnetic configuration at zero temperature we encounter first a first-order phase transition to a paramagnetic state, then another first-order phase transition to a partially polarized state and then another second-order transition back to the paramagnetic configuration. We attribute the appearance of the big partially polarized phase for temperatures above T_F to the fact that the 1RDM is "uncorrelated" and therefore the entropy is underestimated. It would be interesting to investigate, how a FT-LSDA from DFT would perform in the FT-RDMFT framework, but unfortunately this theory does not exist so far. We will therefore resort to an approximate inclusion of temperature effects by employing the temperature-dependent RPA approximation from FT-MBPT (see Section 8.3).
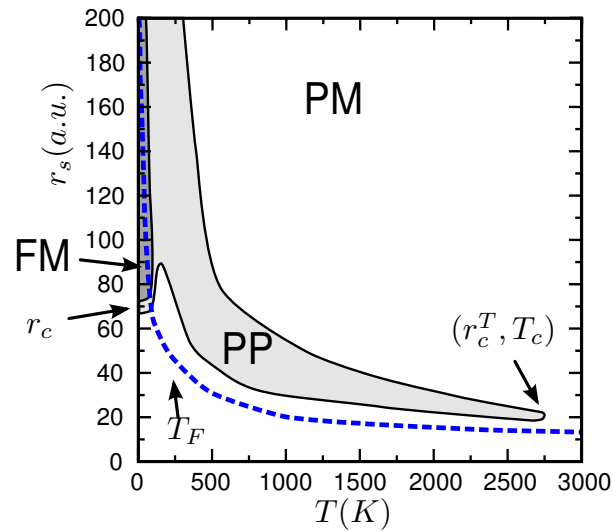
Figure 8.22: Collinear phase diagram of the HEG for the DFT-LSDA functional. FM: ferromagnetic phase, PM: paramagnetic phase, PP: partially polarized phase. The dotted blue line denotes the Fermi temperature T_F.

8.6.2 FT-DFT-RPA correlation

From our investigation of the FT-MBPT contributions on the phase diagram of the HEG in Sections 8.3.2 and 8.3.3, we deduce that an inclusion of the second-order Born approximation does more harm than good. We therefore include only the finite-temperature RPA contribution as defined in Eqs. (8.36) and (8.37). The resulting phase diagram is shown in Figure 8.23. As can be seen from
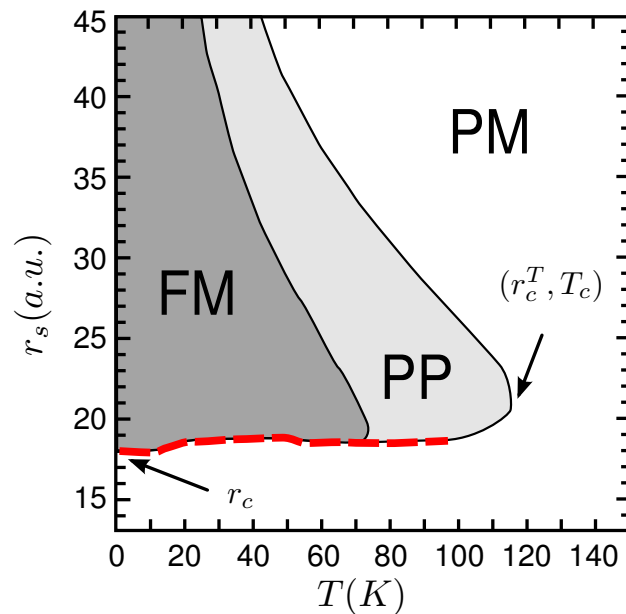

Figure 8.23: Collinear phase diagram of the HEG for the FT-DFT-RPA functional. The thick dashed red line denotes first-order phase transitions. T_F is too big to fit in the graph.

these results, the inclusion of the DFT-RPA contribution leads to a decrease of the ferromagnetic phase. The shape of the phase diagram stays the same as for the Hartree-Fock functional. It exhibits both characteristic phase transitions, a first-order and a second-order one. Because the 1RDM is "uncorrelated", at zero temperature the momentum distribution will be the same as in the FT-MBPT treatment, namely a step function. Therefore, we recover the critical RPA Wigner-Seitz radius of $r_c \approx 18a.u.$. The critical temperature T_c becomes $\approx 120K$ which is an order of magnitude smaller than the Fermi temperature $T_F \approx 1300K$ of the corresponding critical radius $r_c^T \approx 21a.u.$. When we compare the phase diagram from our FT-RDMFT treatment in Figure 8.23 with the corresponding one from FT-MBPT in Figure 8.8, we see that the ferromagnetic phase is reduced. This is in accordance with our investigation of the behaviour of the energy contributions in Section 8.4.1 (see Figure 8.13). Because the ferromagnetic phase in FT-MBPT RPA exists at a temperature much smaller than T_F, the FT-RDMFT variation of the momentum distribution will lead to a favourisation of the paramagnetic configuration compared to the FT-MBPT treatment.

This concludes our investigation of the effect of DFT correlation functionals in FT-RDMFT. As we have seen, the uncorrelated nature of the resulting eq-1RDM leads to several properties of the resulting phase diagrams which do not match our expectation from Section 8.1. These were e.g. the appearance of partially polarized phases above the Fermi temperature or critical temperatures far below the Fermi temperature. We will now try to remedy these problems by considering correlation functionals from the zero-temperature version of RDMFT.

8.6.3 Zero-temperature RDMFT correlation

Both DFT methods for the inclusion of correlation effects described so far exhibit severe shortcomings and qualitatively wrong results with respect to the equilibrium momentum distributions and phase diagrams. As a third option, we therefore employ correlation functionals from zero-temperature RDMFT. These functionals, by construction, are independent of the temperature and therefore have to be seen as first steps towards the development of truly temperature-dependent correlation functionals in the framework of FT-RDMFT.

At first, we will consider the α functional as defined in Eq. (3.16) with $f(n_i, n_j) = (n_i n_j)^\alpha$. We already mentioned in Section 3 that because of its spin-channel seperability, the α functional is intrinsically incapable of accurately reproducing the equilibrium free energies of both unpolarized as well as polarized HEGs together. However, because it is a successful representative of zero-temperature xc functionals, we investigate its finite-temperature performance, hoping to gain some insight into its behaviour at arbitrary temperatures, including the zero-temperature case. For our discretized 1RDM, the xc functional contribution becomes

$$\Omega_{xc}^\alpha[\{n_{\sigma i}\}] = \sum_{\sigma i,j} n_{\sigma i}^\alpha n_{\sigma j}^\alpha K_{i,j}, \tag{8.80}$$

with $K_{i,j}$ given by Eq. (8.52). Repeating some of our statements from Section 3, $\alpha = 1$ reproduces the first-order approximation, neglecting correlation completely. Choosing $\alpha = 0.5$ corresponds to the Müller functional [70, 71] which at zero temperature is known to overestimate the correlation contribution in spin-unpolarized situations (see Figure 3.1). We calculated the phase diagram for several values of α and show the values for r_c, T_c, r_c^T in Table 8.3. $\alpha = 0.55$ was shown in [31] to reproduce the correlation energy of the HEG for $0.2 < r_s < 9.0$ quite accurately.

To understand the effect of the α functional on the phase diagram it is instructive to review the important aspects of the first-order functional mentioned at the end of the previous section. A decreasing α now has two main effects.

First of all, because $0 \leq n_i \leq 1$ and $\alpha < 1$,

$$\Omega_{xc}^\alpha[\gamma] \leq \Omega_x[\gamma]. \tag{8.81}$$

Therefore, the α functional yields a bigger contribution to the free energy than the first-order functional.

α	1	.9	.8	.7	.6	.55
$r_c(a.u.)$	5.56	5.45	5.39	5.28	4.70	$\approx$5
$T_c(K)$	10500	9400	8500	7200	6500	4600
$r_c^T(a.u.)$	7.10	7.25	7.75	8.25	9.00	9.50

Table 8.3: Critical temperatures and densities for various values of α. The energy differences decrease with decreasing α. For $\alpha = .55$ we could not get an accurate estimate for r_c within our energy resolution.
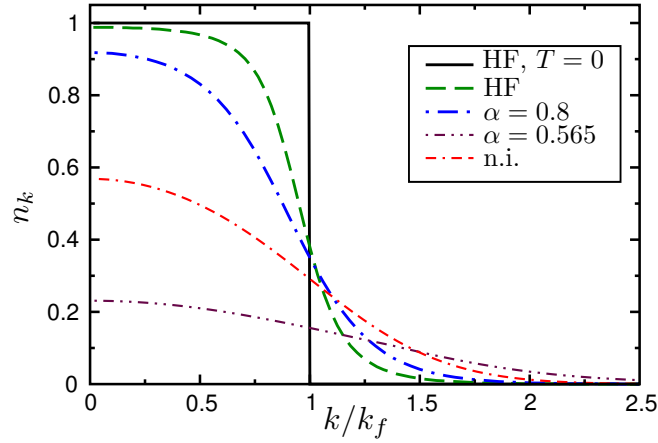

Figure 8.24: Equilibrium momentum distributions for a paramagnetic configuration at $r_s = 10a.u.$. The solid black line denotes the Hartree-Fock (or $\alpha = 1$) solution at zero temperature. The other graphs show the equilibrium momentum distributions for $T = 5000K$ for different values of α. The noninteracting solution is given by the red 2-dash-1-dot line.

The second effect is due to the nonanalyticity of Ω_{xc}^α for vanishing ONs. As explained in Section 3, this leads to an occupation of all ONs and therefore to a smoothing of the momentum distribution of the eq-1RDM. We show two representative distributions in Figure 8.24. Such a smoother momentum distribution leads to a bigger entropy contribution which in turn favours the paramagnetic phase.

These two effects compete and from our results we see that for low temperatures, the first one dominates, leading to a decrease of the critical density r_c as shown in Table 8.3. With increasing temperature, the second effect finally overcomes the first effect and therefore, with decreasing α, the critical temperature T_c and the critial Wigner-Seitz radius r_c^T increase.

When considering PSS states, it was shown in [139] that an increase of α leads to a decrease of the amplitudes of the PSS states at zero temperature. In accordance with these results, we could not observe any PSS phase for $\alpha < 0.8$. Furthermore, as mentioned before, the smoothing of the momentum distribution, due to the decrease of α, increases the effect of temperature when compared to the first-order FT-RDMFT functional. A decrease of α therefore leads to a reduction of the critical temperature of the PSS phase. The values of T_c^{PSS} for some values of α are given in Table 8.4.

From these results, we see that the α functional is capable of capturing some effects of correlation

α	1	0.95	0.9	0.85
$T_c^{PSS}(K)$	4500	3000	2000	500

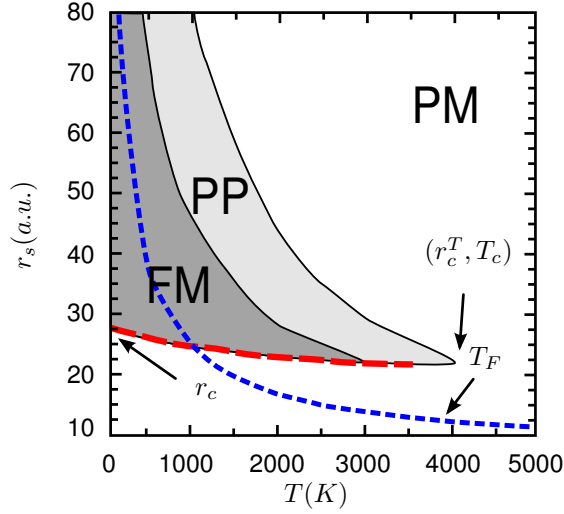Table 8.4: T_c^{PSS} for various values of α

Figure 8.25: Collinear phase diagram of the HEG for the BOW-TIE functional. FM: ferromagnetic phase, PM: paramagnetic phase, PP: partially polarized phase. The thick dashed red line denotes a first-order phase transition. The dotted blue line denotes the Fermi temperature T_F.

also at finite temperature, like the broadening of the momentum distribution and the reduction of the ferromagnetic phase. It fails, however, to increase r_c which is known to be one order of magnitude higher than the Hartree-Fock result. Making the parameter α polarization-dependent does not manage to increase r_c. As we have seen in Section 3, the choice of $\alpha(\xi)$ which reproduces the correlation energies best fails to reproduce a magnetic phase transition. Therefore, as a second example of a zero-temperature RDMFT correlation functional, we are now going to investigate the BOW functional as defined in Section 3.3. To recover the magnetic phase transition we use the TIE-modification from Eq. (3.30) which yields $r_c \approx 30 a.u.$ and reproduces the correlation energies over the whole range of densities and polarizations quite accurately. The resulting phase diagram for collinear spin configuration is shown in Figure 8.25. It reproduces most the features expected (see Table 8.1 and Figure 8.2).

The investigation of PSS states in the BOW functional cannot be easily achieved by a change of the prefactors in the exchange contribution. This can be understood from the following. Let us recapitulate the exchange contribution to the free energy of Eq. (8.61). We now want to include an additional coupling between the ↑↑ and ↓↓ contributions of the 1RDM. We model this additional term as

$$\Omega_c^+[\gamma] = -\frac{1}{2} \int d^3r d^3r' w(\boldsymbol{r} - \boldsymbol{r}')(\gamma_{\uparrow\uparrow}(\boldsymbol{r}, \boldsymbol{r}')\gamma_{\downarrow\downarrow}(\boldsymbol{r}', \boldsymbol{r}) + \gamma_{\downarrow\downarrow}(\boldsymbol{r}, \boldsymbol{r}')\gamma_{\uparrow\uparrow}(\boldsymbol{r}', \boldsymbol{r})). \quad (8.82)$$

Using the SDW-1RDM, as defined in Eqs. (8.60)-(8.60), one gets

$$\Omega_c^+[\gamma] = -\frac{1}{2n} \int \frac{d^3k_1}{(2\pi)^3} \frac{d^3k_2}{(2\pi)^3} \frac{4\pi}{|\boldsymbol{k}_1 - \boldsymbol{k}_2 - \boldsymbol{q}|^2}$$
$$\left(n_{1\boldsymbol{k}_1} \cos^2\left(\frac{\Theta_{\boldsymbol{k}_1}}{2}\right) + n_{2\boldsymbol{k}_1} \sin^2\left(\frac{\Theta_{\boldsymbol{k}_1}}{2}\right) \right) \left(n_{2\boldsymbol{k}_2} \cos^2\left(\frac{\Theta_{\boldsymbol{k}_2}}{2}\right) + n_{1\boldsymbol{k}_2} \sin^2\left(\frac{\Theta_{\boldsymbol{k}_2}}{2}\right) \right) \quad (8.83)$$

We see that, in contrast to the exchange contribution, this correlation functional explicitly depends on the PSS wavevector $\boldsymbol{q}$. Carrying out the product in the integrand, one will then acquire four products of two ONs. These could then be replaced by $f(n_i n_j)$, as presented in Section 3.1.1, to

model correlation effects. The implementation and testing of these functionals is left for further studies and will not be dealt with in this work.

As a final approach to the problem of describing correlation effects in FT-RDMFT we will now consider the perturbative methodology, as derived in Section 6. We will show that a straightforward inclusion of a given subset diagrams is fairly complicated and could lead to a variational collapse.

8.6.4 FT-RDMFT perturbation expansion

Whereas the contributions $\Omega_k, \Omega_{ext}, S_0$, and Ω_x depend only on the momentum distribution directly, Ω_{2b} and Ω_r (and all higher-order diagrams which exhibit more independent momenta than noninteracting Green's functions) also depend explicitly on the Kohn-Sham energies. This becomes a problem in FT-RDMFT as we will show in the following. Using the fundamental one-to-one correspondence $n \leftrightarrow v_{KS}$, we see that n determines v_{KS} which determines $\varepsilon(\mathbf{k})$. Hence the $\varepsilon(\mathbf{k})$ are functionals of n and Ω_r can be viewed as an implicit functional of $\varepsilon(\mathbf{k})$. To get a rough idea of the behaviour of this functional we parametrize the Kohn-Sham energies in the following way.

$$\varepsilon(m; \mathbf{k}) = \frac{k^2}{2m} \tag{8.84}$$

m is the variational parameter and can be interpreted as an effective mass. We note that the fugacity shows a simple dependence on m, namely $\alpha(t; m) = \alpha(mt)$, and the momentum distribution becomes

$$n(t, m; \mathbf{k}) = \frac{1}{1 + e^{\frac{k^2}{mt} - \alpha(mt)}} = n(mt, 1; \mathbf{k}). \tag{8.85}$$

The general effect of m on the momentum distribution is then that a decrease of m leads to a smoother momentum distribution. We are therefore able to investigate qualitatively the behaviour of FT-RDMFT functionals under a change in $n(\mathbf{k})$. The contributions up to first-order show the following dependence on m.

$$\Omega_k(t, m) = \Omega_k(mt, 1) \tag{8.86}$$
$$\Omega_{ext}(t, m) = \Omega_{ext}(mt, 1) \tag{8.87}$$
$$N(t, m) = N(mt, 1) \tag{8.88}$$
$$S_0(t, m) = S_0(mt, 1) \tag{8.89}$$
$$\Omega_x(t, m) = \Omega_x(mt, 1) \tag{8.90}$$
$$F(t, m) = E_k(mt, 1) + \Omega_{ext}(mt, 1) - 1/\beta S_0(mt, 1) + \Omega_x(mt, 1) \tag{8.91}$$

It has to be noted that because of the temperature prefactor of S_0, $F(t, m) \neq F(mt, 1)$. The second-order Born diagram, as well as the RPA contribution, shows different behaviour because of the explicit dependence on $\varepsilon(m; \mathbf{k})$.

$$\Omega_{2b\sigma}(t, m) = m\Omega_{2b\sigma}(mt, 1) \tag{8.92}$$
$$\chi_\sigma(t, m; q, \nu_a) = m\chi_\sigma(mt, 1; q, \nu_a) \tag{8.93}$$

This choice of diagrams leads to severe problems, as we will show in the following. We assume $t << 1, m >> 1$ and $mt << 1$. A small change in m will therefore change the momentum distribution only negligibly and all contributions up to first-order in the interaction will not change strongly. We can see from Figure 8.6 that Ω_r then decreases for increasing m. Ω_r therefore favours a more "washed-out" momentum distribution. Considering now the limit $t \to 0$, one can choose m arbitrarily big, leading to a divergence of Ω_r. An inclusion of Ω_r only in addition to the first-order functional will therefore lead to a variational collapse for $t \to 0$. We will now investigate the behaviour of Ω_{2b} in our parametrization. With the same restrictions on m and t as before, we see from Figure 8.4 that

Ω_{2b} increases with increasing m and therefore favours a less "washed-out" momentum distribution. Ω_{2b} and Ω_r now compete in a variational minimization w.r.t. m and the problem of variational collapse disappears for this choice of diagrams. However, our calculations show that the results show a qualitatively incorrect density dependence for $t \to 0$. This is due to the fact that Ω_{2b} is independent of the density. With increasing r_s it therefore gains influence when compared to the Ω_r-contribution. This then leads to a less "washed-out" momentum distribution which is in contrast to the expected exact behaviour. When considering high densities, i.e. $r_s \to 0$, the situation is reversed. Ω_r is dominant over Ω_{2b} which leads to a more "washed-out" momentum distribution. Furthermore, the dominance of Ω_r will lead to a big value for m which in turn via Eq. (8.93) leads to free energies which are orders of magnitude below the FT-MBPT results.

A solution to the wrong behaviour for small densities could be a screening of the second-order Born contribution Ω_{2b}. We implemented an RPA screening of Ω_{2b} and found no improvement for our results - a fact not too surprising, considering that the screening vanishes for $m \to 0$.

$$W^{RPA}(t, m) = \frac{W}{1 - mW\chi(mt, 1)} \tag{8.94}$$

The wrong behaviour for small r_s could be corrected by a restriction on the variational parameter m, since one knows that $m = 1$ reproduces the correct result for $r_s \to 0$. But this is against the ideal of having a functional which is capable of reproducing the equilibrium properties of a system by a free variation. It would also not be clear how one would restrict the momentum distribution for different parametrizations.

Taking the previous considerations into account, we come to the conclusion that an inclusion of higher-order diagrams in the methodology derived in Section 6 will most likely lead to ill-behaved functionals, yielding wrong energies and momentum distributions. This does not affect the validity of the results from Section 6. It shows only that the utilization of a subset of diagrams in a variational scheme carries the danger of leading to a variational collapse. This fact is to be attributed to the total freedom of choice for $\varepsilon(\boldsymbol{k})$ by the inclusion of nonlocal potentials, a fact also recently pointed out in the context of GW [140]. As a general recipe for avoiding the problem of variational collapse one might model the perturbative expressions by approximations using the momentum distributions alone. We are going to investigate several first steps in this direction in the following.

As we have seen before, the divergence in Ω_r stems from the fact that the eigenenergies $\varepsilon_\sigma(\boldsymbol{k})$ appear exlicitely in the definition of χ_σ. A first guess to remedy this problem is to fix these eigenenergies to the noninteracting values.

$$\varepsilon_\sigma(\boldsymbol{k}) = \varepsilon_\sigma^0(\boldsymbol{k}) = \frac{k^2}{2} \tag{8.95}$$

We have implemented this correlation functional and found that it yields qualitatively incorrect results. The correlation functional in this approximation favours less washed out momentum distributions.

This drawback lets us formulate a functional resting on exact properties of the polarization propagator. As a first step in our approximation process we will model $\chi(\boldsymbol{q}, \nu_a)$ as being frequency independent, much in the spirit of the Coulomb hole plus screened exchange approximation (COHSEX) [141]. Using the relation

$$\frac{\partial n(\boldsymbol{k})}{\partial \varepsilon(\boldsymbol{k})} = -\beta n(\boldsymbol{k})(1 - n(\boldsymbol{k})), \tag{8.96}$$

the $\boldsymbol{q} \to 0$ limit of the kernel of $\chi(\boldsymbol{q}, 0)$ can be calculated up to second order to give

$$\frac{n(\boldsymbol{k} + \boldsymbol{q}) - n(\boldsymbol{k})}{\varepsilon(\boldsymbol{k} + \boldsymbol{q}) - \varepsilon(\boldsymbol{k})} = \frac{\partial n(\boldsymbol{k})}{\partial \varepsilon(\boldsymbol{k})} \left(1 + \frac{\beta(n(\boldsymbol{k}) - \frac{1}{2}) \sum_{i,j} q_i q_j \frac{\partial \varepsilon(\boldsymbol{k})}{\partial k_i} \frac{\partial \varepsilon(\boldsymbol{k})}{\partial k_j}}{\sum_i q_i \frac{\partial \varepsilon(\boldsymbol{k})}{\partial k_i}} \right). \tag{8.97}$$

We assume the ONs and eigenenergies to be point symmetrical around the origin, i.e. $n(\boldsymbol{k}) = n(-\boldsymbol{k})$ and $\varepsilon(\boldsymbol{k}) = \varepsilon(-\boldsymbol{k})$. Accordingly, the second term in Eq. (8.97) vanishes in the integration over $\boldsymbol{k}$. The polarization propagator in the limit $\boldsymbol{q} \to 0$ therefore becomes

$$\chi_\sigma(\boldsymbol{q}) \xrightarrow{q \to 0} -\beta \int \frac{d^3k}{(2\pi)^3} n_\sigma(\boldsymbol{k})(1 - n_\sigma(\boldsymbol{k})) + O(q^2). \tag{8.98}$$

We now need to describe the momentum dependence for big $\boldsymbol{q}$. We restate the main expression for the RPA correlation grand potential Eq. (8.36):

$$\Omega_r = \frac{1}{\beta}(2\pi)^{-2} \int dq q^2 \left\{ \ln(1 - W(\boldsymbol{q})\chi(\boldsymbol{q})) + W(\boldsymbol{q})\chi(\boldsymbol{q}) \right\}. \tag{8.99}$$

It is now possible to estimate the behaviour of Ω_r. If $W(\boldsymbol{q})\chi(\boldsymbol{q})$ is big, the logarithm in the kernel of Ω_r becomes negligible. The main object defining whether or not $W(\boldsymbol{q})\chi(\boldsymbol{q})$ is big or small is $\beta/(q^2)$. We therefore split the integral in Eq. (8.99) in two parts, one where $q < \widetilde{q} = \sqrt{\beta}$ and one where $q > \widetilde{q}$:

$$\Omega_r \approx \Omega_r^0 + \Omega_r^\infty \tag{8.100}$$

$$\Omega_r^0 = \frac{1}{\beta}(2\pi)^{-2} \int_0^{\widetilde{q}} dq q^2 (W(\boldsymbol{q})\chi(\boldsymbol{q})) \tag{8.101}$$

$$= \frac{4\pi}{\beta}(2\pi)^{-2} \int_0^{\sqrt{\beta}} dq \chi(\boldsymbol{q})) \tag{8.102}$$

$$\Omega_r^\infty = -\frac{1}{\beta}(2\pi)^{-2} \int_{\sqrt{\beta}}^\infty dq q^2 \frac{(W(\boldsymbol{q})\chi(\boldsymbol{q}))^2}{2}. \tag{8.103}$$

It can be deduced from Eq. (8.102) that in the limit $T \to 0$, i.e. $\beta \to \infty$, Ω_r^0 diverges unless $\chi(\boldsymbol{q})$ behaves like

$$\chi(\boldsymbol{q}) \xrightarrow{q \to \infty} \propto q^{-\kappa} \tag{8.104}$$

$$\kappa \geq 2. \tag{8.105}$$

We incorporate the findings from the investigation of the exact limits of χ in the following KAPPA-approximation to the polarization propagator in Eq. (8.99).

$$\chi^\kappa[n(\boldsymbol{k})](\boldsymbol{q}) = \sum_\sigma \chi_\sigma^\kappa[n(\boldsymbol{k})](\boldsymbol{q}) \tag{8.106}$$

$$\chi_\sigma^\kappa[n(\boldsymbol{k})](\boldsymbol{q}) = -\frac{\beta}{1 + (q/k_F)^\kappa} \int \frac{d^3k}{(2\pi)^3} n_\sigma(\boldsymbol{k})(1 - n_\sigma(\boldsymbol{k})) \tag{8.107}$$

$$= -\frac{\beta}{1 + (q/k_F)^\kappa} \left(n_\sigma - \langle n_\sigma^2 \rangle \right), \tag{8.108}$$

where

$$\langle n_\sigma^2 \rangle = \int \frac{d^3k}{(2\pi)^3} n_\sigma^2(\boldsymbol{k}). \tag{8.109}$$

The prefactor of β ensures that Ω_r stays nonvanishing in the limit $\beta \to \infty$. The occurrence of $\left(n_\sigma - \langle n_\sigma^2 \rangle \right)$ in this approximation shows that $\chi_\sigma^\kappa[n(\boldsymbol{k})](\boldsymbol{q})$ will favour a more washed out momentum distribution.

We calculated the correlation-energy in the zero-temperature limit for several values of κ and show the results in Figure 8.26. The momentum distributions resulting from $\Omega_r^\kappa[\gamma]$ for $\kappa = 2.9$ are shown in Figure 8.27.
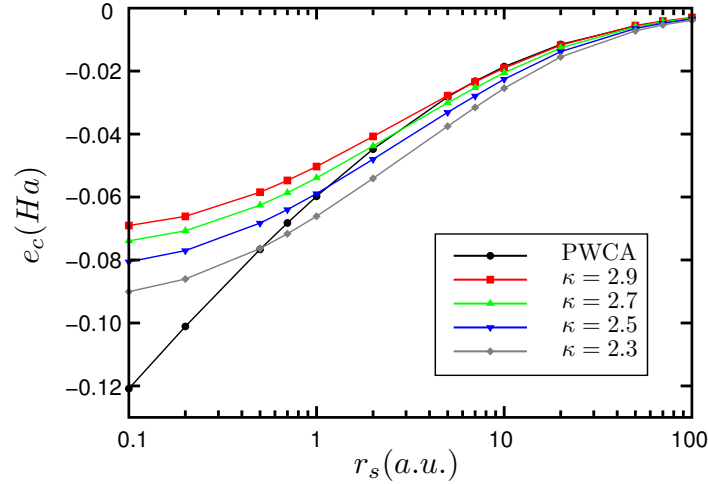
Figure 8.26: Correlation-energy of the three-dimensional electron gas for the KAPPA-functional for various values of κ. The black line denotes Monte-Carlo results in the PWCA [52] parametrization.

Unfortunately, the KAPPA-functional becomes spin-channel seperable in the $T \rightarrow 0$ limit. As in our discussion of zero temperature RDMFT we can make the parameter polarization dependent to describe the partially polarized HEG correctly (see Table 8.5). However, for the same reasons as in the previous discussions the descreasing parameter for decreasing polarization leads to a favourisation of the unpolarized phase in the low density limit and therefore to the absence of a phase transition.
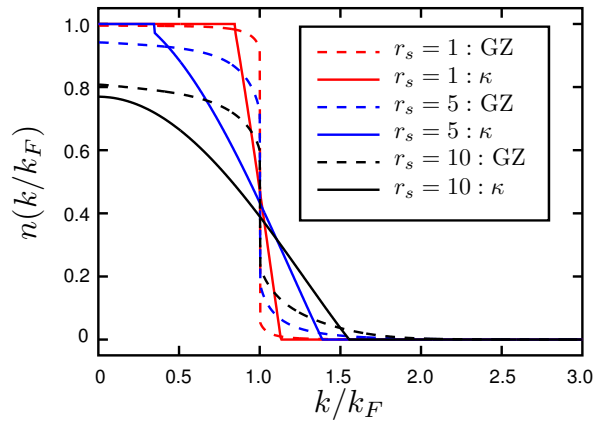
Figure 8.27: Momentum distributions of the HEG for $r_s \in \{1, 5, 10\} a.u.$ from the parametrization by Gori-Giorgi and Ziesche (GZ) [55] and from the KAPPA-functional for $\kappa = 2.9$.

KAPPA-functional										
ξ	0.0	0.1	0.2	0.3	0.4	0.5	0.6	0.7	0.8	0.9	1.0
κ	2.9	2.9	2.9	3.0	3.0	3.0	3.1	3.1	3.1	3.2	3.2

Table 8.5: Best parameters to describe the correlation-energy of a HEG in three dimensions in the range $1 < r_s < 100$ for the KAPPA-functional.

	κ	c
KAPPA-TIE	3.2	0.24

Table 8.6: Best parameters for the KAPPA-TIE-functional as defined in Eq. (8.107).
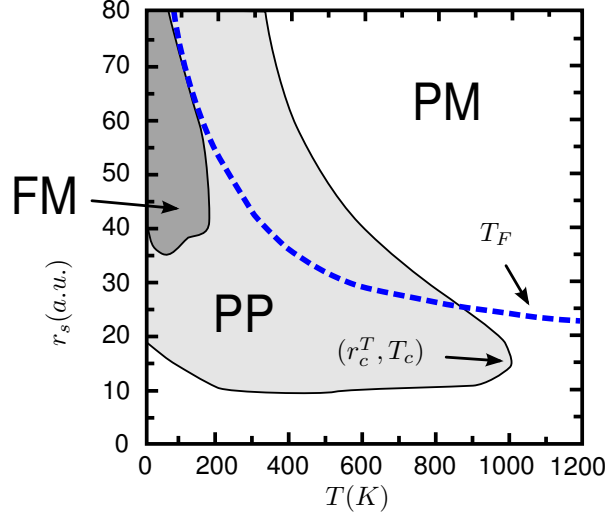
Figure 8.28: Collinear phase diagram of the HEG for the KAPPA-TIE functional. There are no first-order phase transitions. The dotted blue line denotes the Fermi temperature T_F.

We therefore propose a modification similar to the BOW-TIE functional, named KAPPA-TIE, as in Eq. (3.30) to recover a favourisation of the ferromagnetic phase for low densities.

$$\chi_\sigma^{\kappa-TIE}[n(\boldsymbol{k})](\boldsymbol{q}) = -\chi_\sigma^\kappa[n(\boldsymbol{k})](\boldsymbol{q}) - c\frac{\beta}{1 + q^2/k_F^2} \int \frac{d^3k}{(2\pi)^3} n_\uparrow(\boldsymbol{k})n_\downarrow(\boldsymbol{k})(1 - n_\uparrow(\boldsymbol{k})n_\downarrow(\boldsymbol{k})) \qquad (8.110)$$

The parameters which lead to an accurate description of correlation energies for arbitrary polarization over the whole range of densities and a decrease in the critical density are shown in Table 8.6.

We conclude our work by showing the phase diagram as resulting from the KAPPA-TIE functional with this choice of parameters in Figure 8.28. We see that the unphysical instantaneous quantum phase transition disappears and an increase in temperature slightly favours a partially polarized configuration over a paramagnetic one. In summary, the KAPPA-TIE functional constitutes an intrinsically temperature dependent true FT-RDMFT functional which describes the correlation-energy of a HEG at zero temperature with arbitrary polarization accurately, yields a qualtitatively improved momentum distribution, as compared to previously used RDMFT functionals, and leads to a reasonable magnetic collinear phase diagram.

8.7 Summary and outlook

In this final section of our work, we investigated the phase diagram of the three-dimensional HEG. Because the exact phase diagram is not known, we collected several properties we believe are prevalent in the exact phase diagram. We then reviewed existing methods for the calculation of the free energy of a HEG in grand canonical equilibrium. The first constituted a replacement of the Coulomb interaction by a model contact interaction, which leads to a qualitatively correct phase diagram.

We then employed FT-MBPT approximations. We chose exchange-only, exchange+RPA, and exchange+RPA+second-order Born diagrams and investigated the resulting phase diagrams. Both

exchange-only and exchange+RPA phase diagrams exhibit the correct shape when compared to our assumptions. However, both exhibit a critical Wigner-Seitz radius which is too low and additionally the exchange+RPA phase diagram leads to a critical temperature far below the Fermi temperature. The inclusion of the second-order Born diagram leads to several undesired properties of the phase diagram, the reasons of which we discussed.

After these applications of existing methods we turned to the description of the free energy via our novel framework of FT-RDMFT. We focussed on the first-order functional whose solution we had shown before to be equivalent to the FT-HF approximation. The resulting phase diagram is similar to the exchange-only diagram from FT-MBPT, exhibiting both the good overall shape as well as the bad critical density. However, the FT-RDMFT treatment was able to remedy some intrinsic problems of the FT-MBPT method. These were e.g. the equal smoothing of the momentum distribution of the different spin channels for partially polarized configurations and the increase of the free energy for low temperatures.

Besides the investigation of the collinear spin phase we also considered a phase exhibiting a chiral spin symmetry, which we termed PSS states. We showed that, in contrast to a conjecture by Overhauser, the PSS states exhibit a first-order phase transition when the temperature is increased. This phase transition could be attributed to an instantaneous jump in the optimal wavevector of the PSS state rather than to the reduction of the amplitude by temperature. Interestingly, we found that at small temperatures the amplitude of the PSS state actually increases compared to the zero-temperature amplitude.

The fact that the first-order FT-RDMFT functional is capable of reproducing the FT-HF solution was utilized to calculate the temperature dependence of the HF single particle dispersion relation. We found that for the three- and two-dimensional HEG in collinear spin configuration, as well as for the three-dimensional HEG in PSS configuration, an increase in temperature first leads to a vanishing of the characteristic "valleys" in the dispersion relations. This might serve as an argument why, for medium temperatures, a description via an effective mass might be justified. A further increase in temperature then lets the eigenenergies approach the noninteracting dispersion relation, as expected.

Crawling to the finish line, we studied the effect of correlation effects in the framework of FT-RDMFT. We could show that an inclusion of correlation functionals from DFT will inevitably lead to uncorrelated eq-1RDMs. The inclusion of the LSDA functional leads to several features of the phase diagram which are expected to be qualitatively wrong, like the subsequent phase transitions from ferromagnetic to paramagnetic to partially polarized to paramagnetic. The inclusion of FT-DFT-RPA, on the other hand, reproduced the shape of the phase diagram correctly but underestimated both the critical Wigner-Seitz radius as well as the critical temperature, in comparison to the Fermi temperature. Subsequently, we employed correlation functionals from zero-temperature RDMFT. The phase diagram resulting from the spin-separable α functional shows no improvement over the HF phase diagram. It leads to a slight decrease of the critical Wigner-Seitz radius as well as to a vanishing of the PSS phase. To overcome these problems and to get a qualitatively correct phase diagram, we then investigated the phenomenologically derived BOW-TIE functional from Section 3.3. By construction, it leads to a critical Wigner-Seitz radius comparable to the exact one. Additionally, we find that the resulting phase diagram also exhibits most properties we expect from the exact one. Finally, we considered true temperature dependent functionals depending on the full 1RDM. As a backdraw, we found that the inclusion of higher orders in a perturbative treatment, as derived in Section 6, is very complicated and will most likely lead to ill-behaved functionals. As a first remedy to this problem we proposed a method, similar to the existing COHSEX approximations, relying on several exact properties of the polarization propagator. The resulting KAPPA functional yields a reasonable collinear magnetic phase diagram and qualitatively correct momentum distributions. We summarize the agreement of the several approximations we investigated with the exact properties from Table 8.1 in Table 8.7.

We had already seen in Section 3.3 that the BOW functional is also capable of a qualitatively

	(1)	(2)	(3)	(4)	(5)	(6)	r_c
Stoner (Figure 8.3)					X		
FT-MBPT							
x-only (Figure 8.5)		X					X
x+RPA (Figure 8.8)		X			X		X
x+RPA+second Born (Figure 8.9)		X			X		X
FT-RDMFT							
first-order (FT-HF) (Figure 8.19)		X					X
x+DFT-LSDA (Figure 8.22)					X		
x+FT-DFT-RPA (Figure 8.23)		X			X		X
BOW-TIE (Figure 8.25)		X			X		X
KAPPA-TIE (Figure 8.28)							X

Table 8.7: Agreement of phase diagrams for different approximations with the properties from Table 8.1. An X in one of the first six columns denotes properties which are not fulfilled. An X in column 7 means, that the critical density at zero temperature is not reproduced.

correct description of the momentum distribution at zero temperature. As a task for the future we therefore propose the implementation and testing of the BOW and BOW-TIE functionals as well as of the KAPPA and KAPPA-TIE functionals for real physical systems. Questions of great theoretical interest concern then the dependence of the eq-symmetry on the temperature as well as the temperature dependence of the quasi-particle spectrum in solids.

A APPENDIX

A.1 Probabilistic interpretation of the ONs of the 1RDM

We are now going to investigate the ONs of a eq-1RDM which stems from a eq-SDO $\hat{D} = \sum_i w_i |\psi_i\rangle\langle\psi_i|$. The 1RDM is given as

$$\gamma(x, x') = \sum_i w_i \langle\psi_i|\hat{\Psi}^+(x')\hat{\Psi}(x)|\psi_i\rangle \tag{A.1}$$

$$= \sum_i n_i \phi_i^*(x')\phi_i(x). \tag{A.2}$$

The NOs $\{\phi\}$ can be used to build Slater determinants $\{|\chi\rangle\}$ which form a basis of the Hilbert space. We can now expand $|\psi_i\rangle$ in terms of $|\chi_i\rangle$.

$$|\psi_i\rangle = \sum_l c_{ij}|\chi_j\rangle \tag{A.3}$$

$$c_{ij} = \langle\chi_i|\psi_j\rangle \tag{A.4}$$

The SDO then becomes

$$\hat{D} = \sum_{ijk} w_i c_{ij}^* c_{ik} |\chi_j\rangle\langle\chi_k|. \tag{A.5}$$

Because we used the eigenfunctions of γ as basis for the Slater determinants, the expansion of the product of the field operators $\hat{\psi}^+(x')\hat{\psi}(x)$ in terms of creation and annihilation operators $(\hat{a}^+, \hat{a})$ will yield no offdiagonal contributions in the expectation value of Eq. (A.1). Using that $|\chi_i\rangle$ are Slater determinants, Eq.(A.1) then becomes

$$\gamma(x, x') = \sum_i \left(\sum_{jk} w_j |c_{jk}|^2 \langle\chi_k|\hat{n}_i|\chi_k\rangle \right) \phi_i^*(x')\phi_i(x). \tag{A.6}$$

This expression has a probabilistic interpretation if one identifies $|c_{jk}|^2$ with $P(\chi_k|\psi_j)$, i.e. the conditional probability of finding $|\chi_k\rangle$ in a measurement if we know that the system is in the state $|\psi_j\rangle$. Additionally, $\langle\chi_k|\hat{n}_i|\chi_k\rangle$ can be interpreted as $P(\phi_i|\chi_k)$, the conditional probability that $|\phi_i\rangle$ is part of the Slater determinant $|\chi_k\rangle$. And finally, w_j can be seen as the probability $P(\psi_i)$, i.e. the probability that $|\psi_j\rangle$ contributes to the eq-SDO. This leads to the following representation of the eq-1RDM

$$\gamma(x, x') = \sum_i \left(\sum_{jk} P(\psi_j)P(\chi_k|\psi_j)P(\phi_i|\chi_k) \right) \phi_i^*(x')\phi_i(x). \tag{A.7}$$

One can now use the result from probability theory that the probability of event A is given as a sum over the probability of event B times the conditional probability of A, given B:

$$P(A) = \sum_B P(A|B)P(B). \tag{A.8}$$

We then arrive at the following equation:

$$\gamma(x, x') = \sum_i P(\phi_i)\phi_i^*(x')\phi_i(x). \tag{A.9}$$

Therefore, $n_i = P(\phi_\alpha)$ can be interpreted as the probability that the actual state of the system, described by $\hat{D}$, contains $|\phi_i\rangle$ in an expansion of the form (A.5) with the weights w_i. The situation becomes simpler at zero temperature where the SDO is a single projection operator on the gs of the system, i.e. $w_i = \delta_{i0}$.

A.2 Equilibrium ONs in general systems

As we have pointed out in Section 4.2.3, ONs of an eq-1RDM of a noninteracting system are given by

$$n_i = \frac{1}{1 + e^{\beta(\varepsilon_i - \mu)}} \tag{A.10}$$

and will therefore be strictly between 0 and 1. We will now show that the latter is also true for the occupation numbers of eq-1RDMs of arbitrary systems, including interacting ones.

We start from the spectral representation of the eq-1RDM:

$$\gamma(x, x') = \sum_i n_i \phi_i^*(x') \phi_i(x). \tag{A.11}$$

The occupation number operator $\hat{n}_i$ is now defined as

$$\hat{n}_i = \hat{c}_i^+ \hat{c}_i \tag{A.12}$$

where c_i^+ (c_i) creates (annihilates) the natural orbital ϕ_i.

An arbitrary occupation number of the eq-1RDM in grand canonical equilibrium can then be written as

$$n_i = \text{Tr}\{\hat{D}\hat{n}_i\} = \sum_e w_e \langle \Psi_e | \hat{n}_i | \Psi_e \rangle. \tag{A.13}$$

The $\{\Psi_e\}$ are eigenfunctions of the Hamiltonian of the system and form a basis of the underlying Hilbert space. Another basis is formed by the Slater determinants $\{\Phi_\alpha\}$ which are constructed out of the natural orbitals $\{\phi_i\}$ of the eq-1RDM of the system. The transformation between these bases is governed by the expansion coefficients $c_{e\alpha}$ via

$$\Psi_e = \sum_\alpha c_{e\alpha} \Phi_\alpha. \tag{A.14}$$

Due to completeness and normalization of the $\{\Psi_e\}$ and $\{\Phi_\alpha\}$, the coefficients fulfill

$$\sum_e |c_{e\alpha}|^2 = \sum_\alpha |c_{e\alpha}|^2 = 1. \tag{A.15}$$

Expanding the $\{\Psi_e\}$ in Eq. (A.13) in terms of the $\{\Phi_\alpha\}$ then leads to

$$n_i = \sum_e w_e \sum_{\alpha\beta} c_{e\alpha}^* c_{e\beta} \langle \Phi_\alpha | \hat{n}_i | \Phi_\beta \rangle \tag{A.16}$$

Since the Slater determinants $\{\Phi_\alpha\}$ are constructed to be eigenfunctions of the occupation number operator $\hat{n}_i$, this reduces to

$$n_i = \sum_\alpha \underbrace{\left(\sum_e w_e |c_{e\alpha}|^2 \right)}_{f_\alpha} \underbrace{\langle \Phi_\alpha | \hat{n}_i | \Phi_\alpha \rangle}_{g_{i\alpha}}. \tag{A.17}$$

Using Eq. (A.15) and the properties of the thermal weights, $w_e > 0$ and $\sum_e w_e = 1$, we see that

$$f_\alpha > 0 \tag{A.18}$$
$$\sum_\alpha f_\alpha = 1. \tag{A.19}$$

The factors $g_{i\alpha}$ are equal to 1 if the natural orbital ϕ_i appears in the Slater determinant Φ_α and 0 otherwise. The summation over α corresponds to a summation over a basis of the Hilbert space, which is in the situation of a grand canonical ensemble the Fock space. Therefore, for a fixed i, there will be at least one α, so that $g_{i\alpha} = 1$ and at least one α for which $g_{i\alpha} = 0$. Applying this result, together with Eqs. (A.18) and (A.19), to Eq. (A.17) yields the desired inequality relations:

$$0 < n_i < 1. \tag{A.20}$$

A.3 Zero-temperature mapping between potentials and wavefunctions

To investigate the nature of the mapping between the nonlocal external potential and the corresponding gs-wavefunction we will consider the relationship between the potential and the gs-1RDM and then use Gilbert's theorem [26] to translate the results.

Assume an arbitrary Hamiltonian $\hat{H}$ with gs-1RDM γ_{gs}:

$$\hat{H} = \hat{T} + \hat{V} + \hat{W} \tag{A.21}$$

$$\gamma_{gs}(x, x') = \sum_i n_i \phi_i^*(x')\phi_i(x). \tag{A.22}$$

Due to Gilbert's theorem, the wavefunction can be formally written as a functional of the 1RDM and therefore an energy functional $E[\gamma]$ can be defined as

$$E[\gamma] = \langle \Psi[\gamma]|\hat{H}|\Psi[\gamma]\rangle. \tag{A.23}$$

From the variational principle, this functional is minimal for the gs-1RDM $\gamma_{gs}(x, x')$ and therefore the following relations hold

$$\left.\frac{\partial E[\gamma]}{\partial n_i}\right|_{\gamma_{gs}} = \begin{cases} a_i > \mu & , n_i = 0 \\ \mu & , 0 < n_i < 1 \\ b_i < \mu & , n_i = 1 \end{cases} \tag{A.24}$$

where μ can be identified as the chemical potential of the system. We will now be able to show that the mapping between potential and gs-1RDM is one-to-one if and only if there are no pinned occupation numbers, i.e. occupation numbers equal to 0 or 1. This will be done in two steps. At first we show that in the case of unpinned occupation numbers the external potential is uniquely determined up to a constant. Secondly, we will consider gs-1RDMs with pinned occupation numbers and show that one can explicitly construct infinitely many potentials which leave the gs-1RDM invariant.

• unpinned states:

The absence of pinned states allows us to use the following Euler-Lagrange equation

$$\left.\frac{\delta E[\gamma]}{\delta\gamma(x, x')}\right|_{\gamma_{gs}} = \mu \left.\frac{\delta N[\gamma]}{\delta\gamma(x, x')}\right|_{\gamma_{gs}} = \mu\delta(x, x'). \tag{A.25}$$

The addition of an arbitrary external potential contribution $U[\gamma] = \int dx dx' u(x', x)\gamma(x, x')$ to the energy functional, $E_u[\gamma] = E[\gamma] + U[\gamma]$, then yields

$$\left.\frac{\delta E_u[\gamma]}{\delta\gamma(x, x')}\right|_{\gamma_{gs}} = \mu\delta(x, x') + u(x, x'). \tag{A.26}$$

If we now claim that the minimizing 1RDM from $E[\gamma]$ is also the optimal one for $E_u[\gamma]$, we can deduce that the only possible choice of $u(x, x')$ which leaves the gs-1RDM invariant is

$$u(x, x') = c\delta(x, x'). \tag{A.27}$$

● pinned states:

As in the case of pinned occupation numbers the minimum of $E[\gamma]$ will be at the boundary of the domain, we cannot use Eq. (A.25). It would be possible to adjust the Euler-Lagrange equation by an incorporation of Kuhn-Tucker multipliers [94] but there is a simpler way, as described in the following.

The fact that for pinned states, the derivatives are allowed to be different from μ allows us to construct a one-particle potential which leaves the gs-1RDM invariant. This potential shall be governed by the generally nonlocal kernel $u(x, x')$. By choosing it to be diagonal in the basis of natural orbitals of the gs-1RDM we ensure that the orbitals will not change upon addition of the potential. For simplicity, we choose only one component to be non-vanishing.

$$u(x, x') = u\phi_\alpha^*(x')\phi_\alpha(x) \tag{A.28}$$

The new energy functional is then given by

$$E_\alpha[\gamma] = E[\gamma] + \int dx dx' u(x, x')\gamma(x', x) \tag{A.29}$$

and the derivative with respect to the occupation numbers becomes

$$\left.\frac{\partial E_\alpha[\gamma]}{\partial n_i}\right|_{\gamma_{gs}} = \begin{cases} a_i + u\delta_{i\alpha} & , n_i = 0 \\ \mu + u\delta_{i\alpha} & , 0 < n_i < 1 \\ b_i + u\delta_{i\alpha} & , n_i = 1 \end{cases} \tag{A.30}$$

These considerations can now be employed to show the ambiguity of the external potential in RDMFT for groundstates with pinned occupation numbers. For simplicity we will now assume that there is exactly one pinned occupation number with $n_\beta = 0$. We then construct a potential of the form of Eq. (A.28) with $\alpha = \beta$. From Eq. (A.30) we see that every choice of $u > \mu - a_\beta$ leads to a situation where the β-orbital exhibits a derivative bigger than μ, leaving the gs-1RDM invariant. For one pinned occuppation number $n_\beta = 1$ we can choose $u < \mu - b_\beta$ which lets the derivative of the β-orbital always surpass μ which again leads to the same gs-1RDM. When considering gs-1RDM with several pinned states these arguments are readily translated which proves the ambiguity of the one-particle potential for gs-1RDM with pinned occupation numbers.

A.4 Noninteracting grand canonical equilibrium

We are now going to investigate the grand canonical equilibrium of a noninteracting system. We will show that one can express the ONs and NOs of the eq-1RDM easily via the eigenvalues and eigenfunctions of the noninteracting one-particle Hamiltonian. Furthermore, we will show that both the grand potential Ω_0 as well as the entropy S_0 are simple functionals of the ONs of the eq-1RDM γ. The eq-SDO $\hat{D}$ is given by

$$\hat{D} = \frac{e^{-\beta(\hat{H}-\mu\hat{N})}}{Z} = \sum_i w_i|\chi_i\rangle\langle\chi_i|, \tag{A.31}$$

where the noninteracting one-particle Hamiltonian $\hat{H}^{(1)}$ is given in second quantization as

$$\hat{H} = \int dx dx' h(x, x')\hat{\Psi}^+(x')\hat{\Psi}(x). \tag{A.32}$$

$\hat{H}$ commutes with the 1RDM operator $\hat{\gamma}$, given by

$$\hat{\gamma} = \int dx dx' \gamma(x, x')\hat{\Psi}^+(x')\hat{\Psi}(x), \tag{A.33}$$

from which we can deduce that $h(x, x')$ and $\gamma(x, x')$ have the same eigenfunctions. The eq-1RDM γ will be denoted by

$$\gamma(x, x') = \sum_i w_i \langle \chi_i | \hat{\Psi}^+(x') \hat{\Psi}(x) | \chi_i \rangle \tag{A.34}$$

$$= \sum_i n_i \phi_i^*(x') \phi_i(x). \tag{A.35}$$

We will now express the field operators $\hat{\Psi}(x)$ in the basis of NOs of γ:

$$\hat{\Psi}(x) = \sum_i \hat{c}_i \phi_i(x). \tag{A.36}$$

Knowing that with this choice $\hat{\Psi}^+(x')\hat{\Psi}(x)$ will yield no offdiagonal contributions in γ, we can reformulate Eq. (A.34)

$$\gamma(x, x') = \mathrm{Tr} \left\{ \frac{e^{-\beta(\hat{H} - \mu \hat{N})}}{Z} \hat{\Psi}^+(x') \hat{\Psi}(x) \right\} \tag{A.37}$$

$$= \frac{1}{Z} \sum_i \phi_i^*(x') \phi_i(x) \sum_{n_1, n_2, \dots} \langle n_1, n_2, \dots | e^{-\beta \sum_j \hat{n}_j(\varepsilon_j - \mu)} \hat{n}_i | n_1, n_2, \dots \rangle \tag{A.38}$$

$$= \frac{1}{Z} \sum_i \phi_i^*(x') \phi_i(x) \sum_{n_1, n_2, \dots} \langle n_1 | e^{-\beta \hat{n}_1(\varepsilon_1 - \mu)} | n_1 \rangle \dots \langle n_i | e^{-\beta \hat{n}_\alpha(\varepsilon_i - \mu)} \hat{n}_i | n_i \rangle \dots \tag{A.39}$$

$$= \frac{1}{Z} \sum_i \phi_i^*(x') \phi_i(x) \left(\prod_j \sum_{n_j} \langle n_j | e^{-\beta \hat{n}_j(\varepsilon_j - \mu)} | n_j \rangle \right) \frac{\langle n_i | e^{-\beta \hat{n}_i(\varepsilon_i - \mu)} n_i | n_i \rangle}{\langle n_i | e^{-\beta \hat{n}_i(\varepsilon_i - \mu)} | n_i \rangle}. \tag{A.40}$$

Carrying out the summation over n_j, one gets

$$\gamma(x, x') = \frac{1}{Z} \sum_i \phi_i^*(x') \phi_i(x) \left(\prod_j (1 + e^{-\beta(\varepsilon_j - \mu)}) \right) \frac{1}{(1 + e^{\beta(\varepsilon_i - \mu)})}. \tag{A.41}$$

The partition function Z can now be expressed as

$$Z = \mathrm{Tr} \left\{ e^{-\beta(\hat{H} - \mu \hat{N})} \right\} \tag{A.42}$$

$$= \sum_{n_1, n_2, \dots} \langle n_1, n_2, \dots | \prod_i e^{-\beta \hat{n}_i(\varepsilon_i - \mu)} | n_1, n_2, \dots \rangle \tag{A.43}$$

$$= \prod_i \sum_{n_i} \langle n_i | e^{-\beta \hat{n}_i(\varepsilon_i - \mu)} | n_i \rangle \tag{A.44}$$

$$= \prod_i (1 + e^{-\beta(\varepsilon_i - \mu)}). \tag{A.45}$$

We see that the partition function exactly cancels one factor in Eq. A.41, yielding our final result for the eq-1RDM of a noninteracting system in grand canonical equilibrium:

$$\gamma(x, x') = \sum_i n_i \phi_i^*(x') \phi_i(x) \tag{A.46}$$

$$n_i = \frac{1}{1 + e^{\beta(\varepsilon_i - \mu)}}. \tag{A.47}$$

This relation can simply be inverted to yield

$$\varepsilon_i - \mu = \frac{1}{\beta} \ln\left(\frac{1 - n_i}{n_i}\right). \tag{A.48}$$

The grand potential is generally related to the partition function via

$$\Omega = -\frac{1}{\beta} \ln Z. \tag{A.49}$$

Using Eqs. (A.45) and (A.48), we arrive at

$$\Omega_0 = -\frac{1}{\beta} \sum_i \ln\left(1 + e^{-\beta(\varepsilon_i - \mu)}\right) \tag{A.50}$$

$$= \frac{1}{\beta} \sum_i \ln(1 - n_i). \tag{A.51}$$

The entropy can then be found by using the following thermodynamic relation

$$S = \left.\frac{\partial}{\partial T}\Omega\right|_\mu. \tag{A.52}$$

The derivative of the ONs with respect to the temperature is given as

$$\left.\frac{\partial}{\partial T} n_i\right|_\mu = \frac{1}{T} n_i (1 - n_i) \ln\left(\frac{1 - n_i}{n_i}\right) \tag{A.53}$$

which leads to our final result for the noninteracting entropy in terms of the ONs of the eq-1RDM:

$$S_0 = -\sum_i \left(n_i \ln n_i + (1 - n_i) \ln(1 - n_i)\right). \tag{A.54}$$

A.5 Feynman rules

The rules for the evaluation of the graphical contributions in Section 6 are the common Feynman rules from FT-MBPT with an inclusion of the additional effective one-particle potential v_{eff}. They are listed in the following.

1. For fixed numbers n and m, draw all topologically different connected diagrams, with n interaction, m effective potential, and $2n + 1 + m$ particle lines

2. For every particle line, going from point 2 to point 1, assign a noninteracting Green's function $\mathcal{G}^0(x_1, \tau_1, x_2, \tau_2)$

3. For every two-particle interaction line, going from point 2 to point 1, assign a factor $w(x_1, \tau_1, x_2, \tau_2)$

4. For every one-particle effective-potential line, going from point 2 to point 1, assign a factor $v_{eff}(x_1, x_2)$

5. Integrate all internal variables $\int dx \int_0^\beta d\tau$

6. Take the trace over spins

7. Multiply the diagram by $(-1)^n(-1)^F$, where F is the number of closed fermion loops

8. Green's functions at equal times are evaluated as $\mathcal{G}^0(x, \tau, x', \tau) = \mathcal{G}^0(x, \tau, x', \tau^+)$

A.6 Second-order Born diagram

Starting from Eq. (8.40), the second-order Born contribution to the free energy of a HEG becomes

$$\Omega_{2b} = \frac{1}{n} 2^{-10} \pi^{-9} \int d^3k \int d^3p \int d^3q \frac{W(\boldsymbol{q})W(\boldsymbol{k}+\boldsymbol{p}+\boldsymbol{q})n_{\boldsymbol{k}}n_{\boldsymbol{p}}(1-n_{\boldsymbol{k}+\boldsymbol{q}})(1-n_{\boldsymbol{p}+\boldsymbol{q}})}{\varepsilon_{\boldsymbol{k}+\boldsymbol{q}} + \varepsilon_{\boldsymbol{p}+\boldsymbol{q}} - \varepsilon_{\boldsymbol{k}} - \varepsilon_{\boldsymbol{p}}} \tag{A.55}$$

$$= \frac{1}{n} 2^{-6} \pi^{-7} \int d^3k \int d^3p \int d^3q \frac{n_{\boldsymbol{k}}n_{\boldsymbol{p}}(1-n_{\boldsymbol{k}+\boldsymbol{q}})(1-n_{\boldsymbol{p}+\boldsymbol{q}})}{\boldsymbol{q}^2(\boldsymbol{k}+\boldsymbol{p}+\boldsymbol{q})^2(\boldsymbol{q}^2 + \boldsymbol{q}\cdot(\boldsymbol{k}+\boldsymbol{p}))} \tag{A.56}$$

This can be reformulated with the help of the following variable transformations.

$$\boldsymbol{k} \to \boldsymbol{q} \tag{A.57}$$

$$\boldsymbol{p} \to -(\boldsymbol{k}+\boldsymbol{p}+\boldsymbol{q}) \tag{A.58}$$

$$\boldsymbol{q} \to \boldsymbol{k} \tag{A.59}$$

$$\Omega_{2b} = -\frac{1}{n} 2^{-6} \pi^{-7} \int d^3k \int d^3p \int d^3q \frac{n(\boldsymbol{q})n(\boldsymbol{k}+\boldsymbol{p}+\boldsymbol{q})(1-n(\boldsymbol{k}+\boldsymbol{q}))(1-n(\boldsymbol{p}+\boldsymbol{q}))}{\boldsymbol{k}^2\boldsymbol{p}^2\boldsymbol{k}\cdot\boldsymbol{p}} \tag{A.60}$$

Changing to spherical coordinates, we can integrate over θ_k, ϕ_k, and ϕ_p. We will be left with the following six-dimensional integral:

$$\Omega_{2b} = -\frac{1}{n} 2^{-2} \pi^{-5} \int_0^\infty dk \int_0^\infty dp \int_0^\infty dq \int_0^\pi d\theta_p \int_0^\pi d\theta_q \int_{-\frac{\pi}{2}}^{\frac{\pi}{2}} d\phi_q$$
$$\frac{q^2 \tan(\theta_p)\sin(\theta_q)}{kp} n(\boldsymbol{q})n(\boldsymbol{k}+\boldsymbol{p}+\boldsymbol{q})(1-n(\boldsymbol{k}+\boldsymbol{q}))(1-n(\boldsymbol{p}+\boldsymbol{q})). \tag{A.61}$$

For numerical purposes, it is now helpful to define the following function $F(\boldsymbol{k},\boldsymbol{p},\boldsymbol{q},\theta_p)$ which is semipositive:

$$F(\boldsymbol{k},\boldsymbol{p},\boldsymbol{q},\theta_p) = \int_0^\pi d\theta_q \sin(\theta_q)(1-n(\boldsymbol{k}+\boldsymbol{q})) \int_{-\frac{\pi}{2}}^{\frac{\pi}{2}} d\phi_q n(\boldsymbol{k}+\boldsymbol{p}+\boldsymbol{q})(1-n(\boldsymbol{p}+\boldsymbol{q})). \tag{A.62}$$

To further simplify notation, we introduce the function $G(k,p,q)$ by the following equation:

$$G(k,p,q) = q^2 f_{\boldsymbol{q}} \int_0^{\frac{\pi}{2}} d\theta_p \tan\left(\frac{\pi}{2} + \theta_p\right) \left(F\left(k,p,q,\frac{\pi}{2}+\theta_q\right) - F\left(k,p,q,\frac{\pi}{2}-\theta_q\right)\right). \tag{A.63}$$

The previous definitions in combination with variable transformations of the kind $k \to \ln k$ then lead to the following expression for Ω_{2b}:

$$\Omega_{2b} = -\frac{1}{n} 2^{-2} \pi^{-5} \int_{-\infty}^\infty dk \int_{-\infty}^\infty dp \int_0^\infty dq G(e^k, e^p, q). \tag{A.64}$$

The momenta k, p, and q can now be interpreted as coordinates. The integration therefore runs over half the space, spanned by k, p, and q. One can therefore introduce spherical coordinates for this three-dimensional space:

$$k(\boldsymbol{x}) = x\cos(\theta_x) \tag{A.65}$$

$$p(\boldsymbol{x}) = x\sin(\theta_x)\sin(\phi_x) \tag{A.66}$$

$$q(\boldsymbol{x}) = x\sin(\theta_x)\cos(\phi_x). \tag{A.67}$$

This then leads to our final representation of Ω_{2b} which is suitable for numerical integration:

$$\Omega_{2b} = -\frac{1}{n} 2^{-2} \pi^{-5} \int_0^\infty dx x^2 \int_0^\pi d\theta_x \sin(\theta_x) \int_{-\frac{\pi}{2}}^{\frac{\pi}{2}} d\phi_x G(e^{k(\boldsymbol{x})}, e^{p(\boldsymbol{x})}, q(\boldsymbol{x})). \tag{A.68}$$

B Bibliography

References

[1] E. Schrödinger. *An Undulatory Theory of the Mechanics of Atoms and Molecules. Phys. Rev.*, **28**(6), 1049 (1926), URL http://dx.doi.org/10.1103/PhysRev.28.1049.

[2] D. A. Mazziotti, *Reduced-Density-Matrix Mechanics: With Application to Many-Electron Atoms and Molecules*, chap.3, pp. 19–59, *Variational Two-Electron Reduced-Density-Matrix Theory*, URL http://dx.doi.org/10.1002/9780470106600.ch3.

[3] P. Hohenberg and W. Kohn. *Inhomogeneous Electron Gas. Phys. Rev.*, **136**(3B), B864 (1964), URL http://dx.doi.org/10.1103/PhysRev.136.B864.

[4] W. Kohn and L. J. Sham. *Self-Consistent Equations Including Exchange and Correlation Effects. Phys. Rev.*, **140**(4A) (1965), URL http://dx.doi.org/10.1103/PhysRev.140.A1133.

[5] J. P. Perdew, K. Burke, and M. Ernzerhof. *Generalized Gradient Approximation Made Simple. Phys. Rev. Lett.*, **77**(18), 3865 (1996), URL http://dx.doi.org/10.1103/PhysRevLett.77.3865.

[6] U. V. Barth and L. Hedin. *A local exchange-correlation potential for the spin polarized case. i. J. Phys. C*, **5**(13), 1629 (1972), URL http://dx.doi.org/10.1088/0022-3719/5/13/012.

[7] M. Pant. *Theory of inhomogeneous magnetic electron gas. Solid State Commun.*, **10**(12), 1157 (1972), URL http://dx.doi.org/10.1016/0038-1098(72)90934-9.

[8] G. Vignale and M. Rasolt. *Density-functional theory in strong magnetic fields. Phys. Rev. Lett.*, **59**(20), 2360 (1987), URL http://dx.doi.org/10.1103/PhysRevLett.59.2360.

[9] S. Kurth, M. Marques, M. Lüders, and E. K. U. Gross. *Local Density Approximation for Superconductors. Phys. Rev. Lett.*, **83**(13), 2628 (1999), URL http://dx.doi.org/10.1103/PhysRevLett.83.2628.

[10] E. Runge and E. K. U. Gross. *Density-Functional Theory for Time-Dependent Systems. Phys. Rev. Lett.*, **52**(12), 997 (1984), URL http://dx.doi.org/10.1103/PhysRevLett.52.997.

[11] N. D. Mermin. *Thermal Properties of the Inhomogeneous Electron Gas. Phys. Rev.*, **137**(5A) (1965), URL http://dx.doi.org/10.1103/PhysRev.137.A1441.

[12] E. J. Baerends. *Exact Exchange-Correlation Treatment of Dissociated H2 in Density Functional Theory. Phys. Rev. Lett.*, **87**(13), 133004 (2001), URL http://dx.doi.org/10.1103/PhysRevLett.87.133004.

[13] A. J. Cohen, P. M. Sánchez, and W. Yang. *Fractional spins and static correlation error in density functional theory. J. Chem. Phys.*, **129**(12), 121104 (2008), URL http://dx.doi.org/10.1063/1.2987202.

[14] K. Liu. *Spin density functional theory of the temperature-dependent spin susceptibility: Pd and Pt. J. Magn. Magn. Mater.*, **12**(1), 43 (1979), URL http://dx.doi.org/10.1016/0304-8853(79)90333-0.

[15] N. M. Rosengaard and B. Johansson. *Finite-temperature study of itinerant ferromagnetism in Fe, Co, and Ni. Phys. Rev. B*, **55**(22), 14975 (1997), URL http://dx.doi.org/10.1103/PhysRevB.55.14975.

[16] G. Profeta, C. Franchini, N. N. Lathiotakis, A. Floris, A. Sanna, M. A. L. Marques, M. Lüders, S. Massidda, E. K. U. Gross, and A. Continenza. *Superconductivity in Lithium, Potassium, and Aluminum under Extreme Pressure: A First-Principles Study*. Phys. Rev. Lett., **96**(4), 047003 (2006), URL http://dx.doi.org/10.1103/PhysRevLett.96.047003.

[17] P. Cudazzo, G. Profeta, A. Sanna, A. Floris, A. Continenza, S. Massidda, and E. K. U. Gross. *Ab Initio Description of High-Temperature Superconductivity in Dense Molecular Hydrogen*. Phys. Rev. Lett., **100**(25), 257001 (2008), URL http://dx.doi.org/10.1103/PhysRevLett.100.257001.

[18] A. Kietzmann, R. Redmer, M. P. Desjarlais, and T. R. Mattsson. *Complex Behavior of Fluid Lithium under Extreme Conditions*. Phys. Rev. Lett., **101**(7), 070401 (2008), URL http://dx.doi.org/10.1103/PhysRevLett.101.070401.

[19] M. W. C. Dharma-wardana and F. Perrot. *Density-functional theory of hydrogen plasmas*. Phys. Rev. A, **26**(4), 2096 (1982), URL http://dx.doi.org/10.1103/PhysRevA.26.2096.

[20] F. Perrot and M. W. C. Dharma-wardana. *Spin-polarized electron liquid at arbitrary temperatures: Exchange-correlation energies, electron-distribution functions, and the static response functions*. Phys. Rev. B, **62**(24), 16536 (2000), URL http://dx.doi.org/10.1103/PhysRevB.62.16536.

[21] M. W. C. Dharma-wardana and M. S. Murillo. *Pair-distribution functions of two-temperature two-mass systems: Comparison of molecular dynamics, classical-map hypernetted chain, quantum Monte Carlo, and Kohn-Sham calculations for dense hydrogen*. Phys. Rev. E, **77**(2), 026401 (2008), URL http://dx.doi.org/10.1103/PhysRevE.77.026401.

[22] J. Gavnholt, A. Rubio, T. Olsen, K. S. Thygesen, and J. Schiøtz. *Hot-electron-assisted femtochemistry at surfaces: A time-dependent density functional theory approach*. Phys. Rev. B, **79**(19), 195405 (2009), URL http://dx.doi.org/10.1103/PhysRevB.79.195405.

[23] B. Militzer. *First Principles Calculations of Shock Compressed Fluid Helium*. Phys. Rev. Lett., **97**(17), 175501 (2006), URL http://dx.doi.org/10.1103/PhysRevLett.97.175501.

[24] S. Root, R. J. Magyar, J. H. Carpenter, D. L. Hanson, and T. R. Mattsson. *Shock Compression of a Fifth Period Element: Liquid Xenon to 840 GPa*. Phys. Rev. Lett., **105**(8), 085501 (2010), URL http://dx.doi.org/10.1103/PhysRevLett.105.085501.

[25] R. Redmer, T. R. Mattsson, N. Nettelmann, and M. French. *The phase diagram of water and the magnetic fields of Uranus and Neptune*. Icarus, **211**(1), 798 (2011), URL http://dx.doi.org/10.1016/j.icarus.2010.08.008.

[26] T. L. Gilbert. *Hohenberg-Kohn theorem for nonlocal external potentials*. Phys. Rev. B, **12**(6), 2111 (1975), URL http://dx.doi.org/10.1103/PhysRevB.12.2111.

[27] J. R. Chelikowsky and M. L. Cohen. *Nonlocal pseudopotential calculations for the electronic structure of eleven diamond and zinc-blende semiconductors*. Phys. Rev. B, **14**(2), 556 (1976), URL http://dx.doi.org/10.1103/PhysRevB.14.556.

[28] O. Akinlade. *A nonlocal pseudopotential calculation of the resistivity of liquid metals and the LiPb alloy*. Physica B, **175**(4), 389 (1991), URL http://dx.doi.org/10.1016/0921-4526(91)90075-P.

[29] O. Gritsenko, K. Pernal, and E. J. Baerends. *An improved density matrix functional by physically motivated repulsive corrections*. J. Chem. Phys., **122**(20), 204102 (2005), URL http://dx.doi.org/10.1063/1.1906203.

[30] D. R. Rohr, K. Pernal, O. V. Gritsenko, and E. J. Baerends. *A density matrix functional with occupation number driven treatment of dynamical and nondynamical correlation.* J. Chem. Phys., **129**(16), 164105 (2008), URL http://dx.doi.org/10.1063/1.2998201.

[31] N. N. Lathiotakis, S. Sharma, J. K. Dewhurst, F. G. Eich, M. A. L. Marques, and E. K. U. Gross. *Density-matrix-power functional: Performance for finite systems and the homogeneous electron gas.* Phys. Rev. A, **79**(4), 040501 (2009), URL http://dx.doi.org/10.1103/PhysRevA.79.040501.

[32] D. R. Rohr, J. Toulouse, and K. Pernal. *Combining density-functional theory and density-matrix-functional theory.* Phys. Rev. A, **82**, 052502+ (2010), URL http://dx.doi.org/10.1103/PhysRevA.82.052502.

[33] N. N. Lathiotakis, S. Sharma, N. Helbig, J. K. Dewhurst, M. A. L. Marques, F. Eich, T. Baldsiefen, A. Zacarias, and E. K. U. Gross. *Discontinuities of the Chemical Potential in Reduced Density Matrix Functional Theory.* Z. Phys. Chem., **224**(03-04), 467 (2010), URL http://dx.doi.org/10.1524/zpch.2010.6118.

[34] S. Sharma, J. K. Dewhurst, N. N. Lathiotakis, and E. K. U. Gross. *Reduced density matrix functional for many-electron systems.* Phys. Rev. B, **78**(20), 201103 (2008), URL http://dx.doi.org/10.1103/PhysRevB.78.201103.

[35] H. Englisch and R. Englisch. *V-representability in finite-dimensional spaces.* J. Phys. A: Math. Gen., **16**(18) (1983a), URL http://dx.doi.org/10.1088/0305-4470/16/18/003.

[36] W. Kohn. *v-Representability and Density Functional Theory.* Phys. Rev. Lett., **51**(17), 1596 (1983), URL http://dx.doi.org/10.1103/PhysRevLett.51.1596.

[37] E. H. Lieb. *Density functionals for coulomb systems.* Int. J. Quantum Chem., **24**(3), 243 (1983), URL http://dx.doi.org/10.1002/qua.560240302.

[38] P. E. Lammert. *Coarse-grained V representability.* J. Chem. Phys., **125**(7), 074114 (2006), URL http://dx.doi.org/10.1063/1.2336211.

[39] M. Levy and J. P. Perdew. *Hellmann-Feynman, virial, and scaling requisites for the exact universal density functionals. Shape of the correlation potential and diamagnetic susceptibility for atoms.* Phys. Rev. A, **32**(4), 2010 (1985), URL http://dx.doi.org/10.1103/PhysRevA.32.2010.

[40] M. Levy, W. Yang, and R. G. Parr. *A new functional with homogeneous coordinate scaling in density functional theory: F [rho,lambda].* J. Chem. Phys., **83**(5), 2334 (1985), URL http://dx.doi.org/10.1063/1.449326.

[41] M. Levy. *Asymptotic coordinate scaling bound for exchange-correlation energy in density-functional theory.* Int. J. Quantum Chem., **36**(S23), 617 (1989), URL http://dx.doi.org/10.1002/qua.560360864.

[42] M. Lein, E. K. U. Gross, and J. P. Perdew. *Electron correlation energies from scaled exchange-correlation kernels: Importance of spatial versus temporal nonlocality.* Phys. Rev. B, **61**(20), 13431 (2000), URL http://dx.doi.org/10.1103/PhysRevB.61.13431.

[43] S. Pittalis, C. R. Proetto, A. Floris, A. Sanna, C. Bersier, K. Burke, and E. K. U. Gross. *Exact Conditions in Finite-Temperature Density-Functional Theory.* Phys. Rev. Lett., **107**, 163001 (2011), URL http://dx.doi.org/10.1103/PhysRevLett.107.163001.

[44] T. Baldsiefen and E. K. U. Gross. *Reduced density matrix functional theory at finite temperature. I. Theoretical foundations.* arXiv (2012a), URL http://arxiv.org/abs/1208.4703, submitted to Phys. Rev. A.

[45] P. O. Löwdin. *Quantum Theory of Many-Particle Systems. I. Physical Interpretations by Means of Density Matrices, Natural Spin-Orbitals, and Convergence Problems in the Method of Configurational Interaction.* Phys. Rev., **97**(6), 1474 (1955), URL http://dx.doi.org/10.1103/PhysRev.97.1474.

[46] A. J. Coleman. *Structure of Fermion Density Matrices.* Rev. Mod. Phys., **35**(3), 668 (1963), URL http://dx.doi.org/10.1103/RevModPhys.35.668.

[47] G. F. Giuliani and G. Vignale, *Quantum Theory of the Electron Liquid* (Cambridge University Press, Cambridge, 2005), URL http://dx.doi.org/10.1080/00107510903194710.

[48] D. M. Ceperley and B. J. Alder. *Ground State of the Electron Gas by a Stochastic Method.* Phys. Rev. Lett., **45**(7), 566 (1980), URL http://dx.doi.org/10.1103/PhysRevLett.45.566.

[49] G. Ortiz and P. Ballone. *Correlation energy, structure factor, radial distribution function, and momentum distribution of the spin-polarized uniform electron gas.* Phys. Rev. B, **50**(3), 1391 (1994), URL http://dx.doi.org/10.1103/PhysRevB.50.1391.

[50] C. Attaccalite, S. Moroni, P. Gori-Giorgi, and G. B. Bachelet. *Correlation Energy and Spin Polarization in the 2D Electron Gas.* Phys. Rev. Lett., **88**(25), 256601 (2002), URL http://dx.doi.org/10.1103/PhysRevLett.88.256601.

[51] C. Attaccalite, S. Moroni, P. Gori-Giorgi, and G. B. Bachelet. *Erratum: Correlation Energy and Spin Polarization in the 2D Electron Gas [Phys. Rev. Lett. 88, 256601 (2002)].* Phys. Rev. Lett., **91**(10), 109902 (2003), URL http://dx.doi.org/10.1103/PhysRevLett.91.109902.

[52] J. P. Perdew and Y. Wang. *Accurate and simple analytic representation of the electron-gas correlation energy.* Phys. Rev. B, **45**(23), 13244 (1992), URL http://dx.doi.org/10.1103/PhysRevB.45.13244.

[53] Y. Takada and T. Kita. *New Self-Consistency Relation between the Correlation Energy and the Momentum Distribution Function with Application to the One-Dimensional Hubbard Model.* J. Phys. Soc. Jpn., **60**(1), 25 (1991), URL http://jpsj.ipap.jp/link?JPSJ/60/25/.

[54] Y. Takada and H. Yasuhara. *Momentum distribution function of the electron gas at metallic densities.* Phys. Rev. B, **44**(15), 7879 (1991), URL http://dx.doi.org/10.1103/PhysRevB.44.7879.

[55] P. Gori-Giorgi and P. Ziesche. *Momentum distribution of the uniform electron gas: Improved parametrization and exact limits of the cumulant expansion.* Phys. Rev. B, **66**(23), 235116 (2002), URL http://dx.doi.org/10.1103/PhysRevB.66.235116.

[56] T. Baldsiefen and E. K. U. Gross. *Reduced density matrix functional theory at finite temperature. III. Application to the electron gas: Correlation effects.* arXiv (2012b), URL http://arxiv.org/abs/1208.4707, submitted to Phys. Rev. A.

[57] C. Garrod and J. K. Percus. *Reduction of the N-Particle Variational Problem.* J. Math. Phys., **5**(12), 1756 (1964), URL http://dx.doi.org/10.1063/1.1704098.

[58] H. Kummer. *n-Representability Problem for Reduced Density Matrices.* J. Math. Phys., **8**(10), 2063 (1967), URL http://dx.doi.org/10.1063/1.1705122.

[59] A. J. Coleman. *Reduced density operators and the N-particle problem. Int. J. Quantum Chem.*, **13**(1), 67 (1978), URL http://dx.doi.org/10.1002/qua.560130106.

[60] J. E. Harriman. *Geometry of density matrices. I. Definitions, N matrices and 1 matrices. Phys. Rev. A*, **17**(4), 1249 (1978a), URL http://dx.doi.org/10.1103/PhysRevA.17.1249.

[61] J. E. Harriman. *Geometry of density matrices. II. Reduced density matrices and N representability. Phys. Rev. A*, **17**(4), 1257 (1978b), URL http://dx.doi.org/10.1103/PhysRevA.17.1257.

[62] D. Van Neck, M. Waroquier, K. Peirs, V. Van Speybroeck, and Y. Dewulf. *v-representability of one-body density matrices. Phys. Rev. A*, **64**(4), 042512 (2001), URL http://dx.doi.org/10.1103/PhysRevA.64.042512.

[63] P. W. Ayers and M. Levy. *Generalized density-functional theory: Conquering the N-representability problem with exact functionals for the electron pair density and the second-order reduced density matrix. J. Chem. Sci.*, **117**, 507 (2005), URL http://www.ias.ac.in/chemsci/Pdf-sep2005/507.pdf.

[64] D. Van Neck and P. W. Ayers. *Necessary conditions for the N -representability of the second-order reduced density matrix: Upper bounds on the P and Q matrices. Phys. Rev. A*, **75**(3), 032502 (2007), URL http://dx.doi.org/10.1103/PhysRevA.75.032502.

[65] G. Friesecke. *On the infinitude of nonzero eigenvalues of the singleelectron density matrix for atoms and molecules. Proc. R. Soc. London A*, **459**(2029), 47 (2003), URL http://dx.doi.org/10.1098/rspa.2002.1027.

[66] T. Kato. *On the eigenfunctions of many-particle systems in quantum mechanics. Commun. Pure Appl. Math.*, **10**(2), 151 (1957), URL http://dx.doi.org/10.1002/cpa.3160100201.

[67] R. Requist and O. Pankratov. *Generalized Kohn-Sham system in one-matrix functional theory. Phys. Rev. B*, **77**(23), 235121 (2008), URL http://dx.doi.org/10.1103/PhysRevB.77.235121.

[68] N. Helbig, N. N. Lathiotakis, M. Albrecht, and E. K. U. Gross. *Discontinuity of the chemical potential in reduced-density-matrix-functional theory. Eur. Phys. Lett.*, **77**, 67003 (2007), URL http://dx.doi.org/10.1209/0295-5075/77/67003.

[69] N. Helbig, N. N. Lathiotakis, and E. K. U. Gross. *Discontinuity of the chemical potential in reduced-density-matrix-functional theory for open-shell systems. Phys. Rev. A*, **79**(2), 022504 (2009), URL http://dx.doi.org/10.1103/PhysRevA.79.022504.

[70] A. Müller. *Explicit approximate relation between reduced two- and one-particle density matrices. Phys. Lett. A*, **105**(9), 446 (1984), URL http://dx.doi.org/10.1016/0375-9601(84)91034-X.

[71] M. A. Buijse and Baerends. *An approximate exchange-correlation hole density as a functional of the natural orbitals. Mol. Phys.*, **100**(4), 401 (2002), URL http://dx.doi.org/10.1080/00268970110070243.

[72] S. Goedecker and C. J. Umrigar. *Natural Orbital Functional for the Many-Electron Problem. Phys. Rev. Lett.*, **81**(4), 866 (1998), URL http://dx.doi.org/10.1103/PhysRevLett.81.866.

[73] J. M. Herbert and J. E. Harriman. *Self-interaction in natural orbital functional theory. Chem. Phys. Lett.*, **382**(1-2), 142 (2003), URL http://dx.doi.org/10.1016/j.cplett.2003.10.057.

[74] M. Piris, J. M. Matxain, X. Lopez, and J. M. Ugalde. *Communications: Accurate description of atoms and molecules by natural orbital functional theory. J. Chem. Phys.*, **132**(3), 031103 (2010), URL http://dx.doi.org/10.1063/1.3298694.

[75] M. A. L. Marques and N. N. Lathiotakis. *Empirical functionals for reduced-density-matrix-functional theory. Phys. Rev. A*, **77**(3), 032509 (2008), URL http://dx.doi.org/10.1103/PhysRevA.77.032509.

[76] N. N. Lathiotakis and M. A. L. Marques. *Benchmark calculations for reduced density-matrix functional theory. J. Chem. Phys.*, **128**(18), 184103+ (2008), URL http://dx.doi.org/10.1063/1.2899328.

[77] P. W. Ayers, O. W. Day, and R. C. Morrison. *Analysis of density functionals and their density tails in H2. Int. J. Quantum Chem.*, **69**(4), 541 (1998), URL http://dx.doi.org/10.1002/(SICI)1097-461X(1998)69:4%3C541::AID-QUA11%3E3.0.CO;2-2.

[78] C. A. Ullrich and E. K. U. Gross. *Density Functional Theory of Normal and Superconducting Electron Liquids: Explicit Functionals via the Gradient Expansion. Aust. J. Phys.*, **49**, 103 (1996), URL http://www.publish.csiro.au/paper/PH960103.htm.

[79] D. M. Ceperley. *Path integrals in the theory of condensed helium. Rev. Mod. Phys.*, **67**(2), 279 (1995), URL http://dx.doi.org/10.1103/RevModPhys.67.279.

[80] M. Troyer and U. J. Wiese. *Computational Complexity and Fundamental Limitations to Fermionic Quantum Monte Carlo Simulations. Phys. Rev. Lett.*, **94**(17), 170201 (2005), URL http://dx.doi.org/10.1103/PhysRevLett.94.170201.

[81] G. Csányi, S. Goedecker, and T. A. Arias. *Improved tensor-product expansions for the two-particle density matrix. Phys. Rev. A*, **65**(3), 032510 (2002), URL http://dx.doi.org/10.1103/PhysRevA.65.032510.

[82] J. Cioslowski and K. Pernal. *Constraints upon natural spin orbital functionals imposed by properties of a homogeneous electron gas. J. Chem. Phys.*, **111**(8), 3396 (1999), URL http://dx.doi.org/10.1063/1.479623.

[83] J. C. Kimball. *Short-range correlations and the structure factor and momentum distribution of electrons. J. Phys. A: Math. Gen.*, **8**(9), 1513 (1975), URL http://dx.doi.org/10.1088/0305-4470/8/9/021.

[84] N. N. Lathiotakis, N. Helbig, and E. K. U. Gross. *Performance of one-body reduced density-matrix functionals for the homogeneous electron gas. Phys. Rev. B*, **75**(19), 195120 (2007), URL http://dx.doi.org/10.1103/PhysRevB.75.195120.

[85] F. H. Zong, C. Lin, and D. M. Ceperley. *Spin polarization of the low-density three-dimensional electron gas. Phys. Rev. E*, **66**(3), 036703 (2002), URL http://dx.doi.org/10.1103/PhysRevE.66.036703.

[86] H. Eschrig. *T>0 ensemble-state density functional theory via Legendre transform. Phys. Rev. B*, **82**(20), 205120 (2010), URL http://dx.doi.org/10.1103/PhysRevB.82.205120.

[87] H. Umegaki. *Conditional expectation in an operator algebra. IV. Entropy and information. Kodai Math. Sem. Rep.*, **14**(2), 59 (1962), URL http://dx.doi.org/10.2996/kmj/1138844604.

[88] G. Lindblad. *Entropy, information and quantum measurements. Commun. Math. Phys.*, **33**(4), 305 (1973), URL http://dx.doi.org/10.1007/BF01646743.

[89] M. Ruskai. *Another short and elementary proof of strong subadditivity of quantum entropy. Rep. Math. Phys.*, **60**(1), 1 (2007), URL http://dx.doi.org/10.1016/S0034-4877(07)00019-5.

[90] A. Wehrl. *General properties of entropy. Rev. Mod. Phys.*, **50**(2), 221 (1978), URL http://dx.doi.org/10.1103/RevModPhys.50.221.

[91] S. M. Valone. *A one-to-one mapping between one-particle densities and some n-particle ensembles. J. Chem. Phys.*, **73**(9), 4653 (1980), URL http://dx.doi.org/10.1063/1.440656.

[92] W. Yang, Y. Zhang, and P. W. Ayers. *Degenerate Ground States and a Fractional Number of Electrons in Density and Reduced Density Matrix Functional Theory. Phys. Rev. Lett.*, **84**(22), 5172 (2000), URL http://dx.doi.org/10.1103/PhysRevLett.84.5172.

[93] P. E. Lammert. *Differentiability of Lieb functional in electronic density functional theory. Int. J. Quantum Chem.*, **107**(10), 1943 (2007), URL http://dx.doi.org/10.1002/qua.21342.

[94] H. W. Kuhn and A. W. Tucker, in *Proceedings of 2nd Berkeley Symposium*, edited by J. Neyman (University of California Press., Berkeley, 1951), p. 481, URL http://projecteuclid.org/DPubS/Repository/1.0/Disseminate?handle=euclid.bsmsp/1200500249&view=body&content-type=pdf_1.

[95] Y. Wang and R. G. Parr. *Construction of exact Kohn-Sham orbitals from a given electron density. Phys. Rev. A*, **47**(3), R1591 (1993), URL http://dx.doi.org/10.1103/PhysRevA.47.R1591.

[96] P. A. M. Dirac. *On the Theory of Quantum Mechanics. Proc. R. Soc. London A*, **112**(762), 661 (1926), URL http://dx.doi.org/10.1098/rspa.1926.0133.

[97] J. Chayes, L. Chayes, and M. Ruskai. *Density functional approach to quantum lattice systems. J. Stat. Phys.*, **38**(3), 497 (1985), URL http://dx.doi.org/10.1007/BF01010474.

[98] H. Englisch and R. Englisch. *Hohenberg-Kohn theorem and non-V-representable densities. Physica A*, **121**(1-2), 253 (1983b), URL http://dx.doi.org/10.1016/0378-4371(83)90254-6.

[99] H. Englisch and R. Englisch. *Exact Density Functionals for Ground-State Energies II. Details and Remarks. Phys. Stat. Sol. B*, **124**(1), 373 (1984), URL http://dx.doi.org/10.1002/pssb.2221240140.

[100] T. Baldsiefen and E. K. U. Gross, *Properties of exact functionals in finite-temperature reduced density matrixfunctional theory* (2012c), submitted to Phys. Rev. A.

[101] E. H. Lieb and S. Oxford. *Improved lower bound on the indirect Coulomb energy. Int. J. Quantum Chem.*, **19**(3), 427 (1981), URL http://dx.doi.org/10.1002/qua.560190306.

[102] T. Matsubara. *A New Approach to Quantum-Statistical Mechanics. Prog. Theor. Phys.*, **14**(4), 351 (1955), URL http://dx.doi.org/10.1143/PTP.14.351.

[103] A. Görling and M. Levy. *Correlation-energy functional and its high-density limit obtained from a coupling-constant perturbation expansion. Phys. Rev. B*, **47**(20), 13105 (1993), URL http://dx.doi.org/10.1103/PhysRevB.47.13105.

[104] A. L. Fetter and J. D. Walecka, *Quantum Theory of Many-Particle Systems* (Dover Publications, 2003), URL http://www.worldcat.org/isbn/0486428273.

[105] E. Cancès and K. Pernal. *Projected gradient algorithms for Hartree-Fock and density matrix functional theory calculations. J. Chem. Phys.*, **128**(13), 134108 (2008), URL http://dx.doi.org/10.1063/1.2888550.

[106] M. Piris and J. M. Ugalde. *Iterative diagonalization for orbital optimization in natural orbital functional theory.* *J. Comput. Chem.*, **30**(13), 2078 (2009), URL http://dx.doi.org/10.1002/jcc.21225.

[107] K. Dewhurst, *ELK*, URL http://elk.sourceforge.net/.

[108] T. Baldsiefen and E. K. U. Gross. *Minimization procedure in reduced density matrix functional theory by means of an effective noninteracting system.* *Comp. Theor. Chem.* (2012d), URL http://dx.doi.org/10.1016/j.comptc.2012.09.001.

[109] K. Pernal. *Effective Potential for Natural Spin Orbitals.* *Phys. Rev. Lett.*, **94**(23), 233002 (2005), URL http://dx.doi.org/10.1103/PhysRevLett.94.233002.

[110] G. J. Conduit, A. G. Green, and B. D. Simons. *Inhomogeneous Phase Formation on the Border of Itinerant Ferromagnetism.* *Phys. Rev. Lett.*, **103**(20), 207201 (2009), URL http://dx.doi.org/10.1103/PhysRevLett.103.207201.

[111] H. Iyetomi and S. Ichimaru. *Free energies of electron-screened ion plasmas in the hypernetted-chain approximation.* *Phys. Rev. A*, **34**, 433 (1986), URL http://dx.doi.org/10.1103/PhysRevA.34.433.

[112] S. Ichimaru and S. Tanaka. *Spin-dependent electron interactions in metals across the compressibility and spin-susceptibility anomalies.* *Phys. Rev. B*, **36**(11), 6182 (1987), URL http://dx.doi.org/10.1103/PhysRevB.36.6182.

[113] S. Tanaka and S. Ichimaru. *Spin-dependent correlations and thermodynamic functions for electron liquids at arbitrary degeneracy and spin polarization. Phys. Rev. B*, **39**(2), 1036 (1989), URL http://dx.doi.org/10.1103/PhysRevB.39.1036.

[114] K. S. Singwi, M. P. Tosi, R. H. Land, and A. Sjölander. *Electron Correlations at Metallic Densities.* *Phys. Rev.*, **176**, 589 (1968), URL http://dx.doi.org/10.1103/PhysRev.176.589.

[115] S. Tanaka and S. Ichimaru. *Thermodynamics and Correlational Properties of Finite-Temperature Electron Liquids in the Singwi-Tosi-Land-Sjölander Approximation. J. Phys. Soc. Jpn.*, **55**(7), 2278 (1986), URL http://dx.doi.org/10.1143/JPSJ.55.2278.

[116] H. K. Schweng and H. M. Böhm. *Finite-temperature electron correlations in the framework of a dynamic local-field correction. Phys. Rev. B*, **48**(4), 2037 (1993), URL http://dx.doi.org/10.1103/PhysRevB.48.2037.

[117] M. W. C. Dharma-wardana and F. Perrot. *Spin-Polarized Stable Phases of the 2D Electron Fluid at Finite Temperatures. Phys. Rev. Lett.*, **90**, 136601 (2003), URL http://dx.doi.org/10.1103/PhysRevLett.90.136601.

[118] F. Perrot. *Gradient correction to the statistical electronic free energy at nonzero temperatures: Application to equation-of-state calculations. Phys. Rev. A*, **20**(2), 586 (1979), URL http://dx.doi.org/10.1103/PhysRevA.20.586.

[119] U. Gupta and A. K. Rajagopal. *Exchange-correlation potential for inhomogeneous electron systems at finite temperatures. Phys. Rev. A*, **22**(6), 2792 (1980a), URL http://dx.doi.org/10.1103/PhysRevA.22.2792.

[120] M. W. C. Dharma-wardana and R. Taylor. *Exchange and correlation potentials for finite temperature quantum calculations at intermediate degeneracies. J. Phys. C*, **14**(5), 629 (1981), URL http://dx.doi.org/10.1088/0022-3719/14/5/011.

[121] U. Gupta and A. K. Rajagopal. *Density functional formalism at finite temperatures with some applications.* *Phys. Rep.*, **87**(6), 259 (1982), URL http://dx.doi.org/10.1016/0370-1573(82)90077-1.

[122] F. Perrot and M. W. C. Dharma-wardana. *Exchange and correlation potentials for electron-ion systems at finite temperatures.* *Phys. Rev. A*, **30**(5), 2619 (1984), URL http://dx.doi.org/10.1103/PhysRevA.30.2619.

[123] D. G. Kanhere, P. V. Panat, A. K. Rajagopal, and J. Callaway. *Exchange-correlation potentials for spin-polarized systems at finite temperatures.* *Phys. Rev. A*, **33**(1), 490 (1986), URL http://dx.doi.org/10.1103/PhysRevA.33.490.

[124] R. G. Dandrea, N. W. Ashcroft, and A. E. Carlsson. *Electron liquid at any degeneracy.* *Phys. Rev. B*, **34**(4), 2097 (1986), URL http://dx.doi.org/10.1103/PhysRevB.34.2097.

[125] T. Baldsiefen, F. G. Eich, and E. K. U. Gross. *Reduced density matrix functional theory at finite temperature. II. Application to the electron gas: Exchange only.* *arXiv* (2012), URL http://arxiv.org/abs/1208.4705, submitted to Phys. Rev. A.

[126] D. S. Kosov, M. F. Gelin, and A. I. Vdovin. *Calculations of canonical averages from the grand canonical ensemble.* *Phys. Rev. E*, **77**, 021120 (2008), URL http://dx.doi.org/10.1103/PhysRevE.77.021120.

[127] O. Betbeder-Matibet and M. Combescot. *On the Coulomb energy of a finite-temperature electron gas.* *J. Stat. Phys.*, **75**(5), 953 (1994), URL http://dx.doi.org/10.1007/BF02186752.

[128] U. Gupta and A. K. Rajagopal. *Inhomogeneous electron gas at nonzero temperatures: Exchange effects.* *Phys. Rev. A*, **21**(6), 2064 (1980b), URL http://dx.doi.org/10.1103/PhysRevA.21.2064.

[129] A. Wasserman, T. J. Buckholtz, and H. E. DeWitt. *Evaluation of Some Fermi-Dirac Integrals.* *J. Math. Phys.*, **11**(2), 477 (1970), URL http://dx.doi.org/10.1063/1.1665160.

[130] M. Galassi, *GNU Scientific Library Reference Manual (3rd Ed.)*, URL http://www.gnu.org/software/gsl/.

[131] M. G. Mann and K. A. Brueckner. *Correlation Energy of an Electron Gas at High Density.* *Phys. Rev.*, **106**(2), 364 (1957), URL http://dx.doi.org/10.1103/PhysRev.106.364.

[132] E. W. Montroll and J. C. Ward. *Quantum Statistics of Interacting Particles; General Theory and Some Remarks on Properties of an Electron Gas.* *Phys. Fluids*, **1**(1), 55 (1958), URL http://dx.doi.org/10.1063/1.1724337.

[133] S. H. Vosko and J. P. Perdew. *Theory of spin susceptibility of an inhomogeneous electron-gas via density functional formalism.* *Can. J. Phys.*, **53**(14), 1385 (1975), URL http://dx.doi.org/10.1139/p75-176.

[134] W. Kohn and J. M. Luttinger. *Ground-State Energy of a Many-Fermion System.* *Phys. Rev.*, **118**(1), 41 (1960), URL http://dx.doi.org/10.1103/PhysRev.118.41.

[135] L. Onsager, L. Mittag, and M. J. Stephen. *Integrals in the Theory of Electron Correlations.* *Ann. Phys. (Leipzig)*, **473**(1-2), 71 (1966), URL http://dx.doi.org/10.1002/andp.19664730108.

[136] S. Hong and G. D. Mahan. *Temperature dependence of the Hartree-Fock approximation.* *Phys. Rev. B*, **50**, 7284 (1994), URL http://dx.doi.org/10.1103/PhysRevB.50.7284.

[137] S. Hong and G. D. Mahan. *Spin-polarized Hartree-Fock approximation at nonzero temperatures. Phys. Rev. B*, **51**, 17417 (1995), URL http://dx.doi.org/10.1103/PhysRevB.51.17417.

[138] A. W. Overhauser. *Spin Density Waves in an Electron Gas. Phys. Rev.*, **128**(3), 1437 (1962), URL http://dx.doi.org/10.1103/PhysRev.128.1437.

[139] F. G. Eich, S. Kurth, C. R. Proetto, S. Sharma, and E. K. U. Gross. *Noncollinear spin-spiral phase for the uniform electron gas within reduced-density-matrix-functional theory. Phys. Rev. B*, **81**(2), 024430 (2010), URL http://dx.doi.org/10.1103/PhysRevB.81.024430.

[140] S. Ismail-Beigi. *Correlation energy functional within the GW-RPA: Exact forms, approximate forms, and challenges. Phys. Rev. B*, **81**(19), 195126 (2010), URL http://dx.doi.org/10.1103/PhysRevB.81.195126.

[141] L. Hedin. *New Method for Calculating the One-Particle Green's Function with Application to the Electron-Gas Problem. Phys. Rev.*, **139**(3A) (1965), URL http://dx.doi.org/10.1103/PhysRev.139.A796.

C Deutsche Kurzfassung

Reduzierte-Dichtematrix-Funktionaltheorie (RDMFT) ist ein vielversprechender Kandidat für die Behandlung von Fragestellungen in der Quantenmechanik, welche durch konventionelle Dichtefunktionaltheorie (DFT) nur schwer zu behandeln sind. Dazu gehören die Berechnung von Dissoziationskurven von Molekülen sowie die Bestimmung der elektronischen Energielücke in Übergangsmetall-Oxiden. Bei der Beschreibung des homogenen Elektronengases, welches eines der bedeutensten Modellsysteme für die Familie der Funktionaltheorien darstellt, liefern bestehende Funktionale allerdings keine akkuraten Ergebnisse. In Teil 3 dieser Arbeit haben wir daher ein RDMFT-Funktional hergeleitet, welches sowohl die Korrelationsenergie mit hoher Genauigkeit, als auch die Grundzustands-Impulsverteilung qualitativ korrekt wiedergibt.

Ein weiteres Gebiet, auf dem DFT eher geringe Erfolge vorzuweisen hat ist die Beschreibung quantenmechanischer Eigenschaften von Vielteilchensystemen im thermodynamischen Gleichgewicht. In Teil 4 der vorliegenden Arbeit untersuchen wir daher die Möglichkeit, eine Erweiterung von RDMFT auf großkanonische Systeme vorzunehmen. Ausgehend vom Variationsprinzip konnten wir zeigen, dass ein bijektiver Zusammenhang zwischen dem statistischen Dichteoperator (SDO) im thermischen Gleichgewicht und der dazugehörigen 1-reduzierten Dichtematrix (1RDM) besteht. Dies ermöglicht die Bestimmung der Gleichgewichts-1RDM durch eine variationelle Funktionaltheorie (FT-RDMFT). Sowohl die SDOs, als auch die 1RDMs können als Elemente eines Banachraumes verstanden werden was uns einerseits ermöglichte wichtige Eigenschaften der FT-RDMFT-Funktionale herzuleiten und andererseits den Defininitionsbereich dieser Funktionale auf eine einfach zu charakterisierende Menge von 1RDMs zu erweitern.

Um die Entwicklung von genäherten Funktionalen in FT-RDMFT zu erleichtern, haben wir in Teil 5 dieser Arbeit Eigenschaften der exakten Funktionale untersucht. Als besonders fruchtbar hat sich hierbei die Methode der Skalierung von Parametern erwiesen. Dadurch war es uns möglich, mehrere Beziehungen der verschiedenen Korrelationsbeiträge untereinander herzuleiten, sowie exakte Aussagen über das Skalierungsverhalten der einzelnen Funktionale zu treffen. Diese Resultate können nun benutzt werden um bestehende genäherte Funktionale in FT-RDMFT zu testen oder um als Leitlinien für die Entwicklung neuer Funktionale zu dienen.

Die Entwicklung einer lokalen Dichtenäherung (LDA), wie sie mit überwältigendem Erfolg in DFT angewandt wird, ist in FT-RDMFT vorerst nicht möglich, da keine Monte-Carlo Ergebnisse für thermodynamische Potentiale von Systemen mit nochtlokalem externen Potential in thermodynamischem Gleichgewicht existieren. In Teil 6 der vorliegenden Arbeit entwickelten wir daher eine störungstheoretische Methodik zur Herleitung genäherter Funtionale. Wir konnten zeigen, dass die Minimierung des resultierenden Funktionals erster Ordnung äquivalent zur Lösung der temperaturabhängigen Hartree-Fock Gleichungen ist.

Es gibt im Rahmen von FT-RDMFT, im Gegensatz zur Grundzustands-RDMFT, ein effektives, nicht wechselwirkendes System, welches die Gleichgewichts-1RDM eines wechselwirkenden Systems reproduziert. Dies konnten wir in Teil 7 unserer Arbeit nutzen, um eine selbstkonsistente Minimierungsmethode für Funktionale aus sowohl FT-RDMFT als auch RDMFT zu entwickeln. Durch die Anwendung auf ein Beispielsystem konnten wir die Effektivität und Effizienz dieser Methode belegen.

Nachdem wir in den vorhergegangenen Teilen eine ausführliche Behandlung der theoretischen Grundlagen von FT-RDMFT vorgenommen haben untersuchten wir in Teil 8 unserer Arbeit die Auswirkung von FT-RDMFT auf das homogene Elektronengas. So konnten wir das Phasendiagramm für das Funktional erster Ordnung bestimmen, wobei wir sowohl kollineare, als auch spiralförmige Spin-Konfigurationen untersucht haben. FT-RDMFT ermöglichte es uns weiterhin, die Temperaturabhängigkeit der zugehörigen Quasiteilchen-Dispersionsrelationen zu untersuchen. Dies ist von großem Interesse für die Anwendung auf reale Vielteilchensysteme, z.B. Festkörper. Abschließend haben wir verschiedene Möglichkeiten der Behandlung von Korrelationseffekten in FT-RDMFT untersucht. Dabei war es uns möglich, ausgehend von exakten Eigenschaften des Polarisationspropagators, ein FT-RDMFT-Korrelationsfunktional abzuleiten welches zu einem qualitativ korrekten Phasendiagramm führt.

D Publications

1. *Discontinuities of the Chemical Potential in Reduced Density Matrix Functional Theory*
   N. N. Lathiotakis, S. Sharma, N. Helbig, J. K. Dewhurst, M. A. L. Marques, F. G. Eich, T. Baldsiefen, A. Zacarias, and E. K. U. Gross.
   Zeitschrift für Physikalische Chemie, 224(03-04), p. 467-480 (2010)
   http://dx.doi.org/10.1524/zpch.2010.6118

2. *Minimization procedure in reduced density matrix functional theory by means of an effective noninteracting system*
   T. Baldsiefen and E. K. U. Gross.
   Computational and Theoretical Chemistry, in press (2012)
   http://dx.doi.org/10.1016/j.comptc.2012.09.001

3. *Reduced density matrix functional theory at finite temperature. I. Theoretical foundations*
   T. Baldsiefen and E. K. U. Gross.
   arXiv:1208.4703 (2012), submitted to *Phys. Rev. A*
   http://arxiv.org/abs/1208.4703

4. *Reduced density matrix functional theory at finite temperature. II. Application to the electron gas: Exchange only*
   T. Baldsiefen, F. G. Eich, and E. K. U. Gross.
   arXiv:1208.4705 (2012), submitted to *Phys. Rev. A*
   http://arxiv.org/abs/1208.4705

5. *Reduced density matrix functional theory at finite temperature. III. Application to the electron gas: Correlation effects*
   T. Baldsiefen and E. K. U. Gross.
   arXiv:1208.4707 (2012), submitted to *Phys. Rev. A*
   http://arxiv.org/abs/1208.4707

6. *Properties of exact functionals in finite-temperature reduced density matrix functional theory*
   T. Baldsiefen and E. K. U. Gross.
   submitted to *Phys. Rev. A*

E Acknowledgements

"...hoc loco, qui propter animi voluptates coli dicunt ea studia ... non intellegunt idcirco esse ea propter se expetenda, quod nulla utilitate obiecta delectentur animi atque ipsa scientia, etiamsi incommodatura sit, gaudeant."

Cicero, De Finibus Bonorum et Malorum, Liber Quintus, XIX, 50

First of all, I would like to thank Prof. Gross for giving me the opportunity to follow my scientific interest in a quite unconstrained way. Although this might not always have been the most productive path it surely was a very challenging and satisfying one.

I thank all members of the committee for the time they invested in reviewing my work, especially Prof. Schotte who accepted the burden of being my second referee.

Although their fields of research have been quite disjunct from the ones dealt with in this work, several members of the Gross workgroup took some real interest and spent considerable amounts of time in fruitful discussions. In this context I especially thank F. G. Eich for his interest and input.

As this work was done in both Berlin and Halle(Saale) I would like to thank all members of the staff at the physics institute of the Freie Universität Berlin and the Max-Planck Institute für Mikrostrukturphysik in Halle(Saale). Without their efforts, there would hardly be any time left for research.

I would also like to thank Ms. Muriel Hopwood for proofreading my thesis.

Finally, I would like to point out my sincere gratitude to my family and friends whose support was a great help in this sometimes daunting adventure.

Tim